WestVirginiaUniversity
THE RESEARCH REPOSITORY @ WVU

Graduate Theses, Dissertations, and Problem Reports

2020

Cobalt-Catalyzed Aerobic Oxidative Cyclization Reactions of Bisnucleophiles: New Methodologies and the Role of Bisnucleophiles in O2 Activation

Jiaqi Liu
West Virginia University, jqliu@mix.wvu.edu

Follow this and additional works at: https://researchrepository.wvu.edu/etd

Part of the Inorganic Chemistry Commons, Medicinal-Pharmaceutical Chemistry Commons, and the Organic Chemistry Commons

Recommended Citation

Liu, Jiaqi, "Cobalt-Catalyzed Aerobic Oxidative Cyclization Reactions of Bisnucleophiles: New Methodologies and the Role of Bisnucleophiles in O2 Activation" (2020). *Graduate Theses, Dissertations, and Problem Reports*. 7929.
https://researchrepository.wvu.edu/etd/7929

This Dissertation is protected by copyright and/or related rights. It has been brought to you by the The Research Repository @ WVU with permission from the rights-holder(s). You are free to use this Dissertation in any way that is permitted by the copyright and related rights legislation that applies to your use. For other uses you must obtain permission from the rights-holder(s) directly, unless additional rights are indicated by a Creative Commons license in the record and/ or on the work itself. This Dissertation has been accepted for inclusion in WVU Graduate Theses, Dissertations, and Problem Reports collection by an authorized administrator of The Research Repository @ WVU. For more information, please contact researchrepository@mail.wvu.edu.

Cobalt-Catalyzed Aerobic Oxidative Cyclization Reactions of Bisnucleophiles: New Methodologies and the Role of Bisnucleophiles in O_2 Activation

Jiaqi Liu

Dissertation submitted to:

Eberly College of Arts and Sciences

West Virginia University

In partial fulfillment of the requirements for the degree of

Doctor of Philosophy

in

Chemistry

Jessica Hoover, Ph.D., Committee Chair

Brian Popp, Ph.D.

Carsten Milsmann, Ph.D.

Björn Söderberg, Ph.D.

Hanjing Tian, Ph.D.

Department of Chemistry

Morgantown, West Virginia, 2020

Keywords: cobalt, homogenous catalysis, 2-aminophenol, 2-aminoaniline, isonitrile, aerobic oxidation, nitrogen heterocycles, benzoxazoles, benzimidazoles, cyclization, synthetic methods, cobalt complexes

Copyright 2020 Jiaqi Liu

Abstract

Cobalt-Catalyzed Aerobic Oxidative Cyclization Reactions of Bisnucleophiles: New Methodologies and the Role of Bisnucleophiles in O_2 Activation

Jiaqi Liu

Over the past few decades, transition metals have found wide applications in the development of selective oxidative transformations mediated by molecular oxygen. Due to the benign nature of molecular oxygen as an oxidant and an increasing awareness of green chemistry practice, tremendous progress has been made towards the development of Cu-and Pd-catalyzed aerobic oxidation reactions. As a first-row transition metal alternative to copper, cobalt has been employed in aerobic catalytic transformations for its cost-efficiency and earth abundance; however, redox-active mediators such as benzoquinone (BQ), N-hydroxyphthalimide (NHPI) or salen-type ligands are usually required. To date, reactions mediated by Co/O_2 catalytic systems in the absence of redox mediators are still limited. In this regard, we developed a highly efficient protocol employing a Co/O_2 catalytic system without acquiring external mediators to turn-over the cycle.

This dissertation offers a brief overview of advancements in cobalt-catalyzed aerobic oxidative reactions in chapter 1, where three major classes of oxidation reactions mediated by Co/O_2 systems are particularly addressed. Chapterss 2 and 3 describe the development of a series of new cobalt-catalyzed aerobic cyclization reactions of bis-nucleophiles. When isonitriles are employed as coupling partners, a wide variety of functionalized 2-aminobenzoxazoles and 2-aminobenzimidazoles are afforded as pharmaceutically valuable structures. These protocols are additive-free, ligand-free, highly efficient, and require no external redox-active mediators. Mechanistic studies point to the dual function of the bis-nucleophile as both a substrate and a redox-active ligand, and its importance in activating molecular oxygen as the stoichiometric oxidant. Additionally, the bis-nucleophile may act as a hydrogen atom donor capable of participating in hydrogen atom transfer (HAT) reactions. Chapter 4 elucidates the synthesis and characterization of two unprecedented Co^{II} and Co^{III} complexes consisting of the N-unsubstituted aminophenol ligand. As a continuous effort in deepening mechanistic investigations, these metal complexes are regarded as potential active reaction intermediates and have demonstrated success in enabling O_2 activation thus mediating oxidative cyclization transformations afterward.

I have been taught not to use subjective words in my thesis,
but I don’t care this time.

To my dearest mom and dad,
I could never thank you enough for being the most awesome
parents in the world.

Acknowledgement

When I look back to seven years ago, the first time I came to the United States, I couldn't imagine the journey I have made so far. With semi-broken English, I even didn't know how to order my first meal at the only open place on a quiet Sunday morning. I was brave and ambitious; however, I underestimated the challenges along the path I chose. On this journey of studying abroad, I doubted myself hundreds of times and I even wondered if this path towards the Ph.D. is designed for me. Being an international graduate student who switched the major and tackling with stress from improving language proficiency and unexpected cultural shocks, I must admit the whole process was a pain, but it was a good pain. Without experiencing it I would never see my potential, become a stronger person each time from a fall, and stand at the point where I am now telling the story of the past myself as if I am talking about an old friend.

I would like to express my sincere gratitude to my Ph.D. advisor, Dr. Jessica Hoover, who has played an essential role in this journey. Her guidance on my research not only improved the way I visualize science but also impacted many other ways like how I see and solve problems arise in life. She is a serious scientist and a true educator. She cares about the growth of students both academically and mentally. Her high standard in guiding graduate researchers is an awarding experience when a person looks back. I have seen tremendous progress in myself regarding writing and verbal communication skills. What I truly admire is that she is always open to the words and opinions, which created a resilient group culture and made my graduate study enjoyable. I feel fortunate being one of her students in one of the important times of my life.

I sincerely appreciate every member of my committee, Dr. Brian Popp, Dr. Carsten Milsmann, Dr. Björn Söderberg, and Dr. Hanjing Tian for their guidance and active involvement in my 5 years' career in grad school. I also truly appreciate Dr. Novruz Akhmedov for NMR experimental assistance, Dr. Jeffrey Petersen, and Dr. Brian Dolinar for X-ray diffractometry interpretations, Dr. Michael Gunther for EPR measurements, and members from the WVU BioNano Research Facilities (BNRF) for ESI-MS analysis. I am thankful for all the kind help offered by Randy, Allen, Sherman, and Greg for technical work in maintaining instruments. Without their efforts, my research couldn't have been progressed so smoothly.

I want to show gratitude to all my groupmates for being my colleagues and friends. I am thankful for current group members, Prof. Andreas Baur, Dr. Shannen Lorraine, Rob Crovak, Michael Stanton, Rebekah Krupa, Rabina Basnet, and Karl Golian, their presence makes a great Hoover family. I also want to thank all group alumni who had mentored me, John Riedesel, Dr. Aaron Honeycutt, Dr. Minghao Li, Dr. Anitha Shankara Linge Gowda, Dr. Bhasker Radaram, Dr. Oliver Mitevski, and Dr. Aaron Honeycutt. Additionally, I would like to thank every undergraduate student I have mentored, these mentorships make me a more responsible individual and I appreciate the input from all of them in their transformation into scientists. I want to thank Dr. Kerry-Ann Green particularly for being an awesome team member and a friend for three years in the Hoover group, I appreciate she is always there for sincere advices and believing in me.

I am deeply grateful to all the lovely persons I have met in the United States. Their friendship and sincerity make me a warm home in this country. I also truly appreciate all the love and the care my families in China have sent along these years. I want to thank a great guy Suhil, my boyfriend. He has shown incredible patience with me and my occasionally occurred irregular temper, and always send me positive vibes even life might be hard for him sometimes. I could never thank my amazing parents enough for their inspiration, drive, and unconditional support. Nothing I do could fully show my gratitude for them. They are not only my parents; they are my teachers. They have guided me so far throughout the journey, and I know their wisdom and support will keep enlightening my future path, no matter where I will be and how far I will go.

Finally, I acknowledge the C. Eugene Bennett Department of Chemistry at West Virginia University for the generous offer and financial support to make the accomplishment of my Ph.D. study true.

Table of Contents

Title Page i

Abstract ii

Dedications iii

Acknowledgements iv

Table of Contents vi

List of Schemes xi

List of Figures xiv

List of Tables xvi

List of Abbreviations xviii

Chapter 1. Cobalt-catalyzed Aerobic Oxidation Reactions: An Overview 1

1.1. Transition-Metal Catalyzed Oxidation of Organic Substrates with O_2 Oxidant 1

1.2. Historic Overview of Co/O_2 Catalysis 3

1.2.1. Mukaiyama Olefin Oxygenation and Oxidative Cyclization of Alkenols 3

1.2.2. Co/NHPI-Catalyzed Aerobic Oxidative Reactions 6

1.2.3. Cobalt Schiff Base Complexes in Aerobic Oxidation Reactions 10

1.3. Conclusion 16

Chapter 2. Cobalt-Catalyzed Aerobic Oxidative Cyclization of 2-Aminophenols with Isonitriles: 2-Aminophenol Enabled O_2 Activation by Cobalt(II) 17

2.1. Introduction 17

2.2. Results 18

2.2.1. Condition Optimization for Cobalt-Catalyzed Oxidative Cyclization of 2-Aminophenol with *tert*-Butyl Isonitrile 18

2.2.2. Substrate Scope of Substituted 2-Aminophenols and Isonitriles 20

2.2.3. Preliminary Mechanistic Investigations 22

2.2.3.1. Testing the Presence of Trappable Radical Intermediates. 22

2.2.3.2. The Importance of O_2 in Oxidative Cyclization and a Plausible Path for O_2 Activation. 24

2.2.3.3. Probing the Reaction Mechanism Through UV-Visible Studies .26

2.2.3.4. Other Considerations 28

2.3. Conclusive Summary 29

2.4. Experimental Section 29

2.4.1. General Considerations 29

2.4.2. Procedure for Screening of the Reaction Conditions 29

2.4.3. Synthesis and Characterization of the 2-Aminobenzoxazoles 32

2.4.4. Procedures for Control Experiments 43

2.4.4.1. Control Experiments under a Nitrogen Atmosphere 43

2.4.4.2. Control Experiment with a Cobalt(III) Source 44

2.4.4.3. Control Experiment with a Peroxide Oxidant 45

2.4.4.4. Control Experiments with Radical Trapping Reagents 46

2.4.4.5. Control Experiments in the Absence of Isonitrile 47

2.4.4.6. Experimental Procedures for UV-Visible Experiments 50

Chapter 3. Cobalt-Catalyzed Aerobic Oxidative Cyclization of 2-Aminoanilines with Isonitriles: Facile Access to Substituted 2-Aminobenzimidazoles 56

3.1. Introduction 56

3.2. Results 59

3.2.1. Condition Optimization of Cobalt-Catalyzed Aerobic Oxidative Cyclization of *o*-Phenylenediamine with *tert*-Butyl Isonitrile 59

3.2.2. Substrate Scope of *o*-Phenylenediamines and Isonitriles 62

3.2.3. Application of the Cobalt-Catalyzed Oxidative Cyclization of *o*-Phenylenediamines with Isonitriles 65

3.2.4. Radical Trapping Experiments for the Standard Reaction 69

3.3. Conclusive Summary 70

3.4. Experiment Section 70

3.4.1. General Considerations 70

3.4.2. Optimization of the Reaction Condition 71

3.4.3. Reaction Parameter Assessment 74

3.4.4. Alternative Reaction Setups 79

3.4.5. Synthesis and Characterization of 2-Aminobenzimidazoles (**5**) and Other Reaction Products (**6**) 81

3.4.6. Synthesis of 2-Aminobenzimidazoles (**5s** and **5t**) 91

3.4.7. Procedures for Control Experiments with Radical Trapping Agents 94

3.4.8. Attempts in the Synthesis of Mebendazole from 2-Amino-5-Benzoyl Benzimidazole 95

Chapter 4. Synthesis, Isolation and Characterization of the Well-Defined Co^{II} and Co^{III} Complexes bearing NH_2-unsubstituted Aminophenol Ligands and Their Reactivity Studies in the Aerobic Oxidative Cyclization Reactions 99

4.1. Introduction 99

4.2. Results 104

4.2.1. Synthesis of Co^{II} complex bearing 2-amino-4,6-di-*tert*-butylphenol ligands Co^{II}(2-amino-4,6-tert-butylphenolate)$_2$(2-amino-4,6-tert-butylphenol)$_2$ 104

4.2.2. Synthesis of Co^{III} complex bearing 2-amino-4,6-di-*tert*-butyl phenol ligands Co_2^{III}(2-amino-4,6-*tert*-butylphenolate)$_2$(2-amino-4,6-*tert*-butylphenol)(μ-2-amido-4,6-*tert*-butylphenolate)$_2$ 107

4.2.3. Evaluations of the Electronic Properties of Co^{II}-AP^{ditBu} (**7**) and Co^{III}-AP^{ditBu} (**8**) Complexes 111

4.2.3.1. UV-Visible Spectroscopy 111

4.2.3.2. Cyclic Voltammetry 112

4.2.3.3. EPR Measurements 113

4.2.4. Aerobic Oxidation of Co^{II}(2-amino-4,6-*tert*-butylphenolate)$_2$(2-amino-4,6-tert-butylphenol)$_2$ in Solution 115

4.2.5. Reactivity of Co^{II} and Co^{III} Complexes in the Standard Aerobic Oxidative Coupling Systems 116

4.2.5.1. Catalytic and Stoichiometric Reactivity of Co^{II} Complex (**7**) in the Oxidative Cyclization Reactions 116

4.2.5.2. Catalytic and Stoichiometric Reactivity of Co^{III} Complex (**8**) in the Oxidative Cyclization Reactions 118

4.3. Conclusive Summary 121

4.4. Experimental Section 122

4.4.1. General Considerations 122

4.4.2. Synthesis of 2-amino-4,6-di-*tert*-butylphenol ligand 122

4.4.3. Synthesis of 5,7-di-*tert*-butyl-2-(tert-butylamino)benzoxazole (**3w**) by Aerobic Oxidative Cyclization Reaction 123

4.4.4. Synthesis of Co^{II}-AP^{ditBu} Complex Co^{II}(2-amino-4,6-*tert*-butylphenolate)$_2$(2-amino-4,6-*tert*-butylphenol)$_2$ and Co^{III}-AP^{ditBu} Complex Co_2^{III}(2-amino-4,6-*tert*-butylphenolate)$_2$(2-amino-4,6-*tert*-butylphenol)(μ-2-amido-4,6-*tert*-butylphenolate)$_2$ 124

4.4.5. Reactivity Studies of Co^{II}-AP^{ditBu} Complex (**7**) and Co^{II}-AP^{ditBu} Complex (**8**) 125

4.4.6. Crystallography Data 130

4.4.6.1. Description of the X-ray Structural Analysis of Co^{II}-AP^{ditBu} Complex (**7**) 130

4.4.6.2. Description of the X-ray Structural Analysis of Co^{III}-AP^{ditBu} Complex (**8**) 147

References 169

Appendix 181

List of Schemes

Scheme 1.1. Industry Radical Autoxidation Process Employing Transition-Metals and Molecular Oxygen. 2

Scheme 1.2. Simplified Mechanism of Metalloenzyme-Catalyzed Aerobic Oxidation. 2

Scheme 1.3. Mukaiyama Olefin Oxygenation with Co/O_2 Catalytic System 4

Scheme 1.4. First and Second Generations of Cobalt Catalysts in Mukaiyama Oxidative Cyclization. 5

Scheme 1.5. Extension of Mukaiyama Oxidative Cyclization: Reductive and Brominative Alkenol Cyclization. 6

Scheme 1.6. Pioneer Work by Ishii on Aerobic C-H Oxidation Using Combined Catalytic System of Co and NHPI.. 7

Scheme 1.7. Solvent-Free Aerobic Oxidation of Alkylbenzenes Catalyzed by Co/DDAB/NHPI 8

Scheme 1.8. Oxygenation of Heteroarenes by Co/NHPI Catalytic System (Stahl). 9

Scheme 1.9. Autoxidation of Aryl-Capped Alkynyl α-Cyano Alkanones by CoII/NHPI Catalytic System. 10

Scheme 1.10. Two Forms of Co(salen) Complexes with Molecular Oxygen 11

Scheme 1.11. Generalized Mechanism For Co(salen)-Catalyzed Aerobic Oxidation of Lignin-like Phenols to Form Quinones and Aldehydes 12

Scheme 1.12. Simplified Mechanism for the Coupled Redox Cycles Employing Co(salophen) and Hydroquinone Co-catalyst in Pd-Catalyzed Allylic Acetoxylation 14

Scheme 1.13. Co(salen)-Catalyzed Aerobic Oxidative Cross-Coupling of Phenols in the Waste-Free System 15

Scheme 2.1. Redox-Active Mediators in Cobalt-Mediated Aerobic Oxidative Reactions in Enabling O_2 Activation in Prior Studies and This Work... 18

Scheme 2.2. Aerobic Oxidative Cyclization Conducted in the Presence of Radical Trapping Reagents 23

Scheme 2.3. Oxidative Cyclization of 2-Aminophenol and tert-Butyl Isonitrile Mediated by Cobalt Under N_2 25

Scheme 2.4. (a) Proposed Pathway for Co-Catalyzed Aerobic Oxidation of Catechol in Literature and (b) Proposed Pathway for Aerobic 2-Aminophenol Oxidation in This Work 26

Scheme 2.5. (a) The standard reaction conditions and control experiments with (b) 10 mol% $Co(OAc)_2$ and (c) 1 equiv $Co(OAc)_2$ conducted under a nitrogen atmosphere.. 43

Scheme 2.6. Control experiment with (a) $Co(acac)_3$ as a cobalt(III) source and (b) the corresponding catalytic reaction with $Co(acac)_2$ 44

Scheme 2.7. Control experiment with di-*tert*-butyl peroxide as the oxidant 45

Scheme 2.8. Control experiment with (a) TEMPO, (b) 9,10-dihydroanthracene (DHA), and (c) 1,1-diphenylethylene included as radical trapping agents 46

Scheme 2.9. Control experiments conducted in the absence of isonitrile both (a) without and (b) with TEMPO 47

Scheme 3.1. Selected conventional routes for the synthesis of 2-aminobenzimidazoles..... 57

Scheme 3.2. 2-aminobenzimidazole synthesis via transition-metal catalyzed oxidative cyclization of bisnucleophiles with isonitriles 59

Scheme 3.3. Synthesis of *N*-subsittuted diamino quinoxazoline..... 64

Scheme 3.4. Synthesis of *N*-substituted 2-aminobenzimidazoles 65

Scheme 3.5. Application of unsubstituted 2-aminobenzimidazoles in pharmaceutical-related synthesis 66

Scheme 3.6. Synthesis of the unsubstituted 2-aminobenzimidazoles **5s** and **5t** via acid-promoted dealkylation 67

Scheme 3.7. Attempted synthesis of mebendazole from 2-amino-5-benzoyl-1*H*-benzimidazole **5t** under varied reaction conditions 68

Scheme 3.8. Synthesis of mebendazole from 2-amino-5-benzoylbenzimidazole in literature 69

Scheme 3.9. Control experiments with TEMPO and 1,1-diphenylethylene as radical trapping agents. 70

Scheme 3.10. Attempts in the synthesis of mebendazole from 2-amino-5-benzoyl benzimidazole and methyl chloroformate 96

Scheme 4.1. Oxidation states of the bidentate *o*-aminophenol as a redox-active ligand 99

Scheme 4.2. Proposed mechanism for the catalytic oxidation of primary alcohols by dioxygen employing complexes of a tetradentate redox non-innocent ligand 102

Scheme 4.3. Negishi-type cross-coupling reaction of alkyl halides with organozinc reagents by Co^{III}bis(*o*-amidophenolato) complex 103

Scheme 4.4. Proposed mechanism for oxidative ring cleavage of 2-amino-4-*tert*-butylphenol to the picolinic acid in the presence of O_2 104

Scheme 4.5. Cobalt-catalyzed oxidative coupling of 2-amino-4,6-di-*tert*-butyl phenol and *tert*-butyl isonitrile under the standard reaction conditions 105

Scheme 4.6. Synthesis and condition optimization of Co^{II}-AP^{ditBu} complex Co^{II}(2-amino-4,6-*tert*-butylphenolate)$_2$(2-amino-4,6-*tert*-butylphenol)$_2$ by varying metal to ligand ratio 106

Scheme 4.7. Attempted synthesis of Co^{III}-AP^{ditBu} complex in the aqueous medium under ambient atmosphere 108

Scheme 4.8. Solid state oxidation observed by Wieghart group for the oxidation of the Co^{II} complex $[Co^{II}(L_S^{AP})_2]_2 \cdot 2CH_3CN$ in the presence of air (L_S^{AP}= 2-amino-4,6-di-*tert*-butylthiophenol) 109

Scheme 4.9. Solid-state oxidation of metal complex Co^{II}(2-amino-4,6-tert-butylphenolate)$_2$(2-amino-4,6-*tert*-butylphenol)$_2$ under air 109

Scheme 4.10. Catalytic control experiments of Co^{II}-AP^{ditBu} complex **(7)** in the aerobic oxidative cyclization reactions 117

Scheme 4.11. Stoichiometric control experiments of Co^{II}-AP^{ditBu} complex **(7)** under anaerobic reaction conditions 118

Scheme 4.12. Catalytic control experiments of Co^{III}-AP^{ditBu} complex **(8)** under aerobic oxidative cyclization conditions 119

Scheme 4.13. Stoichiometric control experiments with Co^{III}-AP^{ditBu} complex **(8)** under both aerobic and anaerobic atmosphere 120

Scheme 4.14. Reactivity of Co^{III}-AP^{ditBu} complex in oxidative cyclization reactions under N_2 atmosphere 121

List of figures

Figure 1.1. Proposed Mechanism for the Co(salophen)-Catalyzed Aerobic Oxidation of *p*-Hydroquinone 13

Figure 2.1. (a) Absorption spectrum of $Co(acac)_2$ only and $Co(acac)_2$ with CN*t*Bu in CH_3CN under N_2 and after exposed to air overnight. (b) Absorption spectrum of $Co(acac)_2$ and 2-aminophenol under N_2 and after exposed to air overnight 27

Figure 2.2. Absorption spectrum of $Co(acac)_2$ with 2-aminophenol in CH_3CN under N_2 and after exposed to air overnight stacked with the final trace spectrum of $Co(acac)_3$ with 2-aminophenol under air exposure 28

Figure 2.3. ^{1}H NMR spectrum of the crude reaction mixture of the Co-catalyzed, TEMPO-mediated dimerization of 2-aminophenol for the synthesis of 2-aminophenoxazin-3-one (reaction b in **Scheme 2.9**) in DMSO-d_6 at 400 MHz 49

Figure 2.4. ^{1}H NMR spectrum of standard 2-aminophenozaxin-3-one purchased from AstaTech (95% pure) in DMSO-d_6 at 400 MHz 50

Figure 2.5. UV-Visible spectra of $Co^{II}(acac)_2$ (5.05×10^{-2} mM in MeCN) prepared under N_2 (orange trace), and then exposed to air and monitored over the course of 12 h at room temperature (blue trace) 51

Figure 2.6. UV-Visible spectra of (a) Co^{II}(acac)2 (5.05×10^{-2} mM in MeCN) prepared under N2 (red trace), and then *tert*-butylisonitrile (8 equiv) was added (green trace), and final, exposed to air overnight (dark blue trace) 52

Figure 2.7. UV-Visible spectra of (a) $Co^{II}(acac)_2$ (5.05×10^{-2} mM in MeCN) prepared under N_2 (yellow trace), and then treated with 2-aminophenol to reach a total of 2 equiv added (deep blue trace), and (b) $Co^{II}(acac)_2$ (5.05×10^{-2} mM in MeCN) and 2-aminophenol (2 equiv, purple trace) exposed to air and monitored over the course of 12 h at room temperature (orange trace) 53

Figure 2.8. (a) $Co(acac)_2$ (5.0×10^{-5}M) in MeCN under N_2 (red trace) with the addition of 3 equiv of 2-aminophenol (yellow trace), and (b) $Co(acac)_2$ and 2-aminophenol (3 equiv, yellow trace) exposed to air overnight (deep blue trace) 54

Figure 2.9. (a) $Co(acac)_3$ (2.5×10^{-5} M) in MeCN under N_2 (blue trace) with the addition of 3 equiv of 2-aminophenol (yellow trace) and (b) $Co(acac)_3$ (2.5×10^{-5} M) and 2-aminophenol (3 equiv, red trace) exposed to air overnight (blue trace) 55

Figure 3.1. Condition-based sensitivity assessment experiment. (a) Four steps involved in sensitivity assessment procedure (b) Sensitivity assessment of key parameters in Co-catalyzed aerobic oxidative cyclization of *o*-phenylenediamine with *tert*-butyl isonitrile 62

Figure 3.2. Reaction set up for parameter assessment studies 76

Figure 3.3. Reaction setup under N_2 atmosphere (left side) and O_2 atmosphere (right side, stopcocks are closed) 77

Figure 3.4. Radar diagram generated from parameter assessment data shown in **Table 3.9** 78

Figure 3.5. Reaction setup using a pressure tube with a headspace filled with air..... 80

Figure 3.6. Mixture of the two mebendazole structural isomers from the model transformation 97

Figure 3.7. ^{1}H NMR for structural elucidation of mebendazole isomer with 1-acylation..... 97

Figure 3.8. ^{1}H NMR for Structural elucidation of mebendazole isomer with 3-acylation 98

Figure 3.9. ^{13}C NMR for the mixture of two mebendazole isomers..... 98

Figure 4.1. Selected Examples for Cobalt Complexes with 3,5-di-*tert*-butyl-*o*-aminophenols 100

Figure 4.2. The structure of Co(2-amino-4,6-*tert*-butylphenolate)$_2$(2-amino-4,6-*tert*-butylphenol)$_2$..... 107

Figure 4.3. The structure of Co$_2$(2-amino-4,6-*tert*-butylphenolate)$_2$(2-amino-4,6-*tert*-butylphenol)(μ-2-amido-4,6-*tert*-butylphenolate)$_2$ 110

Figure 4.4. UV-visible spectroscopy of Co^{II}-AP^{ditBu} **(7)** and Co^{III}-AP^{ditBu} **(8)**..... 112

Figure 4.5. Cyclic voltammograms of Co^{II}-AP^{ditBu} **(7)** and Co^{III}-AP^{ditBu} **(8)**..... 113

Figure 4.6. EPR spectra For Co^{II}-AP^{ditBu} Complex **(7)** and Co^{III}-AP^{ditBu} Complex **(8)**..... 114

Figure 4.7. Aerobic oxidation of the Co^{II}-AP^{ditBu} complex with dissociation of a ligand monitored by ^{1}H NMR spectroscopy 115

Figure 4.8. Deuterium Exchange Experiment of the Oxidized Cobalt Intermediate. Standard Spectrum of the Ligand was Included for Reference..... 116

List of Tables

Table 2.1. Optimization of Reaction Conditions 19

Table 2.2. Scope of Substituted 2-Aminophenols 20

Table 2.3. Scope of Substituted Isonitriles 21

Table 2.4. Optimization of the reaction temperature and base in the oxidative cyclization of 2-aminophenol and *tert*-butylisonitrile 30

Table 2.5. Optimization of the base in the oxidative cyclization of 2-aminophenol and *tert*-butylisonitrile 31

Table 2.6. Optimization of the catalyst loading and reaction time in the oxidative cyclization of 2-aminophenol and *tert*-butylisonitrile 31

Table 3.1. Optimization of Reaction Conditions 60

Table 3.2. Scope of *ortho*-Phenylenediamine and Isonitrile Coupling Partners 63

Table 3.3. Unsuccesful Isonitrile and Diamine Coupling Partners 65

Table 3.4. Optimization of the cobalt source in the oxidative cyclization of *ortho*-phenylenediamine and *tert*-butylisonitrile 72

Table 3.5. Optimization of the solvent in the oxidative cyclization of *ortho*-phenylenediamine and *tert*-butylisonitrile 72

Table 3.6. Optimization of the base in the oxidative cyclization of *ortho*-phenylenediamine and *tert*-butylisonitrile 73

Table 3.7. Optimization of the temperature in the oxidative cyclization of *ortho*-phenylenediamine and *tert*-butylisonitrile 73

Table 3.8. Conditions used for reaction parameter assessment 75

Table 3.9. Results of Parameter Assessment of the Standard Reaction 78

Table 4.1. Crystal data and structure refinement for Co^{II}-AP^{ditBu} Complex (**7**) 132

Table 4.2. Fractional Atomic Coordinates ($\times 10^4$) and Equivalent Isotropic Displacement Parameters ($Å^2 \times 10^3$) for Co^{II}-AP^{ditBu} Complex (**7**) 133

Table 4.3. Anisotropic Displacement Parameters ($Å^2 \times 10^3$) for Co^{II}-AP^{ditBu} Complex (**7**) 136

Table 4.4. Bond Lengths for Co^{II}-AP^{ditBu} Complex (**7**) 138

Table 4.5. Bond Angles for Co^{II}-AP^{ditBu} Complex (**7**) 140

Table 4.6. Hydrogen Atom Coordinates (Å×10^4) and Isotropic Displacement Parameters (Å^2×10^3) for Co^{II}-AP^{ditBu} Complex (**7**) 142

Table 4.7. Atomic Occupancy for Co^{II}-AP^{ditBu} Complex (**7**) 145

Table 4.8. Crystal data and structure refinement for Co^{III}-AP^{ditBu} Complex (**8**). 149

Table 4.9. Fractional Atomic Coordinates (×10^4) and Equivalent Isotropic Displacement Parameters (Å^2×10^3) for Co^{III}-AP^{ditBu} Complex (**8**) 151

Table 4.10. Anisotropic Displacement Parameters (Å^2×10^3) for Co^{III}-AP^{ditBu} Complex (**8**) 154

Table 4.11. Bond Lengths for Co^{III}-AP^{ditBu} Complex (**8**). 157

Table 4.12. Bond Angles for Co^{III}-AP^{ditBu} Complex (**8**) 158

Table 4.13. Torsion Angles for for Co^{III}-AP^{ditBu} Complex (**8**). 161

Table 4.14. Hydrogen Atom Coordinates (Å×10^4) and Isotropic Displacement Parameters (Å^2×10^3) for Co^{III}-AP^{ditBu} Complex (**8**) 164

Table 4.15. Atomic Occupancy for Co^{III}-AP^{ditBu} Complex (**8**). 168

List of Abbreviations

acac: acetylacetonate

AP: abbreviated aminophenol ligand

AP^{ditBu}: 2-amino-4,6-di-*tert*-butylphenol ligand (only used in the context in this dissertation)

BQ: benzoquinone

Co(salen): [N, N′-bis-(salicylidene)-ethane-1,2-diaminato]cobalt

CV: cyclic voltammetry

DCC: dicyclohexylcarbodiimide

DDAB: di-n-decyl-di-methyl ammonium bromide

DIC: 1,3-diisopropylcarbodiimde

DFT: density functional theory

DHA: 9.10-hydroanthracene

DMSO: dimethyl sulfoxide

DTBP: di-*tert*-butyl peroxide

EDC: *N*-(3-dimethylaminopropyl)-*N'*-ethylcarbodiimide hydrochloride

EPR: electron paramagnetic resonance

ESI-MS: electrospray ionization mass spectrometry

FTIR: fourier-transform infrared spectroscopy

HAA: hydrogen atom abstraction

HAT: hydrogen atom transfer

PCET: proton-coupled electron transfer

HFIP: 1,1,1,3,3,3-hexafluoropropan-2-ol

NHPI: *N*-hydroxyl phthalimide

NMR: nuclear magnetic resonance

PINO: phthalimide-*N*-oxyl

DDAB: di-n-decyl-di-methyl ammonium bromide

MLVs: multi-lamellar Vesicles

NC: isocyanide group

PTC: phase-transfer conditions

Sq: iminosemiquinoate

tBu: *tert*-butyl group

THF: tetrahydrofuran

Ts: toluenesulfonyl

OAc: acetate group

Chapter 1. Cobalt-catalyzed Aerobic Oxidation Reactions: An Overview

1.1. Transition-Metal Catalyzed Oxidation of Organic Substrates with O_2 Oxidant

Molecular oxygen is a highly abundant, environmentally benign, and atom economical oxidant, which makes it an ideal choice for oxidation reactions of organic substrates. However, due to the high energy barrier associated with O_2 activation, the incorporation of catalysts in the reaction is usually necessary.[1] With the increasing awareness of green chemistry practice in recent decades, more efforts have been sought towards the development of the new catalytic oxidation reactions to replace the conventional methods involving the use of stoichiometric quantities of toxic inorganic oxidizing reagents, such as dichromate and permanganate.[2] An ideal system for "Green Oxidation" employs molecular oxygen as the primary oxidant together with recyclable catalysts in a non-toxic solvent to minimize waste disposal. Thus, designing effective catalytic systems that allow the activation of molecular oxygen at ambient conditions for selective oxidation reactions is highly practical. A few applications have been translated to industrial processes and have demonstrated great successes over the past decades (**Scheme 1.1**), such as the palladium-catalyzed Wacker oxidation of alkenes to carbonyl compounds,[3] "KA oil" production via radical-chain autoxidation of cyclohexane to a mixture of cyclohexanone and cyclohexanol, and the synthesis of terephthalic acid from p-xylene in the presence of manganese and cobalt salt, using molecular oxygen as the terminal oxidant.[2]

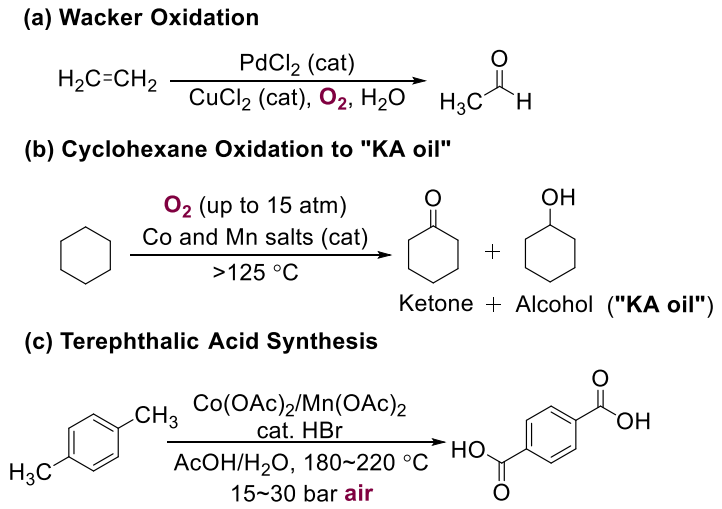

Scheme 1.1. Industry Radical Autoxidation Process Employing Transition-Metals and Molecular Oxygen.

Metalloenzymes that catalyze selective aerobic oxidation reactions have provided valuable frameworks for the design of new catalysts over the century. These enzymes are characterized into two major classes based on the fate of oxygen atom from the molecular oxygen, oxygenase, and oxidase. Oxygenases provide oxygen atom transfer from the molecular oxygen to the substrates, affording the oxygen-incorporated products, while oxidases just use molecular oxygen as the electron or proton acceptor during the oxidation of substrates.[4] The simplified mechanistic elucidation of these two main categories of metalloenzyme is shown in **Scheme 1.2**.

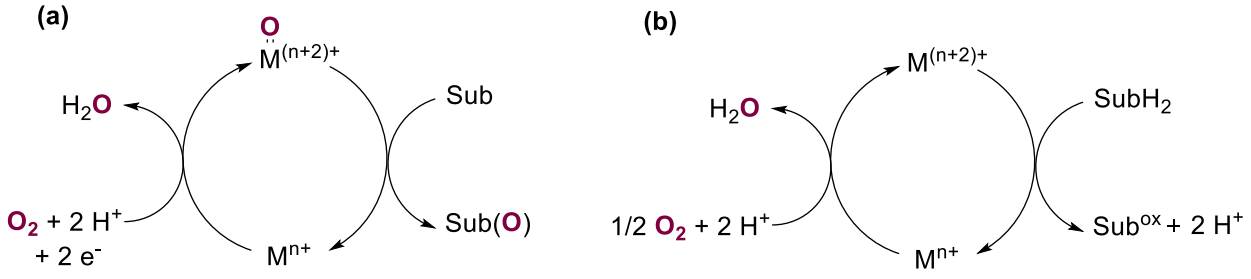

Scheme 1.2. Simplified Mechanism of Metalloenzyme-Catalyzed Aerobic Oxidation. (a) Oxygenase Pathway Featuring Oxygen Atom Transfer from O_2 to Substrate. (b) Oxidase Pathway Featuring O_2 as a $2H^+/2e^-$ Acceptor in Substrate Oxidations.

Studies on these natural oxidation processes have offered lots of insights and inspirations for chemists aiming to utilize O_2 for selective oxidation reactions. "Oxygenase-type" oxidation reactions have demonstrated great successes in asymmetric catalysis, such as Sharpless asymmetric epoxidation, where molecular oxygen or dioxygen surrogates such as amine *N*-oxides, alkyl peroxides, or hydrogen peroxide are employed.[4] The "oxidase-type" oxidation reactions allow any oxidation reaction to being coupled to O_2 reduction when the catalyst can mediate both redox cycles of substrate oxidation by the oxidized catalyst and re-oxidation of the reduced catalyst by O_2. Over the course of seeking effective catalytic oxidation systems, a broad scope of oxidative transformations has been developed using molecular oxygen as the terminal oxidant, catalyzed by a vast range of transition metals.[2, 5-9] These transformations include but are not limited to alcohol oxidations, alkene epoxidation, alkene oxidation to alcohols and ketones, benzylic and allylic oxidation, aromatic C-H oxidation, sulfoxidation, and Baeyer-Villiger oxidation. While numerous contributions have been made toward this field of study, this chapter will mainly focus on three major categories of aerobic oxidative transformation mediated by cobalt-catalysts, including perspectives from both "oxygenase-type" and "oxidase-type" reactions.

1.2. Historic Overview of Co/O_2 Catalysis

1.2.1. Mukaiyama Olefin Oxygenation and Oxidative Cyclization of Alkenols

In the late 80s of the last century, Mukaiyama and co-workers had uncovered a few efficient methods for introducing dioxygen functionality to the carbon-carbon double bond under mild reaction conditions.[10] The development of these methods made a significant contribution to the selective oxygenation of olefins with molecular oxygen paired with cobalt salts, rather than employing cobalt complexes consisting of Schiff-base ligands or porphyrin ligands. These discoveries built foundations to their later reported olefin activation study, with O_2 as the oxidant and $EtSiH_3$ as the reducing agent, the corresponding triethylsilyl peroxide was generated by using a Co^{II} catalyst at room temperature.[11] They also found that the variation of silane agents could produce the alcohol directly from the olefin. When phenyl silane was used in place of triethyl silane, hydration of the olefin proceeded smoothly at room temperature with high efficiency (**Scheme 1.3**).[10]

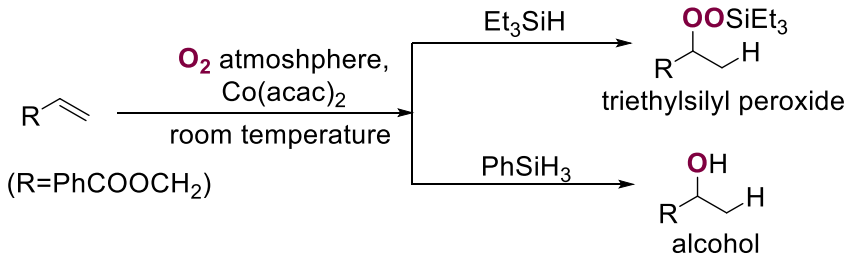

Scheme 1.3. Mukaiyama Olefin Oxygenation with Co/O_2 Catalytic System

In 1990, Mukaiyama reported a Co^{II}-catalyzed oxidative cyclization of 5-hydroxy-1-alkene for the preparation of trans-2-hydroxymethyltetrahydrofurans with molecular oxygen as the oxidant.[12] Employing a $Co(modp)_2$ catalyst, various 2-hydroxymethyl-tetrahydrofurans were attained with extremely high trans-selectivity (**Scheme 1.4a**). Though three decades have passed since the discovery of this oxidative cyclization of alkenols, this reaction still interests a lot of researchers as the diastereoselective synthesis of functionalized cyclic ethers is of significant importance. Tetrahydrofurans (THFs) are key structural elements that are naturally occurring in many substances with potent biological activities.[13] The Mukaiyama oxidation usually proceeds in excellent diastereoselectivity (>99:1 dr) and moderate to good yields, however, the catalyst can be extremely difficult to remove from the THF products when modp ligand is employed, introducing unnecessary challenges to the NMR characterization of the desired product. Also, the difficulties associated with the purification of the products counterbalanced the synthetic advantage of this cobalt catalyst. Later on, Pagenkopf and co-workers developed the second generation of water-soluble cobalt catalyst for Mukaiyama oxidative cyclization reactions.[14] This catalyst was equipped with a piperazine unit, which was believed to help with the solubility of the cobalt catalyst when the acidic workup is used (**Scheme 1.4b**). This method retained the efficiency of the Mukaiyama oxidative cyclization while also providing significantly increased polarity of the cobalt catalyst, and was expected to find applications in total synthesis.

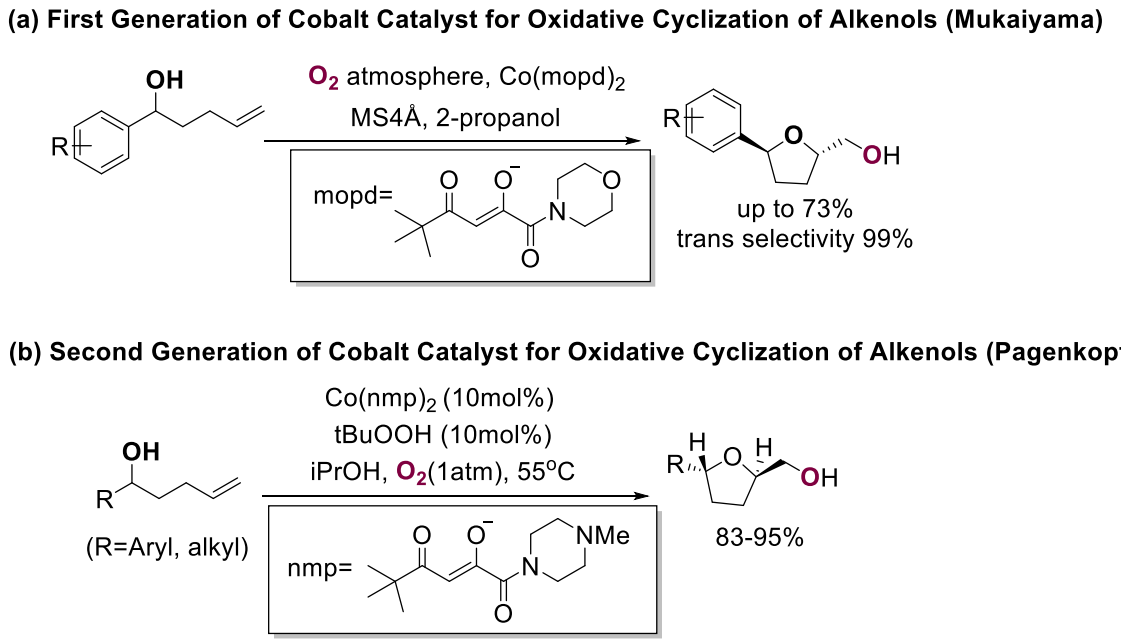

Scheme 1.4. First and Second Generations of Cobalt Catalysts in Mukaiyama Oxidative Cyclization.

Hartung and co-workers further developed a few methods to expand the existing Mukaiyama oxidative cyclization (**Scheme 1.5a**).[15] With the retention of the extraordinary diastereoselectivity (> 99:1 dr) of the original oxidative cyclization of alkenols, heterocycles with different functionality can be obtained employing Co catalyst {4-[3,5-bis(trifluoromethyl)-phenyl]-4-oxybut-3-en-2-one}-cobalt(II) (CoL_2) under an O_2 atmosphere. In their study, they provided evidence that the intermediates generated during catalysis are free carbon radicals, which can be converted into synthetically valuable functional groups with various chemical reagents (**Scheme 1.5b**). In this way, they developed methods for reductive and brominative termination of the aerobic oxidative cyclization of alkenols, with the right choice of the reductant and brominating agents. They later expanded the scope to a broader range of acceptor molecules,[16] such as mono-substituted olefins including methyl acrylate and acrylonitrile; 1,2-disubstituted olefins involving dimethyl fumarate and N-phenylmaleic imide. The protocol can also tolerate ester-substituted alkynes, giving rise to a diastereomerically pure bis-tetrahydrofuran, which was initiated by a cascade process consisting of two aerobic oxidations, an alkyne addition, followed by a hydrogen atom transfer (HAT).

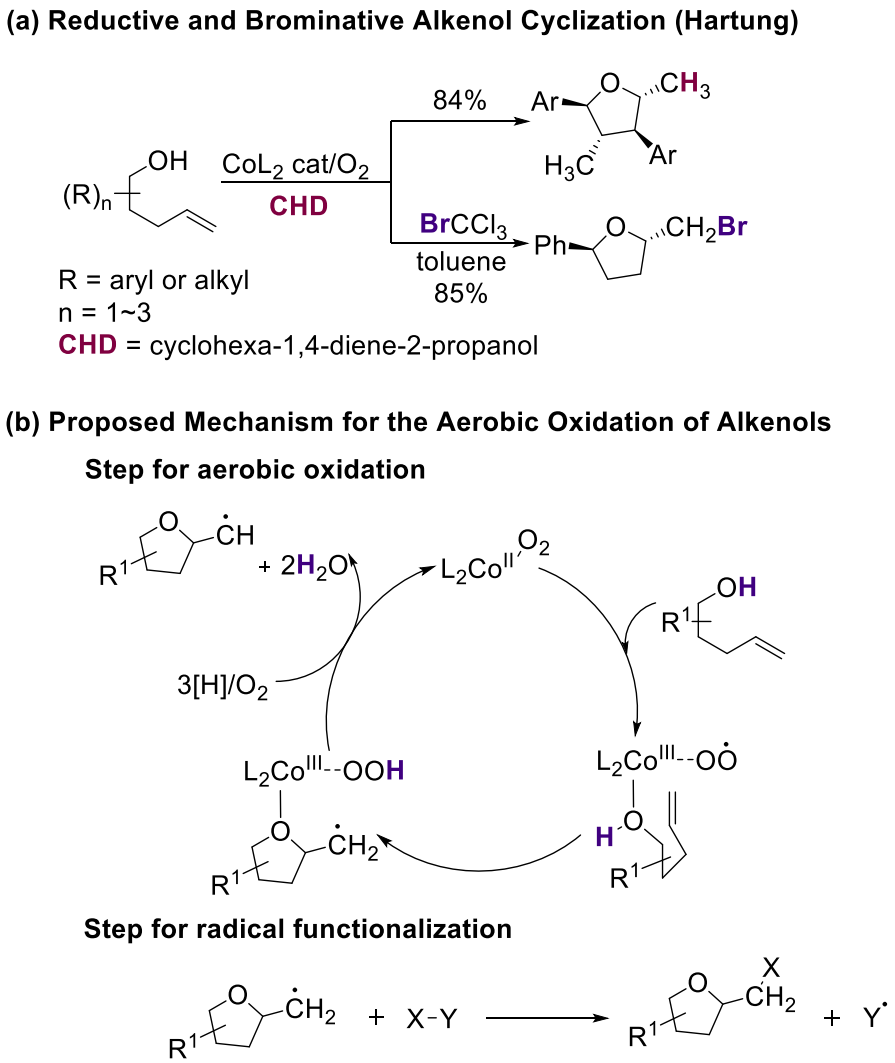

Scheme 1.5. Extension of Mukaiyama Oxidative Cyclization: Reductive and Brominative Alkenol Cyclization.

1.2.2. Co/NHPI-Catalyzed Aerobic Oxidative Reactions

While the discovery of Mukaiyama oxidative cyclization reactions has been a milestone in the cobalt-catalyzed oxidations employing O_2 as the stoichiometric oxidant, it has limited scope to the oxy-functionality of alkenols to generate diastereomerically pure tetrahydrofurans (THFs). A few years later, a practical method had been introduced by Ishii and co-workers to convert alkanes and alkylbenzenes into the corresponding ketones and carboxylic acids using a combined system consisting of N-hydroxyphthalimide (NHPI) and Co(II) (**Scheme 1.6a**).[17-19] This co-catalytic

system was primarily employed in the C-H oxidation of the methylene compounds at ambient pressure. The generalized mechanism shown in **Scheme 1.6b** suggested the in-situ generated phthalimide-N-oxyl radical (PINO) plays a critical role in the catalytic cycle to abstract a hydrogen atom from the substrate. The resulting carbon-centered radical will participate in the oxygenation with O_2, giving rise to the corresponding ketone or carboxylic acid products. Among other transition-metals being investigated, cobalt had shown to be the key promoter to generate the PINO intermediate, other metals demonstrated less efficiency in this aerobic C-H oxidation reaction.[6, 18]

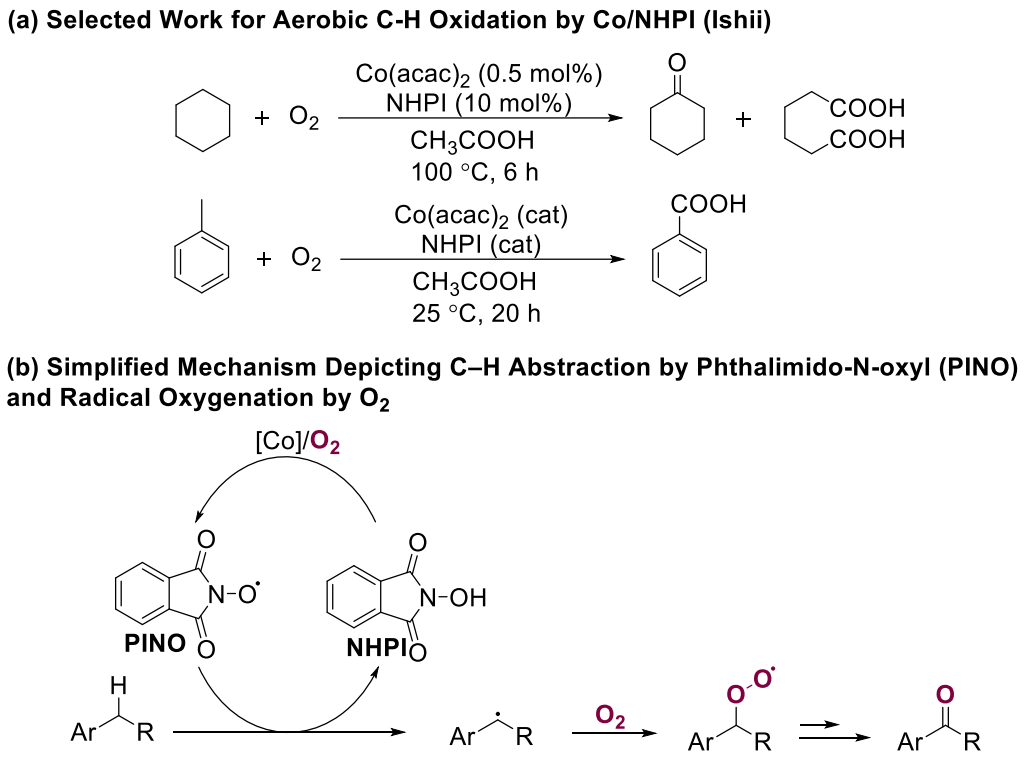

Scheme 1.6. Pioneering Work by Ishii on Aerobic C-H Oxidation Using the Combined Catalytic System of Co and NHPI.

Following these pioneering works, Patil and co-workers later developed a solvent-free, sustainable, and selective reaction for the C-H oxidation of alkylbenzenes by Co/NHPI under phase-transfer conditions (PTC).[20] Although NHPI was proved to be highly efficient and versatile in the aerobic oxidation reactions, it has inherited limitations that prevented translation to the industrial process. For example, there are no proper methods for the reuse and recovery of catalysts; NHPI presented poor solubility in non-polar organic phases, and instability of both NHPI and its

intermediate PINO at the temperature above 80 ºC.[21, 22] The design of this oxidation system aimed at transcending the existing limitations and had demonstrated some success in the preparation of gram scale acetophenone when DDAB (Di-n-decyl-di-methyl ammonium bromide) was used as the phase transfer agent (**Scheme 1.7**). In this work, a light microscope image demonstrated that the multi-lamellar vesicles (MLVs) structures associated with DDAB protected NHPI at high temperatures. Thus, they speculated an efficient recovery and reuse of this ternary catalytic system (Co-NHPI/DDAB) is practical. However, this method only demonstrated excellent tolerance to ethylbenzene and indane, it didn't show much efficiency for tetralin substrates.

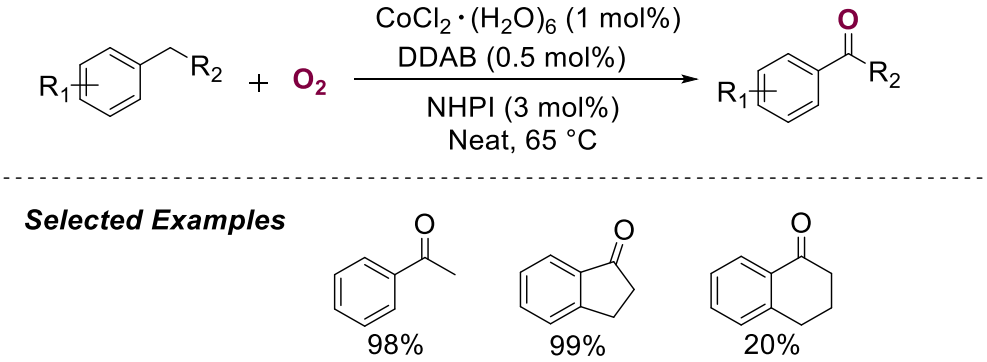

Scheme 1.7. Solvent-Free Aerobic Oxidation of Alkylbenzenes Catalyzed by Co/DDAB/NHPI

In 2017, Stahl and co-workers explored Co/NHPI-catalyzed benzylic oxygenation of heterocyclic substrates including benzimidazoles, thiophenes, and pyridines.[23] This protocol generated benzylic ketones with good to excellent yields, including a gram-scale synthesis of a pharmacologically active compound from its di(hetero) arylmethane precursor with a modified procedure that comprised the use of 500 psi of a mixture (O_2:N_2 9:91) to maintain the limit concentration allowance of molecular oxygen in the solvent BuOAc (**Scheme 1.8**). It was also suggested in this study that radical oxygen reactions would be inhibited with the presence of certain heterocyclic moieties. They attributed the inhibition of the chelation of heterocycles with the metal catalyst, which can be circumvented by an alternative procedure of a cobalt-free, electrochemical NHPI-mediated method they devised at the same time.

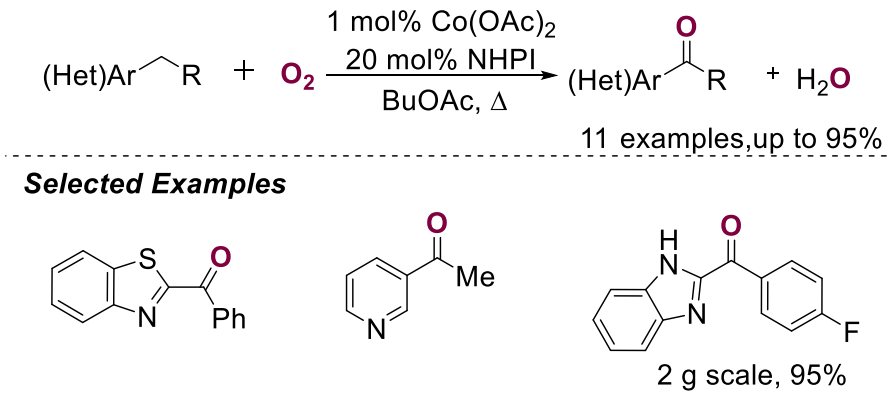

Scheme 1.8. Oxygenation of Heteroarenes by Co/NHPI Catalytic System (Stahl).

Co/NHPI-catalyzed oxygenation not only established great success in the simple oxygenation of the methylene functionalities, but it also proved to be tolerant with oxygen-mediated chain-reactions. The Shia group developed a legitimate protocol of Co/NHPI-catalyzed aerobic oxidation of terminal-capped alkynyl α-cyano alkanone systems.[24] With this method, aryl-, silyl-, and alkyl-capped alkynyl α-cyano alkanone systems can be converted to the corresponding highly functionalized bicyclic products in an effective manner (**Scheme 1.9**). It was also revealed that the substituent capped on the terminal acetylene is structurally variable, although the trialkylsilyl group may play an extraordinary role in inducing the radical chain reaction. According to the proposed mechanism, the chain reaction is initiated by a hydrogen atom abstraction (HAA) at the position α to the cyano group by the in-situ generated phthalimide (PINO) radical, followed by an immediate 5-exo-dig addition to produce a vinyl radical species. Molecular oxygen is then captured by the vinyl radical intermediate to generate a vinyl peroxide species, which undergoes a second hydrogen atom abstraction (HAA) process by NHPI and a 1,4-dehydration to yield the desired product as a highly functionalized bicyclic compound.

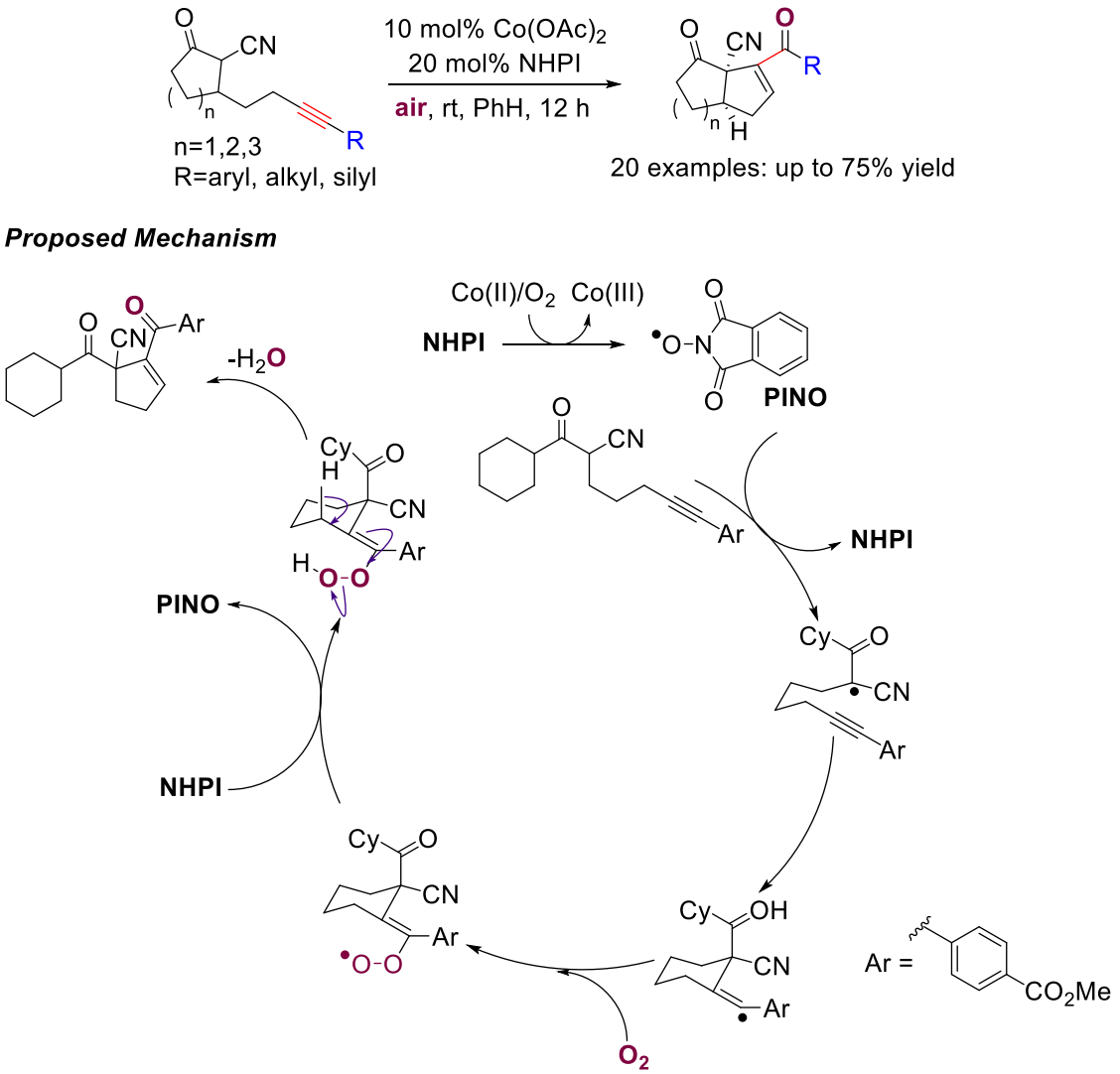

Scheme 1.9. Autoxidation of Aryl-Capped Alkynyl α-Cyano Alkanones by Co^{II}/NHPI Catalytic System.

1.2.3. Cobalt Schiff Base Complexes in Aerobic Oxidation Reactions

The tetradentate, square-planar Schiff base cobalt complex is well known for its O_2 activation behavior. It was first discovered in the 1930s by Tsumaki that solid Co^{II}(salen) ([N, N′-bis-(salicylidene)-ethane-1,2-diaminato]cobalt) can reversibly bind molecular oxygen.[25] This finding spiked tremendous interest among researchers in the oxygen-carrying properties of cobalt complexes with Schiff base ligands.

The Co(salen) complex adapts a square planar geometry. Upon the coordination of molecular oxygen, it adapts an octahedral geometry with the O_2 occupying the axial position.[26] The other axial position is usually occupied by a base, which is believed to help enhance the binding affinity of molecular oxygen to Co(salen) species.[27, 28] Co(salen) complexes typically form either a mononuclear superoxo-complex or a dinuclear complex with a μ-peroxo bridge with molecular oxygen; however, the superoxo complex is assumed to be a radical species and is responsible for aerobic catalytic transformations (**Scheme 1.10**).

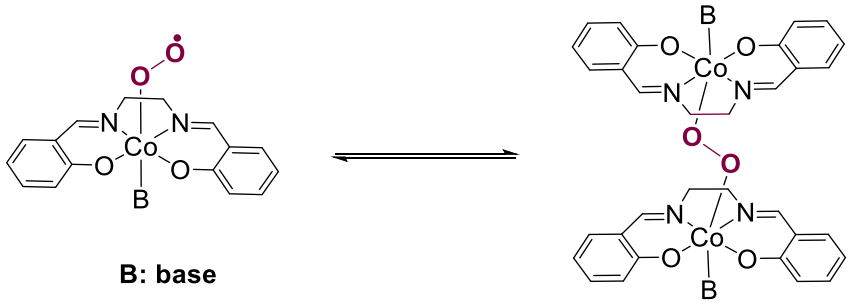

Scheme 1.10. Two Forms of Co(salen) Complexes with Molecular Oxygen. Mononuclear Superoxo Species (Left) and Dinuclear μ-peroxo Species (Right).

Cobalt Schiff base catalysts operate under mild reaction conditions and allow the stoichiometric use of molecular oxygen paired with earth-abundant transition metals. Over the past few decades, it was extensively applied in the phenol oxidations.[27, 29, 30] More recently, this aerobic catalytic system has been translated to the deconstruction of lignin biomass and for the conversion to higher value structures such as quinones and aldehydes. The general mechanism of Co(salen)-catalyzed oxidation is illustrated in **Scheme 1.11** with the *p*-hydroxyphenol lignin model as a substrate.[31, 32] A Co^{III}-superoxide adduct is formed upon activation of molecular oxygen, which readily abstracts a phenolic hydrogen from the substrate to form a phenoxyl radical. This intermediate interacts with the second equivalent of the Co^{III}-superoxide, giving rise to a peroxo species which immediately undergoes a rearrangement to produce quinone and formaldehyde. Alternatively, the same intermediate could also generate an aldehyde upon hydrogen atom abstraction (HAT) from the Co^{III}. The presence of a base such as a pyridine at the axial position of Co(salen) complex has been proved to facilitate the Co^{III}-superoxide formation by increasing the binding affinity of dioxygen species to the metal center.

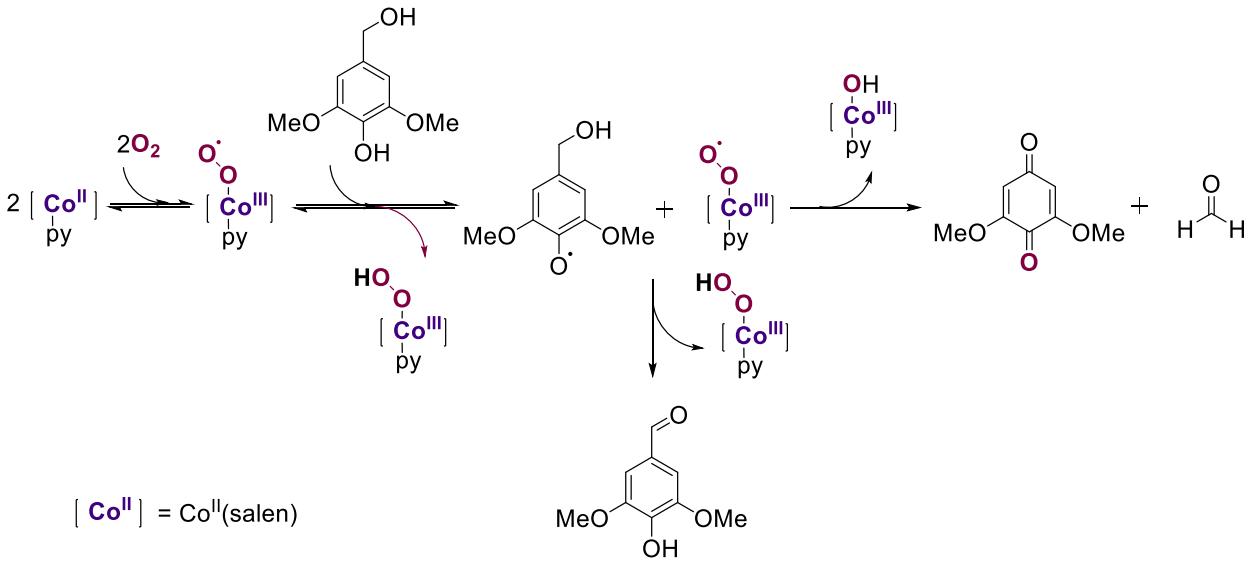

Scheme 1.11. Generalized Mechanism of Co(salen)-Catalyzed Aerobic Oxidation of Lignin-like Phenols to Form Quinones and Aldehydes.

These precedented studies concluded that cobalt Schiff base-catalyzed aerobic phenol oxidations all involve the formation of Co^{III}–hydroxide and Co^{III}–hydroperoxide intermediates. In one of the works published,[32] the proposed Co^{III}-OH intermediate is able to regenerate catalytically active Co^{II} species. Upon hydrogen atom transfer (HAT) from phenol to cobalt hydroxy group, the H_2O can dissociate from the metal center and release the Co(salen) complex to complete the cycle. In 2016, the Stahl group further investigated the Co(salophen)-catalyzed aerobic oxidation of *p*-hydroquinone (**Figure 1.1** left).[33] The mechanism of this catalytic oxidation was examined with a combination of spectroscopy, kinetic measurements, and density functional theory (DFT) calculations. The study suggested that the catalyst resting-state consists of an equilibrium between a Co^{II}(salophen) complex, a Co^{III}-superoxide adduct, and a hydrogen-bonded adduct between the hydroquinone and the Co^{III}–O_2 intermediate (**Figure 1.1** right). The key processes involve a hydrogen atom transfer (HAT) from the *p*-hydroquinone to the Co^{III}-superoxide species and a proton-coupled electron transfer (PCET) between a semiquinone and Co^{III}–hydroperoxo intermediate (Figure 1.1 left bottom). The latter is identified as the turn-over limiting step by combined kinetic experiments and DFT calculations. Subsequently, a coordinated H_2O_2 intermediate of Co^{III} will participate in the oxidation of the second equivalent of *p*-hydroquinone and regenerate the Co^{II} catalyst in the cycle.

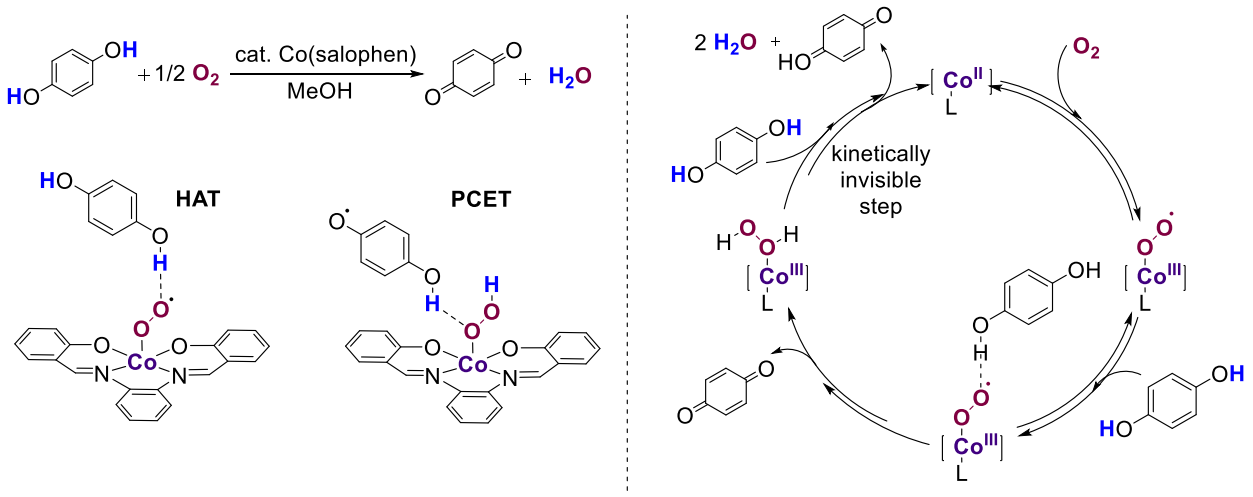

Figure 1.1. Proposed Mechanism for the Co(salophen)-Catalyzed Aerobic Oxidation of *p*-Hydroquinone.

The well-established cycle for aerobic *p*-hydroquinone oxidation by cobalt Schiff base complexes has been widely found in bimetallic-mediated "oxidase" type transformations. These systems all consist of a coupled redox cycle, one cycle for the oxidation of the substrate by the oxidized catalyst, and one cycle for re-oxidation of the reduced catalyst by O_2. Particularly featured in palladium-catalyzed oxidations,[4] benzoquinones and macrocyclic cobalt complexes are usually used as co-catalytic systems in a wide scope of oxidation reactions, such as allylic acetoxylation,[34] Wacker-type oxidation of the alkenes[35], and oxidative C-C cross-coupling reactions.[36] Amongst these impressive findings, Co(salophen) is the most commonly employed co-catalyst in the aerobic oxidative transformations mediated by palladium[37] and ruthenium.[38] **Scheme 1.12** illustrated an example of Pd-catalyzed acetoxylation with a combined redox cycle employing Co(salophen) and hydroquinone as a co-catalyst system. In this system, Co(salophen) and *p*-hydroquinone operate synergistically to generate the active benzoquinone as a co-catalyst meanwhile mediate the electron-transfer to the Pd-catalyzed oxidative C-H functionalization.

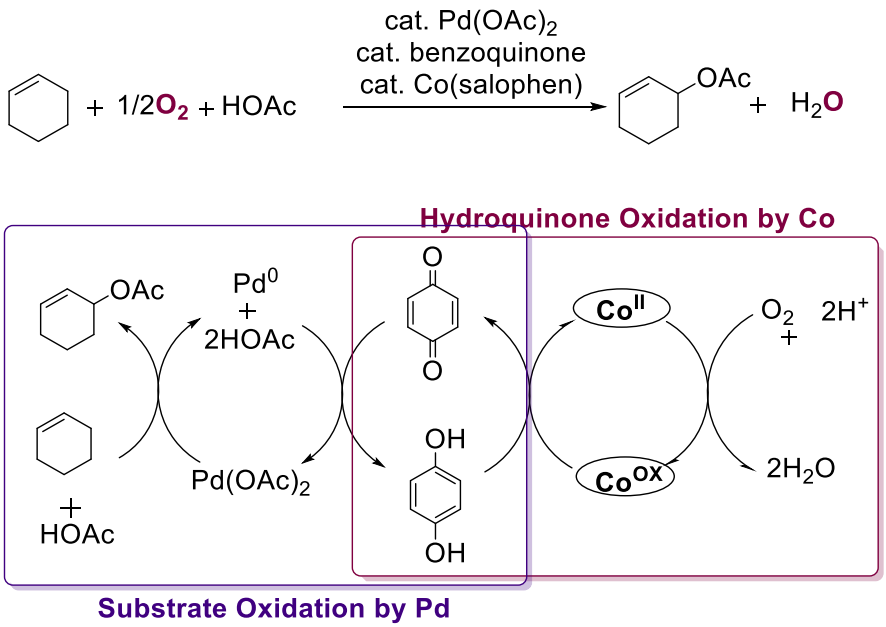

Scheme 1.12. Simplified Mechanism for the Coupled Redox Cycles Employing Co(salophen) and Hydroquinone Co-Catalyst in Pd-Catalyzed Allylic Acetoxylation.

Because of the high efficiency of Co(salen) in the bimetallic systems to function as an electron-transfer mediator when it is paired with a benzoquinone co-catalyst, it has found its application in the selective aerobic oxidative cross-coupling reactions. In 2019, the Pappo group reported a waste-free, selectivity-driven oxidative coupling of phenols employing Co(salen) and air in a recyclable 1,1,1,3,3,3-hexafluoropropan-2-ol (HFIP) solvent (**Scheme 1.13**).[39] This protocol offered a sustainable entry to the synthesis of nonsymmetric biphenols from the readily oxidized phenols and 2-naphthols. A combination of control experiments and kinetic studies pointed to the mechanism shown in Scheme **1.13** (bottom). The catalytic cycle starts with the formation of a dinuclear μ-peroxo species of Co^{III}, which is in equilibrium with the active Co^{III}-superoxide (a). A ligated intermediate with Co^{III}-superoxide (b) is formed when the substituted naphthol was introduced, which readily undergoes a hydrogen atom abstraction from a phenol substrate to generate a Co^{III}-hydrogen peroxide (c) meanwhile liberating a phenoxyl radical. The subsequent steps were kinetically invisible in the proposed cycle, the author suggested a rapid consecutive proton-coupled electron transfer (PCET) from the naphthol to the ligated Co^{III}-hydrogen peroxide, which released a Co^{II}-ligated napthoxyl radical intermediate (d). At this stage, the two radical species underwent a coupling reaction and afford biphenol as the product. The

chemo-selectivity observed in this reaction thus can be attributed to the distinct roles of two phenols during the HAT and PCET processes. Except for aerobic oxidative coupling reactions, Co(salen) has also been used for the aerobic oxidative polymerization of 2,3-dihydroxynaphthalene[40] and polyphenol oxidation.[41] These studies will not be discussed in this chapter.

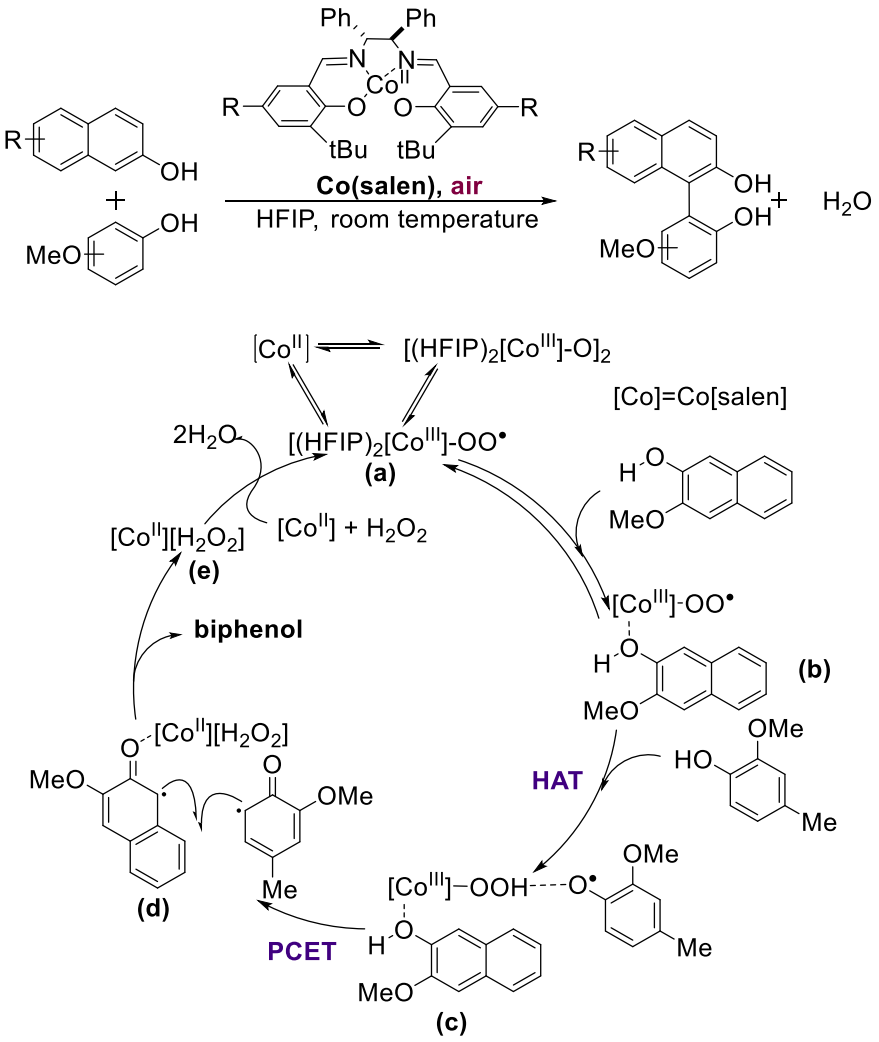

Scheme 1.13. Co(salen)-Catalyzed Aerobic Oxidative Cross-Coupling of Phenols in the Waste-Free System.

1.3. Conclusion

This chapter highlights the significance of developing transition-metal catalyzed oxidative reactions employing molecular oxygen as the stoichiometric oxidant. Two types of metalloenzyme mimic oxidation are introduced, which provide fundamental framework for a vast array of developments of the "oxygenase-type" and "oxidase-type" reactions. Advancements of three major classes of oxidative transformations mediated by Co/O_2 over the past few decades were especially addressed, the Mukaiyama oxidative cyclization, the aerobic oxidation catalyzed by Co/NHPI co-catalyst system, and a variety of powerful transformations facilitated by Co(salen)/O_2 system with and without a *p*-hydroquinone co-mediator. The ideas underlying these brilliant works have inspired the methodology developments and related mechanistic investigations in the next three chapters. A journey towards the development of cobalt-catalyzed aerobic oxidative cyclization reactions with bis-nucleophiles will be uncovered, and the key concepts mentioned in this chapter regarding O_2 carrier chemistry, hydrogen atom transfer (HAT) strategies as well as the role of redox-mediators in Co/O_2-catalyzed oxidation will be well-reflected in the following works.

Chapter 2. Cobalt-Catalyzed Aerobic Oxidative Cyclization of 2-Aminophenols with Isonitriles: 2-Aminophenol Enabled O_2 Activation by Cobalt(II)

2.1. Introduction

The recent decade has witnessed tremendous advances in homogeneous transition-metal-catalyzed aerobic oxidation reactions due to the environmentally benign nature of molecular O_2 as oxidant. As an alternative of widely explored Pd[42, 43] and Cu[44, 45] catalysts in these aerobic oxidation reactions, cobalt has received considerable attention being an earth-abundant first-row transition metal. However, in the cobalt-mediated aerobic oxidative reactions, redox-active co-mediators, such as benzoquinone (BQ)[33], N-hydroxyphthalimide (NHPI)[23, 24] and salen ligands[46, 47] are often employed to enable the activation of molecular oxygen as the terminal oxidant. There are fewer examples of cobalt-catalyzed aerobic oxidation reactions that operate efficiently in the absence of external redox-active co-mediators, despite a surge of studies in Co/O_2-mediated organic transformations.[15, 48, 49]

Achieving aerobic oxidative transformations without requiring external redox-comediators may be particularly challenging as these mediators have been shown in a recent study to prevent the accumulation of peroxide and superoxide intermediates which lead to the generation of undesired oxygenation side products. [33] Inspired by O_2 activation routes in oxidation reactions mediated by Co/BQ and Co/NHPI systems (Scheme 2.1a,b), we hypothesized the dual functionality of a substrate also acts as a hydrogen atom donor that is able to activate molecular oxygen via hydrogen atom transfer (HAT) and therefore selectively oxidize the substrate (Scheme 2.1c). We chose 2-aminophenol as a coupling partner to test our hypothesis due to its relevance to metalloenzymes. Cobalt-containing biomimetic catecholase with N,O donor Schiff-base ligands enables oxidation of a catechol derivative to its corresponding quinone with concomitant reduction of O_2 to H_2O.[50-52] Related N,O-based scaffolds such as *o*-aminophenol derivatives are also commonly explored in cobalt complexes as redox-active ligands.[53] We propose a phenoxyl radical generated in situ in the presence of cobalt catalyst and O_2, which can be trapped efficiently with the proper choice of a coupling partner. Because isonitriles are versatile chemical entities capable

of reacting as electrophiles and nucleophiles, directing this tunable reactivity with metal complexes provides a rapid entry to a vast array of pharmaceutically valuable nitrogenous molecular structures.[54-56] The coupling of 2-aminophenols with isonitriles gives rise to a variety of substituted 2-aminobenzoxazoles;[57] however, the aerobic routes to access these medicinally and biologically important structures are quite limited.[58]

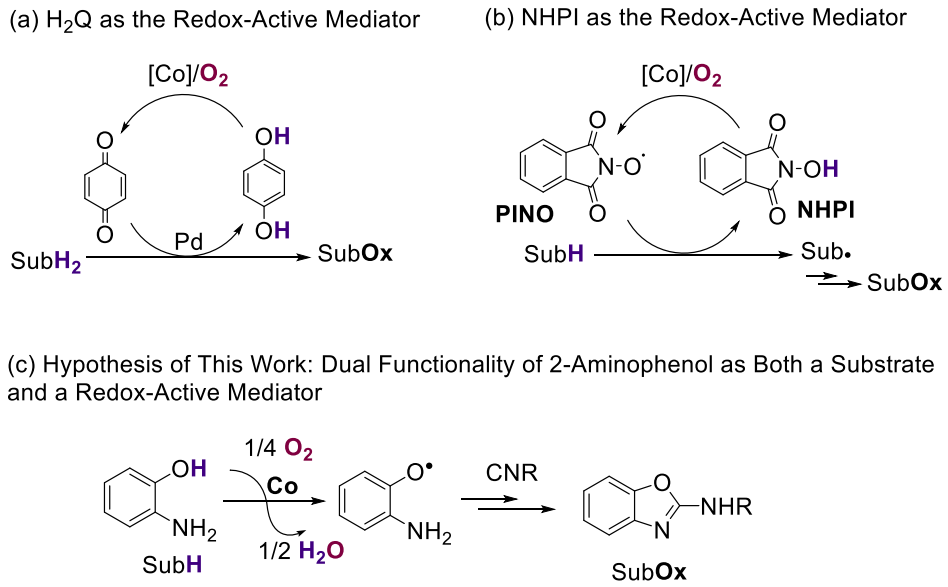

Scheme 2.1. Redox-Active Mediators in Cobalt-Mediated Aerobic Oxidative Reactions in Enabling O_2 Activation in Prior Studies and This Work. (a) Hydroquinone (H_2Q) as a Redox-Active Mediator. (b) N-Hydroxyphthalimide (NHPI) as a Redox-Active Mediator. (c) Hypothesis of This Work: The Dual Functionality of 2-Aminophenol as Both a Redox-Active Mediator and a Substrate.

2.2 Results

2.2.1. Condition Optimization for Cobalt-Catalyzed Oxidative Cyclization of 2-Aminophenol with *tert*-Butyl Isonitrile

We began our studies by evaluating the coupling reaction of 2-aminophenol (**1a**) and tert-butyl isonitrile (**2a**) using air as the supply of the terminal oxidant. In our early studies, air efficiently promoted the oxidative cyclization of these two coupling partners in THF solvent. Of

all Co(II) catalysts being examined, $Co(OAc)_2$ gave the highest yield of the substituted 2-aminobenzoxazole product **3a**. When the solvent is switched to CH_3CN, **3a** was achieved in 93% yield. Shorter reaction times led to slightly reduced yields (entry 12 and 13). A variety of bases were also screened in condition optimization. Though in some cases they afforded the target benzoxazole in high yields they were proved to be a non-necessary component for this reaction (See Table 2.5 in the experimental section). The final optimized reaction conditions featured a simple but efficient combination of $Co(OAc)_2$ as the catalyst, CH_3CN as the solvent, and an air balloon as the source of terminal oxidant. The reaction was carried out at 65 °C for 24 hours. Control experiments were conducted in the absence of either air or Co(II) (Entry 14 and 15), which afforded the desired product with 0% and 14% yields respectively, indicating the importance of both molecular oxygen and the Co(II) source in this oxidative cyclization transformation.

Table 2.1. Optimization of Reaction Conditions[a]

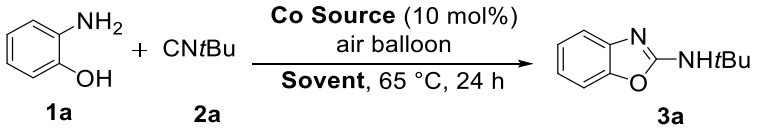

Entry	Co Source	Solvent	Time (h)	% Yield[b]
1	$Co(acac)_2$	THF	24	58[c]
2	$Co(acac)_2 \cdot H_2O$	THF	24	67[c]
3	$CoCO_3$	THF	24	51
4	$CoCO_3 \cdot H_2O$	THF	24	Trace
5	$CoCl_2$	THF	24	46
6	$Co(OAc)_2$	THF	24	86
7	$Co(OAc)_2$	1,4-dioxane	24	89
8	$Co(OAc)_2$	2-Me-THF	24	54
9	$Co(OAc)_2$	DMF	24	86
10	$Co(OAc)_2$	DMSO	24	78
11	**$Co(OAc)_2$**	**CH_3CN**	**24**	**93(90)[c]**
12	$Co(OAc)_2$	CH_3CN	12	85
13	$Co(OAc)_2$	CH_3CN	6	79
14	-	CH_3CN	24	0

15[d]	$Co(OAc)_2$	CH_3CN	24	14

[a]Reaction Conditions: **1a** (0.3 mmol), **2a** (0.3 mmol), cobalt(II) catalysts (10 mol%), solvent (3 mL), at 65 °C with an air balloon for 24 h. [b]The yield of **3a** was determined by ^{1}H NMR spectroscopy with dimethylsulfone as internal standard (0.03 mmol). [c]Isolated yield. [d]The reaction was conducted under N_2.

2.2.2 Substrate Scope of Substituted 2-Aminophenols and Isonitriles

With optimized reaction condition in hand, we next explored the scope of substituted 2-aminophenol coupling partners (**1**, Table 2.2). This protocol showed good tolerance of a variety of functional groups including both electron-rich (**3d**, **3e**, **3h**, and **3i**) and electron-deficient substituents (**3f**, **3g**, and **3k**). The influence of a methyl group in each of the four aromatic positions (**3b**, **3d**, **3i**, and **3l**) reveals only a small steric effect, as the yield of **3b** bearing the 3-methyl group showed a slightly decreased yield. The 4-, 5-, and 6-methyl aminophenols all resulted in high yields of the corresponding 2-aminobenzoxazoles. Similarly, the large phenyl and *tert*-butyl groups afforded the desired cyclized products in good yields (**3c** and **3h**). Finally, the di-substituted electron-deficient 5-nitro-4-chloro-2-aminophenol **1m** afforded the desired benzoxazole product in 64% yield.

Table 2.2. Scope of Substituted 2-Aminophenols[a]

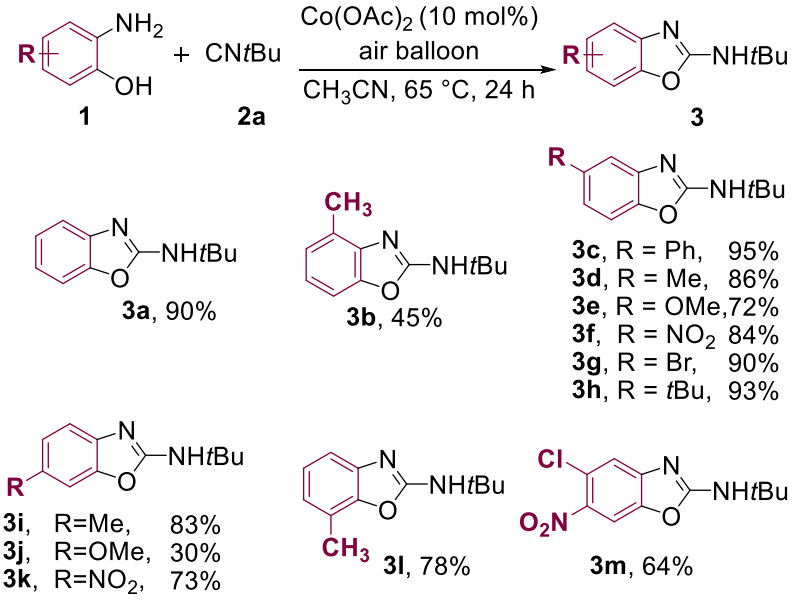

[a]Isolated Yields. Reaction conditions: **1** (0.3 mmol), **2a** (0.3 mmol), and $Co(OAc)_2$ (10 mol%) in 3 mL CH_3CN at 65 °C with an air balloon for 24 h.

To further evaluate the performance of this cyclization reaction, we investigated the scope of isonitriles (**2**, Table 2.3). While tert-butylisonitrile is the most commonly employed isonitrile in related coupling protocols,[54, 59] other bulky aliphatic isonitriles are also excellent coupling partners under our reaction conditions furnishing the corresponding products in high yields (**3n**, **3o** and **3p**). Surprisingly, the isopropyl- and cyclohexyl-substituted isonitriles also generated high yields of the corresponding 2-aminobenzoxazole products (**3p** and **3q**). These products are expected to contain weak C-H bonds (BDE = ~86 kcal mol^{-1})[60] and are plausible substrates for further oxidation. The benzylic isonitrile **2u**, however, did not undergo efficient coupling and instead resulted in only a moderate yield of the coupling product (**3u**, 32%). Also observed was the 3-aminobenzoxazine byproduct (16% yield) which results from insertion of 2 equivalents of isontrile.[61] Surprisingly, no oxygenation byproducts were observed in this reaction, despite the weak C-H bond (~72 kcal·mol^{-1})[62] and the precedent for Co/O_2 enabled benzylic oxygenation.[63] Finally, aryl isonitriles also underwent coupling to yield the corresponding 2-aminobenzoxazole products, with the bulkier aromatic ring of **1t** resulting in the highest product yield.

Table 2.3. Scope of Substituted Isonitriles[a]

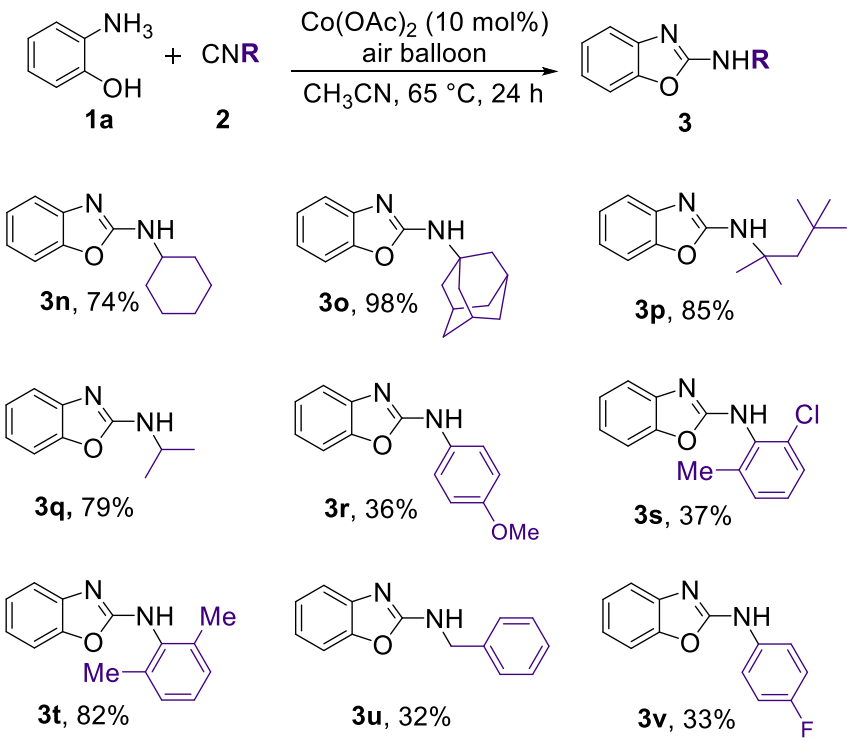

[a]Isolated Yields. Reaction conditions: **1a** (0.3 mmol), **2** (0.3 mmol), and $Co(OAc)_2$ (10 mol%) in 3 mL MeCN at 65 °C with an air balloon for 24 h.

Although a wide variety of functional groups on the 2-aminophenol and isonitrile coupling partners are well tolerated, we observed challenging substrates through our study for which products could not be generated cleanly under the reported reaction conditions (Chart 2.1). This protocol didn't work efficiently for 2-aminophenol substrates bearing a halide in the 5-position. 5-bromo-2-aminophenol and 5-fluoro-2-aminophenol consistently gave the substituted 2-aminobenzoxazole isomers with 5:1 ratio. *p*-Toluenesulfonylmethyl isocyanide underwent competitive oxidation reactions in the presence of O_2 probably due to the liable C-H bond in combination with the active sulfonyl group, and multiple products were generated. This protocol was also not compatible with isonitriles bearing fused-ring systems. Both 1*H*-indol-5-yl isocyanide and protected indol-5-yl isocyanide went through multiple reaction pathways. Similar challenges were observed when 2-naphthyl isocyanide was subjected to the standard reaction system which resulted in multiple unrecognizable products.

Chart 2.1. Products That Were Not Generated Cleanly Under the Reported Conditions

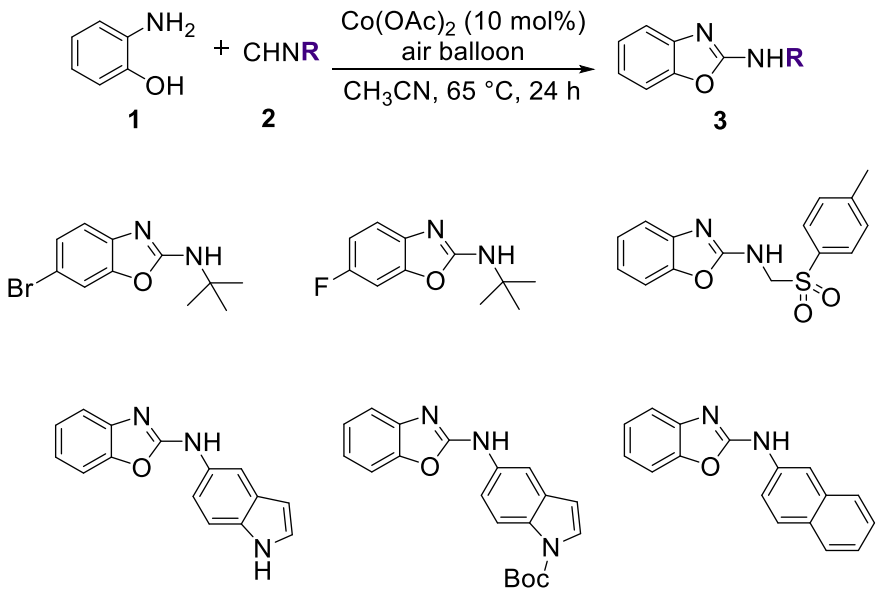

Reaction conditions: **1** (0.3 mmol), **2a** (0.3 mmol), and $Co(OAc)_2$ (10 mol%) in 3 mL CH_3CN at 65 °C with an air balloon for 24 h.

2.2.3 Preliminary Mechanistic Investigations

2.2.3.1. Testing the Presence of Trappable Radical Intermediates

The efficient coupling of isonitriles bearing weak C-H bonds suggested that a free-radical intermediate is unlikely. To test our hypothesis, we sought to trap the free-radical intermediates by a careful selection of radical scavengers. The three commonly used radical scavenger (2,2,6,6-tetramethylpiperidin-1-yl)oxyl (TEMPO), 9,10-dihydroanthracene and 1,1-diphenylethylene showed no evidence of trappable intermediates. Instead, high yields of **3a** were still observed when these reagents were included under the standard reaction conditions (Scheme 2.2a),[64] which were consistent with our hypothesis. When the same reactions are conducted in the absence of isonitrile, oxidative dimerization of 2-aminophenol occurs to form 2-aminophenoxazine-3-one both in the presence and absence of TEMPO (43% and 10% yields, respectively) (Scheme 2.2b),[65] consistent with the presence of aminophenol radicals.[52, 66, 67] The elevated yield in the presence of TEMPO could be a result of a TEMPO-mediated H-atom abstraction pathway to form the aminophenol radical,[68] where TEMPO was acting as a radical initiator rather than a radical-trapping agent.

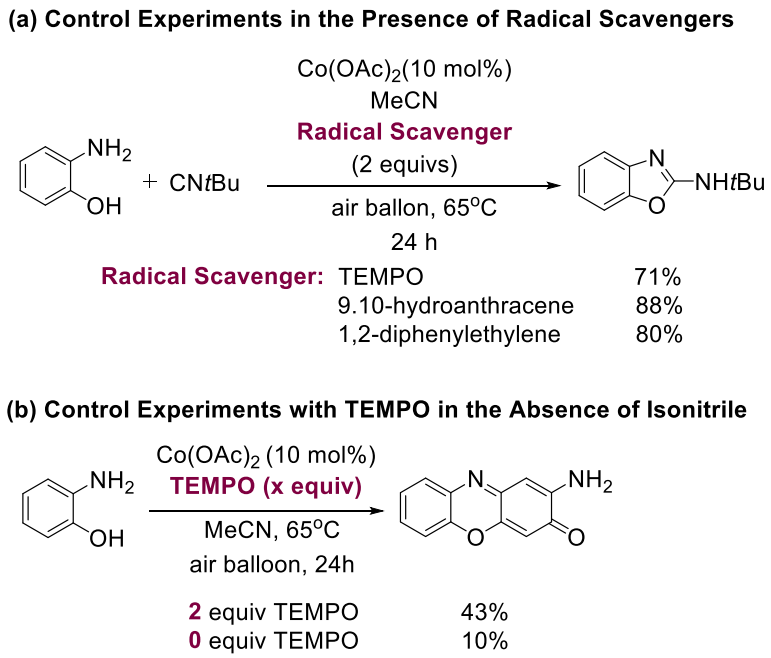

Scheme 2.2. Aerobic Oxidative Cyclization Conducted in the Presence of Radical Trapping Reagents.

2.2.3.2. The Importance of O_2 in Oxidative Cyclization and a Plausible Path for O_2 Activation

We attribute the absence of a trappable intermediate to the possibility of a stabilized ligand radical intermediate. A large series of Co^{II} complexes of aminophenol-, aminothiophenol- and phenylenediamine-derived ligands have been characterized.[53, 55, 69-72] Wieghardt and coworkers have shown aerobic oxidation of these species would form stabilized iminobenzosemiquinonato-type species bearing π-radical ligands (AP^{SQ}).[70] In all of above mentioned cases highly-substituted aminophenols are employed to avoid ligand dimerization and at the same time enable the formation of stable oxidized complexes for isolation purpose. In our case, we believe a similar stabilized ligand radical maybe formed under our reaction conditions from Co^{II} catalyst, O_2 and 2-aminophenol. When isonitrile (CNR) is present, it is a sufficient trap for aminophenol radical while in the absence of isonitrile, dimerization of 2-aminophenol occured and gave rise to 2-aminophenoxazinone.

Then we conducted a series of control experiments in the absence of O_2 to evaluate if O_2 is required for the formation of cyclized benzoxazole products or simply it is responsible for the regeneration of Co^{II} after the product formation (Scheme 2.3). When the standard reaction is conducted with stoichiometric amount of $Co(OAc)_2$ under inert atmosphere, only 10% of product **3a** is obtained, suggesting the need for molecular oxygen to efficiently form the cyclized product. The same reaction was conducted with stoichiometric amount of Co^{III} salt, $Co(acac)_3$ under N_2 atmosphere to test if Co^{III} species an active intermediate for this transformation. This time the cyclized product was formed in 63% yield. The reduced yield obtained with $Co(acac)_3$ related to the standard catalytic conditions was attributed to the slow exchange of the acac ligand. To make a parallel comparison, we set up a control experiment with Co^{II} salt but the same acac ligand. Consistent with our hypothesis, when the standard reaction was conducted with catalytic amount of $Co(acac)_2$ under aerobic atmosphere, 58% of **3a** was obtained. These data combined suggested that O_2 is responsible for the oxidation of Co^{II} to generate an active Co^{III} intermediate or a $Co^{II}AP^{SQ}$ species with oxidized semiquinonato ligands.

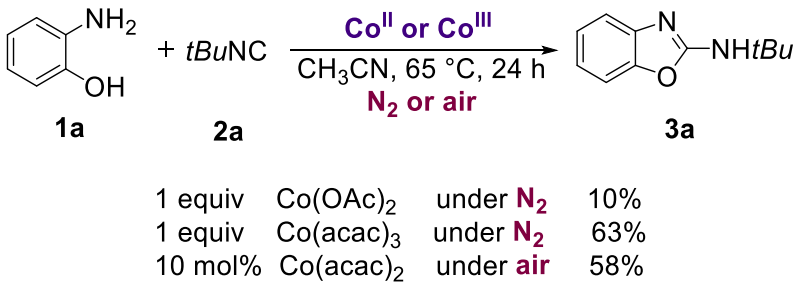

Scheme 2.3. Oxidative Cyclization of 2-Aminophenol and *tert*-Butyl Isonitrile Mediated by Cobalt Under N_2.

Given the importance of oxidation for product formation, we sought to better understand the aerobic oxidation step of this transformation. The oxidation of Co^{II} by molecular oxygen is usually proposed to generate a Co^{III}-superoxide intermediate as demonstrated in a recent study by Stahl, Hammes-Schiffer, and cowokers.[33] In this study, molecular oxygen is activated by a salophen-ligated Co^{II} complex to form a Co^{III}-superoxide intermediate. This superoxide species is responsible for H-atom transfer (HAT) from *p*-hydroquinone to generate a Co^{III}-hydroperoxide intermediate. A second HAT sequence then followed to produce *p*-quinone with concomitant release of H_2O_2 and regeneration of Co^{II}(salophen). Under these reaction conditions, H_2O_2 underwent disproportionation to form H_2O and O_2 (Scheme 2.4a). Comparatively, the re-oxidation of N-hydroxyphthalimide (NHPI) was proposed to go through an analogous HAT sequence.[73] Thus we imagined that a resembling Co^{III}-superoxide species may be responsible for HAT from 2-aminophenol under our oxidative cyclization conditions (Scheme 2.4b). We proposed the molecular oxygen activation by a Co^{II} complex with coordination of two equivalents of 2-aminophenol ligands, which leads to the formation of the corresponding Co^{III}-superoxide as suggested above. H_2O_2 is released after two stepwise HAT sequences from 2-aminophenol ligands to peroxide, giving rise to the active $Co^{II}AP^{SQ}$ intermediate with two oxidized semiquinonato ligands. Consequently, cyclized benzoxazole product is expected in the presence of isonitrile under the aerobic oxidative reaction condition.

Scheme 2.4. (a) Proposed Pathway for Co-Catalyzed Aerobic Oxidation of Catechol in Literature and (b) Proposed Pathway for Aerobic 2-Aminophenol Oxidation in This Work.

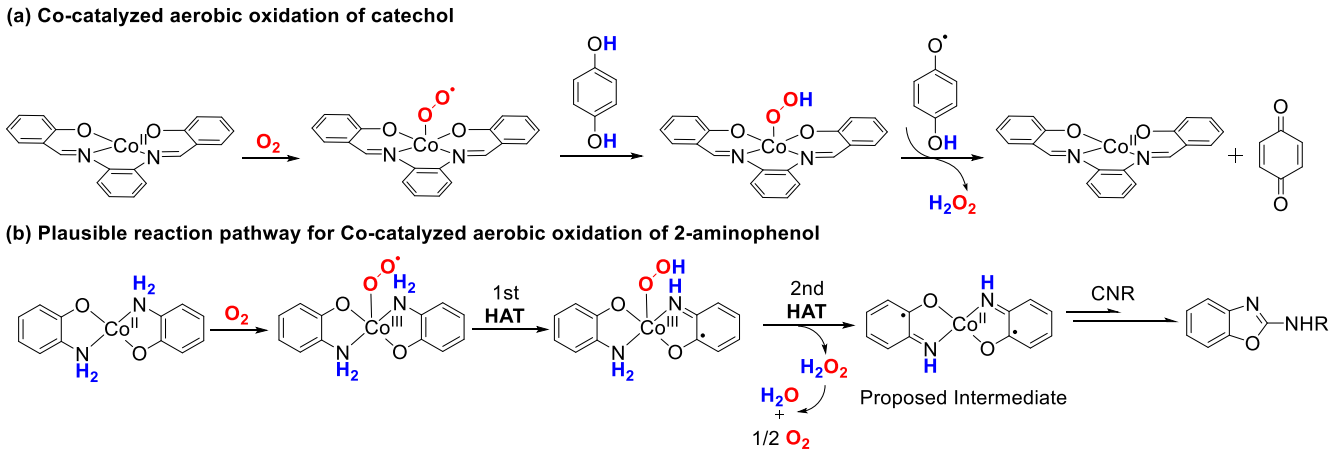

2.2.3.3 Probing the Reaction Mechanism Through UV-Visible Studies

We conducted a series of UV-visible experiments to probe the oxidation step and particularly the ligand environment that enables aerobic oxidation. Three parallel experiments were set up with identical concentration of $Co(acac)_2$ in acetonitrile to investigate potential combination of reaction components that allows the activation of molecular oxygen. Due to the limited solubility of $Co(OAc)_2$ in CH_3CN, $Co(acac)_2$ was employed for these studies which also showed catalytic competency in previous condition optimization. When $Co(acac)_2$ was exposed to air for 24 hours no changes in the absorption spectrum were observed (Figure 2.1a and Figure 2.5 in the Experimental section). Similarly, a mixture of 1:2 equivalents of $Co(acac)_2$ and CN*t*Bu in CH_3CN showed no significant changes in the spectroscopic features after exposure to air (Figure 2.1a and Figure 2.6 in the Experimental section). The mixture of $Co(acac)_2$/CN*t*Bu showed identical maximum absorption with $Co(acac)_2$ in CH_3CN because the absorption of CN*t*Bu can only be detected in the vacuum UV region (λ_{max}~140 nm). In contrast, when a solution of 1:2 ratio of $Co(acac)_2$ and 2-aminophenol was exposed to air a rapid color change was observed from light pink to orange-brown within minutes. This rapid color change was accompanied by an increase in the absorption around 260 nm (Figure 2.1b and Figure 2.7 in the Experimental section). This set

of preliminary data suggested the activation of molecular oxygen only happen in an environment with 2-aminophenol coordination.

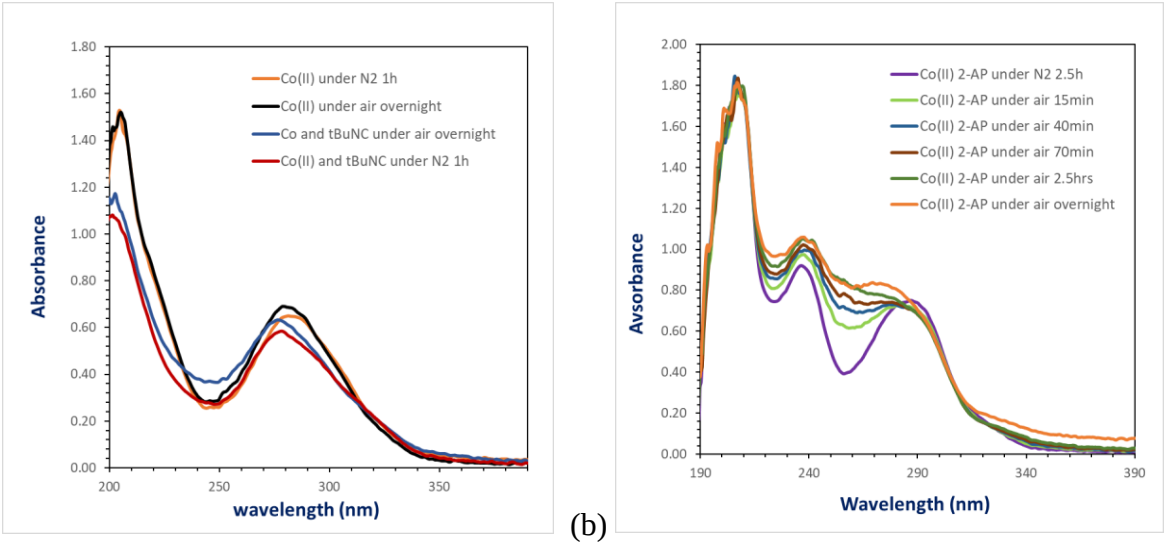

Figure 2.1. (a) Absorption spectrum of $Co(acac)_2$ only and $Co(acac)_2$ with CN*t*Bu in CH_3CN under N_2 and after exposed to air overnight. (b) Absorption spectrum of $Co(acac)_2$ and 2-aminophenol under N_2 and after exposed to air overnight. These experiments were conducted at 5.05×10^{-5}M concentration in CH_3CN.

Based on the above observations, we ruled out the possibility of efficient O_2 activation mediated by Co^{II} only or Co^{II}/CN*t*Bu. We next investigated if the prolonged exposure of Co^{II} and 2-aminophenol mixture under air led to the formation of a Co^{III} intermediate. To test our hypothesis, another set of parallel control experiments were conducted. If the absorption maxima of Co^{II}/2-aminphenol mixture are analogous to those of Co^{III}/2-aminophenol mixture in the presence of O_2, a Co^{III} intermediate may exist in our related catalytic system. In the first experiment, the spectrum of the mixture of 1:3 ratio of $Co(acac)_2$ and 2-aminophenol was taken under anaerobic atmosphere, no spectroscopic changes were observed with extended period of time. When the same solution was exposed to air, we observed a trend of color change comparable to 1:2 ratio mixture and a band around 260 nm on the absorption spectrum was appeared (Figure 2.2). This spectroscopic feature is similar to that observed when $Co(acac)_3$ is combined with 2-aminophenol (λ_{max}= 233 nm, Figure 2.2, Figure 2.8 and Figure 2.9 in the Experimental section). In a related Co system bearing catechol ligands, the semiquinonato species can be obtained when Co^{III} starting materials are treated with catechol.[74, 75] A related redox-equilibrium to access $Co^{II}(AP^{SQ})$ from Co^{III} may be

operative in these aminophenol systems. The absorption band around 410~430 nm of final trace spectrum of $Co(acac)_3$ and 2-aminphenol mixture demonstrated the presence of 2-aminophenoxazine-3-one, the dimerized product of 2-aminophenol under aerobic condition we had observed in the previous control experiment (Scheme 2.2b). This again might be attributed to the slow exchange of the acac ligand and the rate of aminophenol oxidation exceeded the rate of ligand exchange. Overall, these spectroscopic changes suggest aerobic oxidation of Co^{II} is facilitated by the presence of 2-aminophenol.

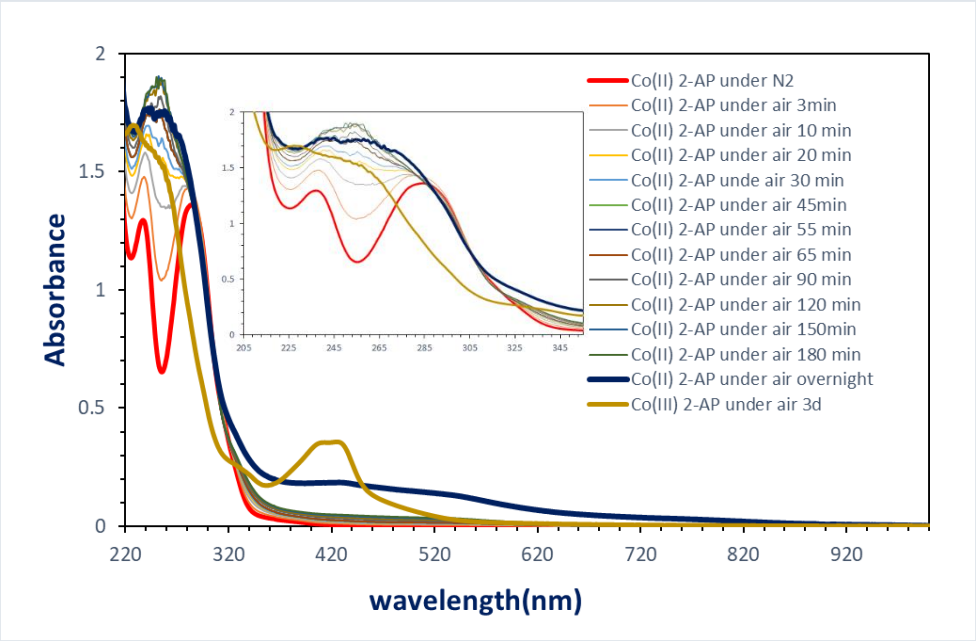

Figure 2.2. Absorption spectrum of $Co(acac)_2$ with 2-aminophenol in CH_3CN under N_2 and after exposed to air overnight stacked with the final trace spectrum of $Co(acac)_3$ with 2-aminophenol under air exposure. These experiments were conducted at 5.05×10^{-5} M concentration in CH_3CN**.**

2.2.3.4. Other Considerations

In related Pd-catalyzed cyclization reactions of aminophenols with isonitriles, the C−N bond-forming step is proposed to proceed via the migratory insertion of the CNR ligand.[61] Based on our spectroscopic studies and related literature precedence, we have proposed a plausible intermediate resulting from the O_2 activation upon the coordination of 2-aminophenol to cobalt center. Although our work here has focused on the step of aerobic oxidation of Co^{II}, we consider the subsequent coupling of the oxidized intermediate with isonitrile may also interest some researchers. Though the investigation of this particular step is not our primary intention, we expect

a radical-based addition to CNR may be operative given the presence of the proposed semiquinoate radical intermediates; [54, 59]however, future endeavors are required to gain a deeper insight into this step of interest.

2.3. Conclusive Summary

In summary, we have developed a convenient and atom efficient route towards the synthesis of 2-aminobenxazoles utilizing an additive free cobalt catalyst system under aerobic conditions. A broad scope of substituted 2-aminophenols and isonitriles are well tolerated. Finally, the importance of 2-aminophenol acting as a ligand to facilitate the aerobic oxidation of Co^{II} was confirmed with a series of UV-visible studies. Future work is directed toward the isolation and characterization of the relevant aminophenol ligated cobalt intermediates.

2.4. Experimental Section

2.4.1. General Considerations

All synthetic reactions were performed on the benchtop unless otherwise noted. All proteo solvents were taken from a Glass Contours solvent system, in which the solvent is passed through a column of activated alumina with a pressure of Argon. All other commercial reagents and NMR solvents were used without further purification unless otherwise stated.

^{1}H and $^{13}C\{^{1}H\}$ NMR spectra were recorded on an Agilent 400 MHz spectrometer, JEOL 400 MHz spectrometer, or a Varian INOVA 600 MHz spectrometer at room temperature, unless otherwise noted. Chemical shifts (δ) are given in parts per million and referenced to the residual solvent signal[76] and all coupling constants (*J*) are reported in Hz. IR spectra were recorded on a Perkin Elmer (Spectrum 100) FT-IR spectrometer. UV-visible spectra were recorded on a Stellar Net Inc. Black Comet Concave Grating Spectrometer with a SL5 Deuterium/Halogen combination lamp and dip probe or Shimadzu UV 1800. High resolution mass spectra were obtained on a Thermofisher Scientific Q Exactive Mass Spectrometer.

2.4.2 Procedure for Screening of the Reaction Conditions

2-Aminophenol (32.7 mg, 0.300 mmol) and cobalt (II) acetate (5.31 mg, 0.0300 mmol) were combined in a 6-inch test tube in a N_2 filled glovebox, and CH_3CN (3.00 mL) and *tert*-butylisonitrile (35.2 μL, 0.300 mmol) were added. The test tube was then sealed with a septum, removed the glovebox, and fitted with an air balloon attached to a needle inserted through the septum. The reaction mixture was then stirred at 65 °C for 24 h. Upon completion, the mixture was cooled to room temperature and filtered through a Pasteur pipette silica gel plug. Ethyl acetate (15 mL) was then passed through the plug and the resulting filtrate was concentrated by rotary evaporation to yield a solid. Dimethylsulfone (3.00 mg, 0.0318 mmol), used as a ^{1}H NMR standard, was added to the solid residue and the crude mixture was dissolved in $CDCl_3$ for ^{1}H NMR analysis. All of the optimization reactions in **Tables 2.4**, **2.5**, and **2.6** were conducted following the standard procedure except for those employing $Co(acac)_2$ or $Co(acac)_2{\cdot}H_2O$. In these cases, the percent yield of the product was determined by column purification (gradient elution from pure hexane to ethyl acetate: hexanes = 1:3) due to the difficulties in removing cobalt from the crude mixture.

Table 2.4. Optimization of the reaction temperature and base in the oxidative cyclization of 2-aminophenol and *tert*-butylisonitrile. [a]

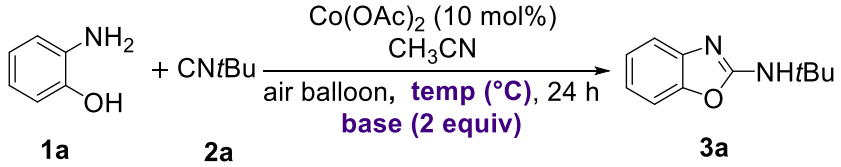

Entry	Base	Temp (°C)	% Yield[b]
1	NaOAc	65	98
2	NaOAc	80	98
3	Na_2CO_3	65	78
4	Na_2CO_3	80	>99
5	-	65	93
6	-	80	91

[a]Reaction conditions: **1a** (0.300 mmol), **2a** (0.300 mmol), $Co(OAc)_2$ (0.0300 mmol), and base (0.0600 mmol) in CH_3CN (3.00 mL) with an air balloon at 65 °C for 24 h. [b]The yield of **3a** was determined by ^{1}H NMR spectroscopy with dimethylsulfone as internal standard (0.03 mmol).

Table 2.5. Optimization of the base in the oxidative cyclization of 2-aminophenol and *tert*-butylisonitrile.[a]

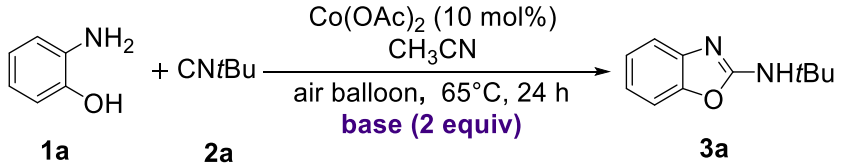

Entry	Base	% Yield[b]
1	Na_2CO_3	78
2	NaOAc	98
3	LiOAc	84
4	Li_2CO_3	87
5	KOAc	82
6	K_2CO_3	31
7	None	86

[a]Reaction conditions: **1a** (0.300 mmol), **2a** (0.300 mmol), $Co(OAc)_2$ (0.0300 mmol), and base (0.0600 mmol) in CH_3CN (3.00 mL) with an air balloon at 65 °C for 24 h. [b]The yield of **3a** was determined by ^{1}H NMR spectroscopy with dimethylsulfone as internal standard (0.03 mmol).

Base was not incorporated in the final catalytic system because base-free reactions gave comparable yields, while enabling a more straight-forward and reliable workup procedure.

Table 2.6. Optimization of the catalyst loading and reaction time in the oxidative cyclization of 2-aminophenol and *tert*-butylisonitrile.[a]

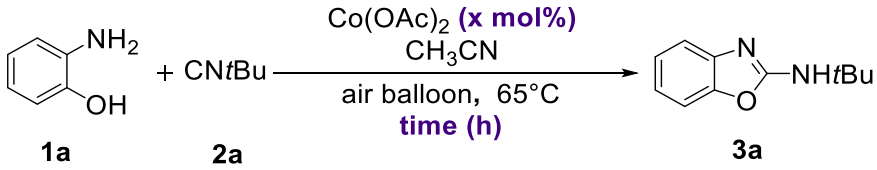

Entry	Co loading (mol%)	Time (h)	% Yield[b]
1	10	6	79
2	10	12	85
3	10	24	93
4	5	24	78

[a]Reaction conditions: **1a** (0.300 mmol), **2a** (0.300 mmol) and $Co(OAc)_2$ (0.0300 mmol) in CH_3CN (3.00 mL) with an air balloon at 65 °C for 24 h. [b]The yield of **3a** was determined by ^{1}H NMR spectroscopy with dimethylsulfone as internal standard (0.03 mmol).

2.4.3. Synthesis and Characterization of the 2-Aminobenzoxazoles

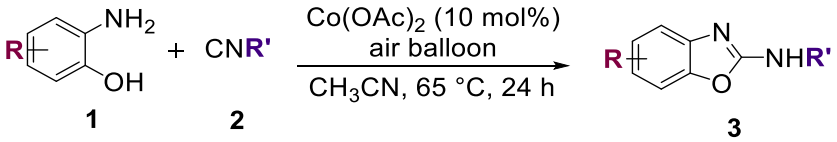

<u>Representative procedure for the synthesis of 2-aminobenzoxazoles</u>

2-(*tert*-butylamino) benzoxazole (3a). 2-aminophenol (32.7 mg, 0.300 mmol) and cobalt(II) acetate (5.31 mg, 0.0300 mmol) were combined in a 6-inch test tube inside a N_2 filled glovebox, and dissolved in dry CH_3CN (3 mL). *tert*-Butyl isocyanide (35.2 μL, 0.300 mmol) was added to the same test tube before it was sealed with a septum and removed from the glovebox. The reaction mixture was then stirred in an oil bath at 65 °C for 24 hours with an air balloon attached to a syringe with a needle inserted through the septum. Upon completion, the reaction mixture was cooled to room temperature and filtered through a Pasteur pipette silica gel plug and washed with ethyl acetate (~15 mL). The resulting filtrate was concentrated by rotary evaporation and the resulting solid was purified by silica column flash chromatography (gradient elution from the pure hexanes to 25% ethyl acetate in hexanes, R_f = 0.5 in 3:1 hexanes : ethyl acetate), to give the title compound as a brown solid in 90 % yield (51.3 mg, 0.270 mmol). All 2-aminobenzoxazoles were prepared according the standard procedure unless otherwise noted.

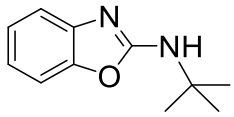

3a

2-(*tert*-butylamino) benzoxazole (3a). The title compound was synthesized according to the standard procedure and purified by silica column chromatography (25% ethyl acetate in hexane, R_f = 0.5 in 3:1 hexanes : ethyl acetate) to yield 51.25 mg (0.27 mmol, 90%) of the title product as a brown solid. ^{1}H NMR (400 MHz, $CDCl_3$) δ = 7.37 (dd, 1H), 7.25 (dd, 1H), 7.16 (td, *J* = 7.7, 1.1 Hz, 1H), 7.02 (td, *J* = 7.8, 1.1 Hz, 1H), 5.75 (s, 1H), 1.51 (s, 9H). ^{13}C NMR (100 MHz, $CDCl_3$): δ = 161.43, 148.25, 143.04, 123.75, 120.47, 116.12, 108.62, 52.09, 29.37. The spectral data are consistent with those reported in the literature. [77, 78]

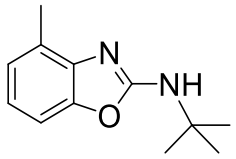

3b

4-methyl-2-(*tert*-butylamino)benzoxazole (3b). The title compound was synthesized according to the standard procedure and purified by silica column chromatography (25% ethyl acetate in hexane, R_f = 0.7 in 3:1 hexanes : ethyl acetate) to yield 27.5 mg (0.13 mmol, 45%) of the title compound as a yellow solid. ^{1}H NMR (400 MHz, $CDCl_3$) ^{1}H NMR (400 MHz, $CDCl_3$) δ 7.10 (dd, *J* = 7.7, 0.6 Hz, 1H), 6.95 (ddd, *J* = 24.5, 8.2, 4.1 Hz, 2H), 4.94 (s, 1H), 2.48 (s, 3H), 1.49 (s, 9H). ^{13}C-NMR (100 MHz, $CDCl_3$): δ = 160.60, 147.97, 141.58, 126.49, 124.61, 120.32, 106.14, 52.20, 29.36, 16.37. HRMS (ESI-MS, m/z) $[M+H]^+$ calcd for $C_{12}H_{16}N_2O$ 205.1263; found 205.1336. The spectral data are consistent with those reported in the literature.[58]

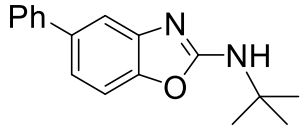

3c

5-phenyl-2-(*tert*-butylamino)benzoxazole. (**3c**) The title compound was synthesized according to the standard procedure and purified by silica column chromatography (20% ethyl acetate in hexane, R_f = 0.3 in 3:1 hexanes: ethyl acetate) to yield 75.9 mg (0.28 mmol, 95%) of the title compound as an off-white solid (m.p. 129-131 °C). ^{1}H NMR (400 MHz, $CDCl_3$): δ = 7.61 (d, *J* = 7.7 Hz, 3H), 7.44 (t, *J* = 7.6 Hz, 2H), 7.29 (dt, *J* = 18.5, 8.0 Hz, 3H), 5.63 (s, 1H), 1.52 (s, 9H). ^{13}C NMR (400 MHz, $CDCl_3$): δ = 161.56, 147.90, 143.88, 141.84, 137.60, 128.80, 127.40, 126.92, 120.04, 115.08, 108.58, 52.21, 29.35. HRMS (ESI-MS, m/z) $[M+H]^+$ calcd for $C_{17}H_{18}N_2O$ 267.1419; found 267.1492. The spectral data are consistent with those reported in the literature.[79]

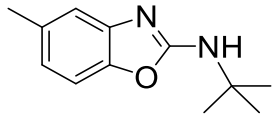

3d

5-methyl-2-(*tert*-butylamino)benzoxazole (3d). The title compound was synthesized according to the standard procedure and purified by silica column chromatography (25% ethyl acetate in hexane, R_f = 0.6 in 3:1 hexanes : ethyl acetate) to yield 52.7 mg (0.26 mmol, 86%) of the title

compound as a yellow solid. ^{1}H NMR (400 MHz, $CDCl_3$): δ = 7.18 (d, *J* = 0.6 Hz, 1H), 7.11 (d, *J* = 8.1 Hz, 1H), 6.84 – 6.79 (m, 1H), 5.24 (s, 1H), 2.39 (s, 3H), 1.49 (s, 9H). ^{13}C NMR (100 MHz, $CDCl_3$): δ = 161.20, 146.42, 143.37, 133.43, 121.32, 116.86, 108.00, 52.12, 29.36, 21.62. HRMS (ESI-MS, m/z) $[M+H]^+$ calcd for $C_{12}H_{16}N_2O$ 205.1263; found 205.1337. The spectral data are consistent with those reported in the literature.[61]

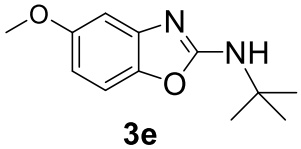

3e

-methoxy-2-(*tert*-butylamino)benzoxazole (3e). The title compound was synthesized according to the standard procedure and purified by silica column chromatography (gradient elution from pure hexanes to hexanes : ethyl acetate = 3:1, R_f = 0.4 in 3:1 hexanes : ethyl acetate) to yield 58.0 mg (0.263 mmol, 74%) of the title compound as a brown solid (m.p.= 111-113 °C) . ^{1}H NMR (400 MHz, $CDCl_3$): δ = 7.10 (d, *J* = 8.7 Hz, 1H), 6.94 (d, *J* = 2.4 Hz, 1H), 6.57 (dd, *J* = 8.6, 2.5 Hz, 1H), 5.32 (s, 1H), 3.80 (s, 3H), 1.48 (s, 9H). ^{13}C NMR (100 MHz, $CDCl_3$): δ = 161.82, 156.95, 144.21, 142.77, 108.45, 107.20, 101.56, 56.02, 52.12, 29.33. HRMS (ESI-MS, m/z) $[M+H]^+$ calcd for $C_{12}H_{16}N_2O_2$ 221.1212; found 221.1249. The spectral data are consistent with those reported in the literature.[61]

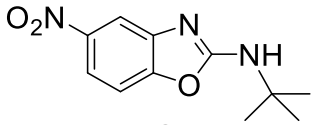

3f

5-nitro-2-(*tert*-butylamino)benzoxazole (3f). The title compound was synthesized according to the standard procedure and purified by silica column chromatography (gradient elution from pure hexanes to 3:1 hexanes: ethyl acetate, R_f = 0.55 in 3:1 hexanes: ethyl acetate) to yield 56.5 mg (0.240 mmol, 80 %) of the title compound as a yellow solid. ^{1}H NMR (400 MHz, $CDCl_3$): δ = 8.17 (d, *J* = 2.2 Hz, 1H), 7.97 (dd, *J* = 8.7, 2.3 Hz, 1H), 7.25 (d, *J* = 8.8 Hz, 1H), 5.36 (s, 1H), 1.50 (s, 9H). ^{13}C NMR (100 MHz, $CDCl_3$): δ = 162.57, 152.26, 145.02, 144.26, 117.31, 111.86, 108.23, 52.76, 29.08. HRMS (ESI-MS, m/z) $[M+H]^+$ calcd for $C_{11}H_{13}N_3O_3$ 236.0957; found 236.1030. The spectral data are consistent with those reported in the literature.[58]

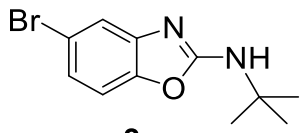

3g

5-bromo-2-(*tert*-butylamino)benzoxazole (3g). The title compound was synthesized according to the standard procedure and purified by silica column chromatography (20% ethyl acetate in hexane, R_f = 0.7 in 3:1 hexanes: ethyl acetate) to yield 72.6 mg (0.27 mmol, 90%) of the title compound as a yellow solid (mp = 102-104 °C). ^{1}H NMR (400 MHz, $CDCl_3$) δ = 7.46 (s, 1H), 7.16 – 7.03 (m, 2H), 5.57 (s, 1H), 1.49 (s, 9H). ^{13}C NMR (100 MHz, $CDCl_3$): δ = 162.50, 147.87, 145.43, 123.30, 119.46, 116.41, 109.72, 52.42, 29.34. IR (ATR, cm^{-1}): 162.50, 147.87, 145.43, 123.30, 119.46, 116.41, 109.72, 52.42, 29.34. HRMS (ESI-MS, m/z) $[M+H]^+$ calcd for $C_{11}H_{13}BrN_2O$ 269.0211; found 269.0287. The spectral data are consistent with those reported in the literature.[61]

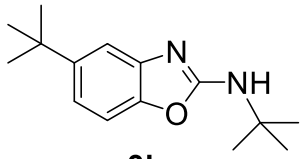

3h

5-tert-butyl-2-(tert-butylamino)benzoxazole (3h). The title compound was synthesized according to the standard procedure and purified by silica column chromatography (20% ethyl acetate in hexane, R_f = 0.7 in 3:1 hexanes: ethyl acetate) to yield 69.0 mg (0.28 mol, 93%) of the title compound as a pink solid (mp =121-123 °C). ^{1}H NMR (400 MHz, $CDCl_3$) δ = 7.44 (d, *J* = 1.6 Hz, 1H), 7.13 (d, *J* = 8.4 Hz, 1H), 7.04 (dd, *J* = 8.4, 1.9 Hz, 1H), 5.07 (s, 1H), 1.48 (s, 9H), 1.33 (s, 9H). ^{13}C NMR (150 MHz, $CDCl_3$): δ = 161.09, 147.18, 146.0, 143.05, 117.87, 113.57, 107.69, 52.04, 34.90, 31.94, 29.26. IR (ATR, cm^{-1}): 3248 (w), 2964 (m), 1640 (s), 1582 (s), 1428 (m), 1480 (m), 1216 (s), 912 (w), 801 (m), 653 (m). HRMS (ESI-MS, m/z) $[M+H]^+$ calcd for $C_{15}H_{22}N_2O$ 247.1732; found 247.1805.

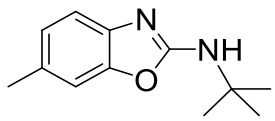

3i

6-methyl-2-(*tert*-butylamino)benzoxazole (3i). The title compound was synthesized according to the standard procedure and purified by silica column chromatography (25% ethyl acetate in hexane, R_f = 0.7 in 3:1 hexanes : ethyl acetate) to yield 51.0 mg (0.25 mmol, 83%) of the title compound as a yellow solid (mp = 104-106 °C). ^{1}H NMR (400 MHz, $CDCl_3$): δ = 7.23 (d, *J* = 7.9 Hz, 1H), 7.06 (s, 1H), 6.95 (dd, *J* = 7.9, 0.8 Hz, 1H), 5.44 (s, 1H), 2.38 (s, 3H), 1.47 (s, 9H). ^{13}C NMR (100 MHz, $CDCl_3$): δ = 160.87, 148.44, 140.76, 130.58, 124.44, 115.71, 109.24, 52.04, 29.36, 21.53. HRMS (ESI-MS, m/z) $[M+H]^+$ calcd for $C_{12}H_{16}N_2O$ 205.1263; found 205.1335. The spectral data are consistent with those reported in the literature.[80]

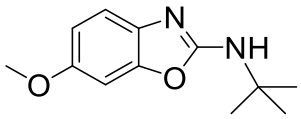

3j

6-methoxy-2-(*tert*-butylamino) benzoxazole (3j). The title compound was synthesized according to the standard procedure on a larger scale. 2-amino-5-methoxyphenol (83.5 mg, 0.600 mmol) and cobalt(II) acetate (10.6 mg, 0.0600 mmol) were combined in a 6-inch test tube inside a N_2 filled glovebox, and dissolved in dry CH_3CN (5 mL). *tert*-Butyl isocyanide (70.4 μL, 0.600 mmol) was added to the test tube before it was sealed with a septum and removed from the glovebox. The reaction mixture was then stirred in an oil bath at 65 °C for 24 hours with an air balloon attached to a syringe and needle inserted through the septum. Upon completion, the reaction mixture was cooled to room temperature and was filtered through a pad of celite. The resulting filtrate was stirred with saturated EDTA solution (100 mL) for three hours, extracted with ethyl acetate (50 mL) and the layers were separated. The aqueous layer was extracted twice with ethyl acetate (2 x 30 mL) and the combined organic layers were washed with saturated sodium chloride solution (80 mL), separated, dried over anhydrous sodium sulfate and concentrated by rotary evaporation to 3 mL. The concentrated crude mixture was passed through a silica gel pipette column, which was then washed with ethyl acetate (10 mL). This step removes any remaining cobalt from the crude mixture. The resulting filtrate was concentrated by rotary evaporation and the resulting solid was purified by silica column flash chromatography (gradient elution from the pure hexanes to hexanes: ethyl acetate = 8:1, R_f = 0.3 in 4:1 hexanes : ethyl acetate), to give the title compound as a light brown solid in 31 % yield (40.9 mg, 0.186 mmol). m.p. = 82-84 °C. ^{1}H NMR (400 MHz, $CDCl_3$): δ 7.23 (d, *J* = 8.5 Hz, 1H), 6.86 (s, 1H), 6.73 (dd, *J* = 8.4, 1.8 Hz, 1H), 5.18 (s, 1H), 3.79 (s, 3H),

1.47 (s, 9H). ^{13}C NMR (100 MHz, $CDCl_3$): δ = 160.34, 155.20, 148.71, 136.88, 116.18, 109.97, 95.85, 56.21, 52.09, 29.30. IR (ATR, cm^{-1}): 3197 (w), 2966 (m), 2834 (w), 1640 (s), 1584 (s), 1486 (s), 1441 (m), 1362 (m), 1270 (m), 1202 (s), 1138 (s), 1027 (m), 996 (m), 863 (w), 803(w). HRMS (ESI-MS, m/z) $[M+H]^+$ calcd for $C_{12}H_{16}N_2O_2$ 221.1285; found 221.1276.

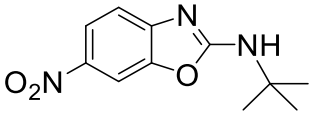

3k

6-nitro-2-(*tert*-butylamino)benzoxazole (3k). The title compound was synthesized according to the standard procedure and purified by silica column chromatography (25% ethyl acetate in hexane, R_f = 0.5 in 3:1 hexanes : ethyl acetate) to yield 51.4 mg (0.22 mmol, 73%) of the title compound as a yellow solid. ^{1}H NMR (400 MHz, $CDCl_3$): δ = 8.21 – 8.07 (m, 2H), 7.33 (d, *J* = 8.7 Hz, 1H), 5.77 (s, 1H), 1.53 (s, 9H). ^{13}C NMR (100MHz, $CDCl_3$): δ = 163.96 150.03, 147.32, 141.50, 121.28, 114.95, 104.99, 53.02, 29.13. HRMS (ESI-MS, m/z) $[M+H]^+$ calcd for $C_{11}H_{13}N_3O_3$ 236.0957; found 236.1029. The spectral data are consistent with those reported in the literature.[80]

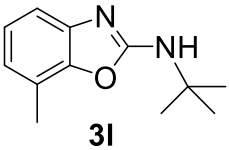

3l

7-methyl-2-(*tert*-butylamino)benzoxazole (3l). The title compound was synthesized according to the standard procedure and purified by silica column chromatography (20% ethyl acetate in hexane, R_f = 0.7 in 3:1 hexanes : ethyl acetate) to yield 47.7 mg (0.23 mmol, 78%) of the title compound as a yellow solid. ^{1}H NMR (400 MHz, $CDCl_3$): δ = 7.10 (d, *J* = 8.7 Hz, 1H), 6.94 (d, *J* = 2.4 Hz, 1H), 6.57 (dd, *J* = 8.6, 2.5 Hz, 1H), 5.32 (s, 1H), 3.80 (s, 3H), 1.48 (s, 9H). ^{13}C NMR (100 MHz, $CDCl_3$): δ = 160.96, 147.25, 142.78, 123.63, 122.14, 118.98, 113.85, 52.08, 29.39, 15.04. IR (ATR, cm^{-1}): 3359 (w), 2977 (w), 1740 (s), 1642 (s), 1580 (s), 1459 (w), 1370 (w), 1270 (m), 1239 (s), 1046 (m), 775 (m), 740 (m). HRMS (ESI-MS, m/z) $[M+H]^+$ calcd for $C_{12}H_{16}N_2O$ 205.1263; found 205.1336.

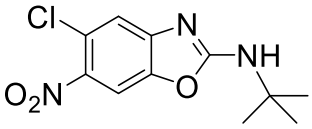

3m

6-nitro-5-chloro-2-(*tert*-butylamino)benzoxazole (3m). The title compound was synthesized according to the standard procedure and purified by silica column chromatography (gradient elution from pure hexanes to 1:1 hexanes: ethyl acetate, R_f = 0.5 in 3:1 hexanes : ethyl acetate) to yield 51.8 mg (0.192 mmol, 64%) of the title compound as a fluffy yellow solid (m.p. = 165-167 °C). ^{1}H NMR (400 MHz, $CDCl_3$): δ = 7.90 (s, 1H), 7.37 (s, 1H), 5.80 (s, 1H), 1.52 (s, 9H). ^{13}C NMR (100MHz, $CDCl_3$): δ = 164.44, 149.04, 145.97, 140.20, 124.61, 118.00, 106.94, 53.23, 29.05. IR (ATR, cm^{-1}): 3203 (w), 2980 (w), 1655 (s), 1575 (s), 1454 (s), 1313 (s), 1263 (s), 1213 (s), 1011 (m), 906 (m), 872 (m), 832 (m), 729 (m), 669 (w). HRMS (ESI-MS, m/z) $[M+H]^+$ calcd for $C_{11}H_{12}ClN_3O_3$ 270.0567; found 270.0640.

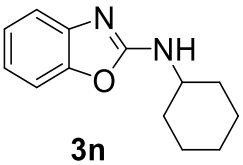

3n

2-(cyclohexylamino)benzoxazole (3n). The title compound was synthesized according to the standard procedure and purified by silica column chromatography (20% ethyl acetate in hexane, R_f = 0.3 in hexanes: ethyl acetate) to yield 47.3 mg (0.22 mmol, 73%) of the title compound as a white solid. ^{1}H NMR (600 MHz, $CDCl_3$) δ = 7.35 (d, *J* = 7.7 Hz, 1H), 7.23 (d, J=7.7Hz, 1H), 7.15 (td, *J* = 7.7, 0.9 Hz, 1H), 7.01 (t, *J* = 7.7 Hz, 1H), 5.14 (s, 1H), 3.76 (s, 1H), 2.13 (dd, *J* = 12.4, 3.1 Hz, 2H), 1.85 – 1.71 (m, 2H), 1.70 – 1.60 (m, 1H), 1.51 – 1.38 (m, 2H), 1.26 (dddd, *J* = 24.9, 15.5, 9.9, 3.4 Hz, 3H). ^{13}C NMR (150 MHz, $CDCl_3$): δ = 161.50, 148.47, 143.08, 123.98, 120.81, 116.29, 108.76, 52.17, 33.57, 25.63, 24.87. HRMS (ESI-MS, m/z) $[M+H]^+$ calcd for $C_{13}H_{16}N_2O$ 217.1263; found 217.1335. The spectral data are consistent with those reported in the literature.[81]

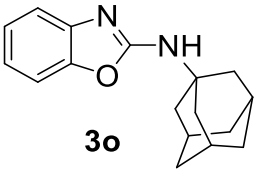

3o

2-(1-admantylamino)benzoxazole (3o). The title compound was synthesized according to the standard procedure and purified by silica column chromatography (25% ethyl acetate in hexanes, R_f = 0.7 in 3:1 hexanes: ethyl acetate) to yield 78.9 mg (0.29 mmol, 98.0 %) of the title compound as a pink solid (m.p. = 160-162 °C). ^{1}H NMR (400 MHz, $CDCl_3$): δ = 7.36 (d, *J* = 7.8 Hz, 1H), 7.26 – 7.21 (d, *J* = 7.8Hz, 1H), 7.14 (t, *J* = 7.7 Hz, 1H), 7.01 (t, *J* = 7.7 Hz, 1H), 5.20 (s, 1H), 2.13 (d, *J* = 21.4 Hz, 9H), 1.79 – 1.67 (m, 6H). ^{13}C NMR (100 MHz, $CDCl_3$): δ = 160.67, 148.15, 143.21, 123.78, 120.65, 116.34, 108.60, 52.47, 42.18, 36.29, 29.63. IR (ATR, cm^{-1}): 3243 (w), 2903 (m), 2851 (w), 1635 (s), 1576 (s), 1460 (m), 1357 (w), 1233 (m), 1011 (w), 813 (w), 740 (m). HRMS (ESI-MS, m/z) $[M+H]^+$ calcd for $C_{17}H_{20}N_2O$ 269.1576; found 269.1648.

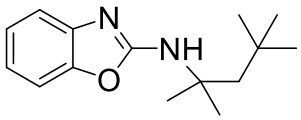

3p

2-(1,1,3,3-tetramethylbutylamino)benzoxazole (3p). The title compound was synthesized according to the standard procedure and purified by silica column chromatography (gradient elution from pure hexanes to 4:1 hexanes: ethyl acetate, R_f = 0.30 in 3:1 hexanes : ethyl acetate) to yield 62.8 mg (0.255 mmol, 85 %) of the title compound as a light yellow solid (m.p.=109-110 ^{o} C). ^{1}H NMR (400 MHz, $CDCl_3$): δ = 7.36 (d, *J* = 7.7 Hz, 1H), 7.23 (d, *J* = 8.0 Hz, 1H), 7.14 (td, *J* = 7.7, 1.0 Hz, 1H), 7.00 (td, *J* = 7.7, 1.1 Hz, 1H), 5.54 (s, 1H), 1.84 (s, 2H), 1.53 (s, 6H), 1.00 (s, 9H). ^{13}C NMR (100 MHz, $CDCl_3$): δ = 160.99, 148.21, 143.33, 123.76, 120.48, 116.30, 108.59, 55.81, 51.90, 31.82, 31.59, 28.85. IR (ATR, cm^{-1}): 3239 (w), 2950 (m), 1655 (s), 1640 (s), 1579 (s), 1459 (s), 1149 (w), 1009 (w), 927 (w), 847 (w), 754 (m), 740 (s). HRMS (ESI-MS, m/z) $[M+H]^+$ calcd for $C_{15}H_{22}N_2O$ 247.1732; found 247.1806.

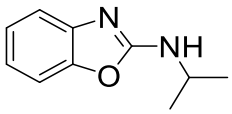

3q

2-(isopropylamino)benzoxazole (3q). The title compound was synthesized according to the standard procedure and purified by silica column chromatography (gradient elution from pure hexanes to 4:1 hexanes : ethyl acetate, R_f = 0.30 in 3:1 hexanes : ethyl acetate) to yield 41.7 mg

(0.237 mmol, 79 %) of the title compound as a light yellow solid. ^{1}H NMR (400 MHz, $CDCl_3$): δ = 7.35 (d, *J* = 7.8 Hz, 1H), 7.28 – 7.20 (m, 1H), 7.15 (dd, *J* = 11.3, 4.0 Hz, 1H), 7.06 – 6.97 (m, 1H), 5.44 (s, 1H), 4.08 (s, 1H) 1.33 (d, *J* = 6.5 Hz, 7H). ^{13}C NMR (100 MHz, $CDCl_3$): δ = 161.63, 148.47, 143.09, 123.95, 120.73, 116.19, 108.78, 45.45, 23.25. HRMS (ESI-MS, m/z) $[M+H]^+$ calcd for $C_{10}H_{12}N_2O$ 177.0950; found 177.1023. The spectral data are consistent with those reported in the literature.[82]

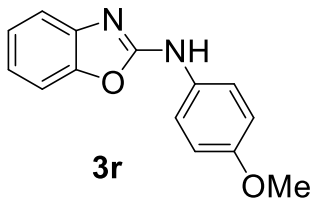

3r

2-(4-methoxyphenylamino)benzoxazole (3r). The title compound was synthesized according to the standard procedure and purified by silica column chromatography (gradient elution from pure hexanes to 1:1 hexanes: ethyl acetate, R_f = 0.55 in 3:1 hexanes : ethyl acetate) to yield 25.6 mg (0.107 mmol, 36 %) of the title compound as a light yellow solid (m.p.= 137-139 ^{o} C). ^{1}H NMR (400 MHz, $CDCl_3$): δ = 8.77 (s, 1H), 7.52 – 7.45 (m, 2H), 7.40 (d, *J* = 7.8 Hz, 1H), 7.31 (d, *J* = 8.0 Hz, 1H), 7.20 (td, *J* = 7.7, 1.0 Hz, 1H), 7.08 (td, *J* = 7.8, 1.1 Hz, 1H), 6.96 – 6.89 (m, 2H), 3.80 (s, 3H). ^{13}C NMR (100 MHz, $CDCl_3$): δ = 156.26, 142.36, 131.16, 124.4, 121.55, 121.19, 116.73, 114.72, 109.21, 55.70. HRMS (ESI-MS, m/z) $[M+H]^+$ calcd for $C_{14}H_{12}N_2O_2$ 241.0972; found 241.0965. The spectral data are consistent with those reported in the literature.[83]

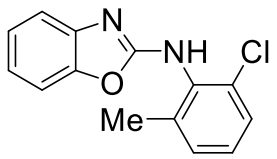

3s

2-(6-chloro-2-methylphenylamino)benzoxazole (3s). The title compound was synthesized according to the standard procedure and purified by silica column chromatography (gradient elution from pure hexanes to 4:1 hexanes : ethyl acetate , R_f = 0.40 in 3:1 hexanes : ethyl acetate) to yield 28.5 mg (0.110 mmol, 37 %) of the title compound as a light yellow solid (m.p.=166-168 °C). ^{1}H NMR (600 MHz, $CDCl_3$): δ = 7.83 (s, 1H), 7.34 (d, *J* = 8.0 Hz, 2H), 7.28 (d, *J* = 6.9 Hz, 1H), 7.26 – 7.13 (m, 3H), 7.07 (t, *J* = 7.7 Hz, 1H), 2.39 (s, 3H). ^{13}C NMR (100 MHz, $CDCl_3$):

δ = 138.14, 133.21, 132.00, 129.82, 129.63, 128.08, 127.63, 124.24, 121.70, 117.16, 109.33, 19.01. IR (ATR, cm^{-1}): 2984 (w), 1639 (m), 1582 (m), 1460 (m), 1372 (m), 1238 (s), 1045 (s), 938 (w), 847 (w), 744 (w), 672 (w). HRMS (ESI-MS, m/z) $[M+H]^+$ calcd for $C_{14}H_{11}ClN_2O$ 259.0560; found 259.0632.

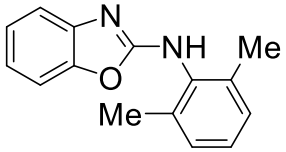

3t

2-(2,6-dimethylphenylamino)benzoxazole (3t). The title compound was synthesized according to the standard procedure and purified by silica column chromatography (gradient elution from pure hexanes to 4:1 hexanes: ethyl acetate, R_f = 0.40 in 3:1 hexanes : ethyl acetate) to yield 58.9 mg (0.247 mmol, 82 %) of the title compound as a light yellow solid. ^{1}H NMR (400 MHz, $CDCl_3$): δ = 8.78 (s, 1H), 7.28 – 7.21 (m, 2H), 7.20 – 7.10 (m, 4H), 7.03 (dd, *J* = 11.3, 4.2 Hz, 1H), 2.36 (s, 6H). ^{13}C NMR (400 MHz, $CDCl_3$): δ = 161.12, 148.49, 142.57, 136.05, 134.33, 128.56, 127.45, 124.03, 120.88, 116.20, 109.09, 18.44. HRMS (ESI-MS, m/z) $[M+H]^+$ calcd for $C_{15}H_{14}N_2O$ 239.1106; found 239.1177. The spectral data are consistent with those reported in the literature.[58]

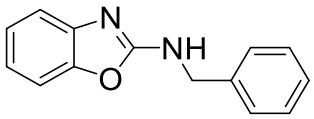

3u

N-(phenylmethyl)-2-benzoxazolamine (3u). The title compound was synthesized according to the standard procedure and purified by silica column chromatography (gradient elution from pure hexanes to 4:1 hexanes : ethyl acetate, R_f = 0.3 in 3:1 hexanes : ethyl acetate) to yield 21.8 mg (0.0972 mmol, 32.4%) of the title compound as a light yellow solid (m.p.= 122-124 °C). ^{1}H NMR (400 MHz, $CDCl_3$): δ = 7.43 – 7.33 (m, 4H), 7.32 – 7.27 (m, 2H), 7.28 – 7.21 (m, 1H), 7.16 (t, *J* = 7.6 Hz, 1H), 7.03 (t, *J* = 7.7 Hz, 1H), 5.63 (s, 1H), 4.68 (s, 2H). ^{13}C NMR (100 MHz, $CDCl_3$): δ = 162.09, 148.75, 143.04, 137.83, 128.98, 128.01, 127.77, 124.09, 121.14, 116.67, 108.96, 47.29. HRMS (ESI-MS, m/z) $[M+H]^+$ calcd for $C_{14}H_{12}N_2O$ 225.1022; found 225.1013. The spectral data are consistent with those reported in the literature.[83]

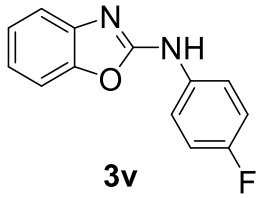

3v

2-(4-fluorophenylamino)benzoxazole (3v) The title compound was synthesized according to the standard procedure on a doubled scale. Cobalt (II) acetate (10.6 mg, 0.0600 mmol), 2-aminophenol (65.4 mg, 0.600 mmol) and 4-fluorophenyl isocyanide (72.7 mg, 0.600 mmol) were combined in a 6-inch test tube inside a N_2 filled glovebox and dissolved in dry CH_3CN (5 mL). The test tube was sealed with a septum and removed from the glovebox. The reaction mixture was then stirred in an oil bath at 65 ˚C for 24 hours with an air balloon attached to a syringe and needle inserted through the septum. Upon completion, the reaction mixture was cooled to room temperature and filtered through a Pasteur pipette silica gel plug and washed with ethyl acetate (~15 mL). The resulting filtrate was concentrated by rotary evaporation and the solid was purified by silica column chromatography (gradient elution from pure hexanes to 10:1 hexanes : ethyl acetate, R_f = 0.65 in 3:1 hexanes : ethyl acetate) to yield 26.8 mg (0.180 mmol, 19.6%) of the title compound as a yellow solid (m.p.= 167-169 °C). ^{1}H NMR (400 MHz, $CDCl_3$): δ = 7.80 (s, 1H), δ 7.63 – 7.53 (m, 2H), 7.47 (d, *J* = 7.8 Hz, 1H), 7.35 (d, *J* = 8.0 Hz, 1H), 7.27 – 7.21 (m, 2H), 7.17 – 7.05 (m, 3H). ^{13}C NMR (100 MHz, $CDCl_3$): δ = 159.97 (s), 158.36 (s), 147.99 (s), 142.31 (s), 133.94 (d, *J* = 2.7 Hz), 124.49 (s), 122.14 (s), 120.43 (d, *J* = 7.9 Hz), 117.32 (s), 116.19 (d, *J* = 22.9 Hz), 109.27 (s). HRMS (ESI-MS, m/z) $[M+H]^+$ calcd for $C_{13}H_9FN_2O$ 229.0699; found 229.0772. The spectral data are consistent with those reported in the literature.[84]

2.4.4 Procedures for Control Experiments

2.4.4.1. Control Experiments under a Nitrogen Atmosphere

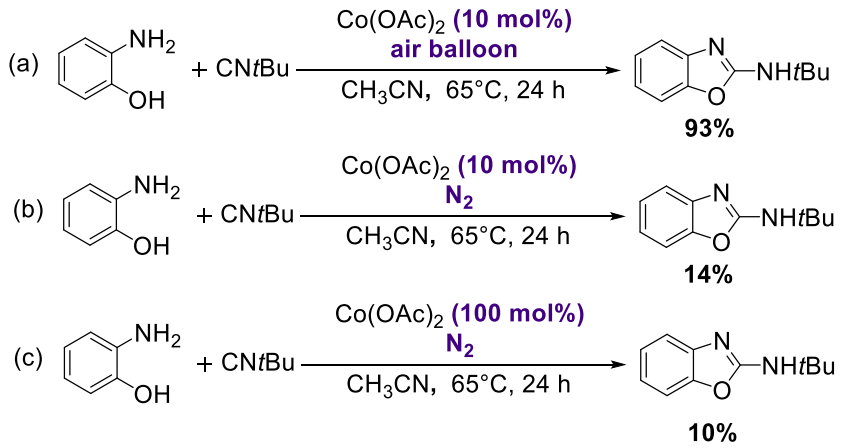

Scheme 2.5. (a) The standard reaction conditions and control experiments with (b) 10 mol% $Co(OAc)_2$ and (c) 1 equiv $Co(OAc)_2$ conducted under a nitrogen atmosphere. Yields are determined by ^1H NMR spectroscopy using dimethylsulfone internal standard.

2-Aminophenol (32.7 mg, 0.300 mmol) and cobalt (II) acetate (either 5.31 mg, 0.0300 mmol or 53.1mg, 0.300 mmol) were combined in a 25 mL Schlenk tube in a N_2 filled glovebox. CH_3CN (3.00 mL) and *tert*-butylisonitrile (35.2 μL, 0.300 mmol) were then added. The Schlenk tube was then sealed with a septum, removed from the glovebox, connected to a Schlenk line and the mixture stirred under N_2 for 24 hours at 65 °C. At the end of this period, the reaction mixture was cooled to room temperature and filtered through a Pasteur pipette silica gel plug. Ethyl acetate (15 mL) was then passed through the plug and the resulting filtrate was concentrated by rotary evaporation to yield a dark brown solid. Dimethylsulfone (3.00 mg, 0.0318 mmol), used as a ^1H NMR standard, was added to the solid residue and the crude mixture was dissolved in $CDCl_3$ for ^1H NMR analysis.

2.4.4.2. Control Experiment with a Cobalt(III) Source

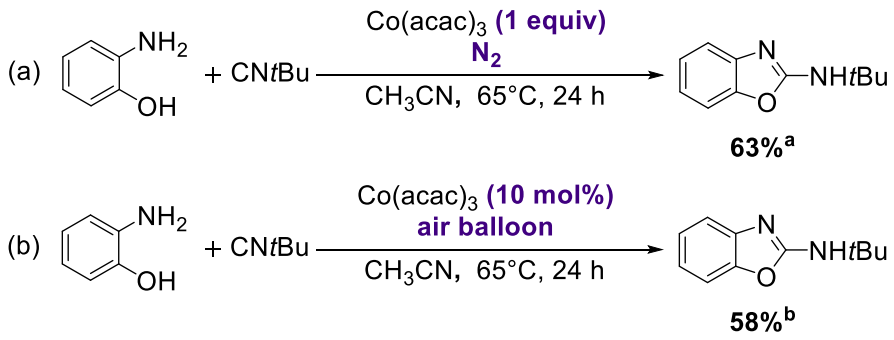

Scheme 2.6. Control experiment with (a) $Co(acac)_3$ as a cobalt(III) source and (b) the corresponding catalytic reaction with $Co(acac)_2$. [a]Isolated yield. [b] Yield determined by ^1H NMR spectroscopy using dimethylsulfone as internal standard.

<u>Procedure for Stoichiometric $Co^{III}(acac)_3$ Control Experiment:</u>

2-Aminophenol (32.7 mg, 0.300 mmol) and cobalt(III) acetylacetonate (106.8 mg, 0.3000 mmol) were combined in a 25 mL Schlenk tube in a N_2 filled glovebox, and CH_3CN (3 mL) and *tert*-butyl isonitrile (35.2 μL, 0.300 mmol) were added. The Schlenk tube was then sealed with a septum, removed from the glovebox and stirred under N_2 on a Schlenk line for 24 hours in a 65 °C oil bath. Upon completion, the reaction mixture was cooled to room temperature and filtered through a pad of Celite via vacuum filtration. The filtrate was then concentrated by rotary evaporation to yield the crude product as a dark brown solid. The crude material was then purified by silica column chromatography (6:1 hexanes: ethyl acetate, R_f = 0.3 in 5:1 hexanes : ethyl acetate) to generate 35.9 mg (0.189mmol, 63%) of the desired product as brown solid.

<u>Procedure for Catalytic $Co^{II}(acac)_2$ Control Experiment:</u>

2-Aminophenol (32.7 mg, 0.300 mmol) and cobalt(II) acetylacetonate (7.71 mg, 0.0300 mmol) were combined in a 25 mL Schlenk tube in a N_2 filled glovebox, and CH_3CN (3 mL) and *tert*-butyl isonitrile (35.2 μL, 0.300 mmol) were added. The Schlenk tube was then sealed with a septum, removed from the glovebox, fitted with an air balloon attached to a needle inserted through the septum and stirred under this aerobic atmosphere for 24 hours in a 65 °C oil bath. Upon completion, the reaction mixture was cooled to room temperature and filtered through a pad of Celite via vacuum filtration. The filtrate was then concentrated by rotary evaporation to yield the crude

product as a dark brown solid. The crude material was then purified by silica column chromatography (6:1 hexanes: ethyl acetate, R_f = 0.3 in 5:1 hexanes : ethyl acetate) to generate 33.1 mg (0.174 mmol, 58%) of the desired product as brown solid.

2.4.4.3. Control Experiment with a Peroxide Oxidant

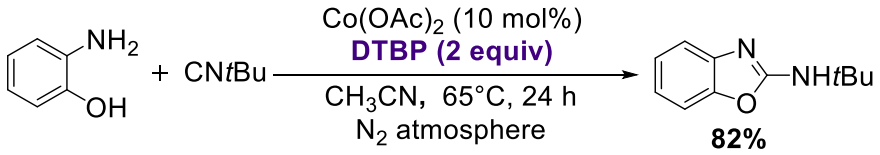

Scheme 2.7. Control experiment with di-*tert*-butyl peroxide as the oxidant. Yield determined by ^{1}H NMR spectroscopy using dimethylsulfone as internal standard.

2-Aminophenol (32.7 mg, 0.300 mmol), di-*tert*-butyl peroxide (87.7 mg, 0.600 mmol) and cobalt (II) acetate (5.31 mg, 0.0300 mmol) were combined in a 25 mL Schlenk tube in a N_2 filled glovebox. CH_3CN (3 mL) and *tert*-butyl isonitrile (35.2 μL, 0.300mmol) were added. The Schlenk tube was then sealed with a septum, removed from the glovebox and the reaction stirred under N_2 on a Schlenk line for 24 hours at 65 °C. Upon completion, the reaction mixture was cooled to room temperature and filtered through a Pasteur pipette silica gel plug. Ethyl acetate (15 mL) was passed through the silica plug and the resulting filtrate was concentrated via rotary evaporation to yield the crude product as a dark brown solid. The yield of the reaction was determined by ^{1}H NMR spectroscopy with dimethylsulfone (3.00 mg, 0.0318 mmol) as the internal standard.

2.4.4.4. Control Experiments with Radical Trapping Reagents

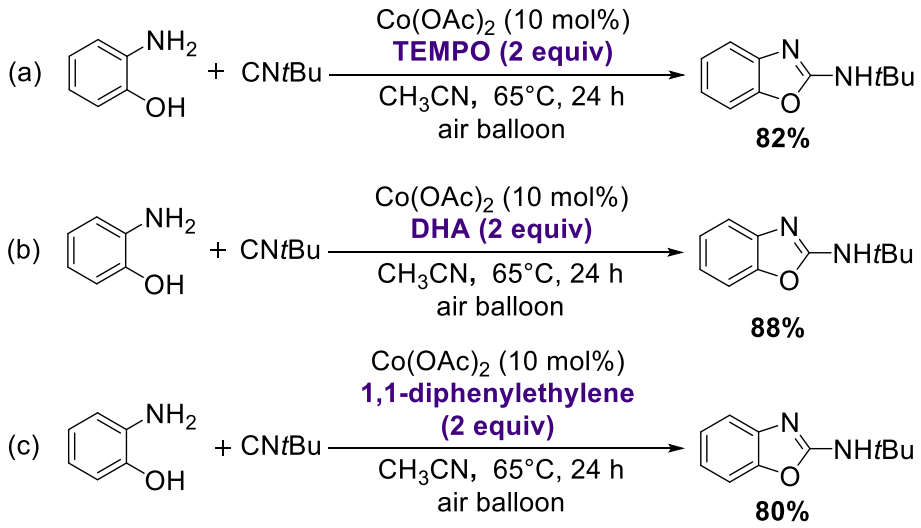

Scheme 2.8. Control experiment with (a) TEMPO, (b) 9,10-dihydroanthracene (DHA), and (c) 1,1-diphenylethylene included as radical trapping agents. Yields determined by ^{1}H NMR spectroscopy using dimethylsulfone as internal standard.

Standard procedure for radical trap experiments. 2-Aminophenol (32.7 mg, 0.300 mmol), radical scavengers (0.6 mmol), and cobalt (II) acetate (5.31 mg, 0.0300 mmol) were combined in a 6 inch test tube in a N_2 filled glovebox, CH_3CN (3 mL) and *tert*-butylisonitrile (35.2 μL, 0.300 mmol) were added. The test tube was then sealed with a septum, removed from the glovebox, and fitted with an air balloon attached to a needle inserted through the septum. The reaction mixture was stirred in an oil bath at 65 °C for 24 hours.

Work up method for control experiment with TEMPO as the radical scavenger. Upon completion of the reaction, the reaction mixture was cooled to room temperature and was diluted with ethyl acetate (20 mL). The resulting mixture was extracted with a saturated solution of $Na_2S_2O_3$ (3 x 20 mL) until the organic layer changed from dark red to light yellow. The organic layer was then washed with saturated sodium chloride solution, separated, dried over anhydrous magnesium sulfate, filtered, and finally concentrated via rotary evaporation to ~3 mL then passed through a Pasteur pipette silica gel plug to remove residue cobalt. The filter plug was flushed with extra 10 mL of ethyl acetate and further concentrated by rotary evaporation to provide the crude

product as a brownish-red solid. The crude yield was determined by ^{1}H NMR spectroscopy with dimethylsulfone (0.0300 mg, 0.0318 mmol) as the internal standard.

Work up method for control experiment with all other radical scavengers. Upon completion, the reaction mixture was cooled to room temperature, filtered through a pad of silica gel with ethyl acetate (20 mL) by vacuum filtration, and the resulting filtrate was concentrated by rotary evaporation to ~3 mL then passed through a Pasteur pipette silica gel plug (to further remove any remaining cobalt). The filter plug was flushed with an extra 10 mL of ethyl acetate and eventually, the solvent was removed by rotary evaporation to generate the crude product as a brownish solid. The crude yield was determined by ^{1}H NMR spectroscopy with dimethylsulfone (0.03 mg, 0.0318 mmol) as the internal standard.

2.4.4.5. Control Experiments in the Absence of Isonitrile

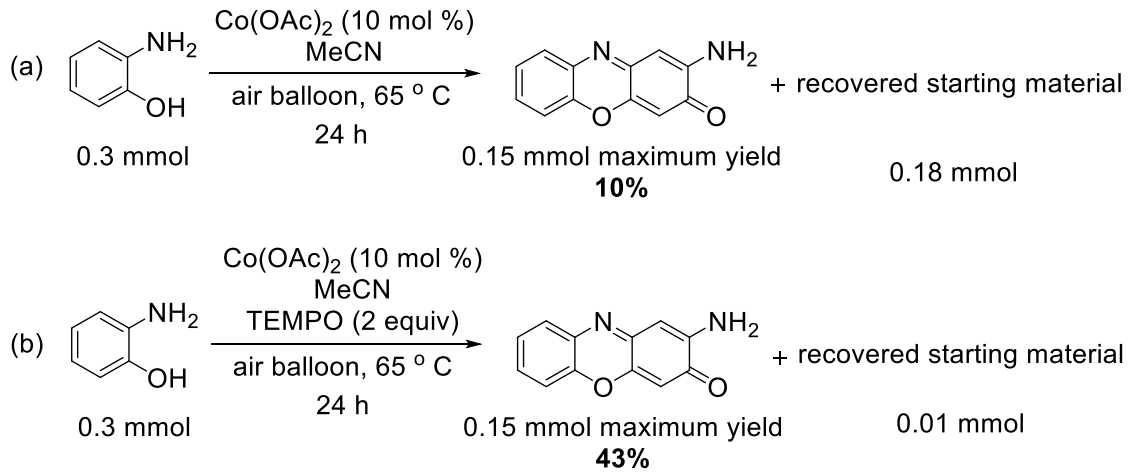

Scheme 2.9. Control experiments conducted in the absence of isonitrile both (a) without and (b) with TEMPO. Yields determined by ^{1}H NMR spectroscopy using a dimethylsulfone internal standard.

<u>Procedure for (a):</u> 2-Aminophenol (32.7 mg, 0.300 mmol) and cobalt(II) acetate (5.31 mg, 0.0300 mmol) were combined in a 25 mL Schlenk tube, and the tube was evacuated and back-filled with air three times. CH_3CN (3.00 mL) was added and the reaction mixture was stirred at 65 °C for 24 h. Upon completion, the reaction mixture was cooled to room temperature, filtered through Celite,

and washed with excess amount of ethyl acetate (50 mL). The filtrate was then concentrated to 3 mL by a rotary evaporation and the resulting mixture was filtered through a silica gel plug to further remove cobalt residues. Then, the plug was rinsed with ethyl acetate (10 mL) and the combined filtrate was concentrated under vacuum to yield the crude product as a brownish solid. Dimethylsulfone (3.00 mg, 0.0318 mmol), used as a ^{1}H NMR standard, was added to the solid residue and the crude mixture was dissolved in DMSO-d_6 for ^{1}H NMR analysis.

Procedure for (b): 2-Aminophenol (32.7 mg, 0.300 mmol), TEMPO (93.4 mg, 0.6 mmol) and cobalt(II) acetate (5.31 mg, 0.0300 mmol) were combined in a 25 mL Schlenk tube, and the tube was evacuated and back-filled with air three times. CH_3CN (3.00 mL) was added and the reaction mixture was stirred at 65 °C for 24 h. Upon completion, the reaction mixture was cooled to room temperature, filtered through Celite, and washed with ethyl acetate (~50 mL). The filtrate was then extracted with a saturated solution of $Na_2S_2O_3$ (3 x 20 mL) until the organic layer changed from dark red to light yellow. This step removes any remaining TEMPO. The organic layer was then washed with saturated sodium chloride solution, dried over anhydrous magnesium sulfate, filtered, and finally concentrated via rotary evaporation to ~3 mL. The resulting mixture was filtered through a silica gel plug to further remove cobalt residues. Then, the plug was rinsed with ethyl acetate (10 mL) and the combined filtrate was concentrated under vacuum to yield the crude product as a brownish solid. Dimethylsulfone (3.00 mg, 0.0318 mmol), used as a ^{1}H NMR standard, was added to the solid residue and the crude mixture was dissolved in DMSO-d_6 for ^{1}H NMR analysis.

In both cases, the reaction yields were determined by ^{1}H NMR spectroscopy with a dimethylsulfone (0.0300 mg, 0.0318 mmol) internal standard. The assignment of the product as 2-aminophenoxazin-3-one was confirmed by both literature evidence[85] as well as comparison with the standard purchased from Asta Tech (95% pure). ^{1}H-NMR (400 MHz, DMSO-d_6) δ 7.70 (d, J = 7.7 Hz, 1H), 7.47 (dd, J = 18.8, 8.0 Hz, 2H), 7.38 (t, J = 7.2 Hz, 1H), 6.80 (s, 2H), 6.36 (d, J = 2.6 Hz, 2H).

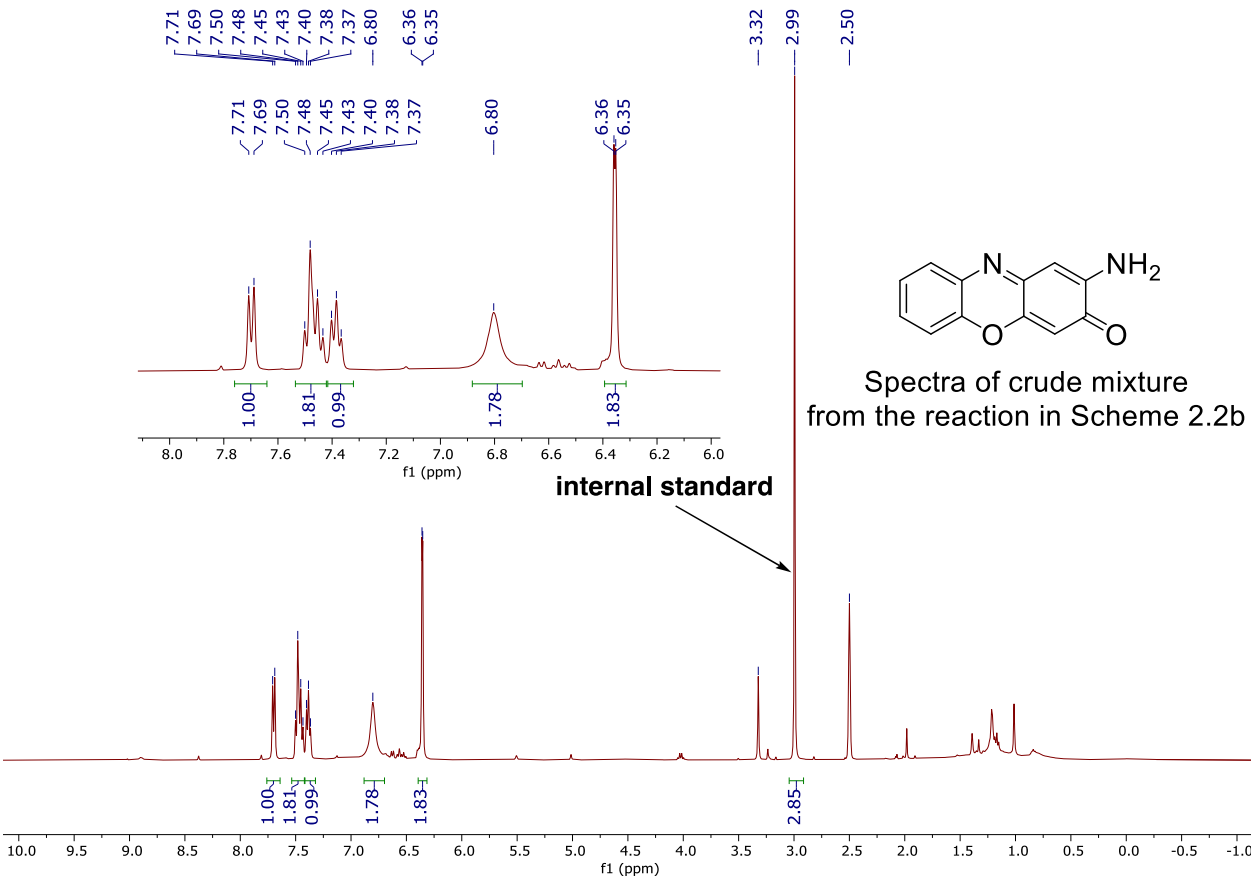

Figure 2.3. ^{1}H NMR spectrum of the crude reaction mixture of the Co-catalyzed, TEMPO-mediated dimerization of 2-aminophenol for the synthesis of 2-aminophenoxazin-3-one (reaction b in **Scheme 2.9**) in DMSO-d_6 at 400 MHz.

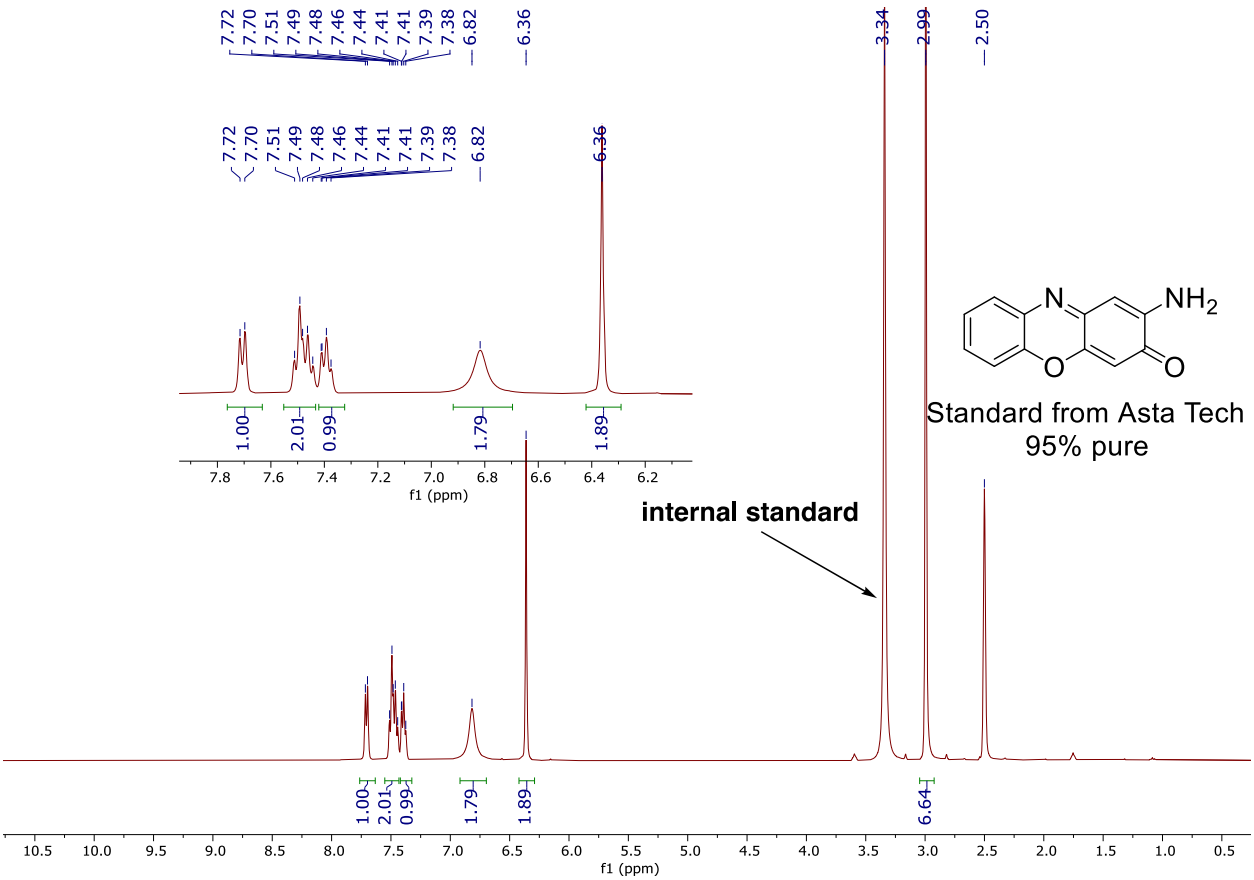

Figure 2.4. ^{1}H NMR spectrum of standard 2-aminophenozaxin-3-one purchased from AstaTech (95% pure) in DMSO-d_6 at 400 MHz.

2.4.4.6. Experimental Procedures for UV-Visible Experiments

<u>The following three experiments (A-C) were conducted with a Stellar Net UV-Vis dip probe.</u>

All cobalt salt and 2-aminphenol solutions for these experiments were prepared by serial dilution under nitrogen using standard Schlenk techniques. The general procedure for preparing $Co^{II}(acac)_2$ and 2-aminophenol solutions in acetonitrile are described below:

<u>Preparation of **$Co^{II}(acac)_2$ solution** in CH_3CN:</u>

To a 25 mL Schlenk tube equipped with a stir bar and a dip probe inserted through the septum, was added $Co^{II}(acac)_2$ (1.3 mg, 5.05×10^{-3} mmol). The tube was evacuated and backfilled with N_2 three times via the side arm and dry acetonitrile (10 mL) was added by syringe. For dilution purposes, 9 mL of the resulting 10 mL solution was removed. To the remaining 1 mL of solution,

was added an additional 9 mL of fresh dry acetonitrile to yield a final 10 mL solution with a concentration of 5.05×10^{-5} M.

Preparation of **2-aminophenol solution** in CH_3CN:

To a 25 mL Schlenk tube equipped with a stir bar and septum, 2-aminophenol (6.5mg, 0.060 mmol) was added and the tube was evacuated and backfilled with N_2 three times via the side arm. Dry acetonitrile (3 mL) was added to yield a final solution with a concentration of 2.0×10^{-2} M.

A. $Co^{II}(acac)_2$ control experiment under N_2 and air atmosphere

During the experiment, the standard spectrum of $Co^{II}(acac)_2$ (5.05×10^{-2} mM in 10 mL MeCN) was taken first under the protection of N_2 atmosphere, then the headspace was exposed to air by inserting an air balloon through the septum. The spectroscopic changes were monitored overnight with stirring. No significant changes were observed upon exposure to air and the spectrum of the cobalt species showed two absorbance maxima at 202 nm and 272 nm under both aerobic and anaerobic conditions (Figure 2.5 below).

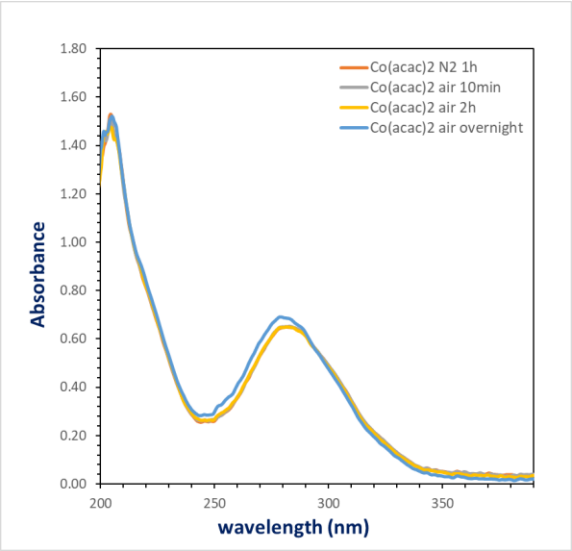

Figure 2.5. UV-visible spectra of $Co^{II}(acac)_2$ (5.05×10^{-2} mM in MeCN) prepared under N_2 (orange trace), and then exposed to air and monitored over the course of 12 h at room temperature (blue trace).

B. $Co^{II}(acac)_2$ control experiment with tBuNC

The standard spectrum of $Co^{II}(acac)_2$ in acetonitrile (5.05×10^{-2} mM in 10 mL MeCN) was taken first under a N_2 atmosphere, then *tert*-butylisonitrile (5 μL, 3.65 mg, 0.044 mmol, 8 equiv) was

added by syringe. The mixture was then exposed to air by inserting an air balloon through the septum and the reaction mixture was stirred under the air atmosphere overnight. No new band were observed and instead only the two absorbance maxima characteristic of $Co^{II}(acac)_2$ were present (202 nm and 272 nm, Figure S4 below).

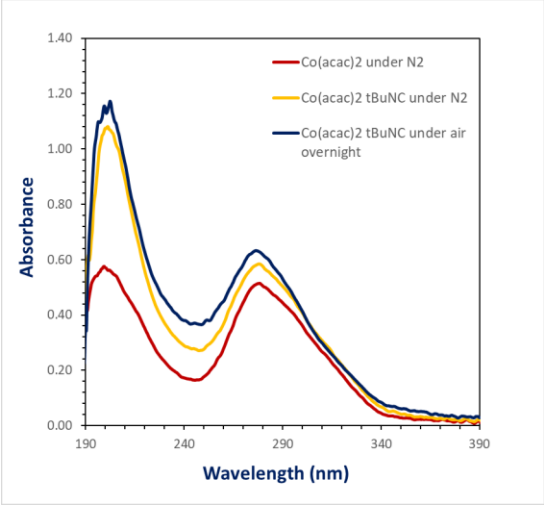

Figure 2.6. UV-Visible spectra of (a) $Co^{II}(acac)_2$ (5.05×10^{-2} mM in MeCN) prepared under N_2 (red trace), and then *tert*-butylisonitrile (8 equiv) was added (green trace), and final, exposed to air overnight (dark blue trace).

C. $Co^{II}(acac)_2$ control experiment with 2 equivalents of 2-aminophenol

First, a UV-visible spectrum of Co^{II} $(acac)_2$ (5.05×10^{-2} mM in 10 mL MeCN) was taken under a N_2 atmosphere. Then 2-aminophenol was added by syringe in 1 equivalent increments (25 μL of the 2.0 $\times10^{-2}$ M aminophenol stock solution in MeCN, described above) until a total of 2 equivalents had been added. Spectra were recorded after each addition. The mixture was then stirred under an inert atmosphere for 2.5 h, then exposed to air by inserting an air balloon through the septum. The resulting mixture was stirred in the closed aerobic system overnight. UV-visible spectra were taken throughout the reaction. Under anaerobic condition, $Co^{II}(acac)_2$ showed absorbance maxima at 202 and 272 nm. Upon the injection of the 2-aminophenol solution in MeCN, accumulation of 2-aminophneol was observed. Changes of absorbance maxima were observed only when the mixture was exposed to air, which was observed as the slow growth of the peak around 270 nm (Figure 2.7, below).

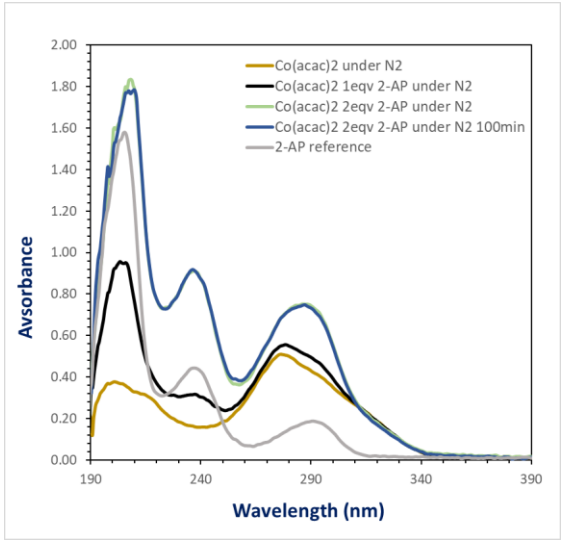

(a)

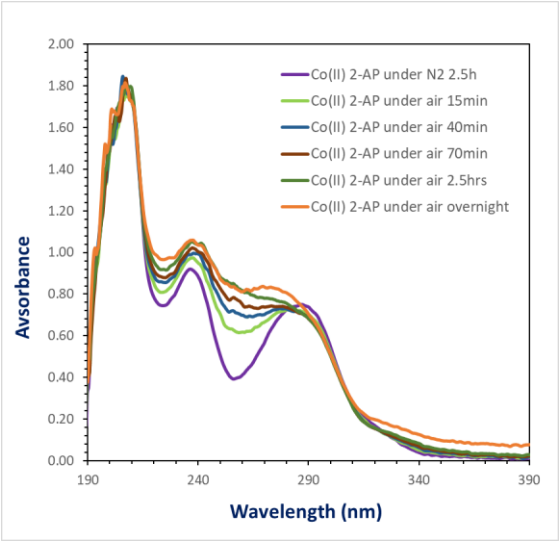

(b)

Figure 2.7. UV-visible spectra of (a) $Co^{II}(acac)_2$ (5.05×10^{-2} mM in MeCN) prepared under N_2 (yellow trace), and then treated with 2-aminophenol to reach a total of 2 equiv added (deep blue trace), and (b) $Co^{II}(acac)_2$ (5.05×10^{-2} mM in MeCN) and 2-aminophenol (2 equiv, purple trace) exposed to air and monitored over the course of 12 h at room temperature (orange trace).

The following two experiments (D and E) were conducted with a Shimadzu UV 1800 instrument

All cobalt salt and 2-aminophenol solutions for these experiments were prepared by serial dilution in a nitrogen-filled glovebox or using standard Schlenk techniques. The general procedure for preparing $Co^{II}(acac)_2$ and 2-aminophenol solutions in acetonitrile are described below:

<u>General procedure for preparing **$Co^{II}(acac)_2$** solution:</u>

To a 20 mL scintillation vial inside the glovebox, $Co(acac)_2$ (1.3 mg, 5.0×10^{-3} mmol) was first dissolved in dry CH_3CN (10 mL). For dilution purposes, 1 mL of the resulting 10 mL solution was transferred to a new clean 20 mL scintillation vial. To this 1 mL of solution was added 19 mL of fresh CH_3CN to yield a final 20 mL solution with concentration of 2.5×10^{-5} M.

<u>General procedure for preparing **$Co^{III}(acac)_3$** solution:</u>

To a 20 mL scintillation vial inside the glovebox, $Co(acac)_3$ (1.8 mg, 2.5×10^{-3} mmol) was first dissolved in dry CH_3CN (10 mL). For dilution purposes, 1 mL of the resulting 10 mL solution was transferred to a new clean 20 mL scintillation vial. To this 1 mL of solution was added 19 mL of fresh CH_3CN to yield a final 20 mL solution with concentration of 2.5×10^{-5} M.

General procedure for preparing **2-aminophenol** solution

To a 25 mL Schlenk tube equipped with a stir bar and septum, 2-aminophenol (8.2 mg, 0.075 mmol) was added and the tube was evacuated and backfilled with N_2 three times. Dry acetonitrile (3 mL) was added via syringe to make a final solution with a concentration of 2.5 $\times 10^{-2}$ M.

D. $Co^{II}(acac)_2$ control experiment with 3 equivalents of 2-aminophenol

Inside a N_2 filled glovebox, a 3 mL aliquot of the standard solution of $Co(acac)_2$ (2.5×10^{-5}M, described above) was transferred to a cuvette. The cuvette was then sealed, removed from the glovebox and an initial spectrum recorded. Then 2-aminophenol was added by syringe in 1 equivalent increments (3 μL of the 2.5 $\times 10^{-2}$ M aminophenol stock solution in CH_3CN, described above) until a total of 3 equivalents had been added. Spectra were recorded after each addition and for 1 hour further under N_2. Under a N_2 atmosphere, no significant changes in the spectra were observed upon addition of 2-aminophenol except for the accumulation of 2-aminophenol in the mixture. Air was then bubbled into the mixture for 3 min by inserting an air balloon through the septum of the cuvette and UV-visible spectra were recorded under this aerobic atmosphere for over 12 hours. Upon exposure of the mixture to air, spectral changes were seen with a rapid growth of the absorbance around 260 nm. (Figure 2.8, below).

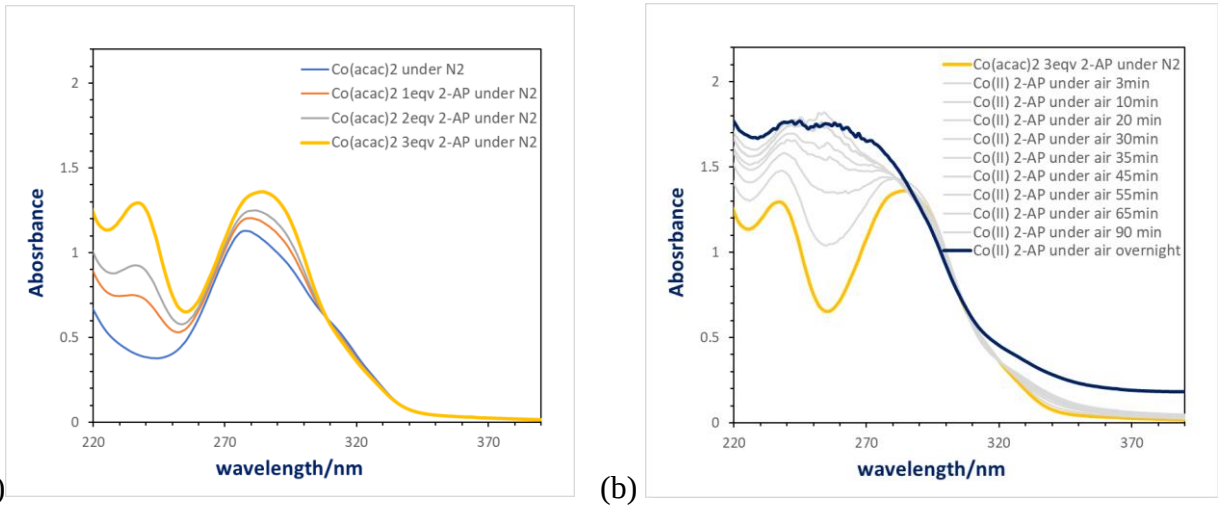

(a) (b)

Figure 2.8. (a) $Co(acac)_2$ (5.0×10^{-5}M) in MeCN under N_2 (red trace) with the addition of 3 equiv of 2-aminophenol (yellow trace), and (b) $Co(acac)_2$ and 2-aminophenol (3 equiv, yellow trace) exposed to air overnight (deep blue trace).

E. $Co^{III}(acac)_3$ control experiment with 3 equivalents of 2-aminophenol

Inside a N_2 filled glovebox, a 3 mL aliquot of the standard solution of $Co(acac)_3$ (2.5×10^{-5}M, described above) was transferred to a cuvette. The cuvette was then sealed, removed from the glovebox and an initial spectrum recorded. Then 2-aminophenol was added by syringe in 1 equivalent increments (3 μL of the 2.5 $\times10^{-2}$ M aminophenol stock solution in CH_3CN, described above) until a total of 3 equivalents had been added. Spectra were recorded after each addition and for 2 hours further under N_2. Air was then bubbled into the mixture by inserting an air balloon through the septum of the cuvette and UV-visible spectra were recorded under this aerobic atmosphere for over 12 hours (Figure 2.9 below).

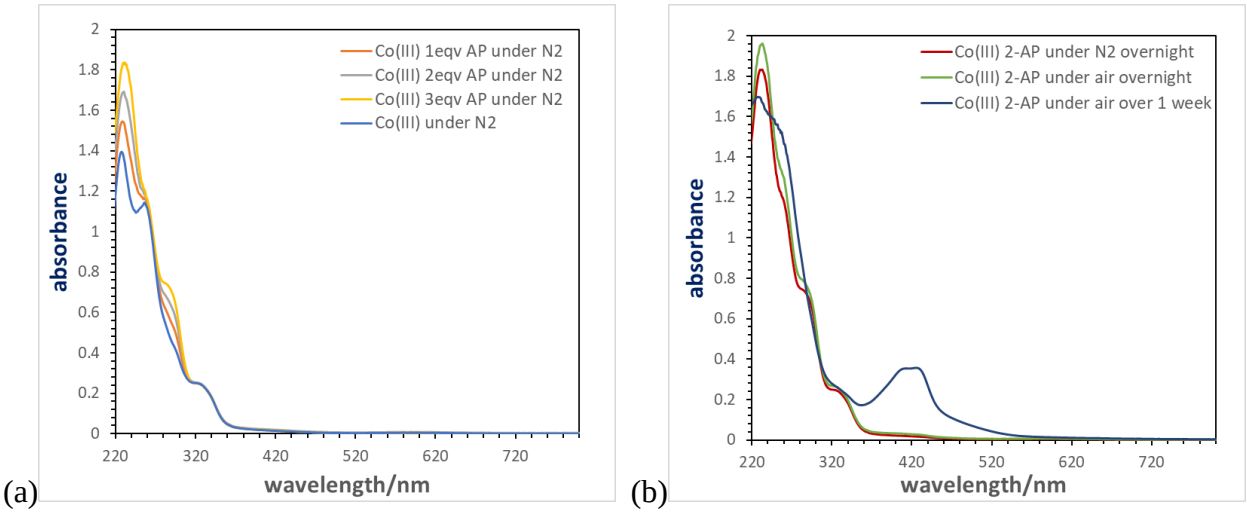

Figure 2.9. (a) $Co(acac)_3$ (2.5×10^{-5} M) in MeCN under N_2 (blue trace) with the addition of 3 equiv of 2-aminophenol (yellow trace) and (b) $Co(acac)_3$ (2.5×10^{-5} M) and 2-aminophenol (3 equiv, red trace) exposed to air overnight (blue trace).

Chapter 3. Cobalt-Catalyzed Aerobic Oxidative Cyclization of 2-Aminoanilines with Isonitriles: Facile Access to Substituted 2-Aminobenzimidazoles

3.1 Introduction

Benzimidazoles are structurally important heterocyclic compounds that are key targets or the intermediates in the synthesis of pharmaceutically valuable and biologically active molecules.[86-90] Specifically, the 2-aminobenzimidazole scaffold is a common substructure in this category that existing widely in a variety of antihistamines (norastemizole and astemizole),[91] antihelmitics (mebendazole),[92] kinase inhibitors,[93, 94] and integrin $\alpha v\beta_3$ antagonists.[95] These structures have also demonstrated anticancer[96] and antimalarial[97] activities among others in related research (Chart 3.1).[98, 99]

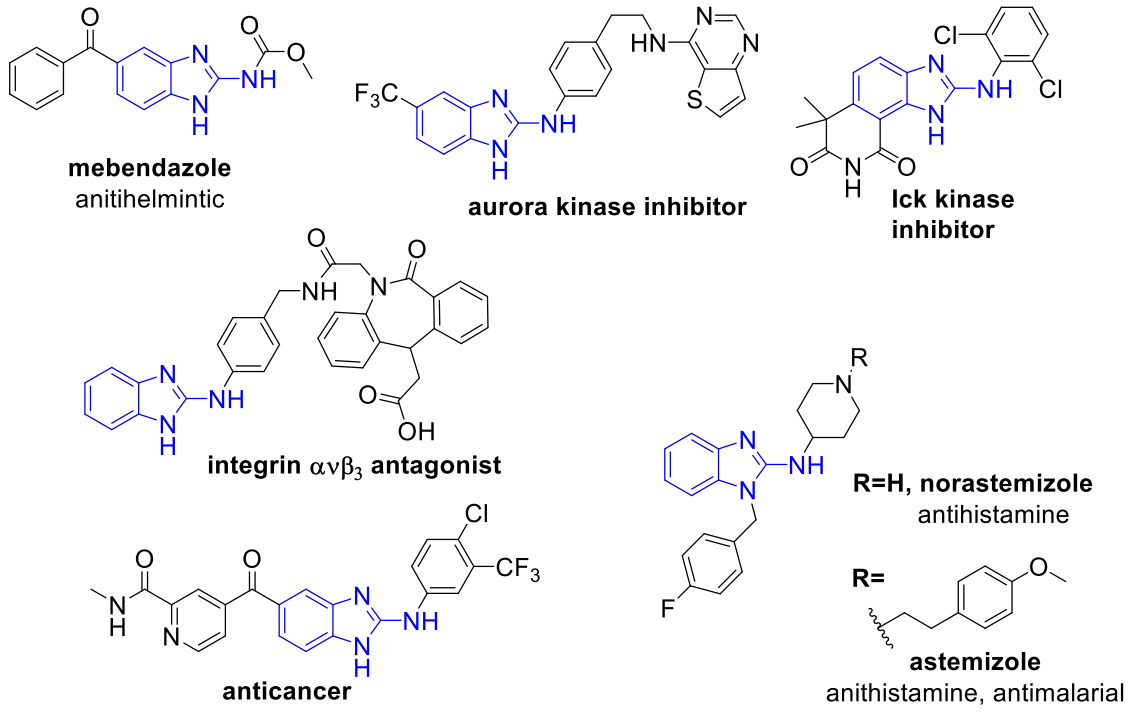

Chart 3.1. Selected biologically active small molecules containing 2-aminobenzimidazole substructure.

One of the most conventional routes to access these heterocyclic structures relies on the desulfurization of a preformed thiourea that can be prepared from either the reduction of the appropriate *ortho*-nitroaryl thiourea[100-104] or the coupling of *ortho*-phenylenediamine with the corresponding isothiocyanate[81, 105-111] (**Scheme 3.1 Route a**). Unfortunately, the pre-functionalization of these starting materials has disadvantages like low yields, poor atom efficiency and the reduction of nitro-group was not always efficient. Also, these reactions require the use of super stoichiometric mercury salts for the ring-closure of thiourea derivatives and toxic/or hazardous desulfurizing agents such as MeI among others.[81, 112] Alternatively, TsCl has been employed under basic conditions[113] and coupling agents such as 1,3-diisopropylcarbodiimde (DIC) or N-(3-dimethylaminopropyl)-N'-ethylcarbodiimide hydrochloride (EDC) or dicyclohexylcarbodiimide (DCC) have also been shown to be efficient in this category of transformations.[102, 114] Whilst effective, these methods suffer from low atom economy and the employment of toxic reagents renders a doubtful feasibility for large scale synthesis and limited industrial applications. Furthermore, the 1,2-diamine substitutions on the arene substrates prior to desulfurization often require a fresh preparation due to the poor stability of these compounds.[115]

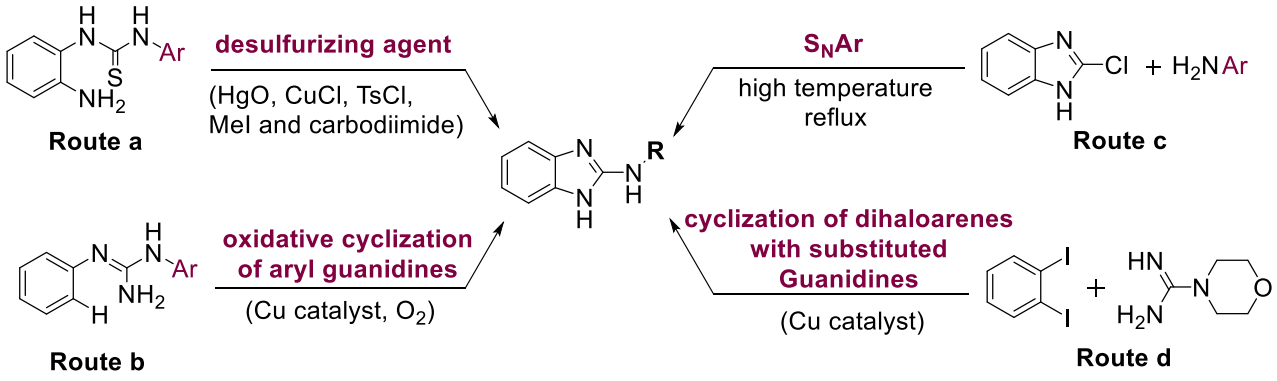

Scheme 3.1. Selected conventional routes for the synthesis of 2-aminobenzimidazoles. Reaction Conditions: (Route a) desulfurization agents such as HgO, carbodiimide or Cu catalyst and base. (Route b) Cu catalyst and O2. (Route c) reflux at high temperature or Pd catalyst. (Route d) Cu catalyst and base.

More recently, transition metal-catalyzed cyclization reactions have provided attractive alternatives to access 2-(N-substituted)-aminobenzimidazoles. The copper-catalyzed intramolecular cyclization reactions of thioureas[116] or guanidines **(Scheme 3.1 Route b)**[115] help

eliminate the requirement of stoichiometric desulfurizing agents. Other approaches enable arylamination of 2-chlorobenzimidazole either by Pd catalysis[117, 118] or S_NAr transformation mediated either by high temperature[119, 120] or high pressure **(Scheme 3.1 Route c)**.[121] Cyclization of dihaloarenes with substituted guanidines mediated by a Cu catalyst also provided an alternative path to achieve 2-aminobenzimidazoles **(Scheme 3.1 Route d)**,[122, 123] however, this protocol is restricted by its inherent limitation that only dihaloarenes can be used and availability of guanidines is another challenge. Finally, transition-metal-free cyclization reactions using I_2[110, 111] or hypervalent iodine-based oxidants[124] have also been developed. To circumvent additional non-trivial synthetic challenges that most methodologies suffer, the ability to utilize readily available coupling partners in combination with environmentally benign oxidants, such as O_2 and air, and abundant first-row transition-metal catalysts would represent a significant advance toward the facile synthesis of substituted 2-aminobenzimidazoles.[57] A variety of cobalt-catalyzed cyclization reactions of isonitriles have been developed. Specifically, Wang and coworkers have reported cyclization reactions with bisnucleophiles employing persulfate-based oxidants[125] and in the last chapter we have revealed an aerobic cobalt-catalyzed oxidative cyclization of aminophenols and isonitriles to generate substituted 2-aminobenzoxazoles.[126] Thus, we wondered if we can expand our aerobic cobalt catalyst system to the efficient synthesis of other heterocycles. In this chapter, we will disclose the cobalt-catalyzed aerobic oxidative cyclization reactions of ortho-phenylenediamines with isonitriles to generate substituted 2-aminobenzimidazoles **(Scheme 3.2)**.

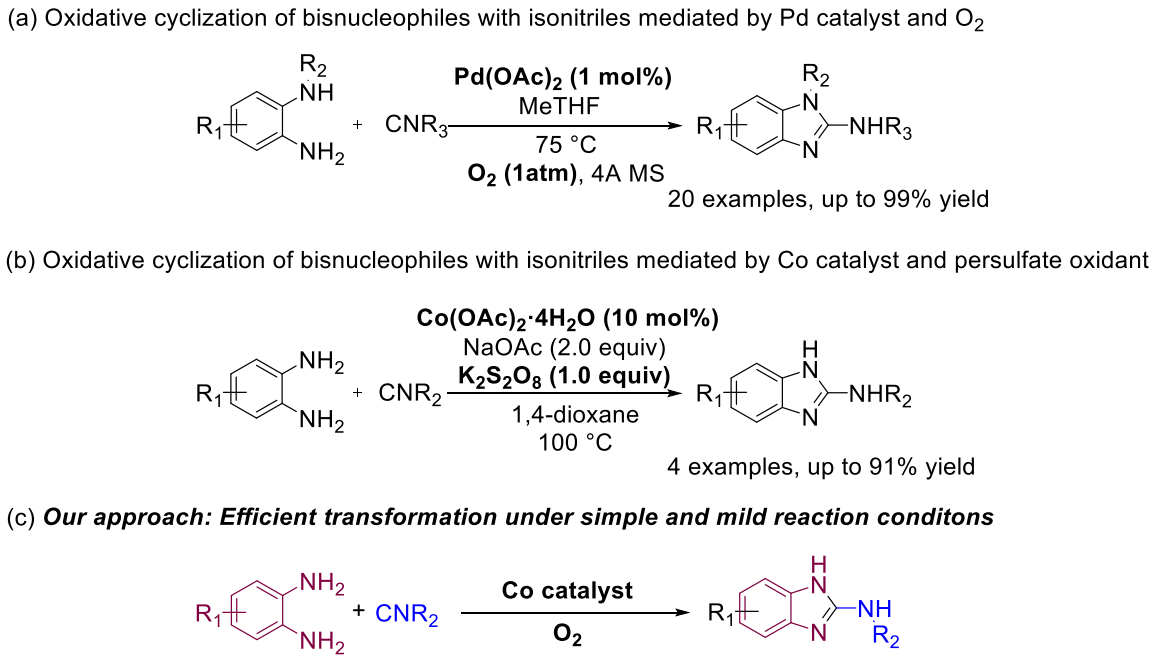

Scheme 3.2. 2-aminobenzimidazole synthesis via transition-metal catalyzed oxidative cyclization of bisnucleophiles with isonitriles. (a) Pd/O_2 mediated oxidative cyclization reactions. (b) Oxidative cyclization reactions mediated by Co catalyst pairing with a persulfate oxidant. (c) Approach of our work in this chapter.

3.2 Results

3.2.1. Condition Optimization of Cobalt-Catalyzed Aerobic Oxidative Cyclization of o-Phenylenediamine with tert-Butyl Isonitrile

We started our condition optimization with the model coupling reaction of *ortho*-phenylenediamine (**4a**) and *tert*-butyl isonitrile (**2a**) under the aerobic cobalt-catalyzed conditions. Of all cobalt salts investigated, $Co(OAc)_2$ was found to provide the highest yield of **5a** in 69% of yield when CH_3CN was employed as a solvent at 65 °C (entries 1-5). Reactions run in CH_3CN provided higher yields of **5a** than other commonly utilized solvents such as dioxane, THF and DMF (entries 5-9). The incorporation of base additives improved the reaction yield, with two equivalents of K_2CO_3 showing the greatest improvement of product in 85% of yield (entries 10-15). Finally, we have found that the increase of the reaction temperature plays a critical role in this

aerobic oxidative cyclization reaction. The yield of **5a** was increased to 95% when the reaction temperature was raised to 80 °C (entry 16). Thus, the optimized reaction conditions employ 10 mol% of $Co(OAc)_2$ with two equivalents of K_2CO_3 and an air balloon in CH_3CN at 80 °C for 24 hours.

Table 3.1 Optimization of Reaction Conditions[a]

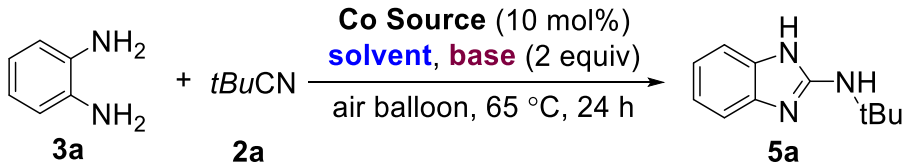

Entry	Co Source	Solvent	Base	% Yield[b]
1	$CoCO_3$	CH_3CN	--	Trace
2	$CoCO_3 \cdot H_2O$	CH_3CN	--	Trace
3	$CoCl_2$	CH_3CN	--	Trace
4	$Co(acac)_2$	CH_3CN	--	41
5	$Co(OAc)_2$	CH_3CN	--	69
6	$Co(OAc)_2$	1,4-dioxane	--	61
7	$Co(OAc)_2$	2-Me-THF	--	69
8	$Co(OAc)_2$	THF	--	54
9	$Co(OAc)_2$	DMF	--	23
10	$Co(OAc)_2$	CH_3CN	K_2CO_3	85
11	$Co(OAc)_2$	CH_3CN	Na_2CO_3	79
12	$Co(OAc)_2$	CH_3CN	Li_2CO_3	67
13	$Co(OAc)_2$	CH_3CN	KOAc	82
14	$Co(OAc)_2$	CH_3CN	NaOAc	62
15	$Co(OAc)_2$	CH_3CN	LiOAc	65
16[c]	**$Co(OAc)_2$**	**CH_3CN**	**K_2CO_3**	**95**

[a]Reaction Conditions: **4a** (0.3 mmol), **2a** (0.3 mmol), cobalt(II) catalysts (10 mol%), solvent (3 mL), at 65 °C with an air balloon for 24 h. [b]The yield of **5a** was determined by ^1H NMR spectroscopy with dimethylsulfone as internal standard (0.03 mmol).[c]The reaction was conducted at 80 °C.

Last year Glorious and co-workers developed an user-friendly assessment tool that enabled the sensitivity to different variants of a protocol to be rapidly assessed.[127] This tool delivers a straightforward overview of the sensitivity of reactions to key parameters by the standardized presentation of the results in a radar diagram. This diagram provides a direct visualization of the general sensitivity of a reaction based on the shape of the black line generated. The round shape around the "0% deviation line" indicates low sensitivity, while any section deflecting from that to the red zone refers to high sensitivity. Specifically, the sharp "arrow-like" deflections immediately demonstrate the most influential parameters. As we aimed to develop a highly efficient but simple transformation delivering the scaffolds of critical pharmaceutical importance, we applied this tool to our standard cobalt-catalyzed aerobic cyclization reaction to test the robustness of the condition screening and reproducibility of this protocol.

In this assessment, O_2 concentration, base stoichiometry, catalyst loading, concentration of reaction mixture and reaction temperature were chosen as key parameters in the standard cyclization reaction. These parameters were evaluated by carefully setting up five sets of experiments with single variation for each, following the systematic four-step procedure reported by Glorious (experimentation, data analysis, calculation and data plotting) (**Figure 3.1a**). From the radar diagram generated upon using this methodology, we realized the almost neglectable influence of reaction mixture concentration and small impact of catalyst loading on the overall performance of this transformation. Also confirmed was the strong dependence of this reaction on the base loading as well as the reaction temperature and O_2 concentration, as indicated by the black "arrow-like" deflections shown in the diagram (**Figure 3.1b**) **(See the details of reaction set up and results of these assessment experiments in the Experimental Section 3.4.3/Tables 3.8 & 3.9/Figures 3.2-3.4)**. By knowing the highly sensitive parameters associated with a chemical transformation, the implementation of this condition-based assessment in our cobalt aerobic cyclization system could help us facilitate higher reproducibility in the later stage substrate scope investigations, and allow the fast application of the new developed protocol in further structural functionalization.

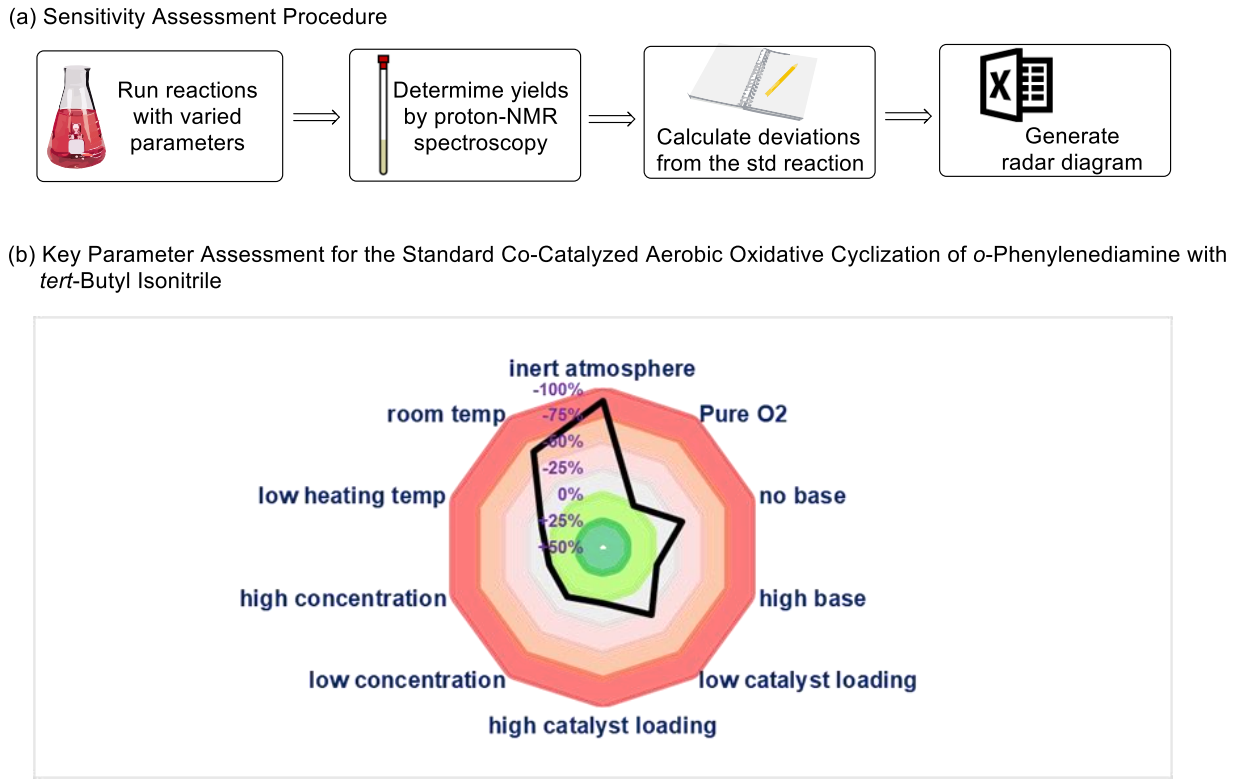

Figure 3.1. Condition-based sensitivity assessment experiment. (a) Four steps involved in sensitivity assessment procedure (b) Sensitivity assessment of key parameters in Co-catalyzed aerobic oxidative cyclization of *o*-phenylenediamine with *tert*-butyl isonitrile.

3.2.2 Substrate Scope of *o*-Phenylenediamines and Isonitriles

With the optimized reaction conditions, we move on to investigate a variety of substituted *ortho*-phenylenediamine coupling partners (**4**, **Table 3.2**). This protocol is broadly tolerant of a wide range functional groups including both electron-rich and electron-deficient substrates. Of the *ortho*-phenylenediamines being explored, the reaction didn't show preference for either electron-MHYHHHHdonating or withdrawing substituents. Electron-withdrawing (**4e-4j**), electron-neutral H(**4a, 4b**) and electron-donating (**4c and 4d**) groups all leads to high yields of the benzimidazole products. Similarly, steric influences on the reaction yield are minimal. For example, high yields of benzimidazoles are obtained in the presence of methyl-substitution in both the 3- and 4-positions of *ortho*-phenylenediamine. Furthermore, functional groups such as a 4-*tert*-butyl (**4c**) or naphthalene (**4m**) are also well tolerated.

Table 3.2. Scope of *ortho*-Phenylenediamine and Isonitrile Coupling Partners[a]

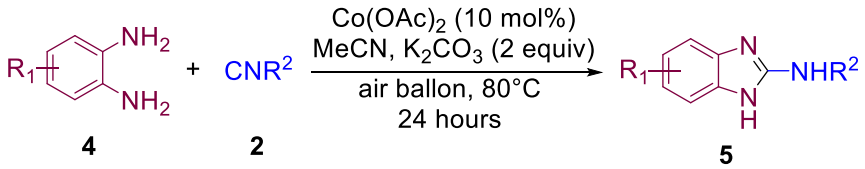

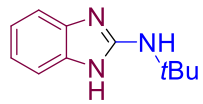

5a, 95%

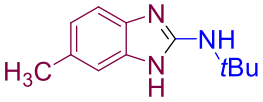

5b, 96%

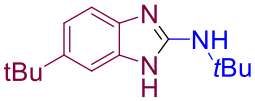

5c, 93%

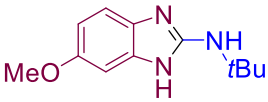

5d, 63%

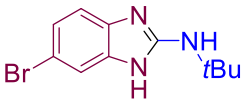

5e, 75%

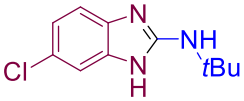

5f, 81%

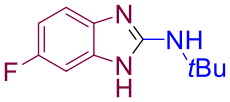

5g, 80%

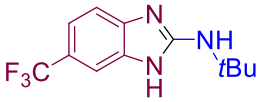

5h, 52%

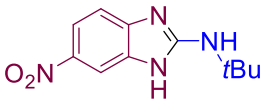

5i, 67%

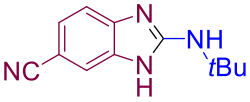

5j, 34% (63%)[b]

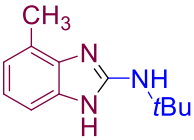

5k, 75%

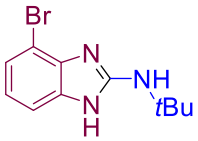

5l, 87%

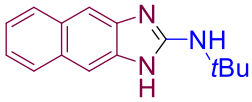

5m, 63%

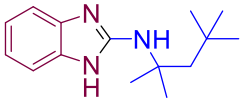

5n, 84%

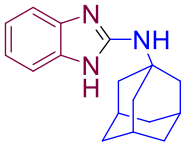

5o, 78%

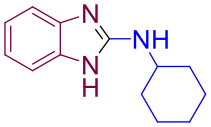

5p, 62%

[a]Isolated Yields. Reaction conditions: **4** (0.3 mmol), **5** (0.3 mmol), K_2CO_3 (0.6 mmol), $Co(OAc)_2$ (10 mol%) in MeCN (3 mL), at 80 °C with an air balloon for 24 h. [b]Yield in parentheses determined by ^{1}H NMR spectroscopy.

In addition to substituted ortho-phenylenediamine coupling partners, various isonitirle coupling partners (**2**) were also explored. Bulky aliphatic substituents, such as tert-butyl,

neopenthyl and admantyl groups delivered the most efficient product formation (**5a, 5n. 5o**). In contrast, less bulky n-pentyl isonitirle undergoes multiple isonitrile insertion steps to generate the corresponding diamino quinoxazoline product (**6**) in 25% yield (**Scheme 3.3**).

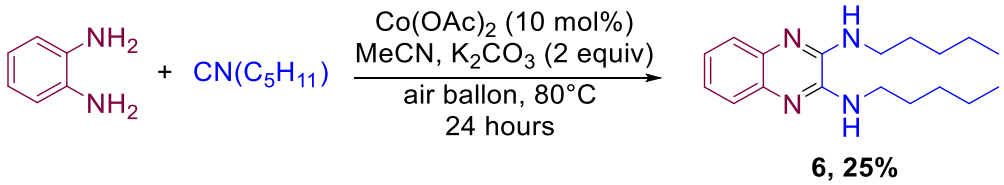

Scheme 3.3. Synthesis of *N*-subsittuted diamino quinoxazoline.

A similar behavior was observed when 2,6-di-methyl phenyl isonitrile was employed as a coupling partner. Different from the case above where the product was generated exclusively from double insertion of isonitrile in this reaction, a complicated compound resulting from triple-insertion of the isonitrile was also found to be one of the major products (**Table 3.3c**). We also explored other isonitrile and diamine coupling partners for this chemical transformation (**Table 3.3**). Isonitirles that had proceeded smoothly with *ortho*-aminophenol coupling partners in our previous study unfortunately revealed to be ineffective in this aerobic cyclization reaction. For example, the oxidative cyclization product was not observed when isopropyl isonitrile was employed as the coupling partner. Interestingly, a product resulting from benzylic oxidation was detected as the major product in the reaction where benzyl isonitirle was used; however, this oxygenation was not observed in the aerobic oxidative cyclization of *ortho*-aminophenol with benzyl isonitrile, indicating the reaction might be operating via a distinct oxidation pathway (**Table 3.3c**). Additionally, we also included a fused-ring system and a heteroaromatic ring in our substrate scope investigation. Unfortunately we found that our system is not tolerant of the fused 2-naphthyl isocyanide. Heterocyclic-based diamines were also shown to be unsuccessful in delievering the desired products in our aerobic system. Both 2,3-diamopyridine and 3,4-diaminopyridine didn't undergo oxidative cyclization with *tert*-butyl isonitrile under our standard reaction conditions (**Table 3.3b**), probably due to the irreversible binding of pyridine substrates to the cobalt catalyst, leading to catalyst deactivation.

Table 3.3. Unsuccesful Isonitrile and Diamine Coupling Partners

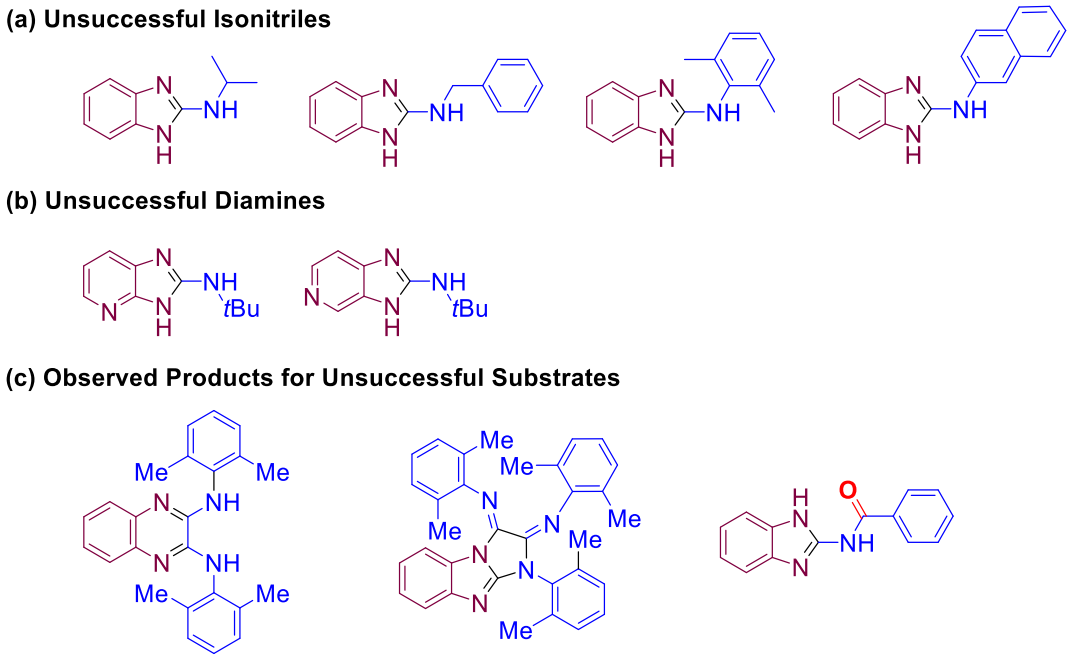

We also explored the reactivity of N-substituted ortho-phenylenediamine coupling partners, the reaction of *N*-methyl- and *N*-phenyl-substituted *ortho*-phenylenediamines (**5q** and **5r**) allow access to the corresponding *N*-subsituted 2-aminobenzimidazoles in moderate yields (**Scheme 3.4**).

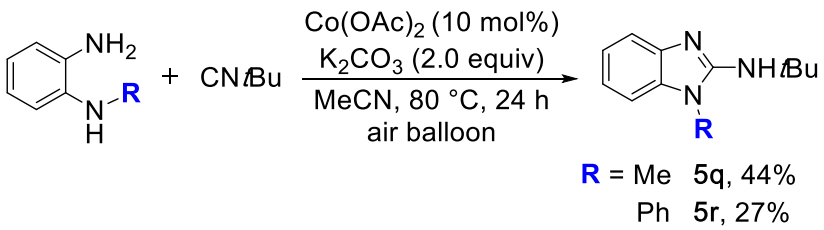

Scheme 3.4. Synthesis of *N*-substituted 2-aminobenzimidazoles.

3.2.3. Application of the Cobalt-Catalyzed Oxidative Cyclization of *o*-Phenylenediamines with Isonitriles

Next, we sought to explore the utilization of this cobalt-catalyzed method to access the unsubstituted 2-aminobenzimidazoles. These compounds are convenient precursors to access a

variety of substituted benzimidazoles readily available as synthetic intermediates or pharmaceutically important drug targets. For example, studies have shown this compound to be an intermediate in the synthesis of biologically active small molecules such as mebendazole (**Scheme 3.5a**)[128] and enviroxime (**Scheme 3.5b**).[129] It also allows access to unique fused heterocyclic structures when treated with aryl sulfonyl chlorides (**Scheme 3.5c)**[130] or oximes (**Scheme 3.5d**).[131] Finally, treating unsubstituted 2-aminobenzimidazole with triphenylphosphine dibromide generates iminophosphoranes, a versatile structure for heterocyclic synthesis (**Scheme 3.5e**).[132]

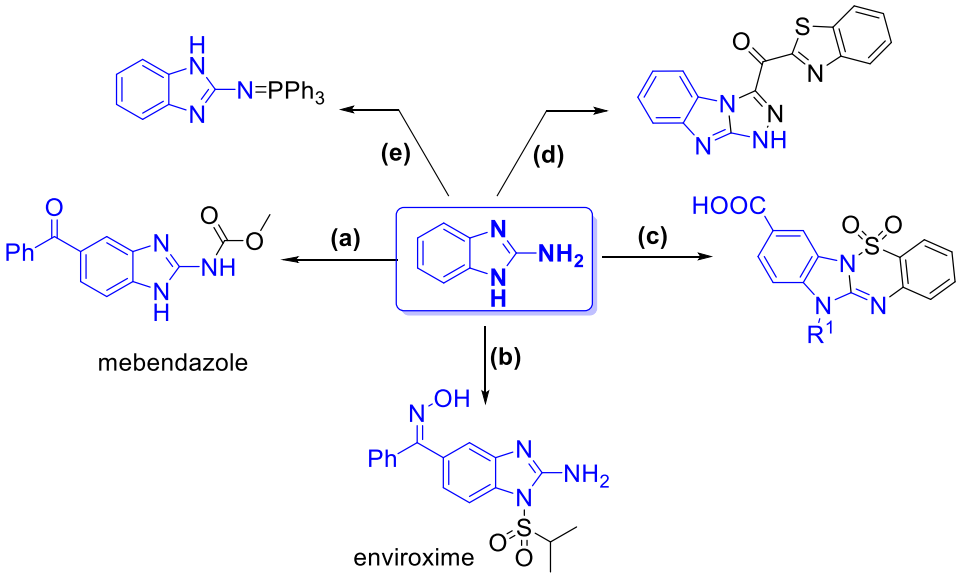

Scheme 3.5. Application of unsubstituted 2-aminobenzimidazoles in pharmaceutical-related synthesis. (a) methyl chloroformate and base[128] (b) isopropylsulfonyl chloride, base and reflux[132] (c) sulfonyl chloride/Cu catalyst then Pd catalyst[130] (d) hydroximoyl chloride and reflux[131] (e) Ph_3PBr_2 and base[132]

Thus, we sought to enable the efficient access to the unsubstituted 2-aminobenzimidazole **5s**. Researchers in other groups have shown the N-tert-butyl benzimidazole to undergo selective dealkylation upon treatment with a strong acid.[57] Based on this precedent, we designed a convenient sequence for facile access to 2-aminobenzimidazole from *ortho*-phenylenediamine and the readily available tert-butyl isonitrile. Upon accomplishment of the reaction under standard condition, the resulting crude product **5a** was treated directly with a strong acid under reflux conditions, giving rise to the unsubstituted 2-aminobenzimidazole **5s** in 82% yield (**Scheme 3.6**).

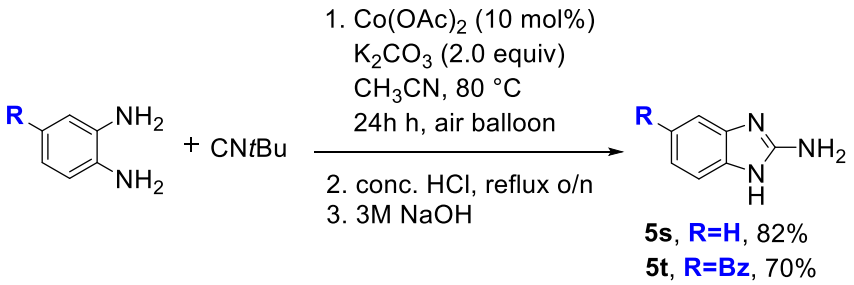

Scheme 3.6. Synthesis of the unsubstituted 2-aminobenzimidazoles **5s** and **5t** via acid-promoted dealkylation.

Finally, we applied this sequence to the synthesis of **5t** (**Scheme 3.6**), an important precursor for accessing antiparasitic small molecule mebendazole and antivirus drug enviroxime. Our method allows access to **5t** in a convenient two-step synthesis from *ortho*-diaminobenzophenone and *tert*-butyl isonitrile in 70% yield. Then we attempted to convert this intermediate to mebendazole by selective acylation of amino group. However, the journey towards this small molecule synthesis led to unexpected challenges. When **5t** was treated with dimethyl dicarbonate and triethylamine under the conventional amino group protection conditions, we didn't observe the generation of mebendazole resulting from the NH_2-functionalization (**Scheme 3.7**). We also attempted the Cu-mediated cross-coupling reaction between 2-amino-5-benzoyl benzimidazole and methyl-chloroformate,[133] and no desired product was detected under the referred reaction condition. More interestingly, when chloroformate was acting as a coupling partner under varied reaction conditions,[134] it consistently generated a mixture of compounds from two distinct N-substitutions (For more details regarding this reaction, see the **Experimental Section 3.4.8**), demonstrating these structural isomers are more thermodynamically favorable under these reaction conditions.

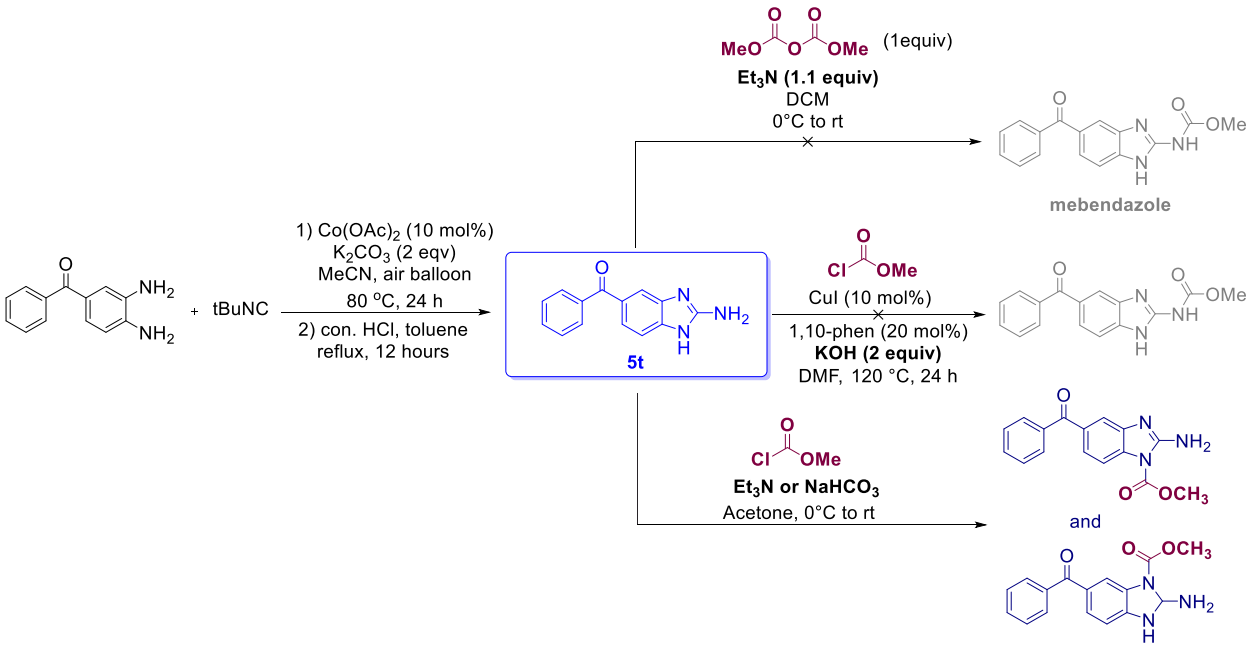

Scheme 3.7. Attempted synthesis of mebendazole from 2-amino-5-benzoyl-1*H*-benzimidazole **5t** under varied reaction conditions.

More endeavors have been made towards a forced base-promoted rearrangement for mebendazole synthesis from the mixture of the structural isomers; however, only starting materials were recovered under the reflux condition for a few hours, suggesting mebendazole isomers are thermodynamically stable and harsher reaction conditions might be required. To track the poor regioselectivity of this transformation, we found support from the literature that the transformation of 2-amino-5-benzoyl benzimidazole to mebendazole can be quite complicated (**Scheme 3.8**).[128] The reaction effectiveness is highly dependent on the choice of solvent and pH value of the reaction mixture. With methyl chloroformate as a coupling partner, the reaction generated exclusively mono-acylated or di-acylated product when acetone or chloroform were employed as a solvent. When the reaction was performed in pH 7.8 environment, a distinct di-acylated product was formed. Although it is suggested mebendazole could be eventually generated through methanolysis (for di-acylated regio-isomer) or base promoted rearrangement (for mono-acylated isomer), we unfortunately didn't generate mebendazole successfully following these protocols. However, we are optimistic that through a thorough tuning of reaction conditions or broad screening, an ideal regioselectivity could be expected, and our protocol of generating 2-aminobenzimidazoles though two-step sequence will provide access to a variety of other 2-aminobenzimidazole substructures that are biologically important.

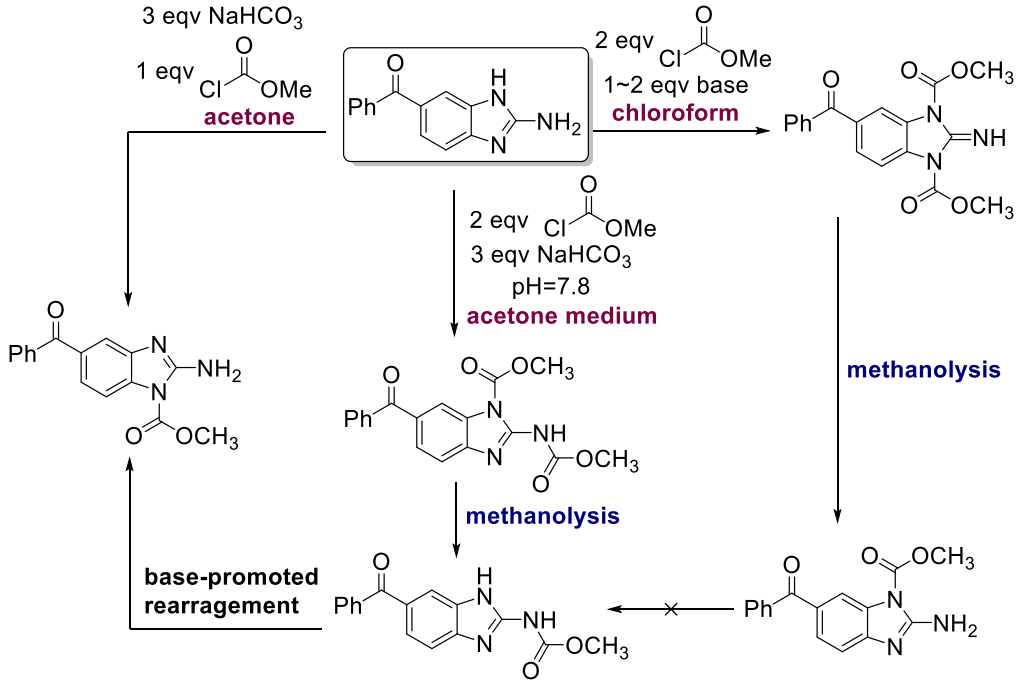

Scheme 3.8. Synthesis of mebendazole from the 2-amino-5-benzoyl benzimidazole in literature.

3.2.4. Radical Trapping Experiments for the Standard Reaction

In our previous studies on the oxidative cyclization of *ortho*-aminophenols with isonitriles,[126] we found the reaction to proceed through a pathway involving initial oxidation of an aminophenol-coordinated cobalt(II) species by O_2 to generate a semiquinoato-type intermediate.[70] Due to the ligand stabilization, these radical intermediates were not trappable with common radical trapping agents. In this study, similarly, no trappable free radicals are observed under the current reaction conditions. When the standard reaction was conducted in the presence of TEMPO, no radical trapped products were obtained, and we observed no significant decrease in the yield of benzimidazole product. Similarly, the incorporation of 1,1-diphenylethylene into the reaction system led to no observation of the radical trapped intermediates. Except for 24% recovery of the starting material, there was no drastic changes in the yield of benzimidazole (**Scheme 3.9**).

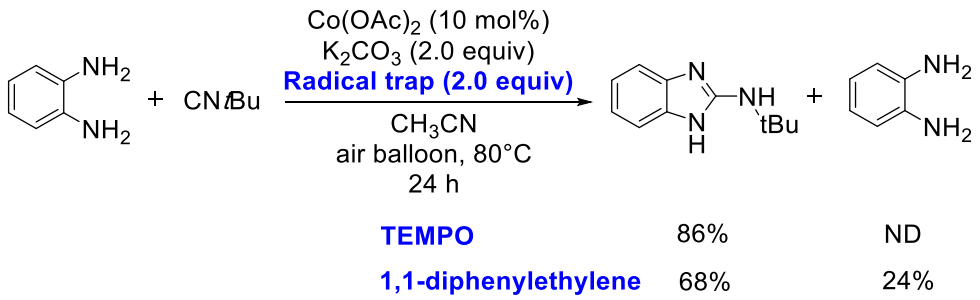

Scheme 3.9. Control experiments with TEMPO and 1,1-diphenylethylene as radical trapping agents.

3.3 Conclusive Summary

In summary, we have described a new cobalt-catalyzed oxidative cyclization of ortho-phenylenediamines with isonitriles to generate the substituted 2-aminobenzimidazoles. This catalytic reaction is efficient under simple and mild ligand-free conditions. It also provides access to the unsubstituted 2-aminobenzimidazoles from an acid-promoted dealkylation of the 2-(tert-butylamino)-benzimidazoles. This route affords structures that can serve as important intermediates in the synthesis of pharmaceutically valuable small molecules.

3.4. Experimental Section

3.4.1. General Considerations

^{1}H, and ^{13}C{^{1}H} NMR spectra were recorded on an Agilent 400 MHz spectrometer or a JEOL 400 MHz spectrometer. Chemical shifts are given in parts per million and referenced to the residual solvent signal;[135] all coupling constants are reported in Hz. High resolution mass spectra were obtained on a Thermo Finnigan Linear Trapping Quadrupole mass spectrometer. IR spectra were recorded on a PerkinElmer (Spectrum 100) FT-IR spectrometer. Column chromatography was performed using Silicycle SiliaFlash P60 silica gel.

Dry solvents were taken from a solvent system which passes the solvent through a column of activated molecular sieves. All deuterated solvents were purchased from Cambridge Isotope

Laboratories. All other chemicals were purchased from commercial sources and used without further purification unless otherwise noted. Air to fill air balloons was obtained from a house compressed air system. O_2 used in control reactions was purchased from Airgas. Both air and O_2 sources were used as received without drying tubes or additional precautions to remove trace water.

3.4.2. Optimization of the Reaction Condition

General Procedure for Screening of Reaction Conditions. *ortho*-Phenylenediamine (32.4 mg, 0.300 mmol) and a cobalt(II) source (0.03 mmol, 10 mol %) were combined in a 6-inch test tube in a N_2 filled glovebox. A base (2 equiv, 0.6 mmol) was added in some instances. Solvent (3 mL) and *tert*-butylisonitrile (35.2 μL, 0.3 mmol) were added and the test tube was sealed with a septum before being removed from the glovebox. Upon removal, an air balloon attached to a needle was inserted through the septum and the reaction mixture was then stirred for 24 hours at 65 or 80 °C in an oil bath. Upon completion, the reaction mixture was cooled to room temperature and passed through a pad of Celite via vacuum filtration. The resulting Celite cake was washed with ethyl acetate (~ 50 mL), the filtrate was collected and concentrated by rotary evaporation to 3 mL, then passed through a silica gel plug Pasteur pipette and rinsed with ethyl acetate (~10 mL). The filtrate was collected and the solvent was removed by rotary evaporation. Dimethyl sulfone (3.00 mg, 0.0318 mmol) was added as an internal standard and the crude mixture was dissolved in DMSO-d_6 for ^{1}H NMR analysis. The reaction yield was determined by ^{1}H NMR spectroscopy.

Table 3.4. Optimization of the cobalt source in the oxidative cyclization of *ortho*-phenylenediamine and *tert*-butylisonitrile.[a]

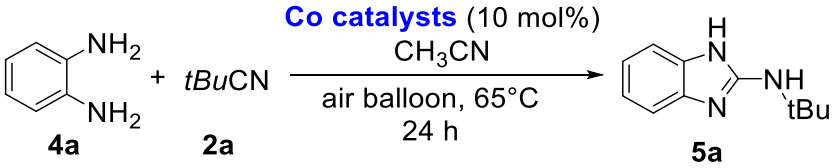

Entry	Co Catalyst	% Yield
1	$CoCO_3$	<5
2	$Co(acac)_2$	41
3	$Co(OAc)_2$	69
4	$CoCl_2$	<5
5	$CoCO_3 \cdot H_2O$	<5

[a]Reaction conditions: **4a** (0.300 mmol), **2a** (0.300 mmol), cobalt catalyst (0.030 mmol), CH_3CN (3.00 mL), with an air balloon at 65 °C for 24 h. The yields of **5a** were determined by ^{1}H NMR spectroscopy with dimethyl sulfone as internal standard (0.0300 mmol).

Table 3.5. Optimization of the solvent in the oxidative cyclization of *ortho*-phenylenediamine and *tert*-butylisonitrile.[a]

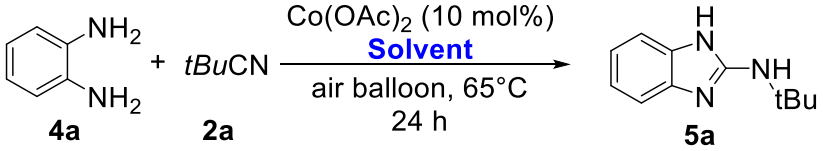

Entry	Solvent	% Yield
1	CH_3CN	69
2	1,4-dioxane	61
3	Me-THF	69
4	THF	54
5	DMF	23

[a]Reaction conditions: **4a** (0.300 mmol), **2a** (0.300 mmol), $Co(OAc)_2$ (0.030 mmol), solvent (3.00 mL), with an air balloon at 65 °C for 24 h. The yields of **5a** were determined by ^{1}H NMR spectroscopy with dimethyl sulfone as internal standard (0.0300 mmol).

Table 3.6. Optimization of the base in the oxidative cyclization of *ortho*-phenylenediamine and *tert*-butylisonitrile.[a]

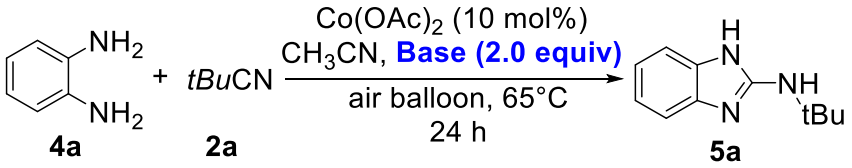

Entry	Base	% Yield
1	LiOAc	65
2	NaOAc	62
3	KOAc	82
4	Li_2CO_3	67
5	Na_2CO_3	79
6	K_2CO_3	85

[a]Reaction conditions: **4a** (0.300 mmol), **2a** (0.300 mmol), $Co(OAc)_2$ (0.030 mmol), CH_3CN (3.00 mL), base (0.600 mmol) with an air balloon at 65 °C for 24 h. The yields of **5a** were determined by ^{1}H NMR spectroscopy with dimethyl sulfone as internal standard (0.0300 mmol).

Table 3.7. Optimization of the temperature in the oxidative cyclization of *ortho*-phenylenediamine and *tert*-butylisonitrile.[a]

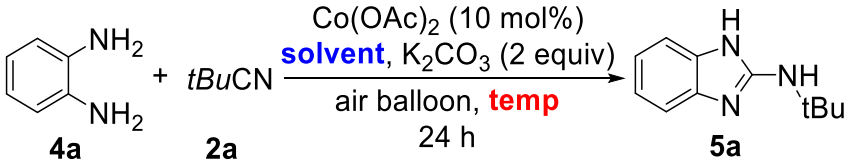

Entry	Solvent	Temp (°C)	% Yield
1	CH_3CN	65	85
2	CH_3CN	80	95
3	Me-THF	80	78

[a]Reaction conditions: **4a** (0.300 mmol), **2a** (0.300 mmol), $Co(OAc)_2$ (0.030 mmol), solvent (3.00 mL), K_2CO_3 (2 equiv) with an air balloon at 65 °C or 80 °C for 24 h. The yields of **5a** were determined by ^{1}H NMR spectroscopy with dimethyl sulfone as internal standard (0.0300 mmol).

3.4.3. Reaction Parameter Assessment

To assess the sensitivity of the reaction to different parameters, a set of control experiments were conducted according to the work reported by Glorius and coworkers.[127] In each experiment only a single parameter is varied while all others are held constant. In our study, the following parameters were varied: oxygen concentration, base loading, catalyst loading, reaction concentration and reaction temperature as described in **Table 3.8** below. Each reaction was conducted according to the standard procedure described below with the exception of the parameter being tested. For each reaction the yield of **5a** was quantified by ^{1}H NMR spectroscopy. The deviation from the standard conditions was calculated in order to provide the visual color-coded radar diagram shown in **Figure 3.4**. For a given parameter, the proximity of the line to the perimeter indicates the significance of the parameter, or the reactions sensitivity to the parameter.

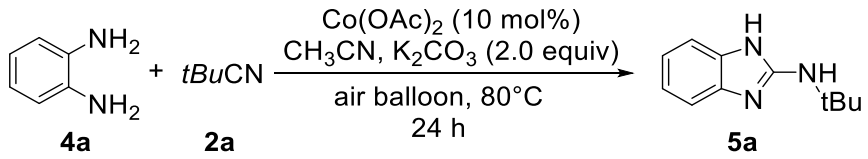

Conditions for reaction parameter assessment. *o*-phenylenediamine (0.3 mmol), *tert*-butyl isocyanide (0.3 mmol), $Co(OAc)_2$ (0.03 mmol), K_2CO_3 (0.6 mmol), MeCN (3 mL), 80 °C, 24 hours. Due to the limited solubility of $Co(OAc)_2$ and K_2CO_3 in MeCN, and volatility of the isonitrile, stock solutions were not prepared. All components of the reaction mixtures with varied parameters were independently weighed. All experiments were set up according to the standard procedure unless otherwise indicated.

Table 3.8. Conditions used for reaction parameter assessment.

Entry	Evaluated Parameter		Reaction prep and setup
1	O_2 content	inert atmosphere	N_2 atmosphere[1]
2		pure O_2 atmosphere	O_2 balloon[2]
3	base	base free	0 equiv of base
4		high base loading	4 equiv of base
5	catalyst	low catalyst loading	5 mol% of $Co(OAc)_2$
6		high catalyst loading	20 mol% of $Co(OAc)_2$
7	concentration	low concentration	with 6.0 mL MeCN
8		high concentration	with 1.5 mL MeCN
9	temperature	low heating temperature	65 °C
10		room temperature	room temperature
11	control	standard reaction conditions	

[1]The reaction was set up in a 25 mL Schlenk tube with Schlenk line technique. See the inert atmosphere procedure below for the detailed description. [2]The reaction was set up in a 25 mL Schlenk tube with an O_2 balloon attached to a needle inserted through the septum. See the O_2 atmosphere procedure below for the detailed description.

Procedure for reaction parameter assessment *ortho*-Phenylenediamine (32.4 mg, 0.300 mmol) and a cobalt(II) acetate (5 mol%, 10 mol % or 20 mol%) were combined in a 6-inch test tube in a N_2 filled glovebox. K_2CO_3 (0 equiv, 2 equiv, or 4 equiv) was added to the same test tube. CH_3CN (1.5 mL, 3 mL or 6 mL) and *tert*-butylisonitrile (35.2 μL, 0.300 mmol) were added and the test tube was sealed with a septum before being removed from the glovebox. Upon removal, an air balloon attached to a needle was inserted through the septum and the reaction mixture was then stirred for 24 hours at room temperature, 65 or 80 °C in an oil bath. Upon completion, the reaction mixture was cooled to room temperature and passed through a pad of Celite via vacuum filtration. The resulting Celite cake was washed with ethyl acetate (~ 50 mL), the filtrate was collected and concentrated by rotary evaporation to 3 mL, then passed through a silica gel plug Pasteur pipette and rinsed with ethyl acetate (~10 mL). The filtrate was collected and the solvent was removed by rotary evaporation. Dimethyl sulfone (3.00 mg, 0.0318 mmol) was added as an internal standard and the crude mixture was dissolved in DMSO-d_6 for ^{1}H NMR analysis. The reaction yield was determined by ^{1}H NMR spectroscopy.

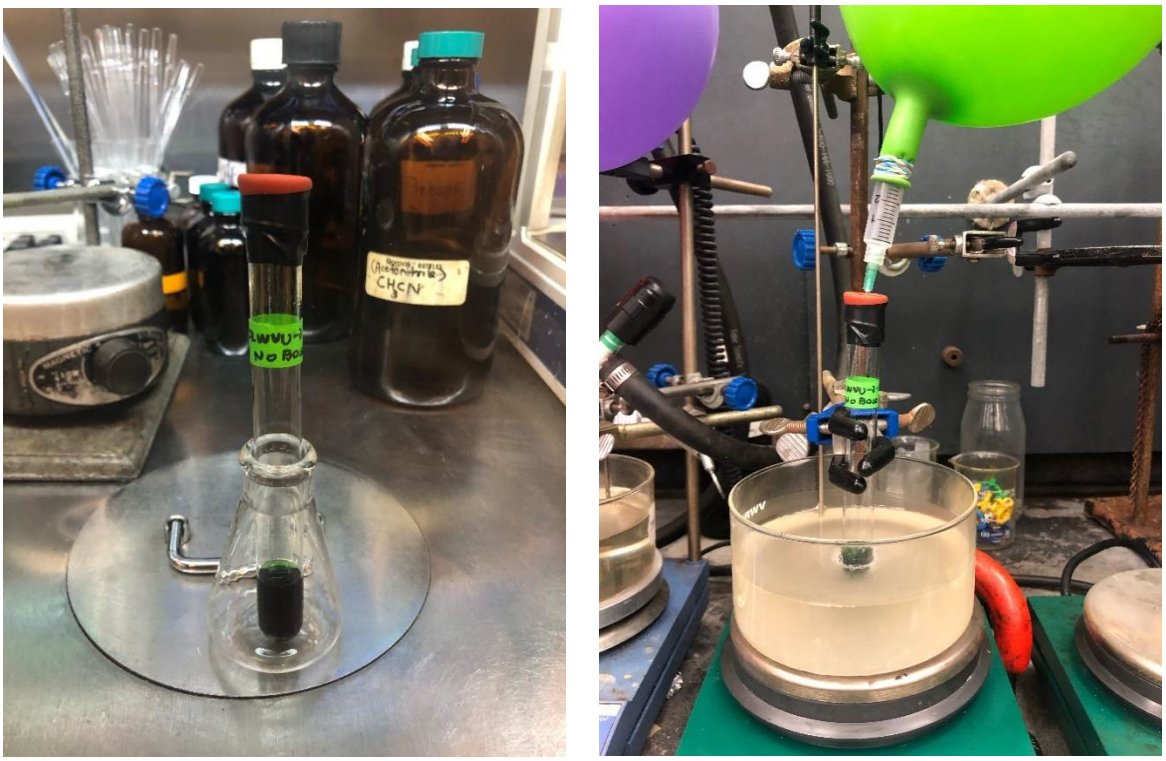

(a) (b)

Figure 3.2. Reaction set up for parameter assessment studies. (a) Preparation of the reaction mixture inside the glovebox. (b) Final reaction setup inside a fume hood with an air balloon.

<u>Procedure for inert atmosphere reaction (Entry 1 in Table 3.8).</u> To a 25 mL Schlenk tube equipped with a stir bar, *ortho*-phenylenediamine (32.4 mg, 0.300 mmol), $Co(OAc)_2$ (5.31mg, 0.0300 mmol), K_2CO_3 (82.9 mg, 0.600 mmol) were combined. The tube was then evacuated and backfilled with N_2 three times. Dry CH_3CN (3 mL) and *tert*-butylisonitrile (35.2 μL, 0.300 mmol) were added under N_2 atmosphere and the reaction mixture was stirred in a 80 °C oil bath for 24 hours. Upon completion, the reaction mixture was cooled to room temperature and passed through a pad of Celite via vacuum filtration. The resulting Celite cake was washed with ethyl acetate (~ 50 mL), the filtrate was collected and concentrated by rotary evaporation to 3 mL, then passed through a silica gel plug Pasteur pipette and rinsed with ethyl acetate (~10 mL). The filtrate was collected and the solvent was removed by rotary evaporation. Dimethyl sulfone (3.00 mg, 0.0318 mmol) was added as an internal standard and the crude mixture was dissolved in DMSO-d_6 for ^{1}H NMR analysis. The reaction yield was determined by ^{1}H NMR spectroscopy.

Procedure for the O_2 atmosphere reaction (Entry 2 in Table 3.8). To a 25 mL Schlenk tube equipped with a stir bar, *ortho*-phenylenediamine (32.4 mg, 0.300 mmol), $Co(OAc)_2$ (5.31mg, 0.0300 mmol), K_2CO_3 (82.9 mg, 0.600 mmol) were combined. The tube was then evacuated and backfilled with O_2 three times using a O_2 balloon. The side arm of the Schlenk tube was sealed and an O_2 balloon attached to a needled was balloon inserted through the septum. Dry CH_3CN (3 mL) and *tert*-butylisonitrile (35.2 μL, 0.300 mmol) were then added and the reaction mixture was stirred in an 80 °C oil bath for 24 hours. Upon completion, the reaction mixture was cooled to room temperature and passed through a pad of Celite via vacuum filtration. The resulting Celite cake was washed with ethyl acetate (~ 50 mL), the filtrate was collected and concentrated by rotary evaporation to 3 mL, then passed through a silica gel plug Pasteur pipette and rinsed with ethyl acetate (~10 mL). The filtrate was collected and the solvent was removed by rotary evaporation. Dimethyl sulfone (3.00 mg, 0.0318 mmol) was added as an internal standard and the crude mixture was dissolved in DMSO-d_6 for ^{1}H NMR analysis. The reaction yield was determined by ^{1}H NMR spectroscopy.

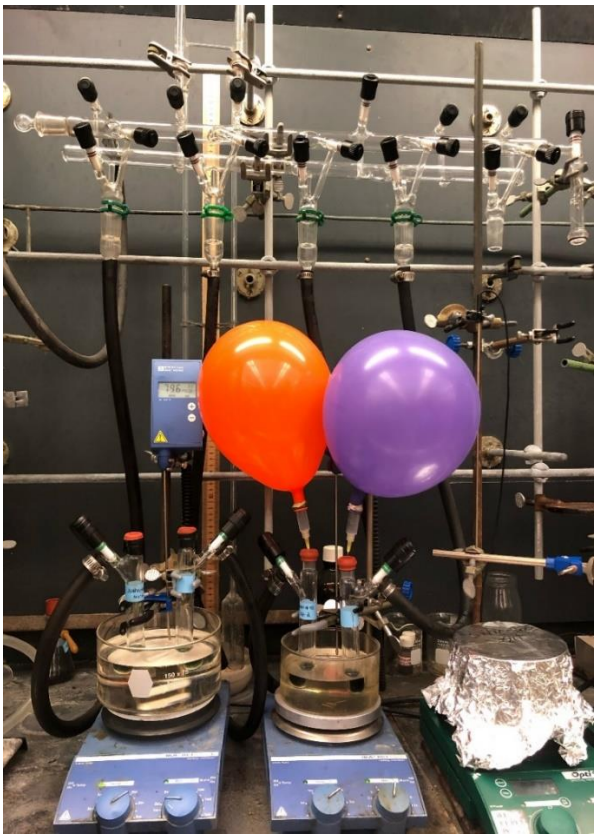

Figure 3.3. Reaction setup under N_2 atmosphere (left side) and O_2 atmosphere (right side, stopcocks are closed).

Table 3.9. Results of Parameter Assessment of the Standard Reaction.

Entry	Evaluated Parameter		Run 1 (%)	Run 2 (%)	Average % Yield	% Deviation
1	O_2 content	inert atmosphere	9	11	10	-89
2		pure O_2 atmosphere	94	97	96	1
3	base	Base free	67	67	67	-29
4		high base loading	92	90	91	-4
5	catalyst	low catalyst loading	67	66	67	-29
6		high catalyst loading	92	92	92	-3
7	concentration	low concentration	86	87	87	-8
8		high concentration	93	89	91	-4
9	temperature	low heating temperature	83	86	85	-11
10		room temperature	37	37	37	-62
11	**control**	**standard reaction condition**	**95**	**95**	**95**	**0**

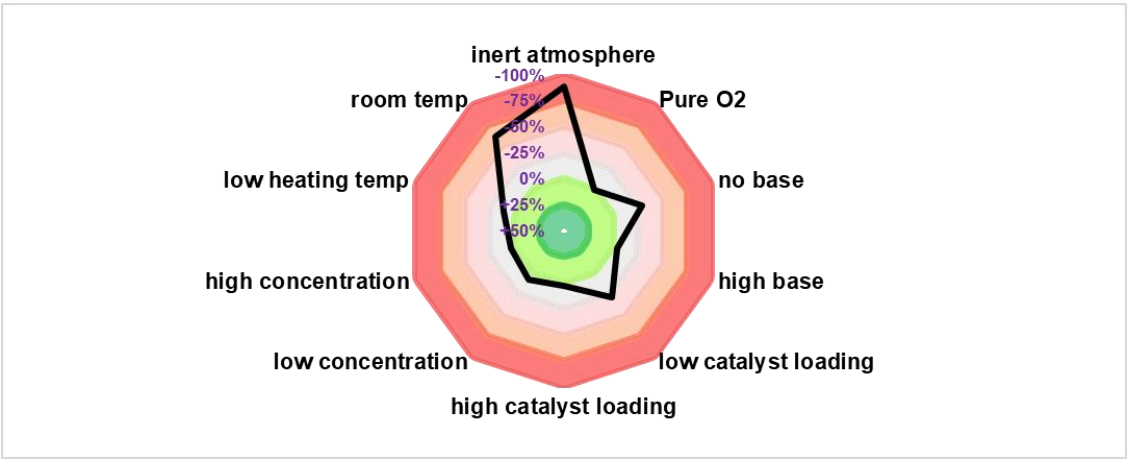

Figure 3.4. Radar diagram generated from parameter assessment data shown in Table 3.9.

The radar diagram indicates the high sensitivity of the standard reaction to an inert atmosphere. Base loading and reaction temperature are also critical factors in influencing the yield of the product **5a**.

3.4.4. Alternative Reaction Setups

Our parameter assessment studies revealed that the standard reaction proceeds efficiently in the presence of a sufficient supply of oxygen. For example, with air as the source of oxygen the reaction yields 95% of **5a**, while with an O_2 balloon 96% yield of **5a** is obtained. Thus, it is possible that the transformation proceeds smoothly in the absence of an air balloon with a headspace filled with air. To test the efficacy of this protocol, we used a sealed 125 mL pressure tube as the vessel for the reaction instead of using our standard 6-inch test tube fitted with an air balloon.

Sealed Reaction Vessel. To a 125 mL pressure tube equipped with a stir bar, *ortho*-phenylenediamine (32.4 mg, 0.300 mmol), $Co(OAc)_2$ (5.31mg, 0.0300 mmol), K_2CO_3 (82.9 mg, 0.600 mmol) were combined in the open air. Dry CH_3CN (3 mL) and *tert*-butylisonitrile (35.2 μL, 0.300 mmol) were added, the pressure tube was sealed and the reaction mixture was stirred in an 80 °C oil bath for 24 hours. Upon completion, the reaction mixture was cooled to room temperature and passed through a pad of Celite via vacuum filtration. The resulting Celite cake was washed with ethyl acetate (~ 50 mL), the filtrate was collected and concentrated by rotary evaporation to 3 mL, then passed through a silica gel plug Pasteur pipette and rinsed with ethyl acetate (~10 mL). The filtrate was collected, and the solvent was removed by rotary evaporation. Dimethyl sulfone (3.00 mg, 0.0318 mmol) was added as an internal standard and the crude mixture was dissolved in DMSO-d_6 for ^{1}H NMR analysis. The reaction gave 95.9% of the desired product indicating the efficiency of the transformation in a sealed vessel with only a headspace of air.

Figure 3.5. Reaction setup using a pressure tube with a headspace filled with air.

The reaction also proceeds smoothly using standard Schlenk technique with reagents stores in a benchtop dessicator without need for a glovebox.

<u>Benchtop Procedure.</u> To an oven-dried 25 mL Schlenk tube equipped with a stir bar, *ortho*-phenylenediamine (32.4 mg, 0.300 mmol), $Co(OAc)_2$ (5.31mg, 0.0300 mmol), K_2CO_3 (82.9 mg, 0.600 mmol) were combined. The tube was connected to the Schlenk line via the sidearm and was evacuated and backfilled with an air balloon three times. The side arm valve was then closed and an air balloon attached to a needle was inserted through the septum. Dry CH_3CN (3 mL) and *tert*-butylisonitrile (35.2 mL, 0.300 mmol) were added and the reaction mixture was stirred in an 80 °C oil bath for 24 hours. Upon completion, the reaction mixture was cooled to room temperature and passed through a pad of Celite via vacuum filtration. The resulting Celite cake was washed with ethyl acetate (~ 50 mL), the filtrate was collected and concentrated by rotary evaporation to 3 mL, then passed through a silica gel plug Pasteur pipette and rinsed with ethyl acetate (~10 mL). The filtrate was collected and the solvent was removed by rotary evaporation. Dimethyl sulfone (3.00 mg, 0.0318 mmol) was added as an internal standard and the crude mixture was dissolved in

DMSO-d_6 for ^{1}H NMR analysis. The reaction yield was determined by ^{1}H NMR spectroscopy to be 95.9% (average of two independent reaction yields).

3.4.5. Synthesis and Characterization of 2-Aminobenzimidazoles (5) and Other Reaction Products (6)

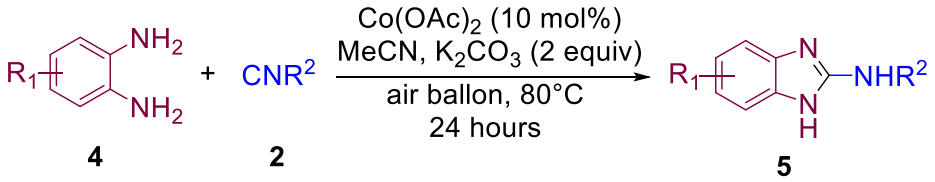

Representative Procedure for the Synthesis of 2-Aminobenzimidazoles (5)

Ortho-phenylenediamine (32.4 mg, 0.300 mmol), $Co(OAc)_2$ (5.31 mg, 0.0300 mmol, 10 mol %), and K_2CO_3 (82.9 mg, 0.600 mmol) were combined in a 6-inch test tube in an N_2 filled glovebox. CH_3CN (3 mL) and *tert*-butylisonitrile (34.2 mL, 0.300 mmol) were added and the test tube was sealed with a septum before being removed from the glovebox. Upon removal, an air balloon attached to a needle was inserted through the septum and the reaction mixture was then stirred for 24 hours at 65 or 80 °C in an oil bath. Upon completion, the reaction mixture was cooled to room temperature and passed through a pad of Celite via vacuum filtration. The resulting Celite cake was washed with ethyl acetate (~ 50 mL), the filtrate was collected and concentrated by rotary evaporation to 3 mL, then passed through a silica gel plug Pasteur pipette and rinsed with ethyl acetate (~10 mL). The solvent was removed by rotary evaporation again. The residue was purified by silica column chromatography (98:2 EtOAc:MeOH). All 2-aminobenzimidazole compounds (**5**) were prepared following the standard procedure unless otherwise noted.

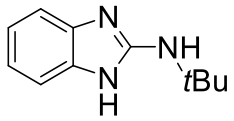

5a

2-(*tert*-butylamino)-benzimidazole (**5a**). The title compound was synthesized according to the standard procedure and purified by silica column chromatography (98:2 EtOAc: MeOH, R_f = 0.20 in 80:15:5 $CHCl_3$: EtOAc: MeOH) to yield 52.6 mg (0.278 mmol, 92.8 % yield) of the title compound as a light-yellow solid (mp = 217-220 ºC). ^{1}H NMR (400 MHz, DMSO-d_6): δ = 10.19 (s, 1H), 7.15 (dd, J = 5.7, 3.2 Hz, 2H), 6.85 (dd, J = 5.7, 3.2 Hz, 2H), 6.18 (s, 1H), 1.42 (s, 9H).

^{13}C NMR (100 MHz, DMSO-d_6): δ = 154.11, 119.05, 111.77, 50.69, 29.09. FTIR (ATR, cm^{-1}): 3428 (w), 3058 (w), 2960 (w), 2868 (w), 2673 (w), 1554 (s), 1481 (m), 1465 (m), 1455 (m), 1414 (m), 1391 (m), 1362 (m), 1265 (m), 1204 (s), 1069 (m), 1008 (m), 923 (m), 865 (m), 839 (m), 760 (m), 734 (s). HRMS (ESI-MS, m/z) $[M+H]^+$ calcd for $C_{11}H_{16}N_3$ 190.1337; found 190.1339. The spectral data are consistent with those reported in the literature.[57]

1.0 Gram Scale Reaction. Upon scaling the reaction, the product yield is reduced, likely due to inefficient gas-liquid mixing. Due to the limited solubility of $Co(OAc)_2$ in CH_3CN under the large scale reaction conditions, a mixed solvent system was used to enhance the solubility of $Co(OAc)_2$. To an oven-dried 250 mL round-bottom flask equipped with a stir bar, *o*-phenylenediamine (1.00g, 9.25 mmol), $Co(OAc)_2$ (163.7mg, 0.925 mmol) and K_2CO_3 (2.56g, 18.5 mmol) were combined. The flask was sealed with a septum under air atmosphere. 125 mL 1:1 ratio of mixed solvent H_2O: CH_3CN was added. With stirring, *tert*-butyl isocyanide (1.05 mL, 9.25 mmol) was added dropwise. The reaction mixture was allowed to stir in an 80 °C oil bath for 48 hours under aerobic atmosphere with two air balloons inserted through the septum. Upon completion of the reaction, the reaction mixture was cooled down to room temperature and CH_3CN were removed via rotary evaporation. The remaining mixture was partitioned in 100 mL ethyl acetate and stirred with 3 M EDTA (100 mL) up to 12 hours. The aqueous layer was separated and extracted with ethyl acetate (2 × 50 mL). The combined organic phase was washed with brine, separated, dried over anhydrous $MgSO_4$, filtered and concentrated via rotary evaporation to generate the crude product as a dark brown solid. The product was purified by column chromatography (gradient elution from pure chloroform to 97:3 $CHCl_3$: MeOH) to yield 377 mg (1.99 mmol, 21.5%) of the desired product as a brown solid.

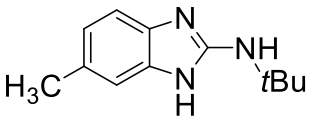

5b

2-(*tert*-butylamino)-5-methylbenzimidazole (**5b**). The title compound was synthesized according to the standard procedure and purified by silica column chromatography (97:1:2 $CHCl_3$: MeOH: Et_3N, R_f = 0.2 in the same solvent) to yield 58.8 mg (0.289 mmol, 96.4 % yield) of the title compound as a brown oil. ^{1}H NMR (400 MHz, $CDCl_3$): δ = 10.64 (s, 1H), 7.17 (d, *J* = 7.9 Hz, 1H), 7.10 (s, 1H), 6.84 (d, *J* = 7.9 Hz, 1H), 5.64 (s, 1H), 2.35 (s, 3H), 1.37 (s, 9H). ^{13}C NMR (100

MHz, $CDCl_3$): δ = 153.81, 136.91, 134.85, 130.50, 121.82, 112.40, 111.75, 51.78, 29.58, 21.61. FTIR (ATR, cm^{-1}): 3277 (w), 2969 (w), 1634 (m), 1596 (m), 1568 (s), 1488 (m), 1459 (m), 1392 (m), 1364 (m), 1273 (m), 1215 (s), 1143 (w), 1034 (w), 956 (w), 938 (w), 861 (w), 802 (m), 750 (s), 665 (s). HRMS (ESI-MS, m/z) $[M+H]^+$ calcd for $C_{12}H_{18}N_3$ 204.1494; found 204.1495. The spectral data are consistent with those reported in the literature.[57]

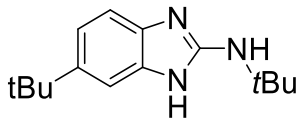

5c

2-(*tert*-butylamino)-5-tert-butylbenzimidazole (**5c**). The title compound was synthesized according to the standard procedure and purified by silica column chromatography (95:2:3 EtOAc: MeOH: Et_3N, R_f = 0.5 in 98:2 EtOAc: MeOH) to yield 68.3 mg (0.278 mmol, 92.6 % yield) of the title compound as a dark brown oil. ^1H NMR (400 MHz, $CDCl_3$): δ = 8.76 (s, 1H), 7.35 (s, 1H), 7.22 (d, *J* = 7.9 Hz, 1H), 7.08 (d, *J* = 7.4 Hz, 1H), 5.29 (s, 1H), 1.40 (s, 9H), 1.32 (s, 9H).^{13}C NMR (100 MHz, $CDCl_3$): δ = 154.57, 143.75, 137.61, 135.61, 117.80, 111.45, 109.01, 51.51, 34.68, 32.01, 29.61. FTIR (ATR, cm^{-1}): 3393 (w), 3310 (w), 3086 (w), 2961 (m), 2867 (m), 1636 (m), 1596 (m), 1567 (s), 1486 (m), 1435 (m), 1391 (m), 1273 (m), 1216 (s), 1134 (w), 1086 (w), 1050 (w), 1024 (m), 934 (w), 870 (w), 811 (m), 752 (s). HRMS (ESI-MS, m/z) $[M+H]^+$ calcd for $C_{15}H_{24}N_3$ 246.1964; found 246.1965.

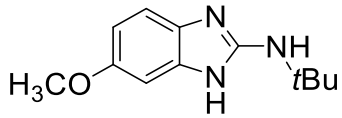

2-(*tert*-butylamino)-5-methoxybenzimidazole (**5d**). The title compound was synthesized according to the standard procedure and purified by silica column chromatography (100:20:10 $CHCl_3$: EtOAc: MeOH, R_f = 0.15 in the same solvent system) to yield 41.3 mg (0.188 mmol, 62.8% yield) of the title compound as a brown oil. ^1H NMR (400 MHz, $CDCl_3$): δ = 8.85 (s, 1H), 7.16 (d, *J* = 7.7 Hz, 1H), 6.87 (s, 1H), 6.63 (d, *J* = 7.6 Hz, 1H), 6.17 (s, 1H), 3.72 (s, 3H), 1.39 (s, 9H). ^{13}C NMR (100 MHz, $CDCl_3$): δ = 155.58, 153.08, 136.61, 129.61, 112.09, 108.63, 97.69, 56.03, 52.06, 29.52. FTIR (ATR, cm^{-1}): 3299 (w), 3085 (w), 2964 (m), 1636 (m), 1601 (m), 1567 (s), 1486 (s), 1446 (s), 1391 (m), 1364 (m), 1302 (m), 1261 (m), 1194 (s), 1152 (s), 1024 (s), 958 (m), 788 (s).

HRMS (ESI-MS, m/z) $[M+H]^+$ calcd for $C_{12}H_{18}N_3O$ 220.1443; found 220.1444. The spectral data are consistent with those reported in the literature.[57]

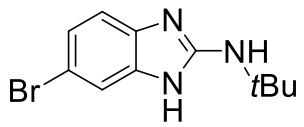

5e

2-(*tert*-butylamino)-5-bromobenzimidazole (**5e**). The title compound was synthesized according to the standard procedure and purified by silica column chromatography (95:2:3 EtOAc: MeOH: Et_3N, R_f = 0.7 in 98:2 EtOAc: MeOH) to yield 63.0 mg (0.226 mmol, 75.4 % yield) of the title compound as a yellow brown solid (mp = 152-155 °C). ^{1}H NMR (400 MHz, $CDCl_3$): δ = 8.73 (s, 1H), 7.37 (s, 1H), 7.08 (s, 2H), 5.26 (s, 1H), 1.41 (s, 9H). ^{13}C NMR (100 MHz, $CDCl_3$): δ = 154.72, 139.63, 136.62, 123.07, 115.24, 112.95, 51.71, 29.55. FTIR (ATR, cm^{-1}): 3322 (w), 3073 (w), 2967 (m), 1630 (m), 1592 (m), 1565 (s), 1462 (s), 1392 (m), 1365 (m), 1341 (w), 1267 (m), 1215 (s), 1048 (m), 1023 (m), 1006 (m), 950 (m), 908 (m), 852 (w), 801 (m), 753 (m), 677 (m). HRMS (ESI-MS, m/z) $[M+H]^+$ calcd for $C_{11}H_{15}N_3Br$ 268.0452; found 268.0444. The spectral data are consistent with those reported in the literature. [57]

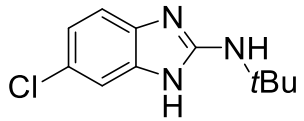

5f

2-(*tert*-butylamino)-5-chlorobenzimidazole (5f). The title compound was synthesized according to the standard procedure and purified by silica column chromatography (98:2:0.3 $CHCl_3$: MeOH: Et_3N, R_f = 0.5 in 96:4:0.3 $CHCl_3$: MeOH: Et_3N) to yield 54.5 mg (0.244 mmol, 81.2 % yield) of the title compound as a dark yellow solid (mp = 178-181 °C). ^{1}H NMR (400 MHz, DMSO-d_6): δ = 7.17 (s, 1H), 7.12 (d, J = 8.2 Hz, 1H), 6.85 (d, J = 8.1 Hz, 1H), 6.47 (s, 1H), 1.40 (s, 9H). ^{13}C NMR (100 MHz, DMSO-d_6): δ =154.92, 123.30, 118.63, 111.90, 50.77, 28.94. FTIR (ATR, cm^{-1}): 3441 (w), 3074 (w), 2975 (w), 1634 (m), 1595 (s), 1567 (s), 1467 (s), 1441 (s), 1392 (m), 1364 (m), 1269 (m), 1213 (s), 1060 (s), 953 (m), 924 (m), 859 (m), 792 (s), 696 (s). HRMS (ESI-MS, m/z) $[M+H]^+$ calcd for $C_{11}H_{15}ClN_3$ 226.0920, found 226.0922. The spectral data are consistent with those reported in the literature.[57]

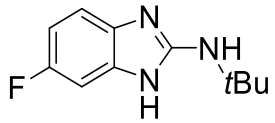

5g

2-(*tert*-butylamino)-5-fluorobenzimidazole (5g). The title compound was synthesized according to the standard procedure and purified by silica column chromatography (98:2:0.3 $CHCl_3$: MeOH: Et_3N, R_f = 0.5 in 96:4:0.3 $CHCl_3$: MeOH: Et_3N) to yield 50.0 mg (0.241 mmol, 80.4 % yield) of the title compound as a beige solid (mp = 203-205 °C). ^{1}H NMR (400 MHz, DMSO-d_6): δ = 7.05 (dd, J = 8.2, 5.0 Hz, 1H), 6.92 (d, J = 9.8 Hz, 1H), 6.61 (t, J = 9.2 Hz, 1H), 6.39 (s, 1H), 1.37 (s, 9H). ^{13}C NMR (100 MHz, DMSO-d_6): δ =158.55, 156.26, 155.03, 110.65, 105.47, 105.23, 99.36, 50.75, 28.97. ^{19}F NMR (376 MHz, DMSO-d_6): δ = -124.51 (s, 1F). FTIR (ATR, cm^{-1}): 3439 (w), 3066 (w), 2979 (w), 2928 (w), 2856 (w), 1637 (m), 1581 (s), 1562 (s), 1486 (s), 1452 (s), 1403 (s), 1284 (m), 1254 (m), 1206 (s), 1139 (s), 1105 (m), 1068 (m), 968 (m), 947 (m), 836 (s), 791 (s), 714 (s). HRMS (ESI-MS, m/z) $[M+H]^+$ calcd for $C_{11}H_{15}FN_3$ 209.1278, found 209.1273. The spectral data are consistent with those reported in the literature.[57]

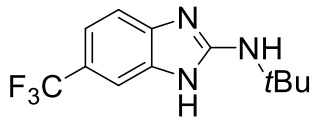

5h

2-(*tert*-butylamino)-5-trifluoromethylbenzimidazole (5h). The title compound was synthesized according to the standard procedure and purified by silica column chromatography (98:2:0.3 $CHCl_3$: MeOH: Et_3N, R_f = 0.4 in 96:4:0.3 $CHCl_3$: MeOH: Et_3N) to yield 40.2 mg (0.156 mmol, 52.1 % yield) of the title compound as a dark yellow solid (mp = 166-168 °C). ^{1}H NMR (400 MHz, CD_3OD): δ = 7.44 (s, 1H), 7.27 (d, J = 8.2 Hz, 1H), 7.21 (d, J = 8.3 Hz, 1H), 1.45 (s, 9H). ^{13}C NMR (100 MHz, Methanol-d_4): δ =156.85, 126.79 (q, J = 269 Hz), 123.14 (q, J = 32 Hz), 118.18 (q, J =4.0 Hz), 115.71, 112.38, 109.77, 52.15, 29.52. ^{19}F NMR (376 MHz, Methanol-d_4): δ = -61.82 (s, 3F). FTIR (ATR, cm^{-1}): 3405 (w), 3082 (w), 2974 (w), 2936 (w), 1637 (m), 1575 (s), 1447 (m), 1366 (m), 1325 (s), 1217 (m), 1159 (m), 1112 (s), 1051 (m), 953 (w), 929 (w), 873 (w), 815 (w), 729 w), 666 (w). HRMS (ESI-MS, m/z) $[M+H]^+$ calcd for $C_{12}H_{15}F_3N_3$ calcd for 259.1246, found 259.1239.

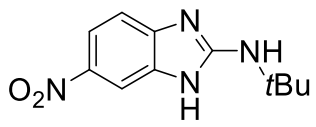

5i

2-(*tert*-butylamino)-5-nitrobenzimidazole (**5i**). The title compound was synthesized according to the standard procedure and purified by silica column chromatography (96:4:0.3 $CHCl_3$: MeOH: Et_3N, R_f = 0.10 in the same solvent system) to yield 47.1 mg (0.201 mmol, 67.0 % yield) of the title compound as a bright yellow solid (mp = 147-149 °C). ^{1}H NMR (400 MHz, CD_3OD): δ = 8.05 (s, 1H), 7.98 – 7.90 (m, 1H), 7.88 (s, 1H), 7.24 (d, *J* = 8.7 Hz, 1H), 1.48 (s, 9H). ^{13}C NMR (100 MHz, CD_3OD): δ = 158.24, 142.63, 118.12, 112.17, 107.87, 52.39, 29.42. FTIR (ATR, cm^{-1}): 3362 (m), 2968 (m), 2214 (w), 1635 (s), 1602 (s), 1572 (s), 1504 (m), 1470 (s), 1437 (m), 1416 (m), 1392 (m), 1360 (m), 1280 (s), 1258 (s), 1211 (s), 1121 (s), 1048 (s), 932 (s), 871 (s), 809 (m), 729 (s), 687 (s), 662 (s). HRMS (ESI-MS, m/z) $[M+H]^+$ calcd for $C_{11}H_{15}N_4O_2$ 235.1191; found 235.1190. The spectral data are consistent with those reported in the literature.[57]

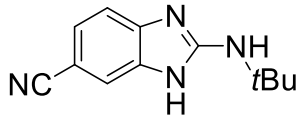

5j

2-(*tert*-butylamino)-5-cyanobenzimidazole (**5j**). The title compound was synthesized according to the standard procedure and purified by silica column chromatography (100:2:0.3 $CHCl_3$: MeOH: Et_3N, R_f = 0.1 in $CHCl_3$: MeOH: Et_3N= 96:4:0.3) to yield 22.1 mg (0.103 mmol, 34.3 % yield) of the title compound as a light brown solid (mp = 185-188 °C). ^{1}H NMR (400 MHz, CD_3OD): δ = 7.50 (s, 1H), 7.31 (d, *J* = 0.8 Hz, 2H), 1.48 (s, 9H). ^{13}C NMR (100 MHz, CD_3OD): δ = 157.06, 143.21, 138.58, 125.91, 121.56, 115.93, 113.49, 103.08, 52.38, 29.43. FTIR (ATR, cm^{-1}): 3331(m), 2969 (m), 2931 (m), 2216 (m), 1632 (s), 1591 (s), 1566 (s), 1467 (s), 1445 (s), 1392 (m), 1364 (m), 1281 (s), 1216 (s), 1120 (m), 1055 (m), 959 (m), 938 (m), 866 (m), 811 (s), 755 (m). HRMS (ESI-MS, m/z) $[M+H]^+$ calcd for $C_{12}H_{15}N_4$ 215.1292; found 215.1291. The spectral data are consistent with those reported in the literature.[57]

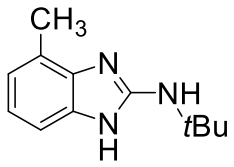

5k

2-(*tert*-butylamino)-4-methylbenzimidazole (**5k**). The title compound was synthesized according to the standard procedure and purified by silica column chromatography (97:1:2 $CHCl_3$: MeOH: Et_3N, R_f = 0.15 in the same solvent system) to yield 45.7 mg (0.225 mmol, 74.9 % yield) of the title compound as a dark brown solid (mp = 146-148 °C). ^{1}H NMR (400 MHz, $CDCl_3$): δ = 9.69 (s, 1H), 7.21 (d, *J* = 7.7 Hz, 1H), 6.95 (t, *J* = 7.6 Hz, 1H), 6.86 (d, *J* = 7.4 Hz, 1H), 5.38 (s, 1H), 2.41 (s, 3H), 1.40 (s, 9H). ^{13}C NMR (100 MHz, $CDCl_3$): δ = 154.02, 139.55, 134.15, 121.56, 120.87, 120.59, 111.28, 51.69, 29.73, 17.00. FTIR (ATR, cm^{-1}): 3386 (w), 3060 (w), 2968 (m), 2163 (w), 2050 (w), 1981 (w), 1627 (s), 1610 (s), 1563 (s), 1491 (m), 1457 (s), 1391 (m), 1363 (s), 1273 (s), 1216 (s), 1160 (m), 1085 (m), 1033 (m), 948 (m), 866 (w), 776 (s), 739 (s). HRMS (ESI-MS, m/z) $[M+H]^+$ calcd for $C_{12}H_{18}N_3$ 204.1495; found 204.1495. The spectral data are consistent with those reported in the literature.[57]

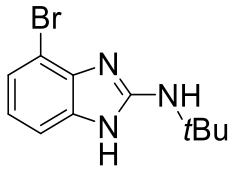

5l

2-(*tert*-butylamino)-7-bromobenzimidazole (**5l**). The title compound was synthesized according to the standard procedure and purified by silica column chromatography (96: 4: 0.3 $CHCl_3$: MeOH: Et_3N, R_f = 0.15 in the same solvent system) to yield 70.3 mg (0.262 mmol, 87.4 % yield) of the title compound as a dark brown solid (mp = 158-160 °C). ^{1}H NMR (400 MHz, $CDCl_3$): δ = 9.57 (s, 1H), 7.25 (d, *J* = 7.2 Hz, 1H), 7.16 (d, *J* = 7.8 Hz, 1H), 6.90 (t, *J* = 7.8 Hz, 1H), 5.22 (s, 1H), 1.40 (s, 9H). ^{13}C NMR (100 MHz, $CDCl_3$): δ = 154.11, 140.10, 135.88, 123.22, 121.93, 112.40, 103.94, 51.95, 29.78. FTIR (ATR, cm^{-1}): 3394 (w), 2968 (m), 1628 (m), 1586 (s), 1565 (s), 1459 (m), 1433 (s), 1392 (m), 1364 (s), 1268 (s), 1214 (s), 1182 (s), 1138 (m), 1044 (m), 930 (m), 77 (s), 730 (s). HRMS (ESI-MS, m/z) $[M+H]^+$ calcd for $C_{11}H_{15}N_3Br$ 268.0448; found 268.0444.

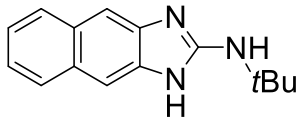

5m

2-(*tert*-butylamino)-naphtho[2,3-d]imidazole (5m). The title compound was synthesized according to the standard procedure and purified by silica column chromatography (80:15:5 $CHCl_3$: EtOAc: MeOH, R_f = 0.15 in the same solvent system) to yield 45.3 mg (0.189 mmol, 63.1% yield) of the title compound as a dark brown solid (mp = 100-102 °C). ^{1}H NMR (400 MHz, $CDCl_3$): δ = 9.76 (s, 1H), 7.73 (d, *J* = 2.4 Hz, 2H), 7.63 (s, 2H), 7.29 (d, *J* = 2.9 Hz, 2H), 6.31 (s, 1H), 1.42 (s, 9H). ^{13}C NMR (100 MHz, $CDCl_3$): δ = 155.83, 137.49, 130.04, 127.39, 123.54, 107.57, 52.10, 29.50. FTIR (ATR, cm^{-1}): 3386 (w), 3054 (w), 2968 (m), 2930 (w), 1651 (m), 1601 (s), 1567 (s), 1463 (m), 1447 (s), 1425 (s), 1392 (m), 1334 (m), 1260 (s), 1207 (s), 1113 (m), 1058 (w), 1034 (w), 944 (m), 852 (s), 783 (m), 742 (s). HRMS (ESI-MS, m/z) $[M+H]^+$ calcd for $C_{15}H_{18}N_3$ 240.1494; found 240.1495.

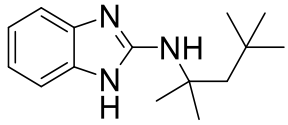

5n

2-(1,1,3,3-tetramethylbutylamino)benzimidazole (**5n**). The title compound was synthesized according to the standard procedure and purified by silica column chromatography (96: 4: 0.3 $CHCl_3$: MeOH: Et_3N, R_f = 0.15 in the same solvent system to yield 61.8 mg (0.252 mmol, 84.0 % yield) of the title compound as a dark brown solid (mp = 143-146 °C). ^{1}H NMR (400 MHz, $CDCl_3$): δ = 10.71 = (s, 1H), 7.31 (s, 2H), 7.04 (s, 2H), 5.47 (s, 1H), 1.73 (s, 2H), 1.48 (s, 6H), 0.90 (s, 9H). ^{13}C NMR (100 MHz, $CDCl_3$): δ = 153.61, 136.83, 120.85, 112.09, 55.66, 52.67, 31.69, 31.56, 29.82. FTIR (ATR, cm^{-1}): 3394 (w), 3060 (w), 2951 (m), 1629 (m), 1599 (m), 1564 (s), 1462 (s), 1421 (m), 1386 (m), 1364 (m), 1271 (m), 1247 (m), 1222 (s), 1150 (m), 1060 (w), 1008 (m), 955 (w), 800 (w), 735 (s). HRMS (ESI-MS, m/z) $[M+H]^+$ calcd for $C_{15}H_{24}N_3$ 246.1964; found 246.1965.

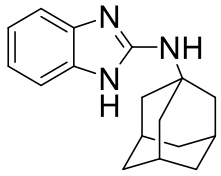

5o

2-(1-admantylamino)benzimidazole (**5o**). The title compound was synthesized according to the standard procedure and purified by silica column chromatography (95:2:3 EtOAc: MeOH: Et_3N, R_f = 0.4 in 98:2 EtOAc: MeOH) to yield 58.3 mg (0.235 mmol, 78.2% yield) of the title compound as a dark reddish-maroon solid (mp = 220-222 °C). ^{1}H NMR (400 MHz, DMSO-d_6): δ = 10.13 (s, 1H), 7.13 (s, 2H), 6.83 (s, 2H), 6.05 (s, 1H), 2.07 (s, 9H), 1.66 (s, 6H).^{13}C NMR (100 MHz, DMSO): δ = 153.57, 118.97, 111.71, 50.82, 41.61, 36.09, 29.05. FTIR (ATR, cm^{-1}): 3386 (w), 3059 (w), 2904 (s), 2850 (m), 1627 (m), 1600 (m), 1567 (s), 1462 (s), 1398 (w), 1358 (s), 1342 (m), 1264 (s), 1139 (m), 1049 (m), 935 (m), 815 (m), 756 (s), 665 (m). HRMS (ESI-MS, m/z) [M+H]$^+$ calcd for $C_{17}H_{22}N_3$ 268.1807; found 268.1808. The spectral data are consistent with those reported in the literature.[136]

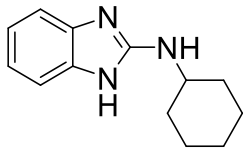

5p

2-(cyclohexylamino)benzimidazole (**5p**). The title compound was synthesized according to the standard procedure and purified by silica column chromatography (97:1:2 $CHCl_3$: MeOH: Et_3N, Rf = 0.15 in the same solvent system) to yield 40.0 mg (0.186 mmol, 61.9 % yield) of the title compound as a yellow oil. ^{1}H NMR (400 MHz, DMSO-d_6): δ = 10.62 (s, 1H), 7.10 (s, 2H), 6.84 (dd, J = 5.3, 2.9 Hz, 2H), 6.56 (d, J = 5.7 Hz, 1H), 3.51 (m, 1H), 1.94 (d, J = 11.1 Hz, 2H), 1.71 (d, J = 12.3 Hz, 2H), 1.59 (d, J = 12.6 Hz, 1H), 1.24 (qd, J = 23.6, 11.8 Hz, 5H). ^{13}C NMR (100 MHz, DMSO-d_6): δ = 154.58, 119.06, 111.38, 50.92, 32.96, 25.37, 24.73. FTIR (ATR, cm^{-1}): 3265 (w), 3056 (w), 2926 (s), 2853 (m), 1665 (m), 1631 (s), 1602 (s), 1577 (s), 1464 (s), 1450 (s), 1402 (m), 1358 (m), 1266 (s), 1213 (m), 1148 (m), 1106 (m), 1024 (m), 890 (m), 810 (m), 738 (s). HRMS (ESI-MS, m/z) [M+H]$^+$ calcd for $C_{13}H_{18}N_3$ 216.1495; found 216.1495. The spectral data are consistent with those reported in the literature.[137]

Synthesis of *N*-Substituted 2-Aminobenzimidazoles (3q and 3r)

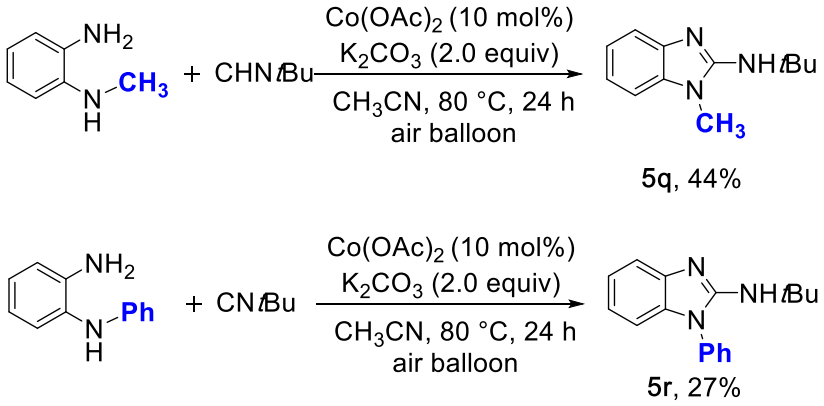

To a 6-inch test tube in an N_2 filled glovebox, *N*-substituted *ortho*-phenylenediamine (0.300 mmol), $Co(OAc)_2$ (5.31mg, 0.0300 mmol), K_2CO_3 (82.9 mg, 0.600 mmol) were combined. CH_3CN (3 mL) and *tert*-butylisonitrile (35.2 □L, 0.300 mmol) was added and the test tube was sealed with a septum before being removed from the glovebox. The reaction mixture was then stirred for 24 hours in an 80 °C oil bath with an air balloon attached to a needle inserted through the septum. Upon completion, the reaction mixture was cooled to room temperature, diluted with 10 mL ethyl acetate and filtered through a pad of Celite. An additional 20 mL of ethyl acetate was used to flush the Celite and the filtrate was concentrated to ~3 mL under vacuum. The resulting concentrate was then passed through a silica gel plug Pasteur pipette and rinsed with ~10 mL ethyl acetate. The solvent was removed by rotary evaporation to generate the crude product as a dark brown solid. Dimethyl sulfone (2.90 mg, 0.03 mmol) was added as an internal standard and the crude mixture was dissolved in DMSO-d_6 for ^{1}H NMR analysis.

***N*-*tert*-butyl-1-methyl-1*H*-benzimidazol-2-amine** (**5q**). ^{1}H NMR (400 MHz, DMSO-d_6): δ = 7.22 (d, *J* = 7.4 Hz, 1H), 7.11 (d, *J* = 7.4 Hz, 1H), 6.91 (p, *J* = 7.5 Hz, 2H), 5.90 (s, 1H), 3.48 (s, 3H), 1.46 (s, 9H). The spectral data is consistent with those reported in the literature.[80]

***N*-*tert*-butyl-1-phenyl-1*H*-benzimidazol-2-amine** (**5r**). ^{1}H NMR (400 MHz, $CDCl_3$): δ = 7.65 – 7.46 (m, 4H), 7.41 (d, *J* = 7.9 Hz, 2H), 7.13 (t, *J* = 7.6 Hz, 1H), 6.98 (t, *J* = 7.6 Hz, 1H), 6.91 (d, *J* = 7.8 Hz, 1H), 4.15 (s, 1H), 1.50 (s, 9H). The spectral data are consistent with those reported in the literature.[138]

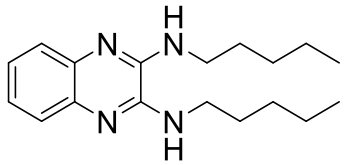

6

***N*²,*N*³-dipentylquinoxaline-2,3-diamine (6).** The title compound was synthesized according to the standard procedure and purified by silica column chromatography (gradient elution from pure hexanes to 6:1 hexanes: ethyl acetate, R_f = 0.55 in 6:1 hexanes: ethyl acetate) to yield 11.5 mg (0.0383 mmol, 25.5% yield) of the title compound as a light brown oil. ^{1}H NMR (400 MHz, $CDCl_3$): δ = 7.67 (dd, *J* = 5.9, 3.5 Hz, 2H), 7.30 (dd, *J* = 6.1, 3.5 Hz, 2H), 4.91 (s, 2H), 3.56 (t, *J* = 7.2 Hz, 4H), 1.84 – 1.56 (m, 4H), 1.49 – 1.29 (m, 9H), 1.26 (s, 2H), 0.91 (t, *J* = 6.8 Hz, 7H), 0.07 (s, 2H). ^{13}C NMR (100 MHz, $CDCl_3$): δ = 144.45, 136.46, 125.35, 124.90, 42.80, 29.49, 29.13, 22.61, 14.15. FTIR (ATR, cm^{-1}): 3341(w), 2956 (m), 2928 (m), 2858 (m), 1649 (w), 1598 (m), 1556 (s), 1505 (s), 1460 (s), 1352 (m), 1330 (m), 1259 (m), 1259 (m), 1214 (s), 1144 (m), 1022 (m), 936 (w), 801 (m), 750 (s), 666 (m). HRMS (ESI-MS, m/z) $[M+H]^+$ calcd for $C_{18}H_{29}N_4$ 301.2387; found 301.2384.

3.4.6. Synthesis of 2-Aminobenzimidazoles (5s and 5t)

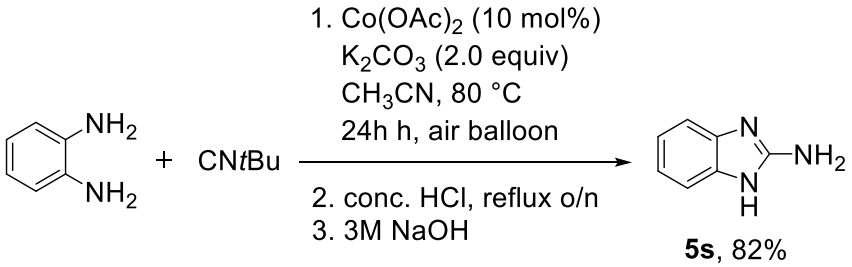

2-aminobenzimidazole (5s). *ortho*-phenylenediamine (32.4 mg, 0.300 mmol), $Co(OAc)_2$ (5.31mg, 0.0300 mmol), K_2CO_3 (82.9 mg, 0.600 mmol) were combined in a 6-inch test tube in an N_2 filled glovebox. CH_3CN (3 mL) and *tert*-butylisonitrile (35.2 □L, 0.300 mmol) were added and the test tube was sealed with a septum before being removed from the glovebox. The reaction mixture was then stirred for 24 hours in an 80 °C oil bath with an air balloon attached to a needled inserted through the septum. Upon completion, the reaction mixture was cooled to room temperature, diluted with ethyl acetate (10 mL) and filtered through a pad of Celite. Additional ethyl acetate

(20 mL) was used to flush the Celite and the resulting filtrate was transferred in a 100 mL two-neck flask and the solvent was removed by rotary evaporation. The flask was then connected to the Schlenk line and evacuated and backfilled with nitrogen three times. Under a N_2 atmosphere, dry toluene (20 mL) was added by syringe followed by a solution of concentrated HCl (1 mL) in toluene (5 mL). The resulting reaction mixture was placed in a 120 °C oil bath and allowed to reflux overnight. Upon completion, the reaction mixture was cooled to room temperature, basified with 3M NaOH until the aqueous layer reached a pH of ~13 (monitored by pH paper) and turned from a black goo to a dark brown suspension. The aqueous layer was extracted with ethyl acetate (3 x 50 mL) and the combined organic layers were washed with brine (50 mL), separated, dried over anhydrous sodium sulfate, filtered, and the solvent removed under vacuum to yield the crude product as a light yellow solid. Dimethyl sulfone (3.00 mg, 0.0318 mmol) was added as an internal standard and the crude mixture was dissolved in DMSO-d_6 for ^{1}H NMR analysis. The reaction yield was determined by ^{1}H NMR spectroscopy to be 82%.

^{1}H NMR (400 MHz, DMSO-d_6): δ = 7.09 (s, 2H), 6.84 (s, 2H), 6.18 (s, 2H). The spectral data are consistent with those reported in the literature.[57]

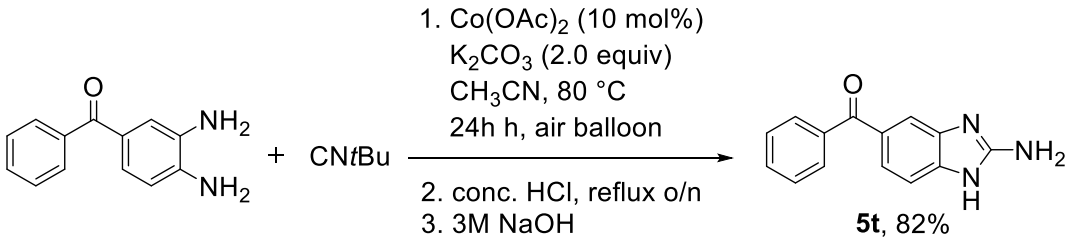

2-Amino-5-benzoyl-*1H*-benzimidazole (5t). In a N_2-filled glovebox, a 6-inch test tube equipped with a stir bar was loaded with 3,4-diaminobenzophenone (63.7 mg, 0.300 mmol), $Co(OAc)_2$ (5.31 mg, 0.0300 mmol), and K_2CO_3 (82.9 mg, 0.600 mmol). Dry CH_3CN (5 mL) was added to the test tube followed by *tert*-butylisonitrile (34.2 mL, 0.300 mmol). The test tube was then removed from the glovebox and the reaction mixture was stirred in an 80 °C oil bath for 24 hours. Upon completion, the reaction mixture was cooled to room temperature, filtered through a pad of Celite, and the Celite was rinsed with 30 mL of ethyl acetate. The filtrate was then transferred to a 100 mL two-neck flask and the solvent was removed under vacuum. The flask was then connected to the Schlenk line, fitted with a water condenser and evacuated and backfilled with N_2 three times. Under a N_2 atmosphere, dry toluene (20 mL) was added via syringe, followed by a mixture of

concentrated HCl (1 mL) in toluene (5 mL). The reaction mixture was heated at 120 °C with stirring overnight to enable complete dealkylation. Upon completion, the reaction mixture was cooled to room temperature, basified with 3M NaOH until the aqueous layer reached a pH of ~13 (monitored by pH paper) and turned from a black goo to a dark brown suspension. The aqueous layer was then extracted with ethyl acetate (3 x 50 mL) and the combined organic layers were washed with brine, separated, dried over anhydrous sodium sulfate, filtered, and concentrated via rotary evaporation to generate the crude product as a dark yellow solid. The product was purified by silica column chromatography (EtOAc: MeOH: Et_3N = 90:10:5, R_f = 0.1 in the same solvent system) to yield the title compound. Due to the presence of triethylamine in the isolated compound, an aqueous extraction was applied to remove remaining triethylamine. The isolated compound was dissolved in 30 mL ethyl acetate and partitioned into 100 mL water. The water layer was extracted ethyl acetate (2 x 20 mL) and the combined organic layers were washed with brine, dried over anhydrous sodium sulfate, filtered, and concentrated via rotary evaporation to provide 49.9 mg of the titled compound (0.210 mmol, 70.1 %) as a yellow solid (m.p.= 169-174 ºC). ^{1}H NMR (400 MHz, DMSO-d_6): δ = 7.71 – 7.64 (m, 2H), 7.64 – 7.48 (m, 4H), 7.40 (d, J = 1.7 Hz, 1H), 7.20 (d, J = 8.2 Hz, 1H), 6.74 (s, 2H). ^{13}C NMR (100 MHz, DMSO-d_6): δ = 195.47, 157.68, 145.25, 139.03, 136.62, 131.51, 129.22, 128.32, 127.78, 123.56, 112.64, 111.92. FTIR (ATR, cm^{-1}): 3320 (w), 3171 (w), 3060 (w), 2923 (w), 2853 (w), 1598 (s), 1565 (s), 1519 (s), 1466 (m), 1433 (s), 1344 (m), 1318 (s), 1283 (s), 1177 (w), 1071 (m), 1026 (m), 975 (w), 930 (w), 873 (m), 851 (m), 825 (m), 790 (s), 709 (s), 695 (s). HRMS (ESI-MS, m/z) $[M+H]^+$ calcd for $C_{14}H_{12}N_3O$ 238.0975; found 238.0974.

3.4.7. Procedures for Control Experiments with Radical Trapping Agents

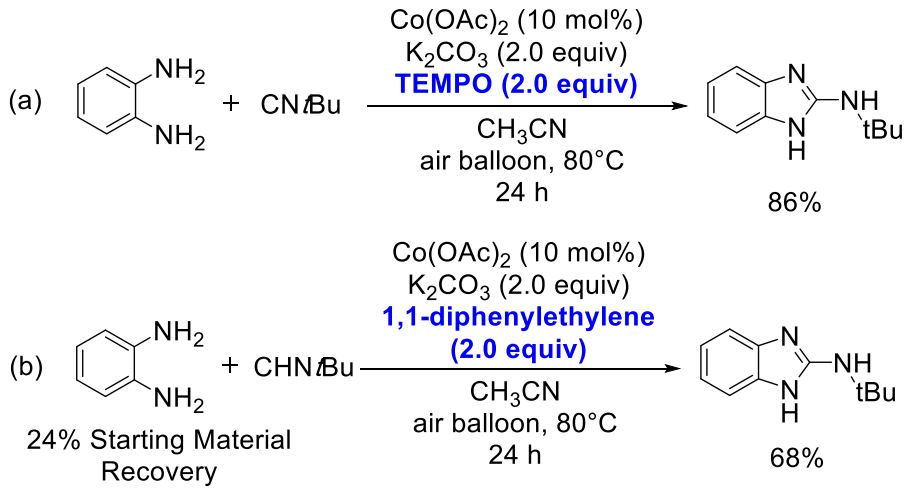

Standard procedure for radical trap experiments. *ortho*-phenylenediamine (32.4 mg, 0.300 mmol), $Co(OAc)_2$ (5.31 mg, 0.0300 mmol), K_2CO_3 (82.9 mg, 0.600 mmol) and radical scavenger (2.0 equiv, 0.600 mmol) were combined in a 6-inch test tube in an N_2 filled glovebox. CH_3CN (3 mL) and *tert*-butylisonitrile (35.2 mL, 0.300 mmol) were added and the test tube was sealed with a septum before being removed from the glovebox. The reaction mixture was then stirred for 24 hours in an 80 °C oil bath with an air balloon inserted through the septum.

Work up method for control experiment with 1,1-diphenylethylene as the radical scavenger. Upon completion, the reaction mixture was cooled to room temperature, diluted with 10 mL ethyl acetate and filtered through a pad of Celite. An additional 20 mL ethyl acetate was used to wash the Celite and the resulting filtrate was concentrated to ~3 mL on the rotary evaporator. The resulting solution was then passed through a silica gel Pasteur pipette to remove any remaining cobalt and the pipette was flushed with additional 10 mL of ethyl acetate. The filtrate was collected and the solvent was removed via rotary evaporation to generate the crude product. Dimethyl sulfone (3.00 mg, 0.0318 mmol) was added as an internal standard and the crude mixture was dissolved in DMSO-d_6 for ^{1}H NMR analysis. The reaction yield was determined by ^{1}H NMR spectroscopy.

Work up method for control experiment with TEMPO as the radical scavenger. After cooling to room temperature, the reaction mixture was diluted with ethyl acetate (20 mL) and the resulting mixture was extracted with a saturated solution of $Na_2S_2O_3$ (3 x 20 mL) until the organic layer

changed from dark red to light yellow. The organic layer was then washed with brine, and the resulting organic layer was dried over anhydrous sodium sulfate, filtered, and finally concentrated via rotary evaporation to ~3 mL. The concentrated sample was then passed through a Pasteur pipette silica gel plug to remove any remaining cobalt and the pipette was flushed with additional 10 mL of ethyl acetate. The filtrate was collected and the solvent was removed via rotary evaporation to generate the crude product as a brownish-red solid. Dimethyl sulfone (3.00 mg, 0.0318 mmol) was added as an internal standard and the crude mixture was dissolved in DMSO-d_6 for ^{1}H NMR analysis. The reaction yield was determined by ^{1}H NMR spectroscopy.

3.4.8. Attempts in the Synthesis of Mebendazole from 2-Amino-5-Benzoyl Benzimidazole

As we stated previously, the formation of mebendazole from 2-amino-5-benzoyl benzimidazole (**5t**) was quite challenging due to the presence of exchangeable NH protons in the starting material. Aside from the methodologies applied in **Scheme 3.8** we especially extended our exploration in this transformation using methyl chloroformate as a coupling partner, but with varied reaction conditions (**Scheme 3.10**). We realized a fully conversion of the starting material in these related reaction conditions; however, these transformations yielded almost 1:1 mixture of mebendazole isomers exclusively regardless of the varied bases and reaction stoichiometry. Suggesting a thermodynamic preference of the following structural isomers over mebendazole under these reaction conditions.

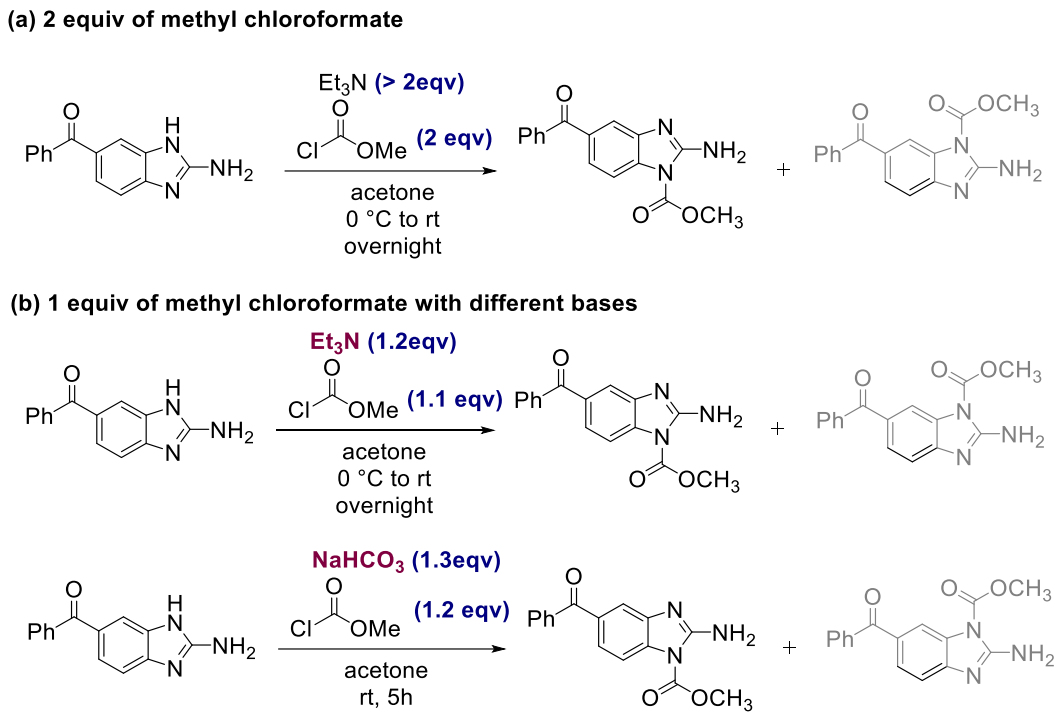

Scheme 3.10. Attempts in the synthesis of mebendazole from 2-amino-5-benzoyl benzimidazole and methyl chloroformate.

Structures of mebendazole isomers are elucidated by ^{1}H-NMR using one of the model reactions from **Scheme 3.10**, where $NaHCO_3$ was employed as a base. Characteristic protons on the benzimidazole ring are highlighted in each structure of the mebendazole isomers. Due to the extreme similarity of the physical properties these two isomers presented, the isolation proved to be impractical. Therefore the structure elucidation here is provided by the sample with mixed isomers (**Figure 3.6-3.9**).

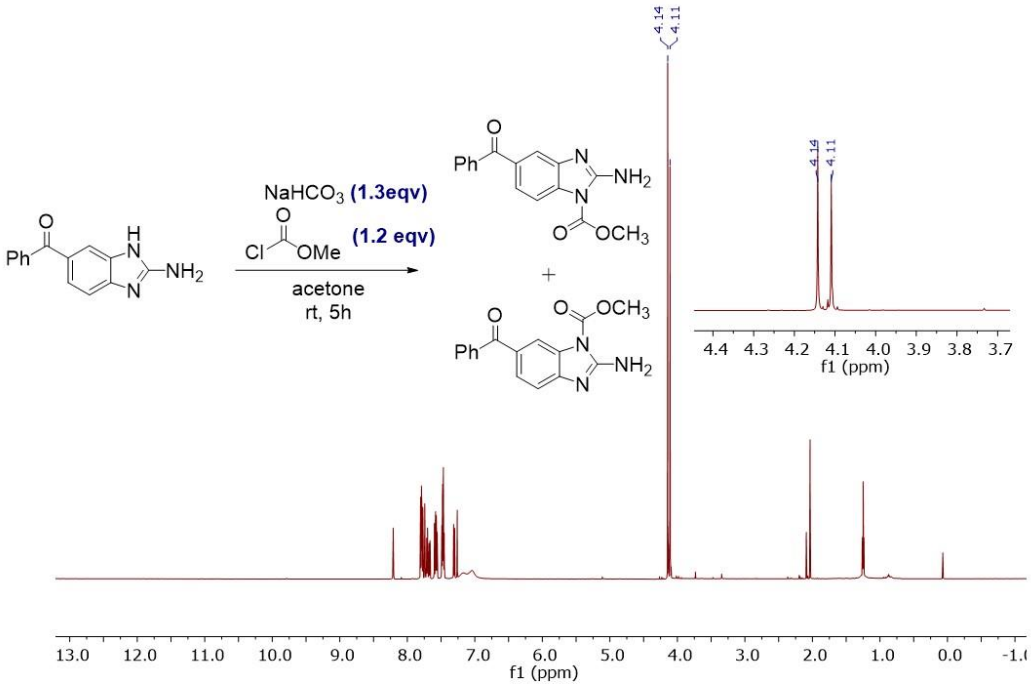

Figure 3.6. Mixture of the two mebendazole structural isomers from the model transformation.

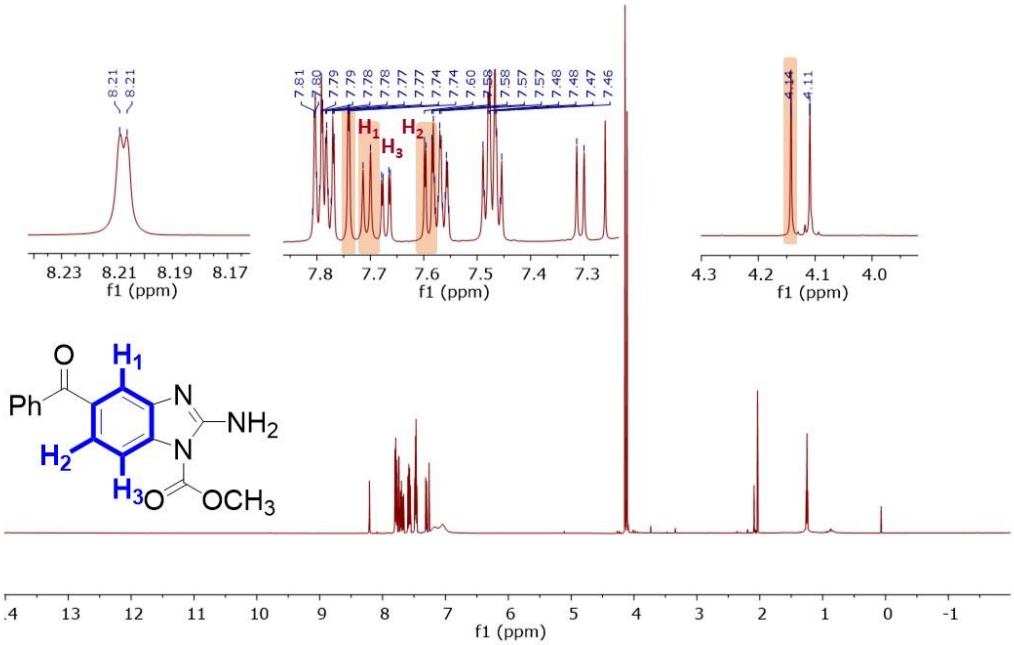

Figure 3.7. ^{1}H NMR for structural elucidation of mebendazole isomer with 1-acylation.

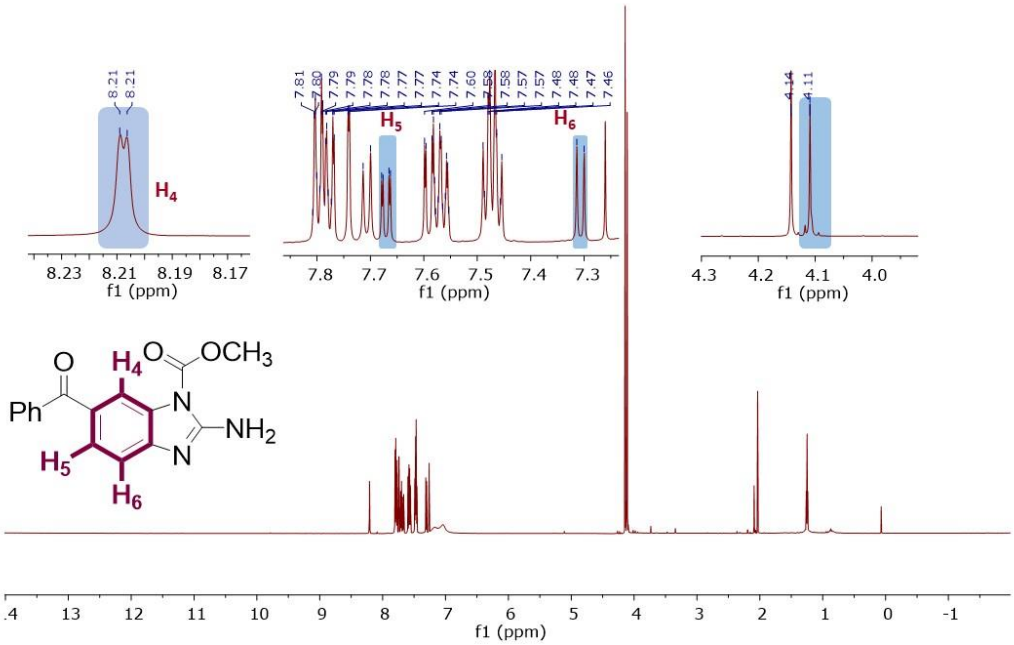

Figure 3.8. ^{1}H NMR for Structural elucidation of mebendazole isomer with 3-acylation.

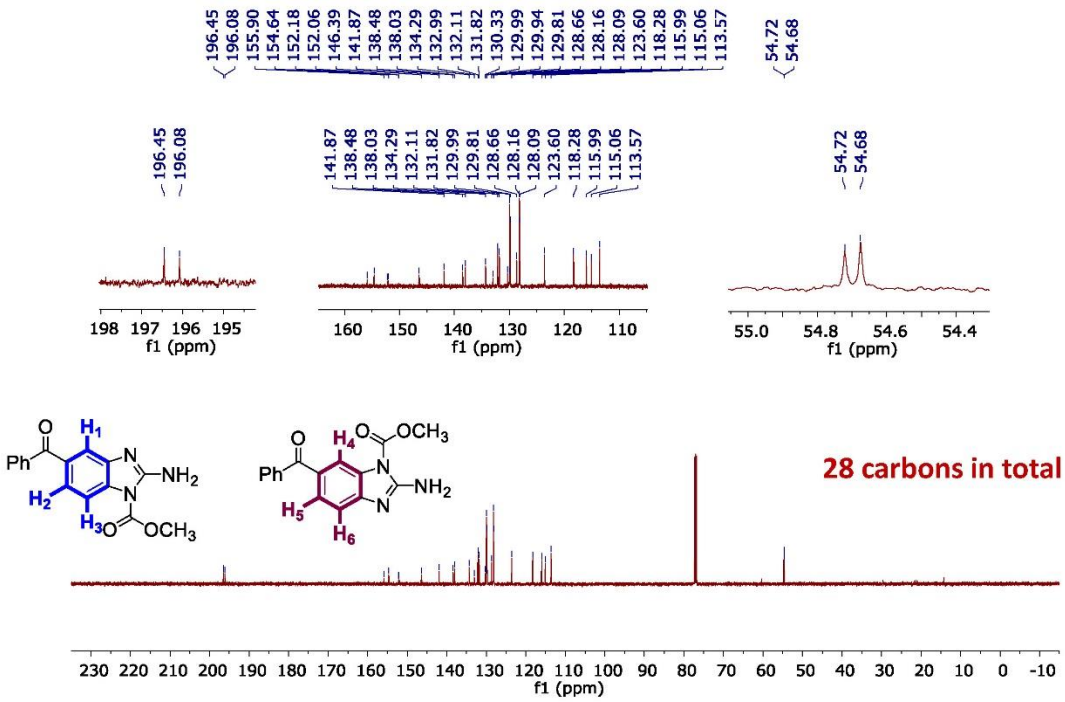

Figure 3.9. ^{13}C NMR for the mixture of two mebendazole isomers.

Chapter 4. Synthesis, Isolation and Characterization of the Well-Defined Co^{II} and Co^{III} Complexes bearing NH_2-unsubstituted Aminophenol Ligands and Their Reactivity Studies in the Aerobic Oxidative Cyclization Reactions

4.1. Introduction

In transition metal catalysis, the property of a complex can be affected by the coordination of ligand to the metal center. Redox non-innocent ligands, which can engage in a ping-pong mechanism by easily being oxidized or reduced by one or more electrons, can have important effects on the redox states of the transition metal center upon coordination. These ligands are capable of stabilizing metal ions with unusual oxidation states through modification of the electrochemical potentials, and act as an electron-reservoirs which allow the transition metal to maintain its most common or stable oxidation state in multielectron transformations by donating or accepting the electron densities. [139-141] *O*-aminophenol, an archetypal example of a redox non-innocent ligand, has been used widely paired with numerous transition-metal catalysts. This ligand can accommodate three stable oxidation states once deprotonated, *o*-aminophenolate, *o*-iminosemiquinoate and *o*-iminobenzoquinone as shown in Scheme 4.1. Metal complexes with one and two electron reduced forms in *o*-aminophenol type ligands have been intensively reported by multiple research groups.[142-146]

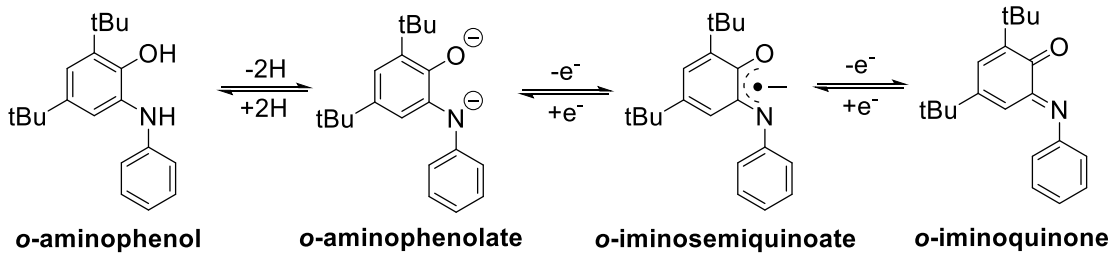

Scheme 4.1. Oxidation states of the bidentate *o*-aminophenol as a redox-active ligand

Among the types of redox non-innocent ligands, extensive studies have focused on 3,5-di-*tert*-butyl substituted *o*-aminophenol ligands. The increased electron-donating property of *tert*-butyl groups enables the deprotonated ligand to stabilize the complex with high oxidation states

efficiently. Also, these substituents play a critical role in facilitating the oxidation of the ligand while suppressing its oxidative decomposition by lowering the oxidation potential of the ligand.[147] With the increasing interest of pairing 3,5-di-*tert*-butyl-*o*-aminophenol with transition-metal catalysts, great efforts have been made on the synthesis and studies of such complexes with a wide range of transition metals, such as iron complexes,[148] uranium complexes,[149] platinum complexes,[150] and zirconium complexes.[151]

While the 2nd and 3rd row late transition metals have a well-established two-electron oxidation state changes in catalysis, first-row base metals don't necessarily undergo the same transformations due to their preference for the single-electron redox changes, for example, Co^{II}/Co^{III} couples. In this regard, the combined behavior of a base metal and a redox non-innocent ligand may facilitate $2e^-$ transformations resembling those of noble metals without compromising to the high energy redox-states for oxidizing the metal by two electrons.[141] The Wieghardt group has made significant contributions in elucidating the electronic structure and the coordination chemistry of redox non-innocent ligands involving catechol, *o*-aminophenol and *o*-phenylenediamine. [69, 70, 152-156] These works have provided valuable insights towards the understanding of how the ligands bind to the metal center and interact with the metal in different oxidation states. Co^{III} complexes consisting of 3,5-di-*tert*-butyl-*o*-aminophenol ligands were amongst those of the most studied by this group. A few examples of these metal complexes are illustrated in **Figure 4.1**. Regardless of the coordination environment of these structures, most of the well-defined Co^{III} complexes exclusively contain *o*-aminophenol ligands with bulky aromatic substitution on each NH moiety, [55, 70, 145] a comprehensive study on a cobalt complex bearing *o*-aminophenol ligands with unsubstituted NH_2 groups has yet to be reported.

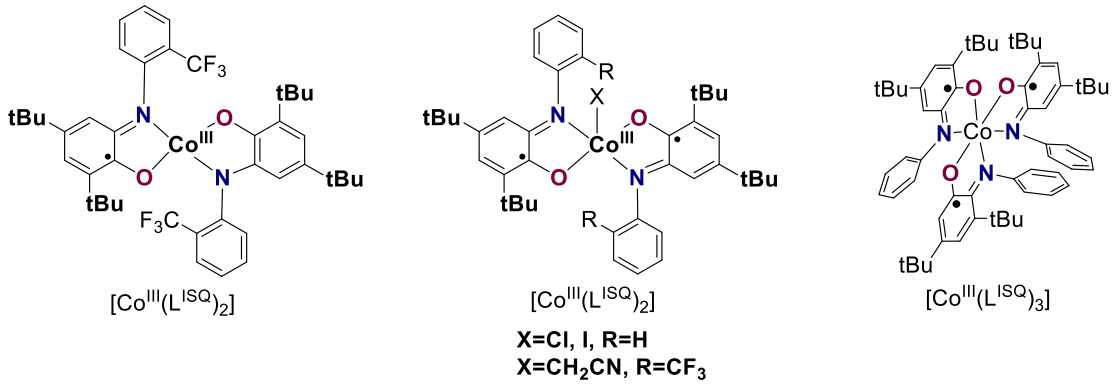

Figure 4.1. Selected examples for cobalt complexes with 3,5-di-*tert*-butyl-*o*-aminophenols.

In these extensively studied Co^{III} complexes the ligand radical anions were assigned. Upon oxidation, the metal center remained Co^{III} while the ligands engaged in the redox changes when coordinated to the metal, resembling the oxidative transformation mediated by noble metals. A few decades prior to these findings, Gary and co-workers had demonstrated that square planner cobalt and nickel complexes with dithiolene ligands were best described as metal (II) species with two ligand radical anions, rather than the assumed metal with +4 oxidation states and ligands with -2.[157, 158] Due to the presence of the extended network of π bonds, these redox non-innocent ligands not only allow themselves to stabilize the radical species but also promote reversible reactions with the metal center, when the formation of radicals are involved.[159] These carbon-centered ligand radicals were not only determined in cobalt complexes, they were also frequently reported in the structural elucidation of other metal complexes such as Ni^{II},[160] Cu^{II},[145, 156] Pd^{II},[145, 154] and Fe^{III} [69, 155] when the same 3,5-di-*tert*-butyl-*o*-aminophenol ligand was employed.

Despite all the notable advances in assigning the true electronic structure of these transition metal complexes involving redox non-innocent ligands, reactivity studies using these metal complexes with radicals on the supporting ligands as catalysts are still underrepresented. Wieghardt and co-workers reported the first examples where redox-active ligands in the metal complexes effectively engaged in C-H bond activations.[161] The work was inspired by enzymatic reactions of galactose oxidase, which performs the two-electron oxidation of alcohols to aldehydes. Using Cu^{II} and Zn^{II} complexes of a tetradentate redox non-innocent ligand, primary alcohols could effectively be oxidized to aldehydes with the reduction of O_2 to H_2O_2 (**Scheme 4.2**). Under aerobic conditions, the single electron oxidized complex (**a)** underwent a stoichiometric oxidation of the primary alcohol and gave rise to complex (**b)**. Through a rate-determining HAA step and electron transfer, the corresponding aldehyde was generated along with the doubly protonated, single-electron reduced species (**d)**, which immediately regenerated complex (**a)** in the presence of molecular oxygen to complete the cycle.

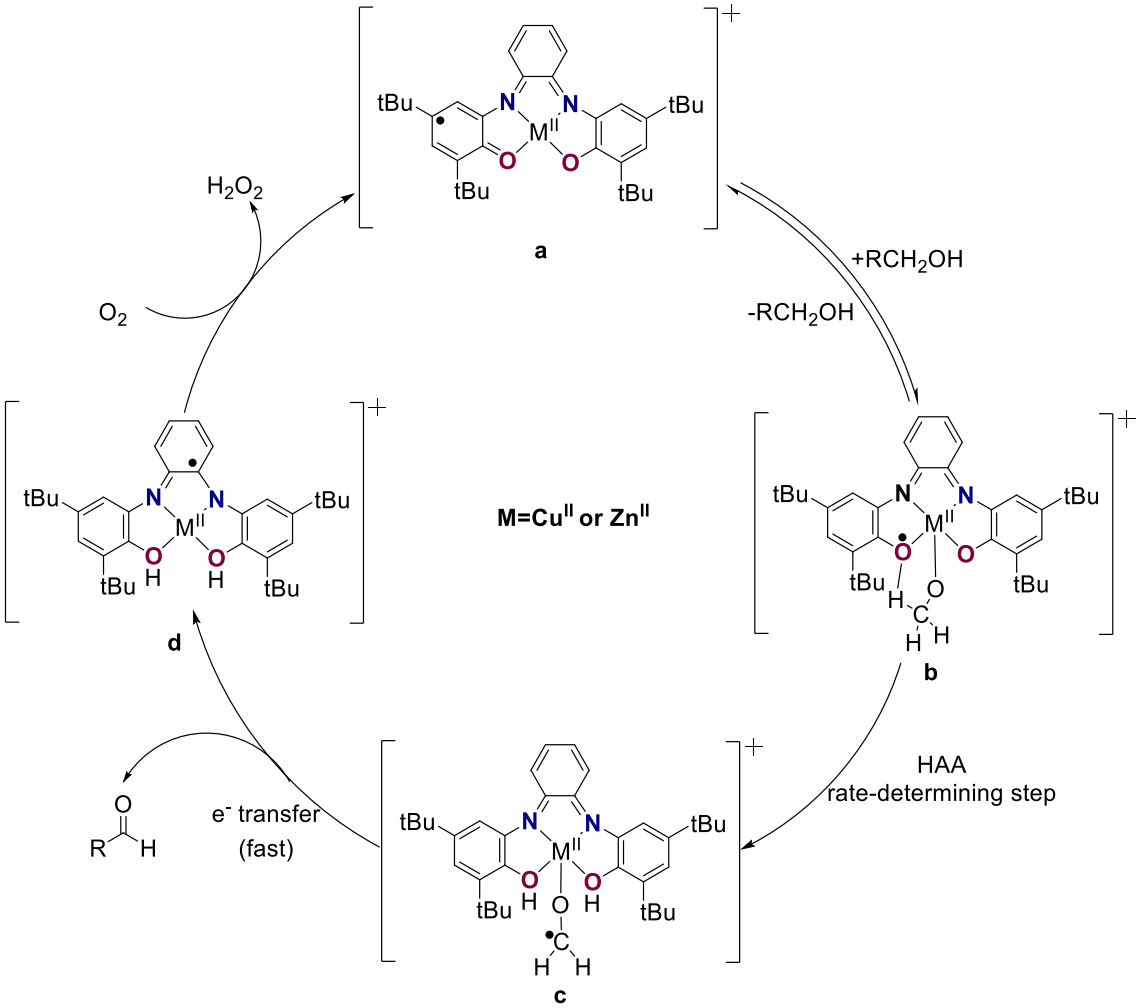

Scheme 4.2. Proposed mechanism for the catalytic oxidation of primary alcohols by dioxygen employing complexes of a tetradentate redox non-innocent ligand.

Although this revolutionary work had shed a lot of light on the later studies of the primary alcohol oxidation reactions using well-characterized metal complexes bearing aminophenol-derived redox non-innocent ligands,[162, 163] implications for cobalt complexes containing redox-active aminophenolate-type ligand in catalysis are still quite limited. To date, the only well-established work demonstrating the reactivity of cobalt aminophenolate complexes was reported by the Soper group,[71] where a square planner Co^{III} complex was capable of catalyzing a Negishi-like cross-coupling reaction of an alkyl halide with an organozinc reagent (**Scheme 4.3**). The starting Co^{III} complex had two bidentate amidophenolato ligands coordinating to the metal center in the anionic aminophenolate form. This complex demonstrated a very unique reactivity to behave

as a nucleophile and react towards the alkylhalide, affording the square pyramidal alkyl complex in quantitative yield. While the cobalt remained the same oxidation state during the oxidative addition, the electrons required for this transformation were provided by the amidophenolato ligands, both of which were oxidized to *o*-iminosemiquinoate (sq^-) oxidation state. Upon treatment of the alkyl complex with zinc bromide, ethyl benzene was observed as a result of C-C bond formation. The starting Co^{III} complex with square planer geometry was regenerated.

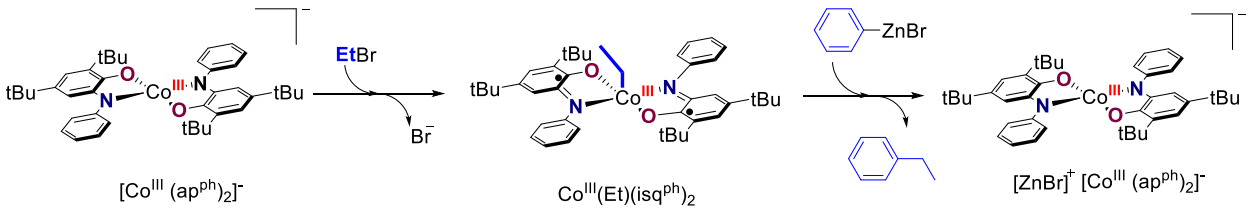

Scheme 4.3. Negishi-type cross-coupling reaction of alkyl halides with organozinc reagents by Co^{III}bis(*o*-amidophenolato) complex.

In this regard, the work in this chapter strives to deepen the understanding of cobalt complexes bearing redox non-innocent aminophenolate ligands, especially their engagement in the oxidative cyclization reactions with bis-nucleophiles through O_2 activation. To date, the cobalt complexes reported in this chapter are the first examples of well-characterized Co^{II} and Co^{III} species bearing redox-active 3,5-di-*tert*-butyl-*o*-aminophenol ligand without NH_2 substitutions. Notably, the bulky N-substitutions on the most commonly used aminophenol-derived ligands play a critical role in stabilizing Co complexes in the presence of O_2. The Paine research group recently reported a biomimetic six-coordinate Fe(II) complex capable of oxidizing 2-amino-4-*tert*-butylphenol to picolinic acid in the presence of O_2 (**Scheme 4.4**),[164] which resembles the activity of the dioxygenase metalloenzymes[165] that are able to catalyze the ring cleavage of numerous organic substrates. This finding suggests that to sustain the stability of carbon-centered ligand radicals against oxidative ring opening reactions in the presence of O_2, both *N*-substitutions and protective tert-butyl groups at the backbone of aminophenol are necessary.

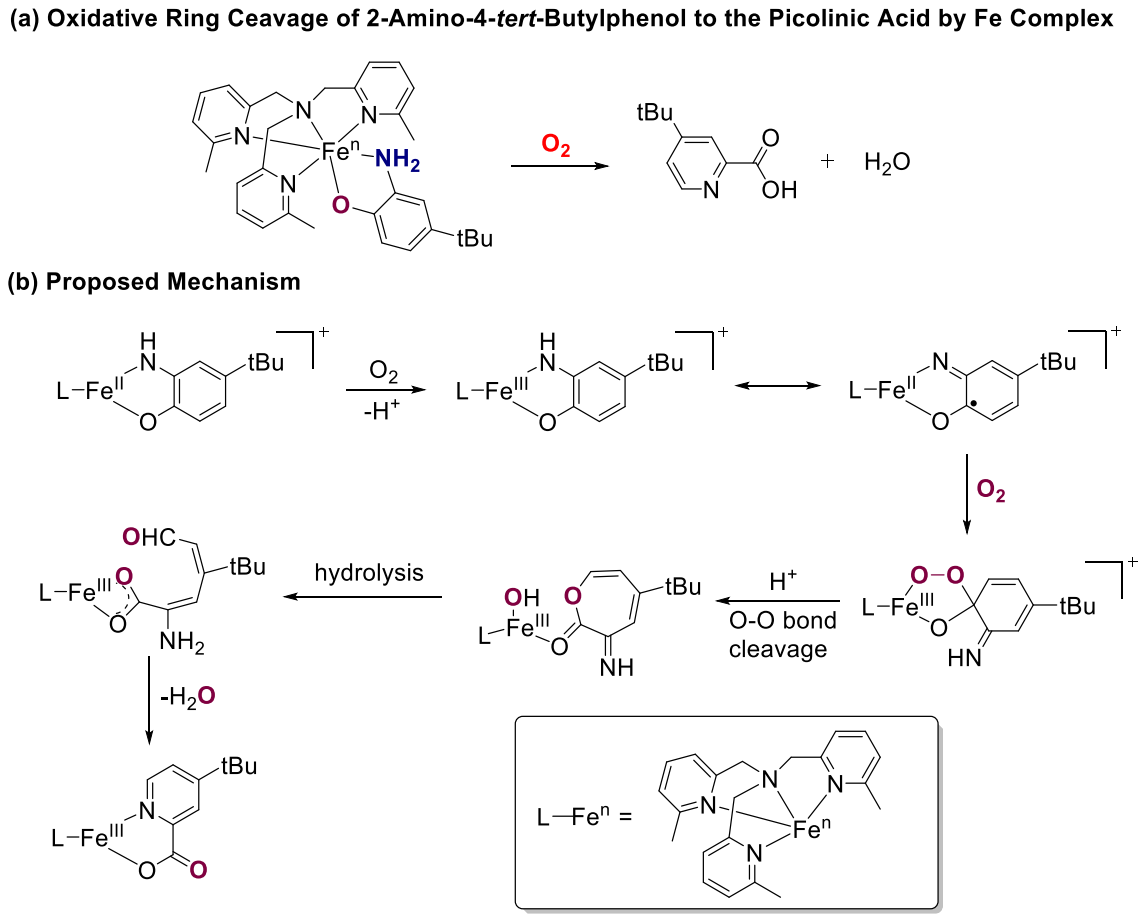

Scheme 4.4. Proposed mechanism for oxidative ring cleavage of 2-amino-4-*tert*-butylphenol to the picolinic acid in the presence of O_2.

As a continuation of our previous mechanistic investigations on the oxidative cyclization reactions with bis-nucleophiles, these extremely challenging complexes were further tested in the model reaction developed in chapter 2 for their ability to effectively mediate aerobic oxidative cyclization reactions as potential active intermediates. Beyond the above investigations, this work expands on the currently limited understanding of first-row base metal species from the structure elucidation to the implementation in the organic transformations.

4.2. Results

4.2.1. Synthesis of Co^{II} complex bearing 2-amino-4,6-ditert-butyl phenol ligands Co^{II}(2-amino-4,6-tert-butylphenolate)$_2$(2-amino-4,6-tert-butylphenol)$_2$

Initially, several attempts to isolate the cobalt complex containing the unsubstituted 2-amino-4-nitrophenol ligands were unsuccessful. Mixtures of products were obtained due to the solubility issues associated with the starting materials and the products. Consequently, the efficacy of 2-amino-4,6-di-tertbutyl phenol was tested in the standard conditions for aerobic oxidative cyclization developed in Chapter 2 (**Scheme 4.5**), where the desired product **3w** was generated with an isolated yield of 78%. Based on the positive results, the 2-amino-4,6-di-tertbutyl phenol was selected as the ligand of choice to synthesize and isolate the cobalt complexes.

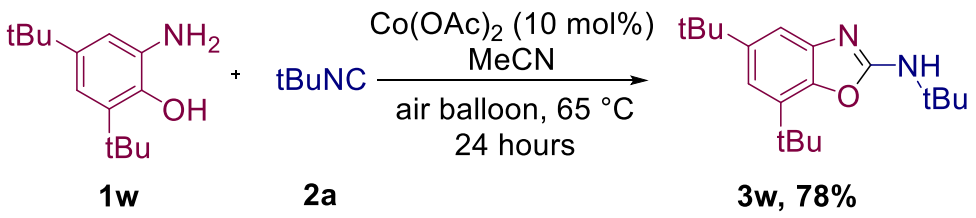

Scheme 4.5. Cobalt-catalyzed oxidative coupling of 2-amino-4,6-di-*tert*-butyl phenol and *tert*-butyl isonitrile under the standard reaction conditions.

The synthesis of the Co^{II} complex was performed under a rigorously inert atmosphere using acetonitrile as the solvent. Triethylamine was introduced as a base to deprotonate the ligand. $CoCl_2$ was chosen as the cobalt source for its greater solubility compared to $Co(OAc)_2$. When 2-amino-4,6-di-*tert*-butylphenol was employed as a ligand, we were delightful to find that under the reaction conditions shown in **Scheme 4.6**, a cobalt complex with a unique coordinating environment was formed in acetonitrile, regardless of the ratio between the metal and the ligand. These results are in contrast to the observations in most other studies, where the corresponding complexes were formed based on the stoichiometry of the ligands introduced;[70, 145] however, the ligands presented in those studies all used bulky *N*-substitutions as detailed in the introduction, which may help to stabilize the 1:2 and 1:3 complexes in solution. In this work, the monomeric cobalt complex was obtained in optimal yield when a 1:4 metal to ligand ratio was employed. A microcrystalline solid was generated with a golden sheen. Based on the extent of acetonitrile solvation, the color of the solid varied from beige to faint greyish green in different batches of synthesis.

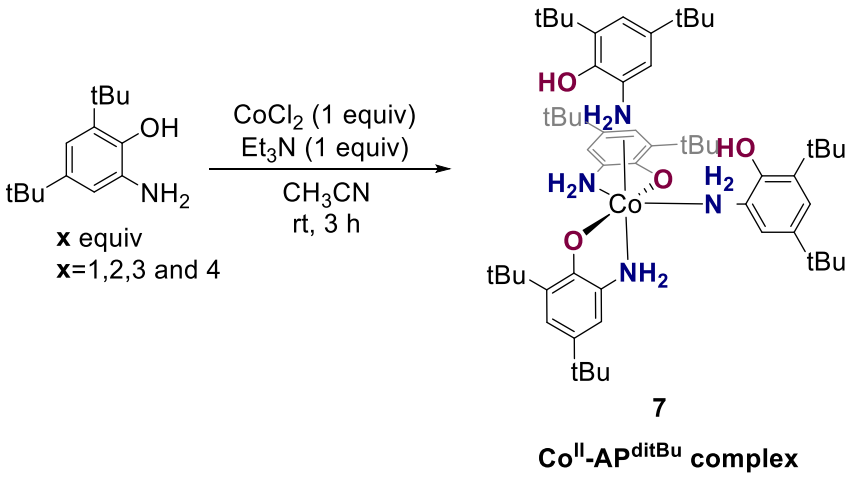

Entry	M:L Ratio	% Yield
1	1:1	43
2	1:2	54
3	1:3	70
4	1:4	93

Scheme 4.6. Synthesis and condition optimization of Co^{II}-AP^{ditBu} complex Co^{II}(2-amino-4,6-*tert*-butylphenolate)$_2$(2-amino-4,6-*tert*-butylphenol)$_2$ by varying metal to ligand ratio.

^{1}H-NMR spectroscopy could not confirm the structure of the Co^{II} complex **7** due to its paramagnetic nature. Single crystals, suitable for X-ray diffraction studies, were acquired by slow evaporation of the mixture under anaerobic conditions upon reaction completion. X-ray crystallography elucidation indicated the space group $Im\bar{3}$ of the resulting cubic light-yellow single crystal. A unique coordinating environment of the Co^{II} complex is determined as shown in **Figure 4.2**, which consists of two monodentate aminophenol ligands *cis* to each other and two bidendate aminophenolate ligands, binding through the octahedral geometry.

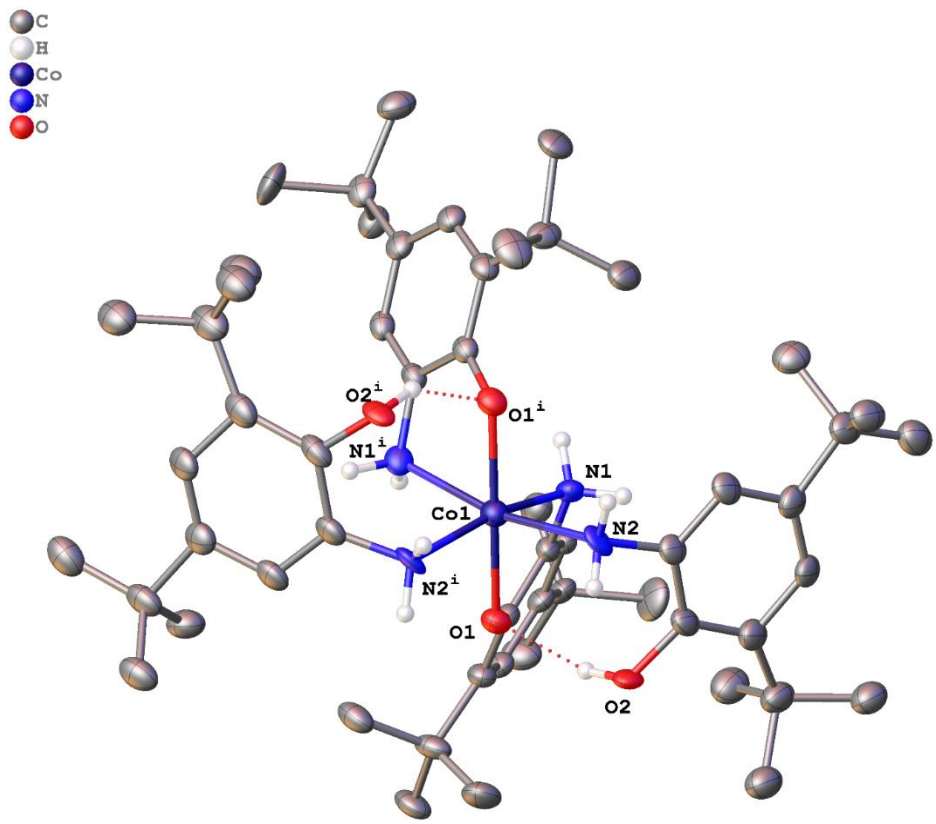

Figure 4.2. The structure of Co(2-amino-4,6-*tert*-butylphenolate)$_2$(2-amino-4,6-*tert*-butylphenol)$_2$. All non-hydrogen atoms are dawn as 40% thermal probability ellipsoids. All hydrogen atoms except those on heteroatoms are omitted for clarity.

4.2.2. Synthesis of Co^{III} complex bearing 2-amino-4,6-di-*tert*-butyl phenol ligands Co_2^{III}(2-amino-4,6-*tert*-butylphenolate)$_2$(2-amino-4,6-*tert*-butylphenol)(μ-2-amido-4,6-*tert*-butylphenolate)$_2$

The synthesis of the Co^{III} complex bearing the same 2-amino-4,6-di-*tert*-butyl phenol was initially attempted by the homogenous aqueous synthesis employing air as the source of oxidant. Under the ambient atmosphere, numerous trials led to the generation of a mixture of products, which was difficult to purify due to the superior solubility of the products in most polar organic solvents or the mixed solvents. In these experiments, $CoCl_2$ was treated with two or three equivalents of the 2-amino-4,6-di-*tert*-butylphenol ligands along with the same equivalents of bases. The reactions were carried out under either room temperature or reflux conditions in the presence of air, but no cobalt species shown in **Scheme 4.7** were isolated as pure substances. The

mixture of the products was extremely soluble in most organic solvents. The lack of bulky N-substitution on the aminophenolate ligand may also contribute to the instability of the formed product in solution when the reactions were carried out under an aerobic atmosphere. These observations were in accordance with similar discoveries by other research groups, that ligands such as catecholate and diamines usually would be unstable in solution when they are bound to metal centers, due to their distinctive ability to form radical species.[159]

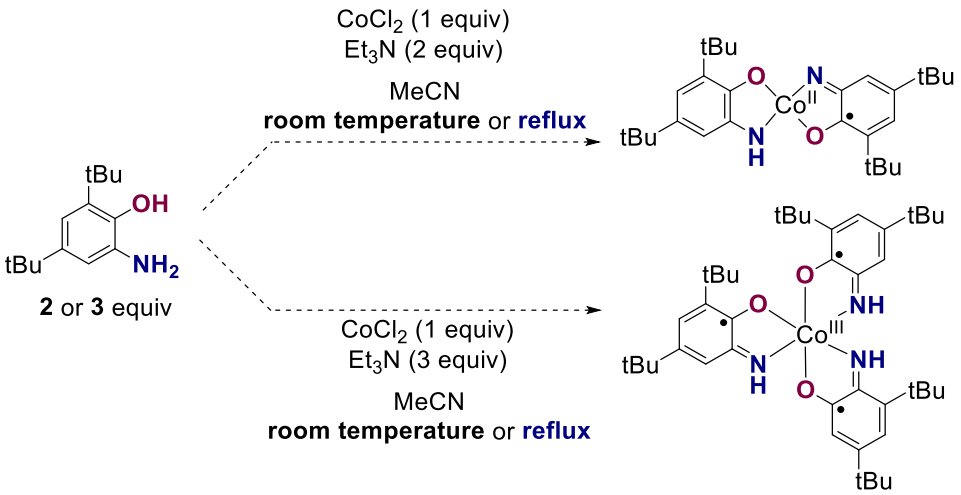

Scheme 4.7. Attempted synthesis of Co^{III}-AP^{ditBu} complex in the aqueous medium under ambient atmosphere. Conditions: $CoCl_2$ (1equiv), 2-amino-4,6-di-*tert*-butylphenol (2 or 3 equivs), triethylamine (2 or 3 equivs), acetonitrile. These reactions were carried out under ambient atmosphere either at room temperature or reflux conditions.

In one of Wieghart's studies, it was disclosed that when a comparable type of redox-active ligand 2-amino-4,6-di-*tert*-butyl thiophenol was employed in the synthesis of Co^{II} complexes, solid state oxidation was observed immediately upon the exposure of Co^{II} complex to the air, as indicated by the color change (**Scheme 4.8**). Inspired by this discovery, a small batch of Co^{II}-AP^{ditBu} was taken out of the glovebox for testing of solid-state oxidation. An instant color change was observed from light grey to shinny dark violet when the compound was exposed to air, demonstrating the efficiency of solid-based oxidation to isolate the Co^{III}-aminophenolate complexes in this study.

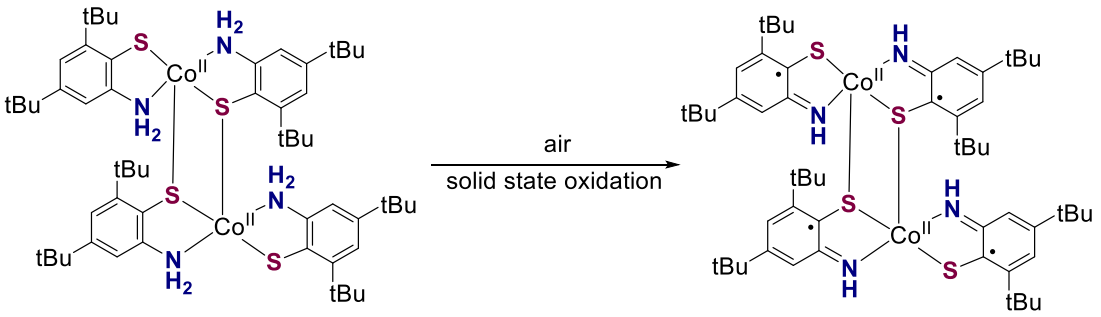

Scheme 4.8. Solid state oxidation observed by Wieghart group for the oxidation of the Co^{II} complex $[Co^{II}(L_S^{AP})_2]_2 \cdot 2CH_3CN$ in the presence of air (L_S^{AP}= 2-amino-4,6-di-*tert*-butylthiophenol).

Subsequently, we concentrated our efforts on the characterization of this oxidized compound. From our observations, the degree of solvation affected the rate at which oxidation of the Co^{II}-AP^{ditBu} complex occurred. The presence of the solvent led to a slower rate of oxidation, whereas, the oxidation occurred in a few hours in the solid state. Elemental analysis confirmed the identity of the oxidized species to be a 3:1 ligand: metal complex, such as a monomeric complex **8a** or **8b** with three ligands coordinating to one cobalt center, as illustrated in the **Scheme 4.9**.

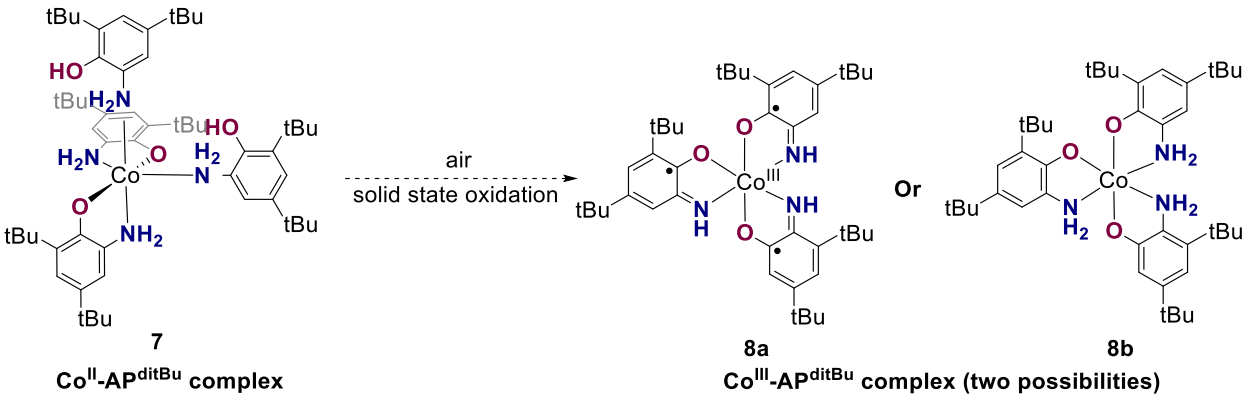

Scheme 4.9. Solid-state oxidation of metal complex Co^{II}(2-amino-4,6-tert-butylphenolate)$_2$(2-amino-4,6-tert-butylphenol)$_2$ under air.

A violet plate-shaped single crystal was able to be obtained by slow diffusion of pentane into dichloromethane dissolved with Co^{III}-AP^{ditBu} complex under the rigorously anaerobic atmosphere and submitted to X-ray diffraction. The structure of the crystal was elucidated as a dimeric metal complex with the space group $P2_1/n$. Each cobalt center possesses three

aminophenol-derived ligands with distinct coordinating environments (**Figure 4.3**), a neutral aminophenol ligand, a monoanionic aminophenolate ligand, and a bridging aminophenolate ligand connecting two cobalt centers via the NH group. Although the structure of this Co^{III}-AP^{ditBu} complex revealed a dimeric species rather than monomeric as proposed, it is consistent with the elemental analysis of the compound collected from the solid-state oxidation.

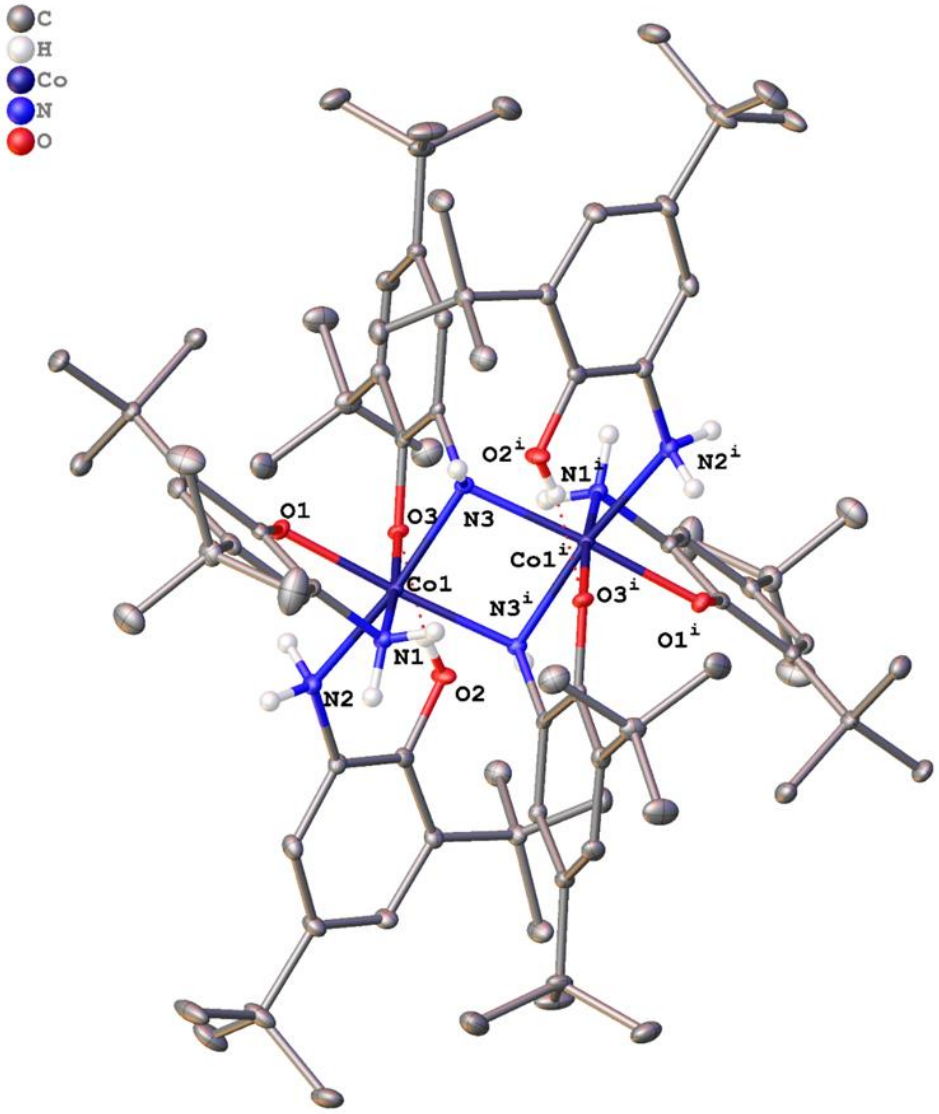

Figure 4.3. The structure of Co_2(2-amino-4,6-*tert*-butylphenolate)$_2$(2-amino-4,6-*tert*-butylphenol)(μ-2-amido-4,6-*tert*-butylphenolate)$_2$. All non-hydrogen atoms are drawn as 50% thermal probability ellipsoids. All hydrogen atoms except those on heteroatoms are omitted for clarity.

4.2.3. Evaluations of the Electronic Properties of Co^{II}-AP^{ditBu} (7) and Co^{III}-AP^{ditBu} (8) Complexes

4.2.3.1. UV-Visible Spectroscopy

The electronic properties of both Co^{II}-AP^{ditBu} (**7**) and Co^{III}-AP^{ditBu} (**8**) were evaluated by UV-visible spectroscopy (**Figure 4.4**). The electronic spectrum of complex **(7)** measured in CH_2Cl_2 displayed no intense absorption maxima above 450 nm, suggesting that the ligands coordinated to the metal center are aromatic, in accordance with the X-ray structure. The electronic spectrum of Co^{III}-AP^{ditBu} (**8**) presented two intense absorption maxima in CH_2Cl_2 solution around 550 nm ($\varepsilon = 3.6\times10^3$ M^{-1} cm^{-1}) and 783 nm ($\varepsilon = 7.5\times10^2$ M^{-1} cm^{-1}), which were absent for the Co^{II} complex, indicating that a ligand to metal charge transfer may be involved. Although the X-ray crystal structure of this Co^{III} compound showed aromatic coordinating ligands of 2-amino-4-6-di-*tert*-butyl phenolate, in solution this compound may have radicals residing on the ligands, as suggested by the structure of **8a**. A series Co^{III} complexes reported by Weighardt and co-workers consisting of N-substituted iminosemiquinoate (sq^-) ligands[70] presented the most intense absorption maxima around 695 nm ($\varepsilon = 1.87\times10^4$ M^{-1} cm^{-1}) and 884 nm ($\varepsilon = 1.03\times10^4$ M^{-1} cm^{-1}). Compared to these observations, the much weaker absorption maxima of our Co^{III} complex may be attributed to the low concentration of the cobalt species involving the ligand centered radical. Because our isolated species doesn't contain the N-substitution for stabilization in solution, the majority of these ligand-centered radicals are possibly delocalized and tautomerized and turn the ligand into aromatic aminophenolate coordinating to the metal center.

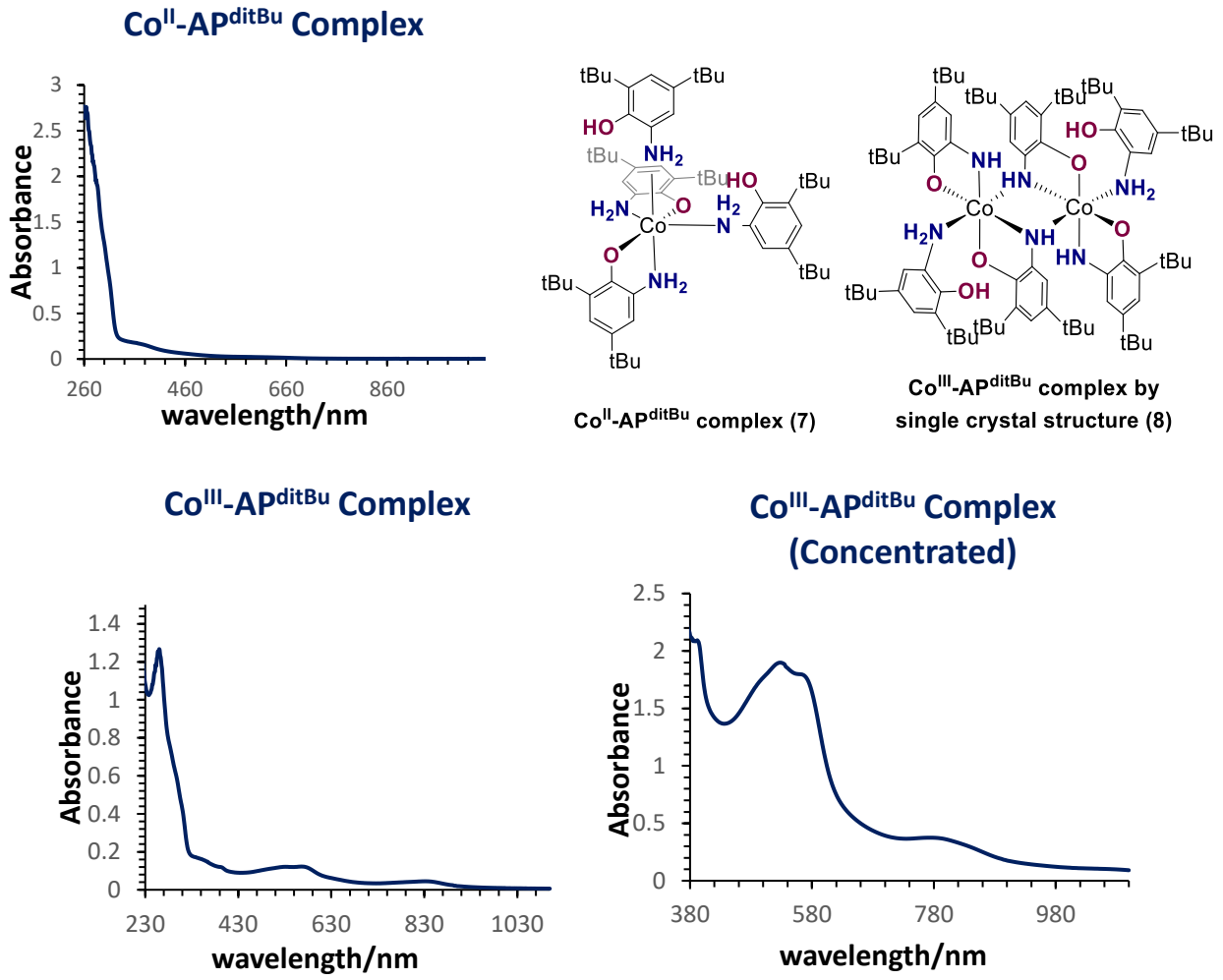

Figure 4.4. UV-visible spectroscopy of Co^{II}-AP^{ditBu} complex **(7)** and Co^{III}-AP^{ditBu} complex **(8)**. Top: Spectrum for Co^{II}-AP^{ditBu} complex **7**. Concentration: 1.1×10^{-4} M in CH_2Cl_2. Bottom left: Spectrum for Co^{III}-AP^{ditBu} complex **8**. Concentration: 5.0×10^{-5} M in CH_2Cl_2. Bottom right: Spectrum for Co^{III}-AP^{ditBu} complex **8**. Concentration: 5.0×10^{-4} M in CH_2Cl_2. All the above measurements were completed under N_2 atmosphere.

4.3.2.2. Cyclic Voltammetry

We further investigated both Co^{II}-AP^{ditBu} (**7**) and Co^{III}-AP^{ditBu} (**8**) complexes by cyclic voltammetry. Co^{II}-AP^{ditBu} complex **7** displayed a significant redox event at $E_{1/2}$ = 0.145V. Based on the $|E_{pa} - E_{pc}|$ values with different scan rates in comparison to ferrocene, this redox process for Co^{II} complex is reversible. Additionally, the compound also exhibited a few irreversible oxidation and reduction events around +1.0 V and -0.8 V. Compared to the Co^{II} species, Co^{III}-AP^{ditBu}

complex **8** presented a significant different behavior under anaerobic atmosphere. The oxidation and reduction processes were completely irreversible when a higher potential (> 0 V) was applied at the starting point. The complex showed a redox behavior highly similar to the Co^{II} complex **7** with a lower applied potential, albeit a narrower window was observed. The redox events of this Co^{III} species are quite different from those in the literature. In a study of a Co^{III} complex consisting of tridentate benzoxazole amidophenoxide ligands,[143] four redox couples were observed at $E_{1/2}$ at -0.67 V, -0.20 V, +0.28 V, and +0.84V respectively. As both oxidation and reduction of this Co^{III} were suggested as ligand-centered behaviors, we speculate that an irreversible decomposition occurred to our Co^{III} complex **8** due to a lack of stabilizing *N*-substitutions.

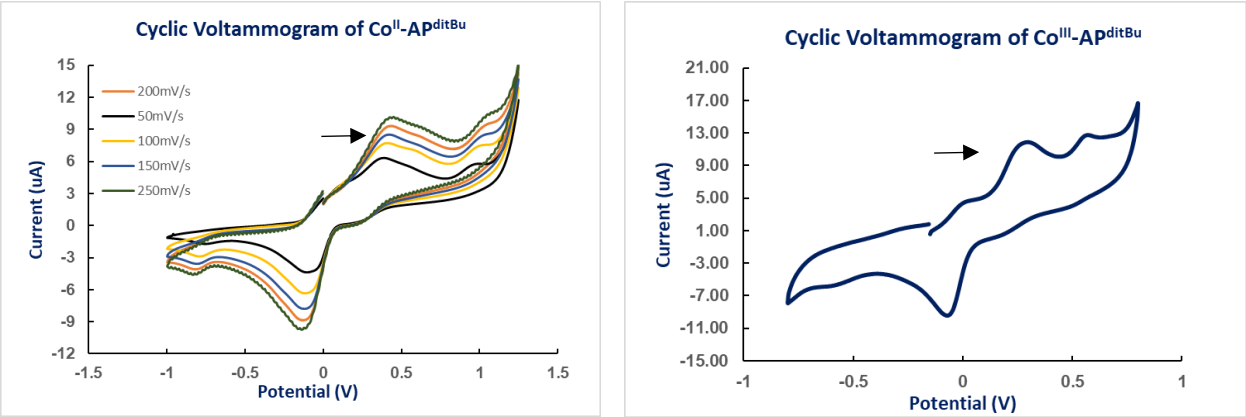

Figure 4.5. Cyclic voltammograms of Co^{II}-AP^{ditBu} **(7)** and Co^{III}-AP^{ditBu} **(8)**. Left: Voltammograms of Co^{II}-AP^{ditBu} **(7)**. Conditions: 10 mM complex, 0.10 M $[nBu_4N]^+[PF6]^-$, scan rate 50, 100, 150, 200, 250 mV·s^{-1}, DMSO solution, 298 K. Right: Voltammograms of Co^{III}-AP^{ditBu} **(8)**. Conditions: 10 mM complex, 0.10 M $[nBu_4N]^+[PF6]^-$, scan rate 100 mV·s^{-1}, DMSO solution, 298 K. All of experiments were done under N_2 atmosphere inside a glovebox.

4.2.3.3. EPR Measurements (New section added)

Both Co^{II}-AP^{ditBu} complex (**7**) and Co^{III}-AP^{ditBu} complex (**8**) were submitted to EPR measurements for the potential presence of ligand-centered radicals (**Figure 4.6**). Under N_2 atmosphere, Co^{II} exhibited no signals at 77 K. When air was introduced into the tube, the sample was immediately sealed and frozen in liquid N_2 for measurements. Intense signals were observed, suggesting radicals were generated in *situ* followed air oxidation (**Figure 4.6** left). The signal of Co^{II} complex upon air oxidation was calculated with a *g* value equals to 2.001. A radical coupled to a nucleus was found with a nuclear spin of 7/2 and an isotropic hyperfine coupling constant of

28.1 Gauss. This hyperfine coupling constant was in a good agreement with a phenoxyl radical coupled to a cobalt ion previously reported from a Co^{III} salen intermediate generated upon introducing the molecular oxygen.[47] Our results combined with the literature precedence highlighted that a phenoxyl radical, or a carbon-centered ligand radical may exist in our system as a result of air oxidation. Compared to the species generated upon aerobic oxidation of Co^{II}, the signals observed for Co^{III}-AP^{ditBu} complex (**8**) were a lot weaker and broader, probably due to the slow rotation of a frozen sample (**Figure 4.6** right). Similarly, a *g* value was calculated for these signals as 2.001. The spectrum of this complex also featured a coupling to one nucleus with a nuclear spin of 7/2 and an isotropic hyperfine coupling constant of 25.0 Gauss. The weak signals may also be attributed to a partial existence of the ligand-centered radicals. We performed the simulations for both Co^{II} and Co^{III} complexes by employing the parameters mentioned above. Simulating those parameters for Co^{II}-AP^{ditBu} complex (**7**) recapitulated the line positions very well. As for Co^{II}-AP^{ditBu} complex (**8**), the simulation fit the positions of the main features of the experimental spectrum very well especially on the low-field side (Simulated spectra not included).

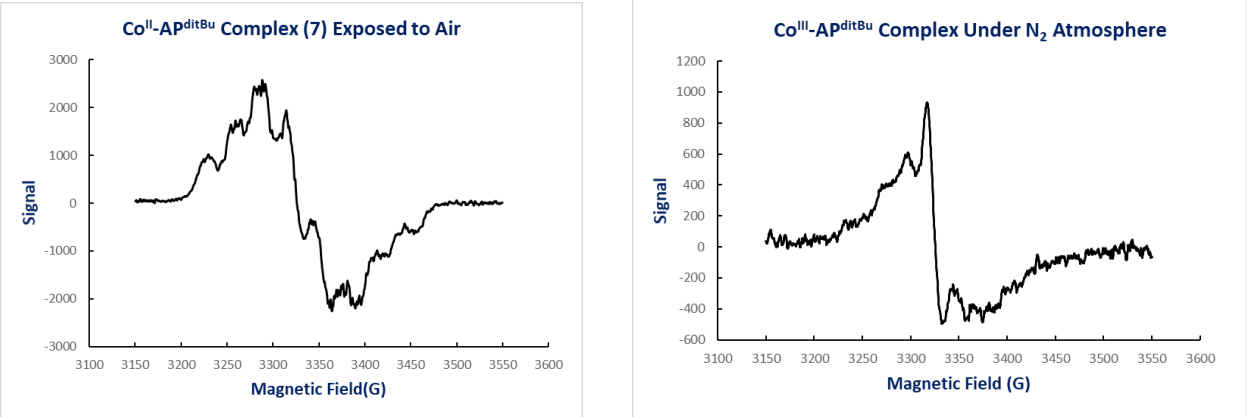

Figure 4.6. EPR spectra for Co^{II}-AP^{ditBu} complex **(7)** and Co^{III}-AP^{ditBu} complex **(8)**. Left: EPR spectrum of Co^{II}-AP^{ditBu} complex **(7)** exposed to air. Concentration: 1 mM cobalt complex in dichloromethane. The sample was prepared inside a N_2 filled glovebox. The spectrum was taken immediately after the sample was exposed to air then frozen in liquid N_2. Spectrum measured at 77K. Right: EPR spectrum of Co^{III}-AP^{ditBu} **(8)**. Concentration: 1 mM cobalt complex in dichloromethane. The sample was prepared inside a N_2 filled glovebox and properly sealed. The spectrum was taken under N_2 at 77K.

4.2.4. Aerobic Oxidation of Co^{II}(2-amino-4,6-*tert*-butylphenolate)$_2$(2-amino-4,6-tert-butylphenol)$_2$ in solution

Next, the oxidation behavior of the isolated Co^{II} complex **7** in solution was investigated. A sample of the Co^{II} complex and dimethyl sulfone as an internal standard were placed in a J. Young NMR tube, then air was introduced into the headspace of the same tube. A 1:1 mixture of deuterated DMSO and chloroform was employed as the solvent system due to the extreme difference in polarity between the low-valent Co^{II} complex and the oxidized intermediate. The in-situ oxidation was monitored with ^{1}H NMR spectroscopy. Upon oxidation, we observed the ligand dissociation shown in the **Figure 4.7**, which was accompanied with the generation of a diamagnetic intermediate. The presence of an internal standard confirmed that the oxidation of the low-valent Co^{II}-AP^{ditBu} to the intermediate accomplished within a few hours. The spectrum indicated an asymmetric structure for the diamagnetic intermediate, which includes 6 distinct aromatic protons and 6 different tert-butyl groups from the oxidized cobalt intermediate along with 6 exchangeable protons associated with NH group. Also found were the protons belonging to the dissociated 2-amino-4,6-di-tertbutyl ligand, and the ratio between the two species was exactly 1:1 according to the calculation based on the internal standard in solution.

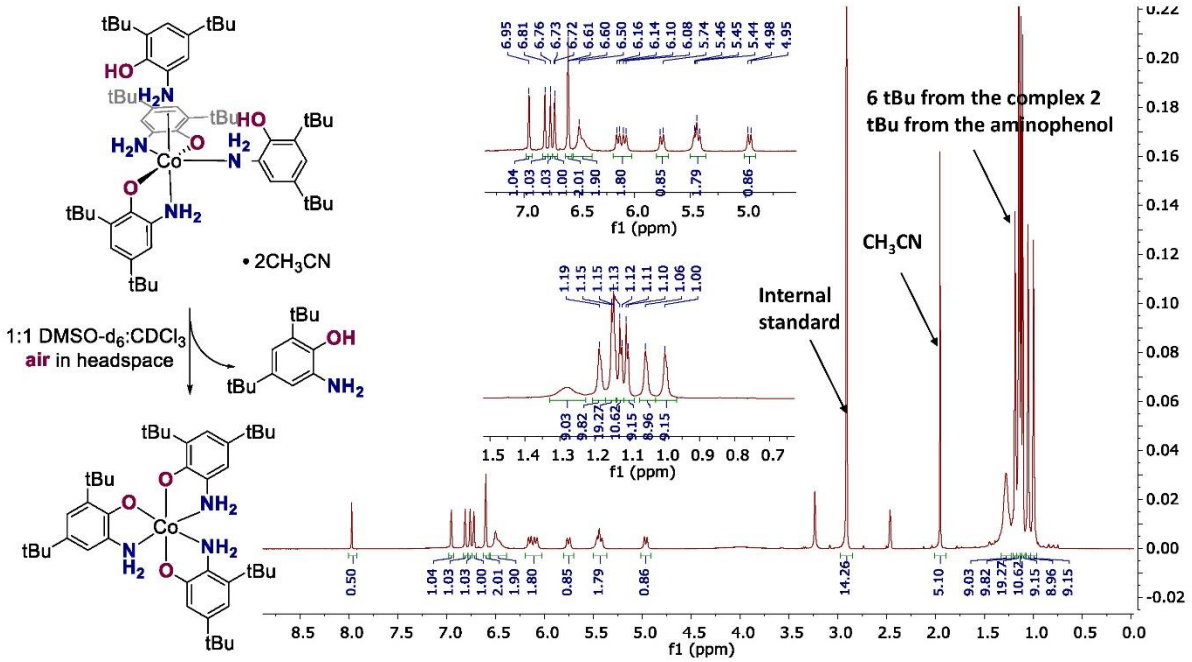

Figure 4.7. Aerobic oxidation of the Co^{II}-AP^{ditBu} complex with dissociation of a ligand monitored by ^{1}H NMR spectroscopy.

The exchangeability of NH protons associated with the diamagnetic cobalt intermediate was further confirmed by the in-situ deuterium-exchange experiment (**Figure 4.8)**. The peaks between 6.5ppm and 5.0ppm all disappeared when the same sample was treated with a few drops of D_2O.

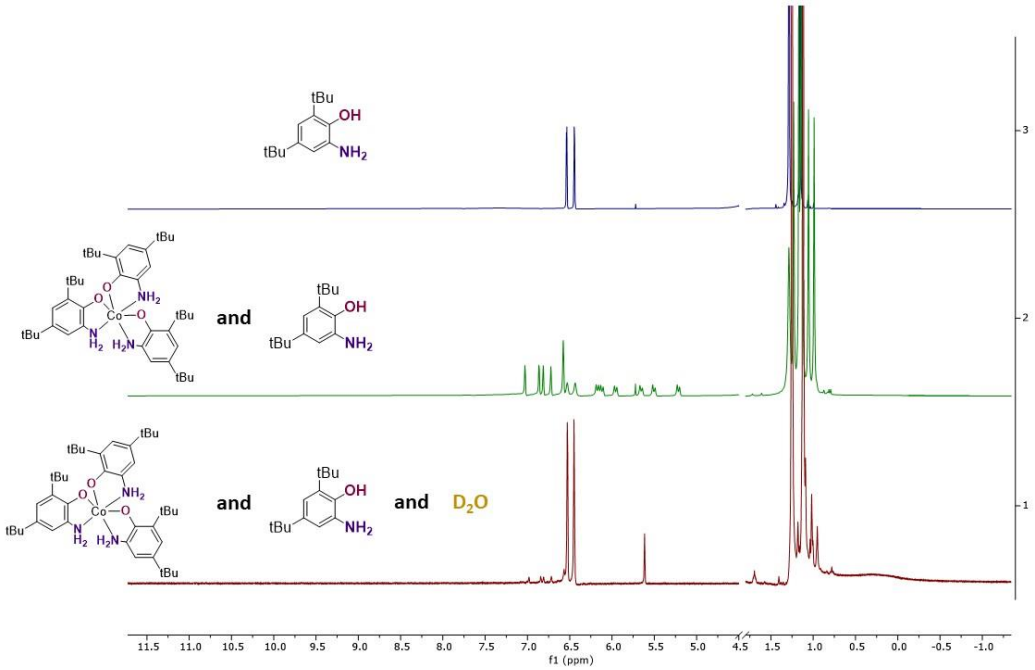

Figure 4.8. Deuterium exchange experiment of the oxidized cobalt intermediate. Standard spectrum of the ligand was included for reference.

4.2.5. Reactivity of Co^{II} and Co^{III} Complexes in the Standard Aerobic Oxidative Coupling Systems

4.2.5.1. Catalytic and Stoichiometric Reactivity of Co^{II}-AP^{ditBu} complex (**7**) in the Oxidative Cyclization Reactions

In order to test for the catalytic competency of the isolated Co^{II} complex **7**, the Co^{II}(2-amino-4,6-tert-butylphenolate)$_2$(2-amino-4,6-tert-butylphenol)$_2$, 10 mol% of catalyst was employed in the experiments shown in **Scheme 4.10**. In the first control experiment **(a)**, 2-amino-4,6-di-*tert*-butyl phenol was employed as both the substrate and the ligand for the Co^{II} complex. The reaction was carried out in acetonitrile for 24 hours with air as the source of stoichiometric

oxidant and delivered exclusively the desired benzoxazole **3w** in 90% yield. However, the formation of two distinct benzoxazoles were observed in the control experiment **(b)** when unsubstituted 2-aminophenol was used as a substrate. With the same reaction conditions, product **3a** from the oxidative cyclization with 2-amionphenol was observed with 55% yield along with the other product **3w** in 32% yield, which derived from 2-amino-4,6-*di*-*tert*-butyl phenolate ligand for the Co^{II} complex. These experiments demonstrated 1) the isolated Co^{II}-AP^{ditBu} complex is catalytically competent; 2) the ligand 2-amino-4,6-*di*-*tert*butyl phenol can dissociate from the cobalt center in solution and engage in the oxidative cyclization reactions with the isocyanide.

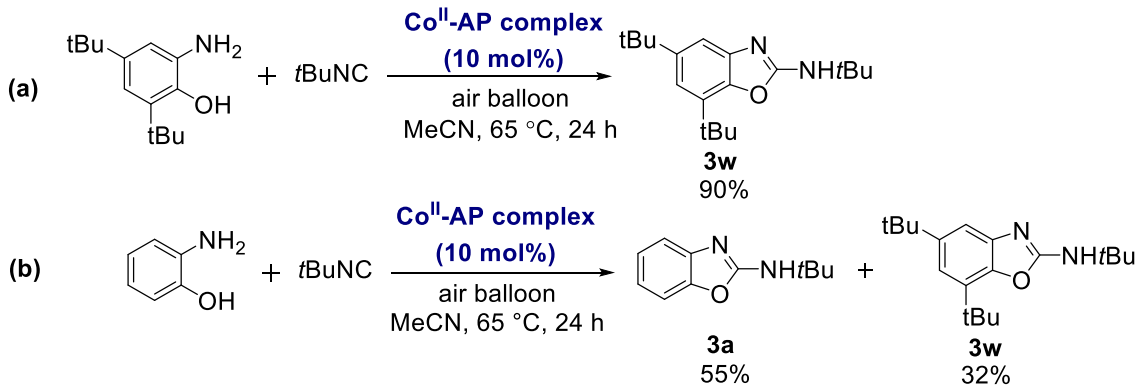

Scheme 4.10. Catalytic control experiments of Co^{II}-AP^{ditBu} complex **(7)** in the aerobic oxidative cyclization reactions.

The experiment was repeated using stoichiometric amounts of Co^{II} complex (**7**) under an anaerobic atmosphere shown in the **Scheme 4.11**. In this case, product **3w** was not observed from the oxidative cyclization. We attribute this observation to the incompetency of the low valent Co^{II} for this transformation, which is in agreement with the findings in Chapter 2. In a stoichiometric control experiment where 1 equiv of $Co(OAc)_2$ was employed to mediate the oxidative cyclization of 2-aminophenol and *tert*-butyl isocyanide under inert atmoshphere, only 10% of the desired product was generated. This result reconfirmed the requirement of an oxidant to initiate the cyclization reactions and stoichiometric amount of Co^{II} is insufficient in this transformation.

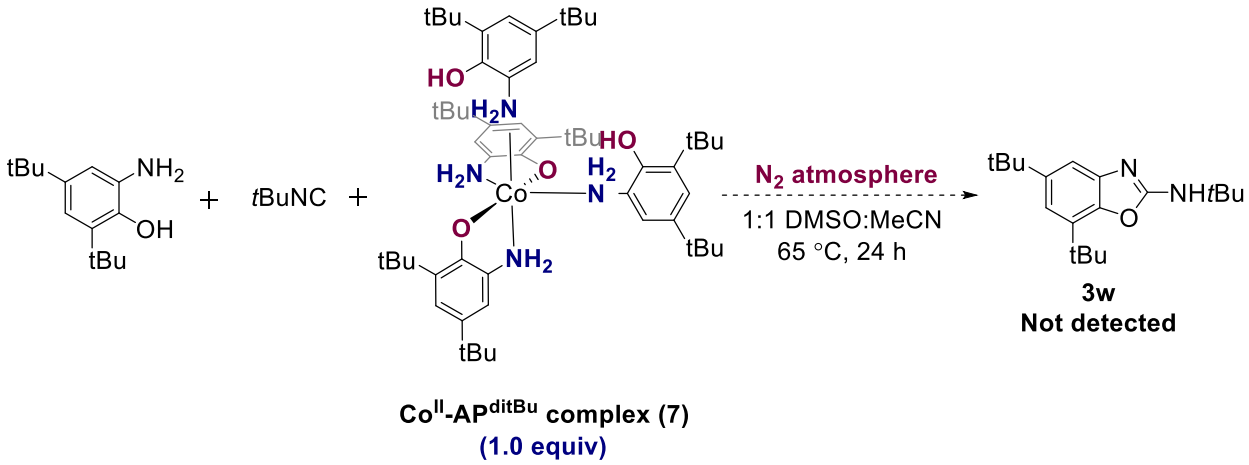

Scheme 4.11. Stoichiometric control experiments of Co^{II}-AP^{ditBu} complex **(7)** under anaerobic reaction conditions.

4.2.5.2. Catalytic and Stoichiometric Reactivity of Co^{III} Complex **(8)** in the Oxidative Cyclization Reactions

The reactivity of the Co^{III}-AP^{ditBu} Complex **(8)** in both catalytic and stoichiometric reaction systems was also evaluated. Catalytic competency of this compound was initially investigated under the aerobic reaction conditions (**Scheme 4.12**). When 2-amino-4,6-di-*tert*-butylphenol was employed as a substrate under the standard condition, only 43% of the compound **3w** was generated as the major product. In the cross-over control experiment shown in **Scheme 4.12b**, unsubstituted *o*-aminophenol was employed to couple with tert-butyl isocyanide and generated **3a** in 55% yield as the only product. This distinct observation compared to the catalytic control with Co^{II} complex **7** demonstrated a significantly different behavior of the Co^{III} complex in terms of the ligand dissociation. When the tert-butyl isocyanide is replaced with cyclohexyl isocyanide in the standard reaction, the desired product **3x** was generated in 53% yield. While in these three catalytic reactions the yields are moderate compared to the reactivity of Co^{II}, these results still demonstrate the catalytic competency of the Co^{III} complex with 4~5 turnovers, albeit the reaction pathway might be completely different. The slightly diminished yields could be attributed to the slow ligand dissociation and reassociation for Co^{III} complex in the presence of O_2. Upon dissociation, the 2-amino-4,6-di-*tert*-butylphenol ligand may be decomposed via an oxidative ring opening pathway as described in the introduction section, which explains the reason that in control experiment (**b**), the formation of the cross-over product was not observed.

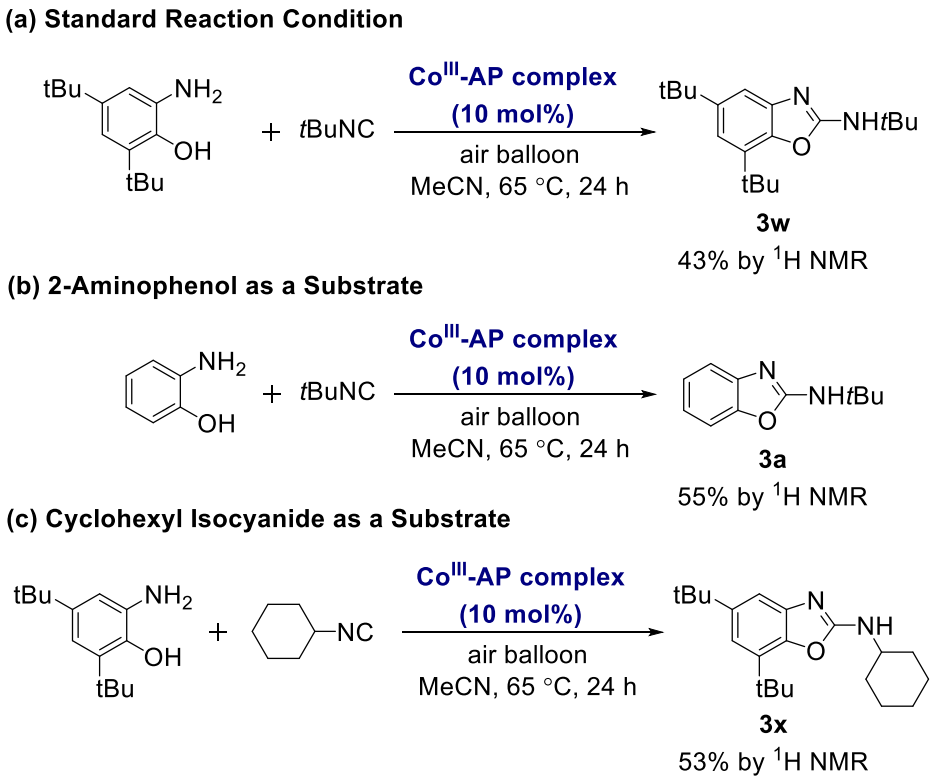

Scheme 4.12. Catalytic control experiments of Co^{III}-AP^{ditBu} complex **(8)** under aerobic oxidative cyclization conditions.

The stoichiometric reactivity of the Co^{III} was also evaluated. Control experiments were carried out by standard Schlenk line operation under both N_2 and O_2 atmosphere with 1 equivalent of the coupling partner, *tert*-butyl isocyanide (**Scheme 4.13**). As no desired product **3w** was observed in either case, the reaction vessel was reinvestigated to reduce the potential loss of the volatile isocyanide through the Schlenk line. When the same reaction was carried out in a pressure tube under inert atmosphere, **3w** was still not detected. Of note, the three control experiments, regardless of the aerobic or anaerobic conditions, gave very comparable results. While no expected product was generated, these reactions yielded identical mixtures as indicated by ^{1}H NMR spectroscopy. These species may be related to one or multiple unknown cobalt complexes bearing 2-amino-4,6-di-*tert*-butylphenol derived ligands, as illustrated by multiple tert-butyl groups in the aliphatic range. Under such reaction conditions, cyclized product of **3w** not being observed may be attributed to 1) slow rate of ligand dissociation from the cobalt metal center and 2) the

concentration of tert-butyl isocyanide is too low to trap any phenoxyl radical and then form the cyclized products.

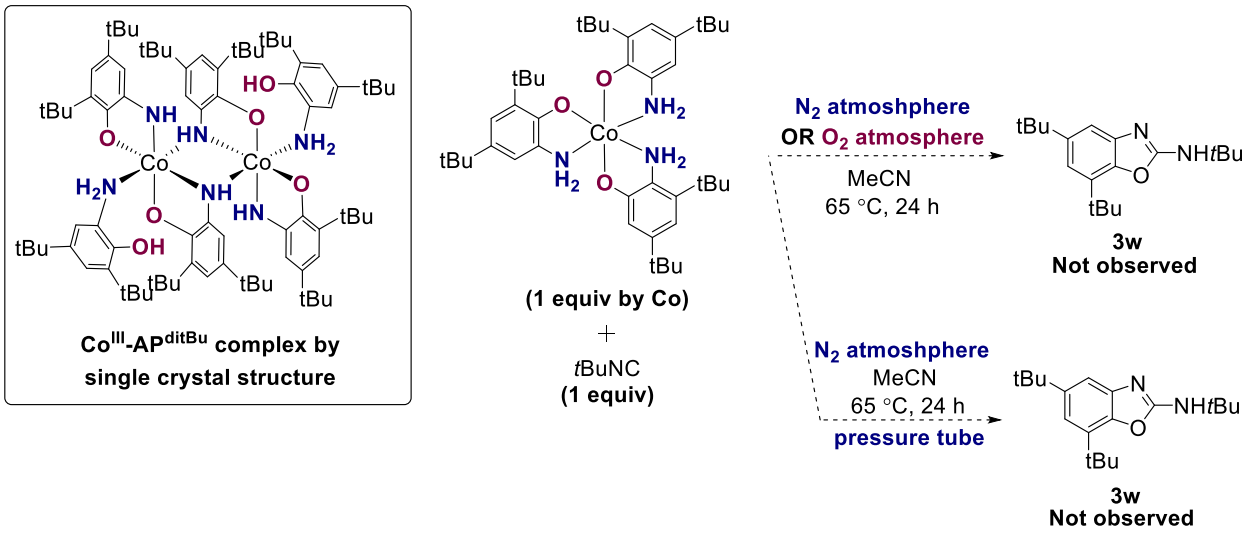

Scheme 4.13. Stoichiometric control experiments with Co^{III}-AP^{ditBu} complex **(8)** under both aerobic and anaerobic atmosphere.

Moving forward, the ability of Co^{III} complex in mediating the oxidative cyclization reactions under anaerobic atmosphere was also investigated. Both 2-amino-4,6-di-*tert*-butylphenol and *tert*-butyl isocyanide were present in this set of experiments with the catalyst loading as the only variation under the N_2 atmosphere (**Scheme 4.14**). It was interesting to find that the yields of the desired product **3w** in this transformation were nearly proportional to the loading of the Co^{III} catalyst (**8**). The reactions carried out with 0.5, 0.7 and 1.0 equivalent of Co^{III} catalyst afforded the product with the yields 42%, 64% and 93% respectively. These results indicated Co^{III} might be the active species in mediating the oxidative cyclization reactions. Combined with the results from the above control experiments in the absence of 2-amino-4,6-di-tertbutyl phenol substrate (**Scheme 4.13**), it was assumed that the dissociated ligand from the Co^{III} complex is not able to reversibly bind to the cobalt center, therefore, in the case where no aminophenol substrate was present, a new cobalt complex from ligand exchange will not be formed thus cannot undergo the transition-metal mediated interaction with *tert*-butyl isocyanide to form the cyclized product. Unfortunately, the fate of the dissociated ligand cannot be confirmed at the current stage, although some type of decomposition is highly suspected.

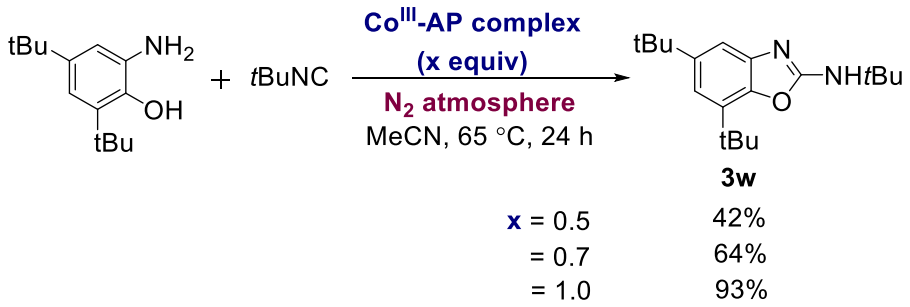

Scheme 4.14. Reactivity of Co^{III}-AP^{ditBu} complex in oxidative cyclization reactions under N_2 atmosphere.

4.3. Conclusive Summary

In summary, the work in this chapter is focused on the synthesis and reactivity studies of cobalt complexes bearing bisnucleophile-derived ligands as potentially active intermediates for aerobic oxidative cyclization transformations developed in the previous two chapters. 2-amino-4,6-di-*tert*-butyl phenol was employed as a model ligand in the metal complex synthesis for solubility and stability considerations. Two unprecedented cobalt complexes were isolated with unique coordinating environments, Co^{II}(2-amino-4,6-tert-butylphenolate)$_2$(2-amino-4,6-tert-butylphenol)$_2$ and Co_2^{III}(2-amino-4,6-tert-butylphenolate)$_2$(2-amino-4,6-tert-butylphenol)(μ-2-amido-4,6-tert-butylphenolate)$_2$. To date, these two compounds are the first examples of well-defined cobalt complexes that bear *ortho*-aminophenol ligands with unsubstituted NH_2 groups. Notably, the bulky *N*-substitutions on the most commonly used aminophenol-derived ligands play a critical role in stabilizing cobalt complexes in the presence of O_2. Preliminary studies on their abilities to mediate oxidative cyclization reactions have demonstrated the catalytic and stoichiometric competencies of both the Co^{II} and Co^{III} complexes. Both complexes are capable of participating in O_2 activation. Under the catalytic reaction conditions, the ligand on Co^{II} complex can reversibly bind to the metal center and engage in the aerobic oxidative cyclization. The interaction of the ligand with the metal center in these Co^{III} complexes is irreversible upon O_2 activation, as suggested by cross-over experiments in the context. In this regard, the Co^{II} and the Co^{III} complexes mediate the reaction via different pathways. Although the fate of the dissociated aminophenol ligands is still not clear at the current stage, these data combined support our earlier proposed mechanistic pathways in Chapter 2. Our study convinced the dual functionality of the

bis-nucleophile as both a substrate and a redox-active ligand. The isolated complexes bearing 2-amino-4,6-di-*tert*-butylphenol ligand are capable of activating molecular oxygen and mediating the oxidative cyclization reactions. We believe these studies on the cobalt complexes derived from our reaction system will shed a light on deeper insights for future relevant works.

4.4. Experimental Section

4.4.1. General Considerations

^{1}H, and ^{13}C{^{1}H} NMR spectra were recorded on an Agilent 400 MHz spectrometer or a JEOL 400 MHz spectrometer. Chemical shifts are given in parts per million and referenced to the residual solvent signal;[135] all coupling constants are reported in Hz. High resolution mass spectra were obtained on a Thermo Finnigan Linear Trapping Quadrupole mass spectrometer. IR spectra were recorded on a PerkinElmer (Spectrum 100) FT-IR spectrometer. Column chromatography was performed using Silicycle SiliaFlash P60 silica gel.

Dry solvents were taken from a solvent system which passes the solvent through a column of activated molecular sieves. All deuterated solvents were purchased from Cambridge Isotope Laboratories. All other chemicals were purchased from commercial sources and used without further purification unless otherwise noted. Air to fill air balloons was obtained from a house compressed air system. O_2 used in control reactions was purchased from Airgas. Both air and O_2 sources were used as received without drying tubes or additional precautions to remove trace water. IR spectra were recorded on a Perkin Elmer (Spectrum 100) FT-IR spectrometer. High resolution mass spectra were obtained on a Thermofisher Scientific Q Exactive Mass Spectrometer. Elemental analyses were performed by Atlantic Microlab, Inc., Norcross, GA.

4.4.2. Synthesis of 2-amino-4,6-*di*-tert-butyl phenol ligand

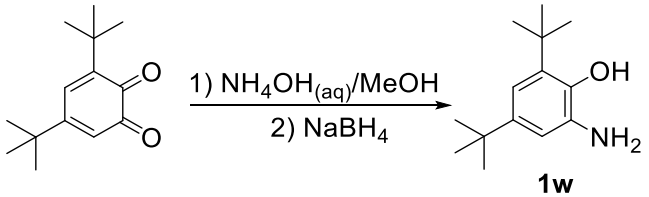

The synthesis was based on the modified literature procedure.[166] In a 500 mL round bottom flask, 3,5-di-tertbutyl-1,2-benzoquinone (7.91g, 35.9 mmol, 1.0 equiv) was dissolved in a mixture of methanol and concentrated ammonium hydroxide (200 mL/80mL) and stirred for 10 min. Upon dissolution, sodium borohydride (3.23g, 85.4 mmol, 2.2. equiv) was added as solid portion by portion over a period of 60 min. The mixture was allowed to stir at room temperature for another 1 hour. Upon completion, the reaction mixture was quenched by pouring slowly into 1L of ice water, then exacted three times with ethyl acetate (3×150 mL). The combined organic phase was washed with brine, separated, dried over anhydrous sodium sulfate and filtered. The solvent was removed via the rotary evaporation to yield the crude compound. High purity 2-amino-4,6-di-tertbutyl phenol **1w** was generated by repetitive washing and decant with hexane, giving the desired product as a pale-yellow powder (5.65g, 25.5 mmol, 71%). Elemental Analysis: calculated $C_{14}H_{23}NO$, C: 75.97; H: 10.47; N: 6.33; found: C: 76.18; H: 10.58; N: 6.32. ^{1}H-NMR (400 MHz, DMSO-D_6) δ 6.54 (d, J = 2.3 Hz, 1H), 6.44 (d, J = 2.3 Hz, 1H), 4.41 (s, 2H), 1.29 (s, 9H), 1.15 (s, 9H).

4.4.3. Synthesis of 5,7-di-*tert*-butyl-2-(tert-butylamino)benzoxazole (3w) by Aerobic Oxidative Cyclization Reaction

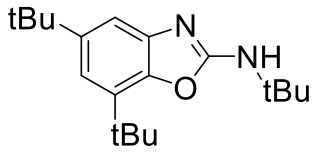

3w

2-amino-4,6-di-tertbutyl phenol (66.4 mg, 0.300 mmol) and cobalt(II) acetate (5.31 mg, 0.0300 mmol) were combined in a 6-inch test tube inside a N_2 filled glovebox, and dissolved in dry CH_3CN (3 mL). *tert*-Butyl isocyanide (35.2 μL, 0.300 mmol) was added to the same test tube after which it was sealed with a septum and removed from the glovebox. The reaction mixture was then stirred in an oil bath at 65 °C for 24 hours with an air balloon attached to a syringe with a needle inserted through the septum. Upon completion, the reaction mixture was cooled to room temperature and filtered through a Pasteur pipette silica gel plug and washed with ethyl acetate (~15 mL). The resulting filtrate was concentrated by rotary evaporation and the resulting solid was

purified by silica column flash chromatography (gradient elution from the pure hexanes to hexane: ethyl acetate = 8:1, R_f = 0.4 in 5:1 hexanes : ethyl acetate), to give the title compound as a light pink microcrystalline solid in 78 % yield (70.9 mg, 0.234 mmol). ^{1}H-NMR (400 MHz, $CDCl_3$) δ 7.30 (s, 1H), 6.98 (s, 1H), 5.33 (s, 1H), 1.51 (s, 9H), 1.44 (s, 11H), 1.34 (s, 10H). ^{13}C-NMR (100 MHz, $CDCl_3$) δ160.87, 146.71, 144.09, 143.11, 131.77, 115.21, 111.43, 51.97, 35.05, 34.20, 32.00, 30.10, 29.43. FTIR (ATR, cm^{-1}): 3156 (w), 3056 (w), 2960 (m), 2868 (w), 1666 (s), 1616 (m), 1589 (s), 1492 (m), 1409 (s), 1362 (s), 1302 (m), 1265 (w), 1047.59 (s), 1016 (s), 981 (w), 919 (s), 854 (s), 736 (s), 661 (m), 612 (w).

4.4.4. Synthesis of Co^{II}-AP^{ditBu} Complex Co^{II}(2-amino-4,6-tert-butylphenolate)$_2$(2-amino-4,6-tert-butylphenol)$_2$ and Co^{III}-AP^{ditBu} Complex Co_2^{III}(2-amino-4,6-tert-butylphenolate)$_2$(2-amino-4,6-tert-butylphenol)(μ-2-amido-4,6-tert-butylphenolate)$_2$

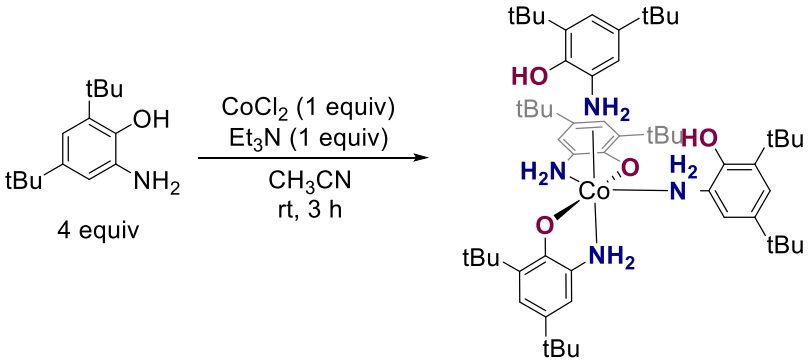

In a N_2-filled glovebox, a 50 mL Erlenmeyer flask equipped with a stir bar was charged with 2-amino-4,6-di-tert-butyl phenol ligand (885.4mg, 4.0 mmol, 1.0 equiv) and anhydrous cobalt (II) chloride (128.8mg, 1.0 mmol, 1 equiv) in dry acetonitrile (40 mL). The resulting mixture was allowed to stir at room temperature for 10 mins to yield a persistent dark green color. It was then filtered and the filtrate was transferred into another clean 50 ml Erlenmeyer flask. Triethylamine (404.8 mg, 4.0 mmol, 4.0 equiv) pre-diluted with 2 mL acetonitrile was added dropwise into the filtrate and the mixture was stirred under room temperature for another three hours. Upon completion, beige to light grey precipitate crushed out from the solution, leaving the solution a

violet supernatant. The precipitate was filtered, washed a couple of times with dry acetonitrile under vacuum to generate the desired Co^{II} complex with up to 93% yield. The complex was further dried under high vacuum to remove excess solvent that binding around, leading to slight color change to light greyish green with a golden sheen. Elemental Analysis: calculated $C_{56}H_{90}CoN_4O_4 \cdot 2CH_3CN$, C: 70.35; H: 9.45; N: 8.20; found, C: 70.13; H: 9.52; N: 7.94.

Solid-state oxidation to Co^{III}: The dry Co^{II}-AP^{ditBu} complex was exposed to air up to 12 hours, yielding the corresponding Co^{III}-AP^{ditBu} as microcrystalline dark violet solid with a golden sheen. Elemental Analysis: calculated $C_{42}H_{66}CoN_3O_3$, C: 70.07; H: 9.24; N: 5.84; found, C: 70.33; H: 9.08; N: 5.70.

4.4.5. Reactivity Studies of Co^{II}-AP^{ditBu} Complex (7) and Co^{II}-AP^{ditBu} Complex (8)

Synthetic Procedure for Catalytic Experiment with Co^{II}-AP^{ditBu} Complex (7)

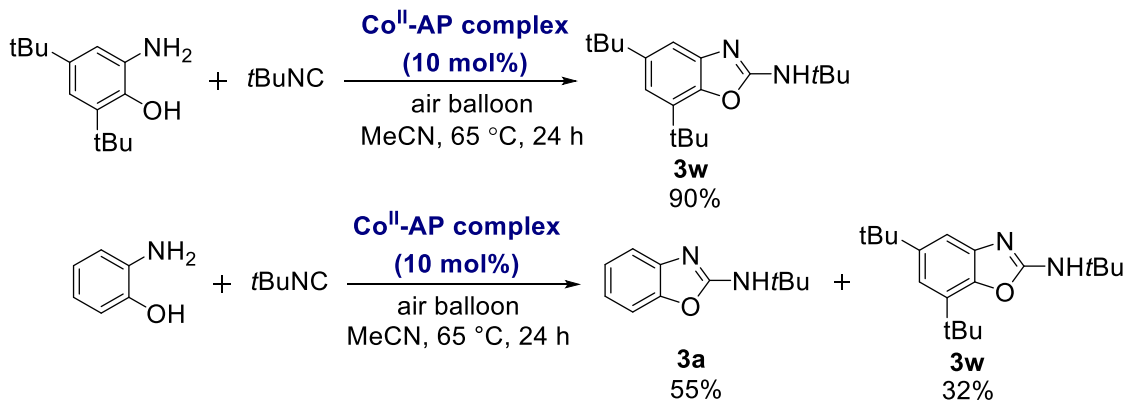

In a 6-inch test tube inside a N_2 filled glovebox, Co^{II}-AP^{ditBu} complex (**7**) (28.27 mg, 0.03 mmol, 0.1 equiv) and 2-amino-4,6-di-tert-butyl phenol (66.40mg, 0.3 mmol, 1.0 equiv) or 2-aminophenol (32.74mg, 0.3 mmol, 1.0 equiv) were combined and dissolved in in dry CH_3CN (3 mL). *tert*-Butyl isocyanide (35.2 μL, 0.300 mmol) was added to the same test tube before it was sealed with a septum and removed from the glovebox. The reaction mixture was stirred in an oil bath at 65 °C for 24 hours with an air balloon attached to a syringe with a needle inserted through the septum. Upon completion, the reaction mixture was cooled to room temperature, partitioned into 30mL ethyl acetate and stirred with 100 mL of 1.0 M EDTA solution for 1 hour. The resulting

mixture was separated, and the aqueous layer was washed another two times with ethyl acetate (2×30 mL). The combined organic phase was washed again with saturated sodium chloride solution, separated, dried over anhydrous sodium sulfate, filtered, concentrated to 10mL solution, and eventually passed through a Pasteur pipette silica gel plug. The resulting filtrate was concentrated by rotary evaporation to yield the crude product. The crude yield was determined by ^{1}H NMR spectroscopy with dimethylsulfone (0.0300 mg, 0.0318 mmol) as the internal standard.

Synthetic Procedure for Stoichiometric Control Experiments of Co^{II}-AP^{ditBu} complex (7) under Anaerobic Reaction Conditions

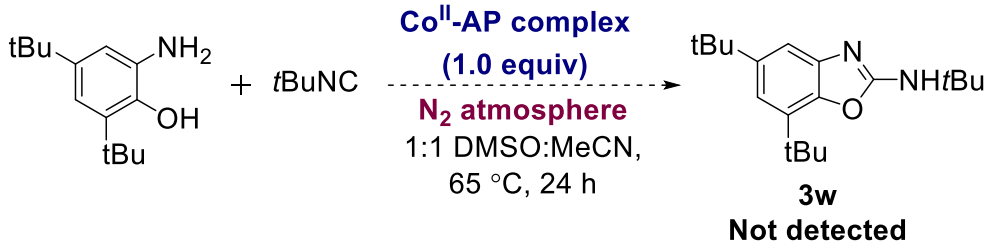

In a 20mL pressure tube inside a N_2 filled glovebox, Co^{II}-AP^{ditBu} complex (**7**) (188.5 mg, 0.2 mmol, 1.0 equiv) and 2-amino-4,6-di-tert-butyl phenol (44.27mg, 0.2 mmol, 1.0 equiv) were combined and dissolved in 5 mL mixture of dry CH_3CN and DMSO (1:1). *tert*-Butyl isocyanide (23.5 μL, 0.2 mmol, 1.0 equiv) was added to the same pressure tube before it was sealed and removed from the glovebox. The reaction mixture was stirred in an oil bath at 65 °C for 24 hours under N_2. Upon completion, the reaction mixture was cooled to room temperature, then CH_3CN was removed via rotary evaporation. The resulting mixture in DMSO was partitioned into 30 mL ethyl acetate and stirred with 100 mL of 1.0M EDTA solution for 1 hour. The resulting mixture was separated, and the aqueous layer was washed twice with ethyl acetate (2×30 mL). The combined organic phase was washed again with saturated sodium chloride solution, separated, dried over anhydrous sodium sulfate, filtered, concentrated to 10mL solution, and eventually passed through a Pasteur pipette silica gel plug. The resulting filtrate was concentrated by rotary evaporation to yield the crude product as a brown solid. No desired product was generated during this reaction by ^{1}H NMR spectroscopy.

Synthetic Procedure for Catalytic Reactivity of Co^{III}-AP^{ditBu} Complex (8) in the Oxidative Cyclization Reactions

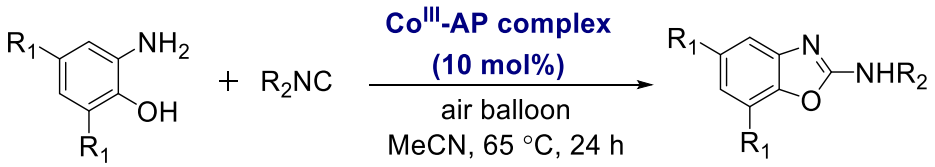

R_1 = *t*Bu	R_2=*t*Bu	**3w** 43% by ^{1}H-NMR
R_1 = H	R_2=*t*Bu	**3a** 55% by ^{1}H-NMR
R_1 = *t*Bu	R_2=cyclohexyl	**3x** 53% by ^{1}H-NMR

<u>Representative procedure for the synthesis of **3w**:</u> In a 6-inch test tube inside a N_2 filled glovebox, Co^{III}-AP^{ditBu} complex (**8**) (21.6 mg, 0.03 mmol, 0.1 equiv) and 2-amino-4,6-di-tert-butyl phenol (66.40 mg, 0.3 mmol, 1.0 equiv) were combined and dissolved in 5 mL mixture of dry CH_3CN. *tert*-Butyl isocyanide (35.2 μL, 0.3 mmol) was added to the same test tube before it was sealed with a septum and removed from the glovebox. The reaction mixture was stirred in an oil bath at 65 °C for 24 hours with an air balloon attached to a syringe with a needle inserted through the septum. Upon completion, the reaction mixture was cooled to room temperature, partitioned into 30 mL ethyl acetate and stirred with 100 mL of 1.0M EDTA solution for 1 hour. The resulting mixture was separated, and the aqueous layer was washed twice with ethyl acetate (2×30 mL). The combined organic phase was extracted again with saturated sodium chloride solution, separated, dried over anhydrous sodium sulfate, filtered, concentrated to 10mL solution, and eventually passed through a Pasteur pipette silica gel plug. The resulting filtrate was concentrated by rotary evaporation to yield the crude product which was later quantified using ^{1}H-NMR spectroscopy with dimethyl sulfone (0.0300 mg, 0.0318 mmol) internal standard.

<u>Synthesis of **3a**:</u> In a 6-inch test tube inside a N_2 filled glovebox, Co^{III}-AP^{ditBu} complex (**8**) (21.6 mg, 0.03 mmol, 0.1 equiv) and 2-aminophenol (32.74 mg, 0.3 mmol, 1.0 equiv) were combined and dissolved in 5 mL mixture of dry CH_3CN. *tert*-Butyl isocyanide (35.2 μL, 0.3 mmol) was added to the same test tube before it was sealed with a septum and removed from the glovebox. The rest of procedures follow the synthesis of **3w**.

<u>Synthesis of **3x**:</u> In a 6-inch test tube inside a N_2 filled glovebox, Co^{III}-AP^{ditBu} complex (**8**) (21.6 mg, 0.03 mmol, 0.1 equiv) and 2-amino-4,6-di-tert-butyl phenol (66.40 mg, 0.3 mmol, 1.0 equiv)

were combined and dissolved in 5 mL mixture of dry CH_3CN. Cyclohexyl isocyanide (37.3 μL, 0.3 mmol) was added to the same test tube before it was sealed with a septum and removed from the glovebox. The rest of procedures follow the synthesis of **3w**.

Synthetic Procedure for Stoichiometric Reactivity of Co^{III}-AP^{ditBu} Complex (8) in the Oxidative Cyclization Reactions

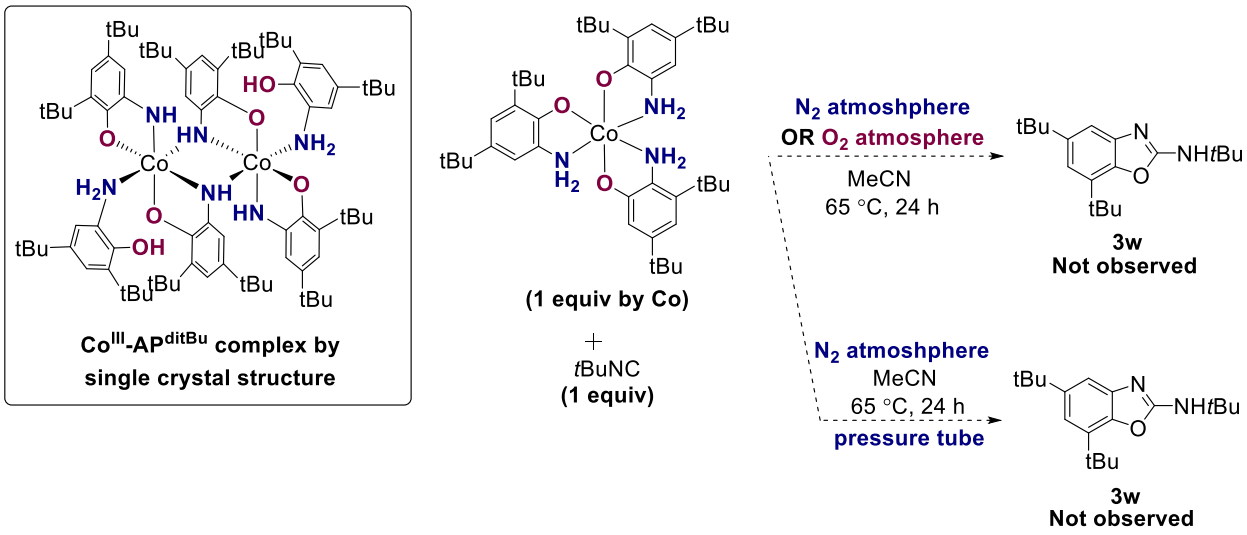

<u>Schlenk Tube Reaction under N_2 (Presentative Procedure):</u> To a 25 mL Schlenk tube inside a N_2 filled glovebox, Co^{III}-AP^{ditBu} complex (**8**) (71.9 mg, 0.1 mmol, 1.0 equiv) was dissolved in 5 mL of dry CH_3CN. *tert*-Butyl isocyanide (11.8 μL, 0.1 mmol) was added to the same Schlenk tube before it was sealed with a septum and removed from the glovebox. The tube was connected to the Schlenk line via the side arm, and tubing was evacuated and backfilled with N_2 three times before the valve on the side arm was opened. The reaction mixture was stirred in an oil bath at 65 ˚C for 24 hours under N_2 atmosphere. Upon completion, the reaction mixture was cooled to room temperature, partitioned into 30 mL ethyl acetate and stirred with 100 mL of 1.0M EDTA solution for 1 hour. The resulting mixture was separated, and the aqueous layer was washed twice with ethyl acetate (2×30 mL). The combined organic phase was extracted again with saturated sodium chloride solution, separated, dried over anhydrous sodium sulfate, filtered, concentrated to 10mL solution, and eventually passed through a Pasteur pipette silica gel plug. The resulting filtrate was concentrated by rotary evaporation to yield the crude product which was later quantified using ^{1}H-NMR spectroscopy with dimethyl sulfone (0.0300 mg, 0.0318 mmol) internal standard.

Schlenk Tube Reaction under O_2: In a 25 mL Schlenk tube, Co^{III}-AP^{ditBu} complex (**8**) (71.9 mg, 0.1 mmol, 1.0 equiv) was added. The tube was sealed with a septum and was connected to the Schlenk line via the side arm. The tube was then evacuated and backfilled with O_2 by inserting a O_2 balloon through the septum for three times. Under O_2 atmosphere, 5 mL of dry CH_3CN was added to dissolve the Co^{III} complex, followed by adding the *tert*-Butyl isocyanide (11.8 μL, 0.1 mmol) into the same Schlenk tube. With a O_2 balloon attached to a syringe with a needle inserted through the septum, the reaction mixture was stirred in an oil bath at 65 °C for 24 hours. The rest procedures follow the above Schlenk Tube Reaction under N_2 (Presentative Procedure).

Pressure Tube Reaction under N_2: In a 20mL pressure tube inside a N_2 filled glovebox, Co^{III}-AP^{ditBu} complex (**8**) (71.9 mg, 0.1 mmol, 1.0 equiv) was added and dissolved in 5 mL of dry CH_3CN. *tert*-Butyl isocyanide (11.8 μL, 0.1 mmol, 1.0 equiv) was added to the same pressure tube before it was sealed and removed from the glovebox. The reaction mixture was stirred in an oil bath at 65 °C for 24 hours under N_2. The rest procedures follow the above Schlenk Tube Reaction under N_2 (Presentative Procedure).

Synthetic Procedure for Stoichiometric Reactivity of Co^{III}-AP^{ditBu} Complex (8) in the Presence of Both Aminophenol and Isonitrile Substrates

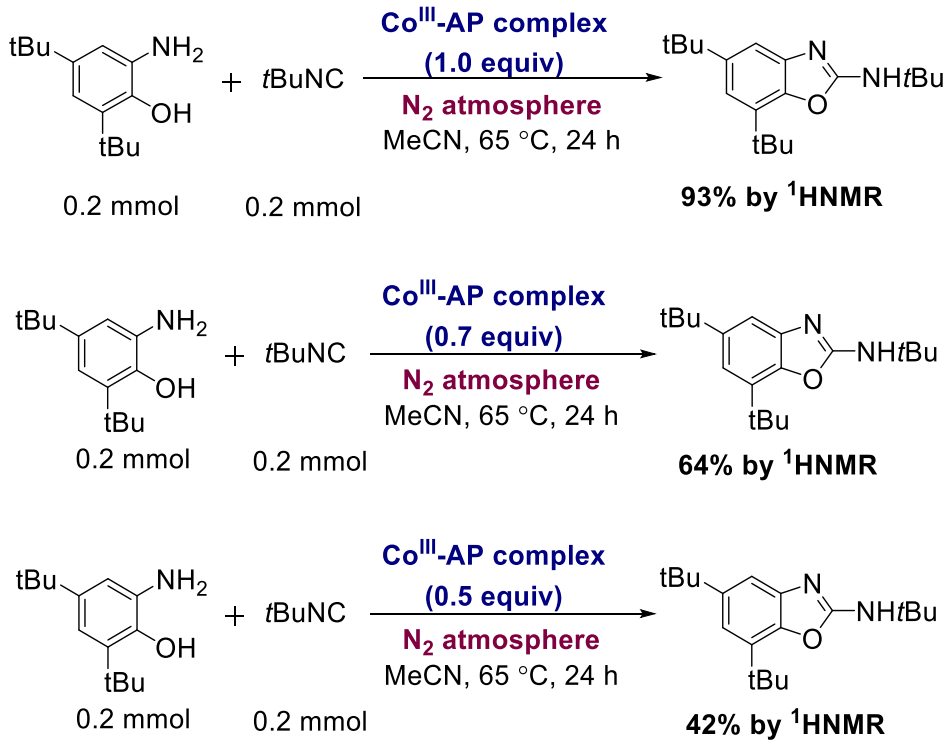

Representative Procedure: In a 20mL pressure tube inside a N_2 filled glovebox, Co^{III}-AP^{ditBu} complex (**8**) (144.0 mg, 0.02 mmol, 1.0 equiv) and 2-amino-4,6-di-tert-butyl phenol (44.27mg, 0.2 mmol, 1.0 equiv) were combined and dissolved in 5 mL of dry CH_3CN. *tert*-Butyl isocyanide (23.5 μL, 0.2 mmol, 1.0 equiv) was added to the same pressure tube before it was sealed and removed from the glovebox. The reaction mixture was stirred in an oil bath at 65 °C for 24 hours under N_2. Upon completion, the reaction mixture was cooled to room temperature, then was partitioned into 30 mL ethyl acetate and stirred with 100 mL of 1.0M EDTA solution for 1 hour. The resulting mixture was separated, and the aqueous layer was extracted twice with ethyl acetate (2×30 mL). The combined organic phase was washed again with saturated sodium chloride solution, separated, dried over anhydrous sodium sulfate, filtered, concentrated to 10mL solution, and eventually passed through a Pasteur pipette silica gel plug. The resulting filtrate was concentrated by rotary evaporation to yield the crude product, which was quantified by ^{1}H NMR spectroscopy using dimethyl sulfone (0.0300 mg, 0.0318 mmol) internal standard.

4.4.6. Crystallography Data

4.4.6.1. Description of the X-ray Structural Analysis of Co^{II}-AP^{ditBu} Complex **(7)**

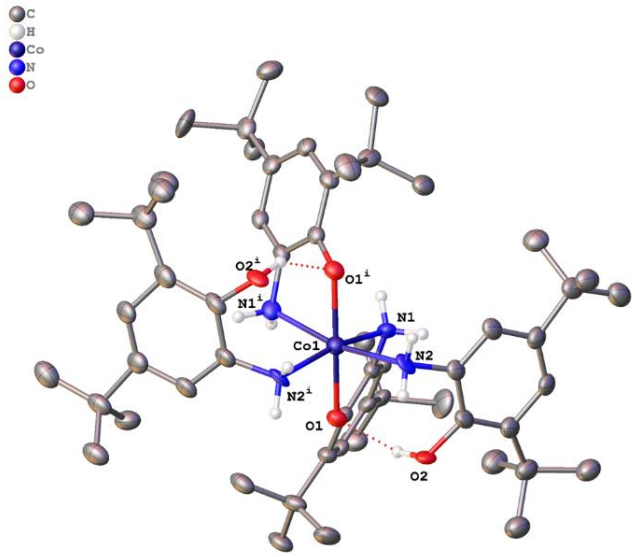

A green-yellow block shaped crystal measuring 0.34 mm x 0.30 mm x 0.17 mm was selected under paratone oil using a MiTeGen Micromount and mounted at 100(1) K to a D8-

Venture diffractometer equipped with a Mo sealed tube X-ray source, a Triumph monochromator, and a Photon CMOS area detector. The unit cell was determined from reflections harvested with a signal to noise ratio (I/σ) of at least 8 from a series of 3 ω scans of 6° with 0.5° frames using APEX3.[1] The data were collected to a resolution of 0.81 Å using 4 ω scans.

The data were integrated using SAINT and corrected for absorption using SADABS.[2] The systematic absences and E-statistics of the data were consistent with the space group $Im\bar{3}$. The structure was solved using the intrinsic phasing routine of SHELXT.[3] The non-hydrogen atoms were located from a Fourier difference map of the electron density and anisotropically refined using the least-squares algorithm of SHELXL.[4] The carbon-based hydrogen atoms were then placed in calculated positions and refined with riding thermal parameters.

The asymmetric unit consists of one half molecule of Co(2-amino-4,6-tert-butylphenolate)$_2$(2-amino-4,6-tert-butylphenol)$_2$ (Figures 1 – 2). The molecule resides on a crystallographic 2-fold axis and a crystallographic mirror plane. The 2-fold axis is a true symmetry element of the molecule and passes through the following points: the midpoint of N2 and N2^i; Co1; and the midpoint of N1 and N1^i. The molecule is disordered over the mirror plane.

Phenol ligand O2 shows additional positional disorder (major component: 27.8(6)%). Geometry and thermal parameter restraints were used to ensure a chemically reasonable and computationally stable refinement.

There was an additional solvent molecule located in the crystal structure. Despite numerous attempts to model this solvent, a computationally stable refinement was not possible. The SQUEEZE algorithm of PLATON was used to correct for the solvent electron density. PLATON calculated that the solvent accessible voids in the structure had a volume of 3077 A^3 (16.2% of the unit cell volume) and consisted of 864 electrons/unit cell. This is consistent with approximately 3 molecules of MeCN per molecule of Co(2-amino-4,6-tert-butylphenolate)$_2$(2-amino-4,6-tert-butylphenol)$_2$ in the structure.

The final structure consisted of 461 parameters refined against 3347 independent reflections, giving refinement residuals of R_1 = 0.0524 (based off F^2 for $I > 2\sigma$) and wR_2 = 0.1617 (based of F^2 for all reflections). The final difference Fourier map was featureless.

References:

1. Bruker-AXS (2016). APEX 3 version 2016.9-0. Madison, Wisconsin, USA
2. (a) Bruker-AXS (2015). *SAINT V8.37A*. Madison, Wisconsin, USA. (b) Krause, L.; Herbst-Irmer, R.; Sheldrick, G.; Stalke, D. J. Appl. Crystallogr. **2015**, *48*, 3-10.
3. Sheldrick, G. M., *Acta Crystallogr. A* **2015**, A71, 3-8.
4. (a) Sheldrick, G. M., *Acta Crystallogr. C* **2015**, C71, 3-8.; (b) Dolomanov, O. V.; Bourhis, L. J.; Gildea, R. J.; Howard, J. A. K.; Puschmann, H., *J. Appl. Crystallogr.* **2009**, *42*, 339-341.

Table 4.1. Crystal data and structure refinement for Co^{II}-AP^{ditBu} Complex (7).

Identification code	Co^{II}-AP^{ditBu} Complex (7)
Empirical formula	$C_{56}H_{90}CoN_4O_4$
Formula weight	942.24
Temperature/K	100.0
Crystal system	cubic
Space group	Im-3
a/Å	26.692(3)
b/Å	26.692(3)
c/Å	26.692(3)
α/°	90
β/°	90
γ/°	90
Volume/$Å^3$	19018(7)
Z	12
ρ_{calc}g/cm^3	0.987

μ/mm^{-1}	0.310
F(000)	6156.0
Crystal size/mm^3	0.34 × 0.3 × 0.17
Radiation	MoKα (λ = 0.71073)
2Θ range for data collection/°	6.106 to 52.046
Index ranges	$-32 \leq h \leq 32$, $-32 \leq k \leq 32$, $-32 \leq l \leq 32$
Reflections collected	231435
Independent reflections	3347 [R_{int} = 0.0988, R_{sigma} = 0.0146]
Data/restraints/parameters	3347/573/461
Goodness-of-fit on F^2	1.181
Final R indexes [I>=2σ (I)]	R_1 = 0.0524, wR_2 = 0.1322
Final R indexes [all data]	R_1 = 0.0757, wR_2 = 0.1617
Largest diff. peak/hole / e $Å^{-3}$	0.42/-0.27

Table 4.2. Fractional atomic coordinates ($\times 10^4$) and equivalent isotropic displacement parameters ($Å^2 \times 10^3$) for Co^{II}-AP^{ditBu} Complex (7). U_{eq} is defined as 1/3 of of the trace of the orthogonalised U_{IJ} tensor.

Atom	***x***	***y***	***z***	**U(eq)**
Co1	5000	8024.6(2)	5000	31.9(2)
O1	5176.3(11)	8053.1(11)	4277.8(11)	33.3(7)
N1	5550.0(11)	8619.1(11)	4994(5)	31.7(8)

C1	5541.7(15)	8821.7(17)	4504.3(15)	29.2(9)
C2	5328.7(15)	8508.2(16)	4144.0(15)	29.0(9)
C3	5296.8(16)	8689.6(18)	3650.7(15)	33.5(10)
C4	5483.3(16)	9157.4(18)	3555.2(16)	33.6(10)
C5	5700.5(18)	9461(2)	3908.1(19)	33.0(11)
C6	5722.4(15)	9280.2(17)	4386.1(15)	30.0(9)
C7	5040(8)	8375.5(17)	3249.1(14)	40(2)
C8	4505(2)	8289(2)	3392.4(18)	46.6(13)
C9	5314(2)	7883(2)	3180(2)	56.2(15)
C10	5055(10)	8642(2)	2741.4(15)	48(3)
C11	5915.5(14)	9966(7)	3790.5(15)	36.4(17)
C12	6484.8(15)	9953(13)	3841(2)	58(4)
C13	5795(2)	10142.6(19)	3258.6(18)	49.9(16)
C14	5716(2)	10372(2)	4145(2)	40.2(12)
O2A	6010(8)	7556(10)	4141(5)	44(3)
N2A	5534(5)	7415(8)	4952(13)	40(3)
C15A	6039(6)	7585(11)	4979(10)	37(2)
C16A	6279(10)	7715(18)	4528(9)	41(3)
C17A	6772(9)	7901(15)	4508(7)	44(2)
C18A	6975(10)	7982(17)	4983(9)	40(2)
C19A	6751(9)	7826(11)	5413(7)	38(2)

C20A	6274(12)	7650(20)	5418(10)	39(3)
C21A	7071(7)	8091(7)	4052(6)	51(2)
C22A	7056(7)	8651(5)	4034(6)	60(3)
C23A	6842(6)	7886(7)	3572(5)	52(3)
C24A	7606(6)	7884(8)	4082(7)	61(3)
C25A	6961(7)	7844(6)	5940(6)	40(2)
C26A	6641(8)	8201(7)	6265(7)	48(3)
C27A	6958(7)	7330(6)	6191(6)	47(3)
C28A	7484(7)	8083(9)	5928(8)	45(3)
O2	5966(6)	7497(7)	4262(4)	36(2)
N2	5562(4)	7429(6)	5170(6)	35(2)
C15	6066(5)	7595(9)	5128(5)	34(2)
C16	6263(9)	7655(16)	4641(6)	40(2)
C17	6741(8)	7877(14)	4542(7)	44(2)
C18	6998(8)	7956(13)	4992(8)	39(2)
C19	6793(8)	7915(13)	5448(7)	40(2)
C20	6333(7)	7727(11)	5538(6)	38(3)
C21	7026(7)	8072(6)	4079(6)	52(2)
C22	6814(6)	8571(6)	3905(5)	59(3)
C23	6997(6)	7709(6)	3645(5)	56(3)
C24	7598(6)	8111(10)	4161(9)	54(3)

C25	7030(7)	8009(7)	5957(7)	46(3)
C26	6664(7)	8381(6)	6216(6)	48(3)
C27	7050(7)	7520(6)	6255(6)	49(3)
C28	7523(6)	8281(6)	5861(8)	55(3)

Table 4.3. Anisotropic displacement parameters ($Å^2 \times 10^3$) for Co^{II}-AP^{ditBu} Complex (7). The anisotropic displacement factor exponent takes the form: $-2\pi^2[h^2a^{*2}U_{11}+2hka^*b^*U_{12}+\ldots]$.

Atom	**U_{11}**	**U_{22}**	**U_{33}**	**U_{23}**	**U_{13}**	**U_{12}**
Co1	31.4(3)	37.5(4)	26.8(3)	0	0	0
O1	36.4(16)	38.4(16)	25.0(14)	-4.3(12)	-3.2(11)	0.9(12)
N1	31.8(13)	38.5(17)	24.9(15)	-10(10)	1(12)	2.0(13)
C1	24.7(19)	40(2)	22.5(19)	-1.7(17)	-2.5(16)	4.9(17)
C2	23.9(19)	39(2)	24(2)	-3.6(17)	1.7(15)	4.3(17)
C3	33(2)	46(3)	22(2)	-5.3(18)	-0.5(17)	1.9(19)
C4	29(2)	46(3)	26(2)	-1.8(18)	6.5(17)	0.1(19)
C5	25(2)	44(3)	29(3)	-5(2)	8(2)	3(2)
C6	23(2)	41(3)	26(2)	-8.3(19)	0.4(16)	1.4(18)
C7	50(6)	49(2)	22.0(15)	-6.9(15)	1(4)	-14(6)
C8	49(3)	63(3)	28(2)	-2(2)	-7(2)	-17(3)
C9	64(4)	66(4)	39(3)	-23(3)	-6(3)	8(3)
C10	54(9)	69(3)	22.5(17)	-2.9(17)	-10(4)	-9(5)

C11	27.9(16)	47(5)	33.7(17)	-11(5)	6.6(13)	6(5)
C12	28(2)	68(11)	77(3)	0(6)	13.2(19)	-20(7)
C13	56(3)	58(4)	35(2)	3(2)	10(2)	-10(2)
C14	35(3)	45(3)	41(3)	-4(3)	5(3)	-5(2)
O2A	47(5)	64(6)	21(6)	0(5)	-5(5)	17(4)
N2A	41(4)	42(4)	38(8)	2(7)	-7(7)	1(4)
C15A	35(4)	40(3)	36(6)	3(6)	-10(6)	13(3)
C16A	40(4)	53(5)	31(5)	-3(5)	-10(5)	19(4)
C17A	37(4)	56(4)	39(4)	-2(4)	-10(4)	18(4)
C18A	28(4)	51(5)	40(4)	2(6)	-2(6)	15(4)
C19A	34(4)	44(5)	37(4)	5(5)	-6(5)	20(4)
C20A	38(5)	41(5)	38(6)	9(5)	-1(5)	15(5)
C21A	48(4)	68(4)	38(4)	-3(4)	2(3)	20(4)
C22A	63(6)	69(6)	49(5)	5(5)	0(5)	-1(6)
C23A	53(6)	64(6)	38(5)	0(5)	6(5)	15(5)
C24A	53(5)	83(7)	46(6)	-3(6)	9(5)	25(6)
C25A	42(4)	44(6)	35(4)	2(4)	-4(3)	13(4)
C26A	50(5)	53(8)	40(5)	3(6)	-8(4)	9(6)
C27A	50(6)	50(8)	40(6)	14(6)	-15(5)	9(6)
C28A	54(6)	47(7)	34(5)	6(6)	-6(5)	21(6)
O2	41(4)	54(5)	13(5)	-5(4)	-1(4)	11(3)

N2	42(4)	40(4)	23(5)	6(5)	-19(4)	5(3)
C15	35(4)	38(3)	30(5)	5(5)	-8(4)	12(3)
C16	40(4)	51(4)	29(5)	-4(5)	-11(4)	16(4)
C17	38(4)	57(4)	38(4)	-3(4)	-7(4)	20(4)
C18	28(3)	49(4)	39(3)	2(6)	-4(6)	17(3)
C19	33(4)	46(5)	41(4)	4(4)	-2(4)	15(4)
C20	41(5)	41(5)	33(5)	6(5)	-11(4)	13(4)
C21	49(4)	68(4)	39(4)	-4(4)	1(3)	22(4)
C22	60(6)	73(6)	44(5)	8(5)	3(5)	16(5)
C23	56(6)	70(7)	42(5)	-4(5)	3(5)	17(5)
C24	51(6)	68(7)	42(6)	-3(6)	6(5)	13(6)
C25	47(4)	55(6)	34(4)	4(5)	-7(4)	21(5)
C26	54(5)	54(8)	35(5)	7(6)	7(4)	2(6)
C27	56(6)	55(7)	37(5)	2(5)	-5(4)	21(6)
C28	55(6)	60(8)	49(6)	-6(7)	-13(5)	15(6)

Table 4.4. Bond Lengths for Co^{II}-AP^{ditBu} Complex (7).

Atom	**Atom**	**Length/Å**	**Atom**	**Atom**	**Length/Å**
Co1	O1	1.986(3)	C17A	C21A	1.539(17)
Co1	N1	2.162(3)	C18A	C19A	1.360(17)
Co1	N2A	2.17(2)	C19A	C20A	1.355(16)
Co1	N2	2.231(15)	C19A	C25A	1.516(17)

O1	C2	1.330(5)	C21A	C22A	1.498(17)
N1	C1	1.415(14)	C21A	C23A	1.521(16)
C1	C2	1.396(6)	C21A	C24A	1.532(16)
C1	C6	1.353(6)	C25A	C26A	1.547(14)
C2	C3	1.405(6)	C25A	C27A	1.526(14)
C3	C4	1.368(6)	C25A	C28A	1.535(16)
C3	C7	1.523(11)	O2	C16	1.351(14)
C4	C5	1.371(7)	N2	C15	1.420(10)
C5	C6	1.365(6)	C15	C16	1.413(14)
C5	C11	1.497(18)	C15	C20	1.353(13)
C7	C8	1.498(19)	C16	C17	1.432(15)
C7	C9	1.515(12)	C17	C18	1.398(16)
C7	C10	1.531(6)	C17	C21	1.544(17)
C11	C12	1.526(6)	C18	C19	1.342(16)
C11	C13	1.531(8)	C19	C20	1.348(15)
C11	C14	1.536(14)	C19	C25	1.518(18)
O2A	C16A	1.328(17)	C21	C22	1.521(17)
N2A	C15A	1.424(12)	C21	C23	1.512(15)
C15A	C16A	1.407(16)	C21	C24	1.545(16)
C15A	C20A	1.341(16)	C25	C26	1.554(16)
C16A	C17A	1.410(16)	C25	C27	1.529(15)

C17A	C18A	1.394(17)	C25	C28	1.525(18)	

Table 4.5. Bond angles for Co^{II}-AP^{ditBu} complex (**7**).

Atom	**Atom**	**Atom**	**Angle/°**	**Atom**	**Atom**	**Atom**	**Angle/°**
O1	Co1	N1	78.7(4)	C20A	C19A	C18A	121.8(16)
O1	Co1	N2	93.7(4)	C20A	C19A	C25A	110.4(16)
N1	Co1	N2	93.9(3)	C15A	C20A	C19A	118.5(17)
C2	O1	Co1	111.6(2)	C22A	C21A	C17A	109.8(18)
C1	N1	Co1	106.1(5)	C22A	C21A	C23A	108.8(13)
C2	C1	N1	114.4(4)	C22A	C21A	C24A	112.7(15)
C6	C1	N1	123.8(4)	C23A	C21A	C17A	109.9(14)
C6	C1	C2	121.8(4)	C23A	C21A	C24A	106.9(14)
O1	C2	C1	119.1(4)	C24A	C21A	C17A	108.8(16)
O1	C2	C3	123.2(4)	C19A	C25A	C26A	109.5(14)
C1	C2	C3	117.6(4)	C19A	C25A	C27A	112.2(13)
C2	C3	C7	119.8(4)	C19A	C25A	C28A	109.3(13)
C4	C3	C2	117.8(4)	C27A	C25A	C26A	107.7(11)
C4	C3	C7	122.3(4)	C27A	C25A	C28A	112.8(12)
C3	C4	C5	124.4(4)	C28A	C25A	C26A	104.9(13)
C4	C5	C11	123.4(4)	C15	N2	Co1	113.5(13)
C6	C5	C4	116.8(5)	C16	C15	N2	117.4(11)
C6	C5	C11	119.8(5)	C20	C15	N2	121.1(11)

C1	C6	C5	121.5(4)	C20	C15	C16	121.3(10)
C3	C7	C10	110.9(8)	O2	C16	C15	115.8(11)
C8	C7	C3	109.5(6)	O2	C16	C17	120.9(13)
C8	C7	C9	110.9(7)	C15	C16	C17	123.2(13)
C8	C7	C10	108.8(14)	C16	C17	C21	136.6(15)
C9	C7	C3	110.3(11)	C18	C17	C16	110.1(12)
C9	C7	C10	106.4(8)	C18	C17	C21	113.2(13)
C5	C11	C12	110.1(15)	C19	C18	C17	124.5(12)
C5	C11	C13	113.0(7)	C18	C19	C20	124.4(14)
C5	C11	C14	111.9(5)	C18	C19	C25	128.9(14)
C12	C11	C13	107.4(6)	C20	C19	C25	106.4(14)
C12	C11	C14	107.9(12)	C19	C20	C15	115.6(13)
C13	C11	C14	106.3(10)	C17	C21	C24	113.3(14)
C15A	N2A	Co1	112.4(16)	C22	C21	C17	110.8(17)
C16A	C15A	N2A	117.8(18)	C22	C21	C24	110.5(15)
C20A	C15A	N2A	122(2)	C23	C21	C17	111.9(15)
C20A	C15A	C16A	120.0(12)	C23	C21	C22	108.0(13)
O2A	C16A	C15A	109.9(16)	C23	C21	C24	101.8(14)
O2A	C16A	C17A	126.0(19)	C19	C25	C26	104.0(16)
C15A	C16A	C17A	123.1(15)	C19	C25	C27	109.8(16)
C16A	C17A	C21A	129.1(16)	C19	C25	C28	106.8(13)

C18A	C17A	C16A	112.5(15)	C27	C25	C26	109.6(12)
C18A	C17A	C21A	117.8(16)	C28	C25	C26	108.2(13)
C19A	C18A	C17A	123.3(15)	C28	C25	C27	117.6(14)
C18A	C19A	C25A	127.7(16)				

Table 4.6. Hydrogen atom coordinates (Å×10^4) and isotropic displacement parameters (Å^2×10^3) for Co^{II}-AP^{ditBu} Complex (7).

Atom	***x***	***y***	***z***	**U(eq)**
H1A	5470	8858	5224	38
H1B	5859	8496	5067	38
H4	5461	9280	3222	40
H6	5868	9481	4641	36
H8A	4491	8123	3720	70
H8B	4343	8077	3140	70
H8C	4329	8611	3411	70
H9A	5668	7948	3108	84
H9B	5164	7698	2900	84
H9C	5286	7683	3487	84
H10A	4877	8962	2766	73
H10B	4894	8431	2488	73
H10C	5404	8703	2645	73

H12A	6575	9897	4193	86
H12B	6625	10273	3729	86
H12C	6620	9681	3635	86
H13A	5953	9917	3016	75
H13B	5923	10483	3211	75
H13C	5431	10141	3209	75
H14A	5351	10395	4111	60
H14B	5867	10695	4059	60
H14C	5801	10285	4492	60
H2AA	5475	7196	5206	48
H2AB	5487	7249	4657	48
H18A	7285	8155	5007	48
H20A	6112	7575	5725	46
H22A	6711	8766	4084	90
H22B	7177	8767	3708	90
H22C	7270	8788	4300	90
H23A	6809	7521	3598	78
H23B	7059	7969	3288	78
H23C	6510	8035	3521	78
H24A	7764	8000	4393	91
H24B	7800	8004	3794	91

H24C	7596	7517	4080	91
H26A	6635	8534	6111	71
H26B	6786	8224	6601	71
H26C	6298	8071	6288	71
H27A	6611	7218	6236	70
H27B	7122	7353	6519	70
H27C	7138	7090	5981	70
H28A	7675	7945	5647	67
H28B	7659	8010	6243	67
H28C	7451	8446	5888	67
H2B	5558	7178	4956	42
H2C	5540	7313	5479	42
H18	7342	8046	4972	46
H20	6204	7689	5868	46
H22D	6464	8528	3806	88
H22E	7009	8694	3619	88
H22F	6834	8814	4180	88
H23D	7193	7409	3723	84
H23E	7132	7868	3343	84
H23F	6647	7615	3587	84
H24D	7668	8376	4405	81

H24E	7762	8191	3843	81
H24F	7726	7791	4288	81
H26D	6622	8678	6004	72
H26E	6802	8481	6541	72
H26F	6339	8218	6265	72
H27D	6708	7403	6321	74
H27E	7223	7578	6573	74
H27F	7231	7266	6061	74
H28D	7756	8055	5690	82
H28E	7668	8387	6181	82
H28F	7461	8575	5650	82
H2A	5740(20)	7760(20)	4170(20)	51(16)

Table 4.7. Atomic occupancy for Co^{II}-AP^{ditBu} complex (**7**).

Atom	***Occupancy***	**Atom**	***Occupancy***	**Atom**	***Occupancy***
O1	0.5	N1	0.5	H1A	0.5
H1B	0.5	C1	0.5	C2	0.5
C3	0.5	C4	0.5	H4	0.5
C5	0.5	C6	0.5	H6	0.5
C7	0.5	C8	0.5	H8A	0.5
H8B	0.5	H8C	0.5	C9	0.5

H9A	0.5	H9B	0.5	H9C	0.5
C10	0.5	H10A	0.5	H10B	0.5
H10C	0.5	C11	0.5	C12	0.5
H12A	0.5	H12B	0.5	H12C	0.5
C13	0.5	H13A	0.5	H13B	0.5
H13C	0.5	C14	0.5	H14A	0.5
H14B	0.5	H14C	0.5	O2A	0.222(6)
N2A	0.222(6)	H2AA	0.222(6)	H2AB	0.222(6)
C15A	0.222(6)	C16A	0.222(6)	C17A	0.222(6)
C18A	0.222(6)	H18A	0.222(6)	C19A	0.222(6)
C20A	0.222(6)	H20A	0.222(6)	C21A	0.222(6)
C22A	0.222(6)	H22A	0.222(6)	H22B	0.222(6)
H22C	0.222(6)	C23A	0.222(6)	H23A	0.222(6)
H23B	0.222(6)	H23C	0.222(6)	C24A	0.222(6)
H24A	0.222(6)	H24B	0.222(6)	H24C	0.222(6)
C25A	0.222(6)	C26A	0.222(6)	H26A	0.222(6)
H26B	0.222(6)	H26C	0.222(6)	C27A	0.222(6)
H27A	0.222(6)	H27B	0.222(6)	H27C	0.222(6)
C28A	0.222(6)	H28A	0.222(6)	H28B	0.222(6)
H28C	0.222(6)	O2	0.278(6)	N2	0.278(6)
H2B	0.278(6)	H2C	0.278(6)	C15	0.278(6)

C16	0.278(6)	C17	0.278(6)	C18	0.278(6)
H18	0.278(6)	C19	0.278(6)	C20	0.278(6)
H20	0.278(6)	C21	0.278(6)	C22	0.278(6)
H22D	0.278(6)	H22E	0.278(6)	H22F	0.278(6)
C23	0.278(6)	H23D	0.278(6)	H23E	0.278(6)
H23F	0.278(6)	C24	0.278(6)	H24D	0.278(6)
H24E	0.278(6)	H24F	0.278(6)	C25	0.278(6)
C26	0.278(6)	H26D	0.278(6)	H26E	0.278(6)
H26F	0.278(6)	C27	0.278(6)	H27D	0.278(6)
H27E	0.278(6)	H27F	0.278(6)	C28	0.278(6)
H28D	0.278(6)	H28E	0.278(6)	H28F	0.278(6)
H2A	0.5				

4.4.6.2. Description of the X-ray Structural Analysis of Co^{III}-AP^{ditBu} Complex **(8)**

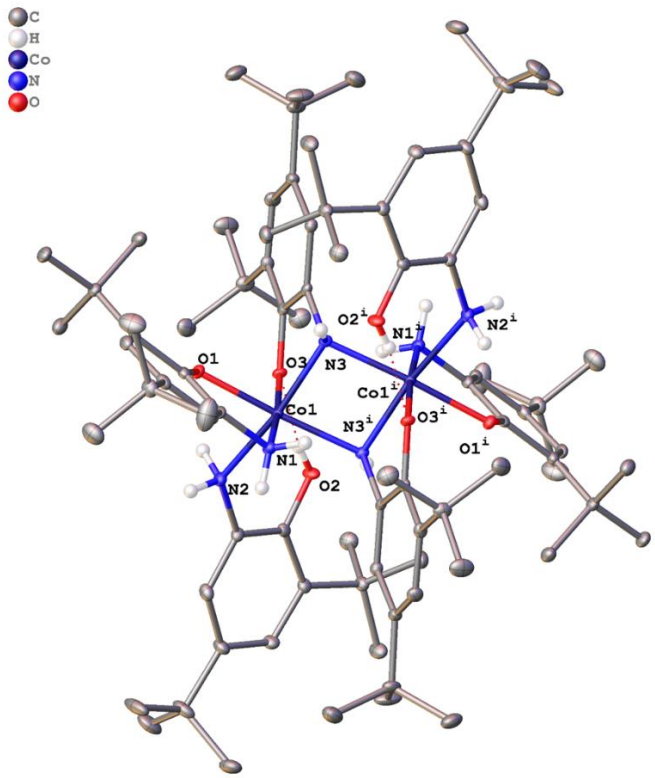

A green-yellow plate shaped crystal measuring 0.357 mm x 0.279 mm x 0.066 mm was selected under paratone oil using a MiTeGen Micromount and mounted at 100(1) K to a D8-Venture diffractometer equipped with a Mo sealed tube X-ray source, a Triumph monochromator, and a Photon CMOS area detector. The unit cell was determined from reflections harvested with a signal to noise ratio (I/σ) of at least 8 from a series of 3 ω scans of 6° with 0.5° frames using APEX3.[1] The data were collected to a resolution of 0.77 Å using 4 ω scans.

The data were integrated using SAINT and corrected for absorption using SADABS.[2] The systematic absences and E-statistics of the data were uniquely consistent with the space group $P2_1/n$. The structure was solved using the intrinsic phasing routine of SHELXT.[3] The non-hydrogen atoms were located from a Fourier difference map of the electron density and anisotropically refined using the least-squares algorithm of SHELXL.[4] The carbon-based hydrogen atoms were then placed in calculated positions and refined with riding thermal parameters. All hydrogen atoms on heteroatoms were located from the Fourier difference map. Their positions were allowed to refine freely and their thermal parameters were constrained to be 1.5 times the thermal parameter of their parent atom.

The asymmetric unit consists of one half molecule Co_2(2-amino-4,6-tert-butylphenolate)$_2$(2-amino-4,6-tert-butylphenol)(μ-2-amido-4,6-tert-butylphenolate)$_2$ and one molecule of dichloromethane (Figures 1 and 2). The dimer resides on a crystallographic inversion center. Tert-butyl group C36 was disordered over two positions (major component: 85.6(4)%). The dichloromethane is also disordered over two positions (major component: 54(3)%). Geometry and thermal parameter restraints were used to ensure a chemically reasonable and computationally stable refinement.

The final structure consisted of 564 parameters refined against 10161 independent reflections, giving refinement residuals of $R_1 = 0.0380$ (based off F^2 for $I > 2\sigma$) and $wR_2 = 0.0896$ (based of F^2 for all reflections). The final difference Fourier map was featureless.

References

1. Bruker-AXS (2016). APEX 3 version 2016.9-0. Madison, Wisconsin, USA

2. (a) Bruker-AXS (2015). *SAINT V8.37A.* Madison, Wisconsin, USA. (b)) Krause, L.; Herbst-Irmer, R.; Sheldrick, G.; Stalke, D. J. Appl. Crystallogr. **2015**, *48*, 3-10.

3. Sheldrick, G. M., *Acta Crystallogr. A* **2015**, A71, 3-8.

4. (a) Sheldrick, G. M., *Acta Crystallogr. C* **2015**, C71, 3-8.; (b) Dolomanov, O. V.; Bourhis, L. J.; Gildea, R. J.; Howard, J. A. K.; Puschmann, H., *J. Appl. Crystallogr.* **2009**, *42*, 339-341.

Table 4.8. Crystal data and structure refinement for Co^{III}-AP^{ditBu} Complex (**8**).

Identification code	Co^{III}-AP^{ditBu} Complex (8)
Empirical formula	$C_{86}H_{136}Cl_4Co_2N_6O_6$
Formula weight	1609.66
Temperature/K	100(1)
Crystal system	monoclinic

Space group	$P2_1/n$
a/Å	15.0642(4)
b/Å	20.4722(5)
c/Å	15.7982(4)
α/°	90
β/°	115.1256(13)
γ/°	90
Volume/$Å^3$	4411.1(2)
Z	2
ρ_{calc}g/cm^3	1.212
μ/mm^{-1}	0.549
F(000)	1728.0
Crystal size/mm^3	0.357 × 0.279 × 0.066
Radiation	MoKα (λ = 0.71073)
2Θ range for data collection/°	5.772 to 55.102
Index ranges	$-19 \leq h \leq 19$, $-26 \leq k \leq 26$, $-20 \leq l \leq 20$
Reflections collected	56144
Independent reflections	10161 [R_{int} = 0.0580, R_{sigma} = 0.0389]
Data/restraints/parameters	10161/259/564
Goodness-of-fit on F^2	1.022

Final R indexes [I>=2σ (I)]	R_1 = 0.0380, wR_2 = 0.0812
Final R indexes [all data]	R_1 = 0.0573, wR_2 = 0.0896
Largest diff. peak/hole / e $Å^{-3}$	0.47/-0.65

Table 4.9. Fractional atomic coordinates ($\times 10^4$) and equivalent isotropic displacement parameters ($Å^2 \times 10^3$) for Co^{III}-AP^{ditBu} complex (8). U_{eq} is defined as 1/3 of of the trace of the orthogonalised U_{IJ} tensor.

Atom	***x***	***y***	***z***	**U(eq)**
Co1	4877.3(2)	698.6(2)	5011.0(2)	8.50(6)
O1	3933.5(8)	1263.1(6)	5152.5(8)	10.9(2)
O2	7311.3(9)	845.7(6)	6410.6(9)	13.7(3)
O3	5578.1(8)	665.9(6)	6340.9(8)	10.1(2)
N1	4052.5(10)	755.4(8)	3681.4(10)	11.1(3)
N2	5633.3(11)	1553.5(7)	5131.8(12)	12.3(3)
N3	4226.8(10)	-66.8(7)	5164.5(10)	9.0(3)
C1	3113.5(12)	1033.6(8)	3556.1(12)	11.2(3)
C2	3111.0(12)	1294.9(8)	4368.2(12)	11.0(3)
C3	2218.3(12)	1576.1(8)	4306.3(12)	11.7(3)
C4	1425.0(12)	1570.7(8)	3432.4(13)	13.2(3)
C5	1431.1(13)	1294.1(9)	2621.3(13)	14.1(4)
C6	2305.7(13)	1019.1(8)	2700.2(12)	12.7(3)
C7	528.1(13)	1326.4(9)	1675.8(13)	16.5(4)

C8	-417.0(14)	1205.3(12)	1795.1(16)	29.3(5)
C9	486.5(15)	2013.5(10)	1272.6(15)	25.4(5)
C10	579.0(17)	825.6(12)	983.8(16)	36.0(6)
C11	2154.2(12)	1851.2(8)	5181.9(12)	12.4(3)
C12	1134.5(13)	2128.7(9)	4967.7(14)	16.9(4)
C13	2367.4(14)	1300.1(9)	5909.0(13)	16.6(4)
C14	2904.4(14)	2401.8(9)	5604.0(14)	17.8(4)
C15	4238.8(12)	-8.4(8)	6078.6(11)	9.6(3)
C16	4995.0(12)	382.6(8)	6700.4(12)	10.2(3)
C17	5136.6(13)	445.7(9)	7634.4(12)	12.7(3)
C18	4452.2(13)	130.2(9)	7875.9(13)	15.1(4)
C19	3662.5(13)	-232.7(8)	7254.0(13)	12.9(3)
C20	3572.4(12)	-312.3(8)	6343.5(12)	11.0(3)
C21	2943.3(14)	-554.2(9)	7588.1(13)	17.5(4)
C22	1988.5(15)	-754.2(12)	6764.3(15)	27.6(5)
C23	2668.7(16)	-73.9(10)	8185.7(15)	24.5(4)
C24	3433.9(17)	-1158.2(10)	8172.1(16)	27.7(5)
C25	5996.7(13)	839.2(9)	8346.0(13)	16.3(4)
C26	5959.6(16)	877.8(11)	9300.5(14)	24.7(4)
C27	6969.6(14)	509.8(11)	8496.1(14)	22.9(4)
C28	5970.3(15)	1543.7(9)	7996.6(14)	21.3(4)

C29	6613.9(12)	1655.5(8)	5193.3(12)	11.7(3)
C30	7399.1(12)	1281.6(8)	5797.1(12)	11.3(3)
C31	8328.5(12)	1346.8(8)	5784.0(12)	11.8(3)
C32	8435.5(13)	1844.8(9)	5231.7(13)	14.3(4)
C33	7674.7(13)	2255.9(9)	4668.2(13)	16.0(4)
C34	6752.5(13)	2138.9(9)	4639.1(13)	14.9(4)
C35	7868.2(14)	2828.4(10)	4136.2(15)	23.8(4)
C39	9171.7(12)	875.6(9)	6341.6(13)	13.4(3)
C40	9487.6(13)	939.7(10)	7397.7(13)	18.4(4)
C41	8851.9(14)	166.2(9)	6029.7(14)	17.4(4)
C42	10076.7(13)	1008.5(10)	6158.0(14)	19.8(4)
C36	8371.3(18)	2573.1(12)	3505.3(18)	25.5(6)
C37	6934.6(19)	3171.0(15)	3490(2)	32.2(7)
C38	8565(2)	3308.2(12)	4835(2)	31.3(7)
C36A	8813(13)	2979(9)	4347(14)	40(3)
C37A	7081(15)	2868(11)	3220(15)	42(3)
C38A	7533(14)	3520(9)	4693(13)	40(3)
Cl1	3942(4)	2856(2)	3846(3)	23.5(9)
Cl2	4049(7)	2107(3)	2327(5)	42.1(12)
C43	3246(9)	2591(6)	2708(9)	23.7(17)
Cl1A	3850(7)	2835(3)	3717(8)	51.9(16)

Cl2A	4266(9)	2048(5)	2407(5)	53.9(17)
C43A	3415(11)	2492(8)	2591(11)	28(3)

Table 4.10. Anisotropic displacement parameters ($Å^2 \times 10^3$) for Co^{III}-AP^{ditBu} complex (**8**). The anisotropic displacement factor exponent takes the form: $-2\pi^2[h^2a^{*2}U_{11}+2hka^*b^*U_{12}+\ldots]$.

Atom	U_{11}	U_{22}	U_{33}	U_{23}	U_{13}	U_{12}
Co1	6.49(10)	10.11(11)	8.86(11)	0.30(9)	3.21(8)	0.60(9)
O1	7.4(5)	13.1(6)	11.6(6)	-0.8(5)	3.5(5)	1.6(5)
O2	7.1(6)	18.2(7)	15.7(6)	5.0(5)	4.9(5)	-0.2(5)
O3	8.8(5)	14.1(6)	8.2(6)	0.1(5)	4.5(5)	-0.4(5)
N1	9.3(7)	13.5(7)	10.7(7)	1.8(6)	4.5(6)	2.1(6)
N2	9.4(7)	12.0(7)	15.6(8)	1.4(6)	5.3(6)	1.6(6)
N3	5.9(6)	12.2(7)	7.5(6)	-0.1(6)	1.5(6)	-0.5(5)
C1	8.3(8)	10.2(8)	16.3(9)	2.3(7)	6.4(7)	1.7(6)
C2	9.1(8)	9.3(8)	15.0(8)	2.2(7)	5.6(7)	-0.4(6)
C3	10.8(8)	9.5(8)	16.4(9)	2.1(7)	7.2(7)	1.2(6)
C4	8.7(8)	12.2(8)	18.9(9)	3.0(7)	6.1(7)	2.7(7)
C5	10.5(8)	11.6(8)	17.2(9)	4.3(7)	3.0(7)	0.0(7)
C6	13.1(8)	11.4(8)	13.5(8)	1.2(7)	5.6(7)	1.2(7)
C7	11.3(8)	17.2(9)	16.1(9)	2.3(7)	1.0(7)	1.9(7)
C8	11.7(9)	41.1(13)	26.9(11)	8.5(10)	0.3(8)	-5.1(9)

C9	19.5(10)	25.6(11)	22.8(10)	8.4(9)	1.1(8)	0.8(8)
C10	24.8(11)	40.1(14)	25.5(12)	-12.8(10)	-6.4(9)	10.5(10)
C11	10.2(8)	12.7(8)	15.9(9)	1.3(7)	7.0(7)	1.9(7)
C12	13.9(8)	17.5(9)	22.8(10)	2.7(8)	11.0(8)	5.1(7)
C13	16.6(9)	17.7(9)	18.4(9)	3.7(7)	10.2(8)	4.5(7)
C14	17.3(9)	16.0(9)	22.9(10)	-4.2(8)	11.2(8)	-1.1(7)
C15	10.4(8)	10.4(7)	8.6(7)	1.5(6)	4.6(6)	3.8(6)
C16	8.7(7)	10.5(8)	12.1(8)	2.2(6)	5.0(7)	2.9(6)
C17	14.2(8)	12.2(8)	10.4(8)	0.1(7)	3.9(7)	1.5(7)
C18	18.5(9)	16.7(9)	11.0(8)	0.1(7)	7.2(7)	0.0(7)
C19	15.1(8)	11.8(8)	14.5(8)	2.3(7)	9.0(7)	1.0(7)
C20	10.0(8)	11.1(8)	11.3(8)	-0.5(6)	3.7(7)	0.5(6)
C21	22.3(9)	19.0(9)	16.6(9)	-1.9(7)	13.7(8)	-5.4(8)
C22	24.3(10)	41.0(13)	23.8(11)	-5.9(10)	16.3(9)	-15.7(10)
C23	25.4(11)	29.2(11)	27.6(11)	-5.7(9)	19.8(9)	-5.1(9)
C24	39.6(12)	20.7(10)	31.1(12)	4.2(9)	22.9(10)	-2.4(9)
C25	16.0(9)	20.3(9)	11.2(8)	-3.1(7)	4.6(7)	-3.6(7)
C26	26.7(11)	33.1(11)	13.6(9)	-6.9(8)	8.1(8)	-10.1(9)
C27	15.3(9)	31.8(11)	16.9(9)	-0.8(8)	2.4(8)	-0.4(8)
C28	27.9(10)	18.6(9)	18.6(10)	-6.8(8)	11.0(8)	-6.4(8)
C29	8.6(8)	10.9(8)	15.1(8)	-1.9(7)	4.6(7)	-0.9(6)

C30	12.0(8)	10.0(8)	11.3(8)	-1.8(6)	4.4(7)	-1.9(7)
C31	9.9(8)	10.7(8)	12.9(8)	-1.3(6)	3.0(7)	-1.4(6)
C32	9.3(8)	16.1(9)	16.5(9)	1.3(7)	4.6(7)	-2.0(7)
C33	13.5(8)	13.0(8)	20.4(9)	4.3(7)	6.1(7)	-1.7(7)
C34	10.9(8)	12.3(8)	18.0(9)	2.3(7)	2.7(7)	1.2(7)
C35	17.6(9)	20.4(10)	28.6(11)	12.7(9)	5.3(9)	-3.5(8)
C39	9.4(8)	13.6(8)	16.4(9)	3.1(7)	4.8(7)	1.6(7)
C40	12.5(8)	22.3(9)	16.5(9)	2.3(8)	2.3(7)	0.9(7)
C41	16.5(9)	13.0(9)	22.3(10)	1.8(7)	7.9(8)	2.9(7)
C42	11.5(8)	21.3(10)	26.5(10)	7.8(8)	8.1(8)	3.3(7)
C36	23.5(12)	29.0(13)	29.0(13)	13.5(11)	15.8(11)	1.8(10)
C37	18.9(12)	30.0(15)	48.2(18)	26.8(14)	14.6(12)	4.5(11)
C38	37.5(15)	20.6(12)	34.1(15)	5.0(11)	13.6(12)	-11.7(11)
C36A	39(5)	43(6)	50(6)	28(5)	31(5)	9(5)
C37A	44(7)	43(7)	49(7)	27(6)	31(6)	15(6)
C38A	53(6)	35(6)	46(6)	13(6)	33(5)	4(6)
Cl1	24.9(11)	26.2(13)	15.1(11)	2.1(9)	4.5(7)	0.9(7)
Cl2	82(3)	24.5(11)	33.5(17)	-0.7(12)	38(2)	-10.8(16)
C43	21(4)	21(3)	25(3)	3(2)	6(2)	3(2)
Cl1A	44(2)	62(3)	50(3)	30.9(19)	20(2)	5.3(17)
Cl2A	66(3)	47(3)	35.2(13)	11.0(14)	9.2(17)	-22(2)

C43A	20(5)	27(5)	27(4)	13(4)	-1(3)	-5(4)

Table 4.11. Bond lengths for Co^{III}-AP^{ditBu} complex (**8**).

Atom	**Atom**	**Length/Å**	**Atom**	**Atom**	**Length/Å**
Co1	Co1[1]	2.8861(5)	C17	C25	1.534(2)
Co1	O1	1.9176(12)	C18	C19	1.393(3)
Co1	O3	1.9104(12)	C19	C20	1.396(2)
Co1	N1	1.9373(15)	C19	C21	1.540(2)
Co1	N2	2.0524(15)	C21	C22	1.530(3)
Co1	N3	1.9172(14)	C21	C23	1.537(3)
Co1	N3[1]	1.9719(14)	C21	C24	1.532(3)
O1	C2	1.331(2)	C25	C26	1.534(3)
O2	C30	1.365(2)	C25	C27	1.538(3)
O3	C16	1.362(2)	C25	C28	1.539(3)
N1	C1	1.458(2)	C29	C30	1.392(2)
N2	C29	1.454(2)	C29	C34	1.395(2)
N3	Co1[1]	1.9720(14)	C30	C31	1.415(2)
N3	C15	1.441(2)	C31	C32	1.395(2)
C1	C2	1.392(2)	C31	C39	1.539(2)
C1	C6	1.383(2)	C32	C33	1.396(3)
C2	C3	1.428(2)	C33	C34	1.391(2)

C3	C4	1.390(2)	C33	C35	1.541(2)
C3	C11	1.534(2)	C35	C36	1.576(3)
C4	C5	1.405(3)	C35	C37	1.514(3)
C5	C6	1.389(2)	C35	C38	1.517(3)
C5	C7	1.536(2)	C35	C36A	1.353(17)
C7	C8	1.534(3)	C35	C37A	1.43(2)
C7	C9	1.534(3)	C35	C38A	1.846(18)
C7	C10	1.524(3)	C39	C40	1.534(3)
C11	C12	1.535(2)	C39	C41	1.544(2)
C11	C13	1.543(2)	C39	C42	1.534(2)
C11	C14	1.534(2)	Cl1	C43	1.739(13)
C15	C16	1.398(2)	Cl2	C43	1.851(11)
C15	C20	1.388(2)	Cl1A	C43A	1.759(15)
C16	C17	1.404(2)	Cl2A	C43A	1.694(14)
C17	C18	1.400(2)			

Table 4.12. Bond angles for Co^{III}-AP^{ditBu} complex (**8**).

Atom	**Atom**	**Atom**	**Angle/°**	**Atom**	**Atom**	**Atom**	**Angle/°**
O1	Co1	$Co1^{1}$	134.73(4)	O3	C16	C15	115.36(15)
O1	Co1	N1	85.65(6)	O3	C16	C17	124.20(15)
O1	Co1	N2	83.39(6)	C15	C16	C17	120.40(15)

O1	Co1	N3[1]	175.75(6)	C16	C17	C25	121.49(16)
O3	Co1	Co1[1]	87.98(4)	C18	C17	C16	116.30(16)
O3	Co1	O1	89.07(5)	C18	C17	C25	122.21(16)
O3	Co1	N1	174.29(6)	C19	C18	C17	124.14(17)
O3	Co1	N2	84.37(6)	C18	C19	C20	118.00(16)
O3	Co1	N3[1]	92.30(5)	C18	C19	C21	120.05(16)
O3	Co1	N3	84.59(6)	C20	C19	C21	121.91(16)
N1	Co1	Co1[1]	94.19(5)	C15	C20	C19	119.48(16)
N1	Co1	N2	97.16(7)	C22	C21	C19	111.53(15)
N1	Co1	N3[1]	92.82(6)	C22	C21	C23	107.02(17)
N2	Co1	Co1[1]	141.03(4)	C22	C21	C24	109.59(17)
N3	Co1	Co1[1]	42.83(4)	C23	C21	C19	110.43(15)
N3[1]	Co1	Co1[1]	41.37(4)	C24	C21	C19	108.77(16)
N3	Co1	O1	91.93(6)	C24	C21	C23	109.48(17)
N3	Co1	N1	93.40(6)	C17	C25	C26	112.04(15)
N3	Co1	N2	168.07(6)	C17	C25	C27	109.62(15)
N3[1]	Co1	N2	100.75(6)	C17	C25	C28	110.12(15)
N3	Co1	N3[1]	84.20(6)	C26	C25	C27	107.52(16)
C2	O1	Co1	111.36(10)	C26	C25	C28	107.34(16)
C16	O3	Co1	108.70(10)	C27	C25	C28	110.13(16)
C1	N1	Co1	108.02(11)	C30	C29	N2	120.71(16)

C29	N2	Co1	129.54(11)	C30	C29	C34	120.69(16)
Co1	N3	Co1[1]	95.81(6)	C34	C29	N2	118.60(15)
C15	N3	Co1[1]	118.49(11)	O2	C30	C29	122.41(15)
C15	N3	Co1	105.62(11)	O2	C30	C31	117.84(15)
C2	C1	N1	114.02(15)	C29	C30	C31	119.75(16)
C6	C1	N1	121.63(15)	C30	C31	C39	120.89(15)
C6	C1	C2	124.33(15)	C32	C31	C30	117.13(16)
O1	C2	C1	118.28(15)	C32	C31	C39	121.97(15)
O1	C2	C3	124.12(16)	C31	C32	C33	123.91(16)
C1	C2	C3	117.59(16)	C32	C33	C35	120.82(16)
C2	C3	C11	120.30(15)	C34	C33	C32	117.09(16)
C4	C3	C2	116.89(16)	C34	C33	C35	122.04(16)
C4	C3	C11	122.80(15)	C33	C34	C29	121.00(16)
C3	C4	C5	124.98(16)	C33	C35	C36	110.24(17)
C4	C5	C7	121.58(16)	C33	C35	C38A	99.8(5)
C6	C5	C4	117.07(16)	C37	C35	C33	112.54(17)
C6	C5	C7	121.27(17)	C37	C35	C36	106.6(2)
C1	C6	C5	119.10(17)	C37	C35	C38	110.4(2)
C8	C7	C5	111.00(16)	C38	C35	C33	109.17(18)
C8	C7	C9	108.83(16)	C38	C35	C36	107.77(19)
C9	C7	C5	107.84(15)	C36A	C35	C33	117.5(7)

C10	C7	C5	112.03(15)	C36A	C35	C37A	124.7(11)
C10	C7	C8	108.14(18)	C36A	C35	C38A	100.4(11)
C10	C7	C9	108.94(18)	C37A	C35	C33	109.1(8)
C3	C11	C12	112.18(15)	C37A	C35	C38A	99.3(11)
C3	C11	C13	109.26(14)	C31	C39	C41	109.70(14)
C12	C11	C13	107.89(14)	C40	C39	C31	111.62(15)
C14	C11	C3	110.18(14)	C40	C39	C41	109.78(15)
C14	C11	C12	107.91(14)	C42	C39	C31	111.36(15)
C14	C11	C13	109.36(15)	C42	C39	C40	107.47(15)
C16	C15	N3	114.30(15)	C42	C39	C41	106.76(15)
C20	C15	N3	124.18(15)	Cl1	C43	Cl2	108.2(7)
C20	C15	C16	121.52(15)	Cl2A	C43A	Cl1A	113.8(9)

Table 4.13. Torsion angles for Co^{III}-AP^{ditBu} complex (**8**).

A	**B**	**C**	**D**	**Angle/°**	**A**	**B**	**C**	**D**	**Angle/°**
Co1	O1	C2	C1	-11.35(18)	C15	C16	C17	C25	176.39(16)
Co1	O1	C2	C3	168.08(13)	C16	C15	C20	C19	-0.7(3)
Co1	O3	C16	C15	21.72(17)	C16	C17	C18	C19	0.1(3)
Co1	O3	C16	C17	-160.52(14)	C16	C17	C25	C26	176.09(17)
Co1	N1	C1	C2	11.58(18)	C16	C17	C25	C27	-64.6(2)
Co1	N1	C1	C6	-167.20(14)	C16	C17	C25	C28	56.7(2)
Co1	N2	C29	C30	-46.8(2)	C17	C18	C19	C20	3.1(3)

Co1	N2	C29	C34	133.63(15)	C17	C18	C19	C21	-179.26(17)
Co1[1]	N3	C15	C16	81.09(16)	C18	C17	C25	C26	-4.0(2)
Co1	N3	C15	C16	-24.65(16)	C18	C17	C25	C27	115.30(19)
Co1	N3	C15	C20	155.87(14)	C18	C17	C25	C28	-123.38(18)
Co1[1]	N3	C15	C20	-98.39(17)	C18	C19	C20	C15	-2.7(2)
O1	C2	C3	C4	179.95(16)	C18	C19	C21	C22	163.48(17)
O1	C2	C3	C11	-1.6(3)	C18	C19	C21	C23	44.6(2)
O2	C30	C31	C32	-172.94(16)	C18	C19	C21	C24	-75.5(2)
O2	C30	C31	C39	8.4(2)	C20	C15	C16	O3	-178.19(15)
O3	C16	C17	C18	178.80(15)	C20	C15	C16	C17	4.0(3)
O3	C16	C17	C25	-1.3(3)	C20	C19	C21	C22	-19.0(2)
N1	C1	C2	O1	-0.4(2)	C20	C19	C21	C23	-137.82(18)
N1	C1	C2	C3	-179.87(15)	C20	C19	C21	C24	102.0(2)
N1	C1	C6	C5	-179.74(16)	C21	C19	C20	C15	179.68(16)
N2	C29	C30	O2	-5.6(3)	C25	C17	C18	C19	-179.87(17)
N2	C29	C30	C31	174.20(16)	C29	C30	C31	C32	7.2(2)
N2	C29	C34	C33	-179.81(17)	C29	C30	C31	C39	-171.46(16)
N3	C15	C16	O3	2.3(2)	C30	C29	C34	C33	0.6(3)
N3	C15	C16	C17	-175.54(15)	C30	C31	C32	C33	-3.0(3)
N3	C15	C20	C19	178.76(15)	C30	C31	C39	C40	-64.4(2)
C1	C2	C3	C4	-0.6(2)	C30	C31	C39	C41	57.5(2)

C1	C2	C3	C11	177.85(15)	C30	C31	C39	C42	175.50(16)
C2	C1	C6	C5	1.6(3)	C31	C32	C33	C34	-2.4(3)
C2	C3	C4	C5	2.0(3)	C31	C32	C33	C35	175.29(18)
C2	C3	C11	C12	-179.84(15)	C32	C31	C39	C40	116.98(19)
C2	C3	C11	C13	-60.3(2)	C32	C31	C39	C41	-121.11(18)
C2	C3	C11	C14	59.9(2)	C32	C31	C39	C42	-3.1(2)
C3	C4	C5	C6	-1.5(3)	C32	C33	C34	C29	3.6(3)
C3	C4	C5	C7	-178.29(16)	C32	C33	C35	C36	55.3(2)
C4	C3	C11	C12	-1.5(2)	C32	C33	C35	C37	174.2(2)
C4	C3	C11	C13	118.12(18)	C32	C33	C35	C38	-62.9(3)
C4	C3	C11	C14	-121.70(18)	C32	C33	C35	C36A	-10.1(11)
C4	C5	C6	C1	-0.3(2)	C32	C33	C35	C37A	139.2(10)
C4	C5	C7	C8	-41.0(2)	C32	C33	C35	C38A	-117.3(7)
C4	C5	C7	C9	78.2(2)	C34	C29	C30	O2	173.95(16)
C4	C5	C7	C10	-161.97(19)	C34	C29	C30	C31	-6.2(3)
C6	C1	C2	O1	178.34(16)	C34	C33	C35	C36	-127.2(2)
C6	C1	C2	C3	-1.1(3)	C34	C33	C35	C37	-8.3(3)
C6	C5	C7	C8	142.40(18)	C34	C33	C35	C38	114.7(2)
C6	C5	C7	C9	-98.5(2)	C34	C33	C35	C36A	167.5(10)
C6	C5	C7	C10	21.4(3)	C34	C33	C35	C37A	-43.2(10)
C7	C5	C6	C1	176.49(16)	C34	C33	C35	C38A	60.3(7)

C11	C3	C4	C5	-176.45(16)	C35	C33	C34	C29	-174.03(18)
C15	C16	C17	C18	-3.5(2)	C39	C31	C32	C33	175.71(17)

Table 4.14. Hydrogen atom coordinates (Å×10^4) and isotropic displacement parameters (Å^2×10^3) for Co^{III}-AP^{ditBu} complex (**8**).

Atom	***x***	***y***	***z***	**U(eq)**
H2	6844(18)	837(12)	6415(17)	21
H1A	3975(16)	372(12)	3472(15)	17
H1B	4292(16)	970(11)	3367(15)	17
H2A	5607(16)	1649(11)	5643(16)	18
H2B	5235(16)	1827(11)	4716(16)	18
H3	3631(16)	-130(10)	4748(15)	13
H4	834	1769	3380	16
H6	2348	824	2173	15
H8A	-376	781	2097	44
H8B	-978	1206	1181	44
H8C	-501	1551	2184	44
H9A	457	2339	1715	38
H9B	-98	2052	679	38
H9C	1074	2088	1167	38
H10A	1135	927	839	54
H10B	-30	840	408	54

H10C	664	388	1259	54
H12A	985	2484	4512	25
H12B	1125	2296	5545	25
H12C	643	1783	4709	25
H13A	1891	947	5639	25
H13B	2315	1472	6465	25
H13C	3031	1131	6085	25
H14A	3567	2230	5781	27
H14B	2853	2576	6159	27
H14C	2773	2751	5142	27
H18	4531	166	8504	18
H20	3059	-572	5909	13
H22A	1699	-373	6368	41
H22B	1529	-925	7000	41
H22C	2126	-1092	6397	41
H23A	3257	41	8747	37
H23B	2188	-278	8369	37
H23C	2385	322	7822	37
H24A	3587	-1472	7784	42
H24B	2988	-1361	8401	42
H24C	4041	-1028	8704	42

H26A	5346	1087	9228	37
H26B	6517	1134	9732	37
H26C	5991	436	9551	37
H27A	6983	64	8728	34
H27B	7518	760	8954	34
H27C	7028	495	7902	34
H28A	6032	1538	7404	32
H28B	6515	1793	8461	32
H28C	5347	1749	7902	32
H32	9064	1908	5240	17
H34	6209	2392	4236	18
H40A	8931	837	7542	28
H40B	9707	1388	7595	28
H40C	10026	636	7731	28
H41A	8316	45	6194	26
H41B	9408	-128	6345	26
H41C	8629	131	5351	26
H42A	10596	697	6513	30
H42B	10310	1454	6354	30
H42C	9903	959	5489	30
H36A	8983	2348	3897	38

H36B	8514	2943	3190	38
H36C	7929	2269	3037	38
H37A	6486	2854	3052	48
H37B	7091	3513	3141	48
H37C	6622	3368	3860	48
H38A	8269	3475	5238	47
H38B	8692	3673	4500	47
H38C	9183	3087	5219	47
H36D	9110	2627	4134	60
H36E	9175	3031	5025	60
H36F	8840	3387	4036	60
H37D	7116	2496	2845	63
H37E	7134	3276	2920	63
H37F	6453	2858	3268	63
H38D	6849	3474	4596	61
H38E	7612	3931	4413	61
H38F	7960	3523	5364	61
H43A	2976	2971	2289	28
H43B	2692	2319	2684	28
H43C	2847	2208	2490	34
H43D	3182	2849	2124	34

Table 4.15. Atomic occupancy for Co^{III}-AP^{ditBu} complex (**8**).

Atom	***Occupancy***	**Atom**	***Occupancy***	**Atom**	***Occupancy***
C36	0.856(4)	H36A	0.856(4)	H36B	0.856(4)
H36C	0.856(4)	C37	0.856(4)	H37A	0.856(4)
H37B	0.856(4)	H37C	0.856(4)	C38	0.856(4)
H38A	0.856(4)	H38B	0.856(4)	H38C	0.856(4)
C36A	0.144(4)	H36D	0.144(4)	H36E	0.144(4)
H36F	0.144(4)	C37A	0.144(4)	H37D	0.144(4)
H37E	0.144(4)	H37F	0.144(4)	C38A	0.144(4)
H38D	0.144(4)	H38E	0.144(4)	H38F	0.144(4)
Cl1	0.54(3)	Cl2	0.54(3)	C43	0.54(3)
H43A	0.54(3)	H43B	0.54(3)	Cl1A	0.46(3)
Cl2A	0.46(3)	C43A	0.46(3)	H43C	0.46(3)
H43D	0.46(3)				

References:

1. Constable, D. J. C.; Dunn, P. J.; Hayler, J. D.; Humphrey, G. R.; Leazer, J. J. L.; Linderman, R. J.; Lorenz, K.; Manley, J.; Pearlman, B. A.; Wells, A.; Zaks, A.; Zhang, T. Y., Key green chemistry research areas—a perspective from pharmaceutical manufacturers. *Green Chem.* **2007,** *9* (5), 411-420.
2. Punniyamurthy, T.; Velusamy, S.; Iqbal, J., Recent advances in transition metal catalyzed oxidation of organic substrates with molecular oxygen. *Chem Rev* **2005,** *105* (6), 2329-63.
3. Sigman, M. S.; Schultz, M. J., The renaissance of palladium(II)-catalyzed oxidation chemistry. *Org Biomol Chem* **2004,** *2* (18), 2551-4.
4. Stahl, S. S., Palladium oxidase catalysis: selective oxidation of organic chemicals by direct dioxygen-coupled turnover. *Angew Chem Int Ed Engl* **2004,** *43* (26), 3400-20.
5. Shi, Z.; Zhang, C.; Tang, C.; Jiao, N., Recent advances in transition-metal catalyzed reactions using molecular oxygen as the oxidant. *Chem Soc Rev* **2012,** *41* (8), 3381-430.
6. Urgoitia, G.; SanMartin, R.; Herrero, M.; Domínguez, E., Recent Advances in Homogeneous Metal-Catalyzed Aerobic C–H Oxidation of Benzylic Compounds. *Catalysts* **2018,** *8* (12).
7. Ho, W. C.; Chung, K.; Ingram, A. J.; Waymouth, R. M., Pd-Catalyzed Aerobic Oxidation Reactions: Strategies To Increase Catalyst Lifetimes. *J Am Chem Soc* **2018,** *140* (2), 748-757.
8. Wang, D.; Weinstein, A. B.; White, P. B.; Stahl, S. S., Ligand-Promoted Palladium-Catalyzed Aerobic Oxidation Reactions. *Chem Rev* **2018,** *118* (5), 2636-2679.
9. Trammell, R.; Rajabimoghadam, K.; Garcia-Bosch, I., Copper-Promoted Functionalization of Organic Molecules: from Biologically Relevant Cu/O_2 Model Systems to Organometallic Transformations. *Chem Rev* **2019,** *119* (4), 2954-3031.
10. Shigeru, I.; Teruaki, M., A New Method for Preparation of Alcohols from Olefins with Molecular Oxygen and Phenylsilane by the Use of Bis(acetylacetonato)cobalt(II). *Chemistry Letters* **1989,** *18* (6), 1071-1074.
11. Isayama, S.; Mukaiyama, T., Novel method for the preparation of triethylsilyl peroxides from olefins by the reaction with molecular oxygen and triethylsilane catalyzed by bis(1,3-diketonato)cobalt(II). *Chemistry Letters* **1989,** *18* (4), 573-576.
12. Inoki, S.; Mukaiyama, T., A convenient method for the stereoselective preparation of trans-(2-hydroxymethyl)tetrahydrofurans by the oxidative cyclization of 5-hydroxy-1-alkenes with molecular oxygen catalyzed by cobalt(II) complex. *Chemistry Letters* **1990,** (1), 67-70.
13. Faisca Phillips, A. M.; Pombeiro, A. J. L.; Kopylovich, M. N., Recent Advances in Cascade Reactions Initiated by Alcohol Oxidation. *ChemCatChem* **2017,** *9* (2), 217-246.
14. Palmer, C.; Morra, N. A.; Stevens, A. C.; Bajtos, B.; Machin, B. P.; Pagenkopf, B. L., Increased yields and simplified purification with a second-generation cobalt catalyst for the oxidative formation of trans-THF rings. *Org Lett* **2009,** *11* (24), 5614-7.
15. Schuch, D.; Fries, P.; Donges, M.; Menendez Perez, B.; Hartung, J., Reductive and brominative termination of alkenol cyclization in aerobic cobalt-catalyzed reactions. *J Am Chem Soc* **2009,** *131* (36), 12918-20.
16. Fries, P.; Muller, M. K.; Hartung, J., An aerobic oxidation/homolytic substitution-cascade for stereoselective methylsulfanyl-cyclization of 4-pentenols. *Org Biomol Chem* **2013,** *11* (16), 2630-7.

17. Ishii, Y.; Nakayama, K.; Takeno, M.; Sakaguchi, S.; Iwahama, T.; Nishiyama, Y., Novel Catalysis by N-Hydroxyphthalimide in the Oxidation of Organic Substrates by Molecular Oxygen. *J. Org. Chem.* **1995,** *60* (13), 3934–3935.
18. Ishii, Y.; Iwahama, T.; Sakaguchi, S.; Nakayama, K.; Nishiyama, Y., Alkane Oxidation with Molecular Oxygen Using a New Efficient Catalytic System: N-Hydroxyphthalimide (NHPI) Combined with Co(acac)n (n = 2 or 3)†. *J. Org. Chem.* **1996,** *61* (14), 4520–4526.
19. Yoshino, Y.; Hayashi, Y.; Iwahama, T.; Sakaguchi, S.; Ishii, Y., Catalytic Oxidation of Alkylbenzenes with Molecular Oxygen under Normal Pressure and Temperature by N-Hydroxyphthalimide Combined with $Co(OAc)_2$. *J. Org. Chem.* **1997,** *62* (20), 6810–6813.
20. Patil, R. D.; Fuchs, B.; Taha, N.; Sasson, Y., Solvent-free and Selective Autooxidation of Alkylbenzenes Catalyzed by Co/NHPI under Phase Transfer Conditions. *ChemistrySelect* **2016,** *1* (13), 3791-3796.
21. Melone, L.; Prosperini, S.; Ercole, G.; Pastori, N.; Punta, C., Is it possible to implement N-hydroxyphthalimide homogeneous catalysis for industrial applications? A case study of cumene aerobic oxidation. *Journal of Chemical Technology & Biotechnology* **2014,** *89* (9), 1370-1378.
22. Baciocchi, E.; Gerini, M. F.; Lanzalunga, O., Reactivity of phthalimide N-oxyl radical (PINO) toward the phenolic O-H bond. A kinetic study. *J Org Chem* **2004,** *69* (25), 8963-6.
23. Hruszkewycz, D. P.; Miles, K. C.; Thiel, O. R.; Stahl, S. S., Co/NHPI-mediated aerobic oxygenation of benzylic C-H bonds in pharmaceutically relevant molecules. *Chem Sci* **2017,** *8* (2), 1282-1287.
24. Huang, J. K.; Wong, Y. C.; Kao, T. T.; Tseng, C. T.; Shia, K. S., Cobalt(II)-Catalyzed Aerobic Oxidation of Terminal-Capped Alkynyl alpha-Cyano Alkanone Systems. An Oxygen-Mediated Radical Chain Reaction. *J Org Chem* **2016,** *81* (22), 10759-10768.
25. Tokuichi, T., Nebenvalenzringverbindungen. IV. Über einige innerkomplexe Kobaltsalze der Oxyaldimine. *Bull. Chem. Soc. Jpn* **1938,** *13* (2), 252-260.
26. Niederhoffer, E. C.; Timmons, J. H.; Martell, A. E., Thermodynamics of oxygen binding in natural and synthetic dioxygen complexes. *Chem. Rev.* **1984,** *84* (2), 137-203.
27. Bozell, J. J.; Hames, B. R.; Dimmel, D. R., Cobalt-Schiff Base Complex Catalyzed Oxidation of Para-Substituted Phenolics. Preparation of Benzoquinones. *J. Org. Chem.* **1995,** *60* (8), 2398–2404.
28. Chen, D.; Martell, A. E., Dioxygen affinities of synthetic cobalt Schiff base complexes. *Inorg Chem* **1987,** *26* (7), 1026-1030.
29. Cedeno, D.; Bozell, J. J., Catalytic oxidation of para-substituted phenols with cobalt–Schiff base complexes/O_2—selective conversion of syringyl and guaiacyl lignin models to benzoquinones. *Tetrahedron Letters* **2012,** *53* (19), 2380-2383.
30. Biannic, B.; Bozell, J. J., Efficient cobalt-catalyzed oxidative conversion of lignin models to benzoquinones. *Org Lett* **2013,** *15* (11), 2730-3.
31. Cooper, C. J.; Alam, S.; Nziko, V. d. P. N.; Johnston, R. C.; Ivanov, A. S.; Mou, Z.; Turpin, D. B.; Rudie, A. W.; Elder, T. J.; Bozell, J. J.; Parks, J. M., Co(salen)-Catalyzed Oxidation of Lignin Models to Form Benzoquinones and Benzaldehydes: A Computational and Experimental Study. *ACS Sustainable Chemistry & Engineering* **2020,** *8* (18), 7225-7234.
32. Zombeck, A.; Drago, R. S.; Corden, B. B.; Gaul, J. H., Activation of molecular oxygen. Kinetic studies of the oxidation of hindered phenols with cobalt-dioxygen complexes. *J Am Chem Soc* **1981,** *103* (25), 7580-7585.

33. Anson, C. W.; Ghosh, S.; Hammes-Schiffer, S.; Stahl, S. S., Co(salophen)-Catalyzed Aerobic Oxidation of *p*-Hydroquinone: Mechanism and Implications for Aerobic Oxidation Catalysis. *J Am Chem Soc* **2016,** *138* (12), 4186-93.
34. Baeckvall, J.-E.; Hopkins, R. B.; Grennberg, H.; Mader, M.; Awasthi, A. K., Multistep electron transfer in palladium-catalyzed aerobic oxidations via a metal macrocycle quinone system. *J Am Chem Soc* **1990,** *112* (13), 5160-5166.
35. Morandi, B.; Wickens, Z. K.; Grubbs, R. H., Practical and general palladium-catalyzed synthesis of ketones from internal olefins. *Angew Chem Int Ed Engl* **2013,** *52* (10), 2944-8.
36. Gigant, N.; Backvall, J. E., Aerobic double dehydrogenative cross coupling between cyclic saturated ketones and simple arenes. *Chemistry* **2014,** *20* (20), 5890-4.
37. Piera, J.; Backvall, J. E., Catalytic oxidation of organic substrates by molecular oxygen and hydrogen peroxide by multistep electron transfer--a biomimetic approach. *Angew Chem Int Ed Engl* **2008,** *47* (19), 3506-23.
38. Purse, B. W.; Tran, L. H.; Piera, J.; Akermark, B.; Backvall, J. E., Synthesis of new hybrid hydroquinone/cobalt Schiff base catalysts: efficient electron-transfer mediators in aerobic oxidation. *Chemistry* **2008,** *14* (25), 7500-3.
39. Reiss, H.; Shalit, H.; Vershinin, V.; More, N. Y.; Forckosh, H.; Pappo, D., Cobalt(II)[salen]-Catalyzed Selective Aerobic Oxidative Cross-Coupling between Electron-Rich Phenols and 2-Naphthols. *J Org Chem* **2019,** *84* (12), 7950-7960.
40. Habaue, S.; Aoyagi, H.; Murakami, S.; Higashimura, H., Asymmetric oxidative coupling polymerization of dihydroxynaphthalene derivatives with cobalt-salen complexes. *Polymer Bulletin* **2007,** *59* (3), 303-310.
41. Haikarainen, A.; Sipilä, J.; Pietikäinen, P.; Pajunenband, A.; Mutikainen, I., Salen Complexes with Bulky Substituents as UsefulTools for Biomimetic Phenol Oxidation Research. *Bioorganic & Medicinal Chemistry* **2001,** *9*, 1633-1638.
42. Campbell, A. N.; Stahl, S. S., Overcoming the "oxidant problem": strategies to use O2 as the oxidant in organometallic C-H oxidation reactions catalyzed by Pd (and Cu). *Acc Chem Res* **2012,** *45* (6), 851-63.
43. Wu, W.; Jiang, H., Palladium-catalyzed oxidation of unsaturated hydrocarbons using molecular oxygen. *Acc Chem Res* **2012,** *45* (10), 1736-48.
44. Wendlandt, A. E.; Suess, A. M.; Stahl, S. S., Copper-catalyzed aerobic oxidative C-H functionalizations: trends and mechanistic insights. *Angew Chem Int Ed Engl* **2011,** *50* (47), 11062-87.
45. Allen, S. E.; Walvoord, R. R.; Padilla-Salinas, R.; Kozlowski, M. C., Aerobic copper-catalyzed organic reactions. *Chem Rev* **2013,** *113* (8), 6234-458.
46. Jain, S. L.; Sain, B., An unconventional cobalt-catalyzed aerobic oxidation of tertiary nitrogen compounds to N-oxides. *Angew Chem Int Ed Engl* **2003,** *42* (11), 1265-7.
47. Vinck, E.; Murphy, D. M.; Fallis, I. A.; Strevens, R. R.; Van Doorslaer, S., Formation of a cobalt(III)-phenoxyl radical complex by acetic acid promoted aerobic oxidation of a Co(II)salen complex. *Inorg Chem* **2010,** *49* (5), 2083-92.
48. Fries, P.; Halter, D.; Kleinschek, A.; Hartung, J., Functionalized tetrahydrofurans from alkenols and olefins/alkynes via aerobic oxidation-radical addition cascades. *J Am Chem Soc* **2011,** *133* (11), 3906-12.
49. Xu, P.; Zhu, T.-H.; Wei, T.-Q.; Wang, S.-Y.; Ji, S.-J., $Co(acac)_2/O_2$-catalyzed oxidative isocyanide insertion with 2-vinylanilines: efficient synthesis of 2-aminoquinolines. *RSC Advances* **2016,** *6* (39), 32467-32470.

50. Dey, S. K.; Mukherjee, A., Catechol oxidase and phenoxazinone synthase: Biomimetic functional models and mechanistic studies. *Coordination Chemistry Reviews* **2016,** *310*, 80-115.
51. Mitra, M.; Raghavaiah, P.; Ghosh, R., A mononuclear cobalt(III) complex and its catecholase activity. *New Journal of Chemistry* **2015,** *39* (1), 200-205.
52. Simandi, T. M.; May, Z.; Szigyarto, I. C.; Simandi, L. I., Hydrogen atom vs electron transfer in catecholase-mimetic oxidations by superoxometal complexes. Deuterium kinetic isotope effects. *Dalton Trans* **2005,** (2), 365-8.
53. Poddel'sky, A. I.; Cherkasov, V. K.; Fukin, G. K.; Bubnov, M. P.; Abakumova, L. G.; Abakumov, G. A., New four- and five-coordinated complexes of cobalt with sterically hindered o-iminobenzoquinone ligands: synthesis and structure. *Inorganica Chimica Acta* **2004,** *357* (12), 3632-3640.
54. Chakrabarty, S.; Choudhary, S.; Doshi, A.; Liu, F. Q.; Mohan, R.; Ravindra, M. P.; Shah, D.; Yang, X.; Fleming, F. F., Catalytic Isonitrile Insertions and Condensations Initiated by RNC-X Complexation. *Adv Synth Catal* **2014,** *356* (10), 2135-2196.
55. Bill, E.; Bothe, E.; Chaudhuri, P.; Chlopek, K.; Herebian, D.; Kokatam, S.; Ray, K.; Weyhermuller, T.; Neese, F.; Wieghardt, K., Molecular and electronic structure of four- and five-coordinate cobalt complexes containing two *o*-phenylenediamine- or two *o*-aminophenol-type ligands at various oxidation levels: an experimental, density functional, and correlated ab initio study. *Chemistry* **2005,** *11* (1), 204-24.
56. Smith, A. L.; Clapp, L. A.; Hardcastle, K. I.; Soper, J. D., Redox-active ligand-mediated Co–Cl bond-forming reactions at reducing square planar cobalt(III) centers. *Polyhedron* **2010,** *29* (1), 164-169.
57. Vlaar, T.; Cioc, R. C.; Mampuys, P.; Maes, B. U.; Orru, R. V.; Ruijter, E., Sustainable synthesis of diverse privileged heterocycles by palladium-catalyzed aerobic oxidative isocyanide insertion. *Angew Chem Int Ed Engl* **2012,** *51* (52), 13058-61.
58. Zhu, T.-H.; Xu, X.-P.; Cao, J.-J.; Wei, T.-Q.; Wang, S.-Y.; Ji, S.-J., Cobalt(II)-Catalyzed Isocyanide Insertion Reaction with Amines under Ultrasonic Conditions: A Divergent Synthesis of Ureas, Thioureas and Azaheterocycles. *Advanced Synthesis & Catalysis* **2014,** *356* (2-3), 509-518.
59. Leardini, R.; Nanni, D.; Zanardi, G., Radical addition to isonitriles: a route to polyfunctionalized alkenes through a novel three-component radical cascade reaction. *J Org Chem* **2000,** *65* (9), 2763-72.
60. Blanksby, S. J.; Ellison, G. B., Bond dissociation energies of organic molecules. *Acc Chem Res* **2003,** *36* (4), 255-63.
61. Liu, B.; Yin, M.; Gao, H.; Wu, W.; Jiang, H., Synthesis of 2-aminobenzoxazoles and 3-aminobenzoxazines via palladium-catalyzed aerobic oxidation of *o*-aminophenols with isocyanides. *J Org Chem* **2013,** *78* (7), 3009-20.
62. Nahakpam, L.; Chipem, F. A.; Chingakham, B. S.; Laitonjam, W. S., Diacetoxyiodobenzene assisted C-O bond formation via sequential acylation and deacylation process: synthesis of benzoxazole amides and their mechanistic study by DFT. *Org Biomol Chem* **2016,** *14* (32), 7735-45.
63. Sharma, V. B.; Jain, S. L.; Sain, B., Cobalt (II) Schiff base catalyzed aerobic oxidation of secondary alcohols to ketones. *Journal of Molecular Catalysis A: Chemical* **2004,** *212* (1-2), 55-59.

64. Yang, W. C.; Wei, K.; Sun, X.; Zhu, J.; Wu, L., Cascade C(sp^3)-S Bond Cleavage and Imidoyl C-S Formation: Radical Cyclization of 2-Isocyanoaryl Thioethers toward 2-Substituted Benzothiazoles. *Org Lett* **2018,** *20* (10), 3144-3147.
65. Bitzer, J.; Große, T.; Wang, L.; Lang, S.; Beil, W.; Zeeck., New Aminophenoxazinones from a Marine Halomonas sp.: Fermentation, Structure Elucidation, and Biological Activity. *J Antibiot* **2006,** *59*, 86-92.
66. Simándi, L. I.; Barna, T.; Németh, S., Kinetics and mechanism of the cobaloxime(II)-catalysed oxidation of 2-aminophenol by dioxygen. A phenoxazinone synthase model involving free-radical intermediates. *J. Chem. Soc., Dalton Trans.* **1996**, 473-478.
67. El-Khalafy, S. H.; Hassanein, M., Oxidation of 2-aminophenol with molecular oxygen and hydrogen peroxide catalyzed by water soluble metalloporphyrins. *Journal of Molecular Catalysis A: Chemical* **2012,** *363-364*, 148-152.
68. Kaizer, J.; Csonka, R.; Speier, G., TEMPO-initiated oxidation of 2-aminophenol to 2-aminophenoxazin-3-one. *J. Mol. Catal. A: Chem.* **2002,** *180* (1-2), 91-96.
69. Chun, H.; Verani, C. N.; Chaudhuri, P.; Bothe, E.; Bill, E.; Weyhermuller, T.; Wieghardt, K., Molecular and electronic structure of octahedral o-aminophenolato and o-iminobenzosemiquinonato complexes of V(V), Cr(III), Fe(III), and Co(III). Experimental determination of oxidation levels of ligands and metal ions. *Inorg Chem* **2001,** *40* (17), 4157-66.
70. Herebian, D.; Ghosh, P.; Chun, H.; Bothe, E.; Weyhermüller, T.; Wieghardt., K., Cobalt(II)/(III) Complexes Containing *o*-Iminothiobenzosemiquinonato(1−) and *o*-Iminobenzosemiquinonato(1−) π-Radical Ligands. *Eur. J. Inorg. Chem.* **2002,** *2002* (8), 1957-1967.
71. Smith, A. L.; Hardcastle, K. I.; Soper, J. D., Redox-active ligand-mediated oxidative addition and reductive elimination at square planar cobalt(III): multielectron reactions for cross-coupling. *J Am Chem Soc* **2010,** *132* (41), 14358-60.
72. Maity, S.; Kundu, S.; Bera, S.; Weyhermüller, T.; Ghosh, P., Mixed-Valence *o*-Iminobenzoquinone and *o*-Iminobenzosemiquinonate Anion Radical Complexes of Cobalt: Valence Tautomerism. *European Journal of Inorganic Chemistry* **2016,** *2016* (22), 3680-3690.
73. Fukuda, O.; Sakaguchi, S.; Ishii, Y., Preparation of Hydroperoxides by N-Hydroxyphthalimide-Catalyzed Aerobic Oxidation of Alkylbenzenes and Hydroaromatic Compounds and Its Application. *Adv Synth Catal* **2001,** *343* (8), 809-813.
74. Adams, D. M.; Noodleman, L., Hendrickson, D. N., Density Functional Study of the Valence-Tautomeric Interconversion Low-Spin $[Co^{III}(SQ)(Cat)(phen)]$ ↔ High-Spin $[Co^{II}(SQ)_2(phen)]$. *Inorg. Chem.* **1997,** *36*, 3966-3984.
75. Evangelio, E.; Ruiz-Molina, D., Valence Tautomerism: New Challenges for Electroactive Ligands. *European Journal of Inorganic Chemistry* **2005,** *2005* (15), 2957-2971.
76. Gottlieb, H. E.; Kotlyar, V.; Nudelman, A. NMR Chemical Shifts of Common Laboratory Solvents as Trace Impurities. *J. Org. Chem.* **1997,** *62* (21), 7512-7515.
77. Cioffi, C. L.; Lansing, J. J.; Yuksel, H., Synthesis of 2-aminobenzoxazoles using tetramethyl orthocarbonate or 1,1-dichlorodiphenoxymethane. *J Org Chem* **2010,** *75* (22), 7942-5.
78. Zhu, T. H.; Wang, S. Y.; Wang, G. N.; Ji, S. J., Cobalt-catalyzed oxidative isocyanide insertion to amine-based bisnucleophiles: diverse synthesis of substituted 2-aminobenzimidazoles, 2-aminobenzothiazoles, and 2-aminobenzoxazoles. *Chemistry* **2013,** *19* (19), 5850-3.
79. Cho, S. H.; Kim, J. Y.; Lee, S. Y.; Chang, S., Silver-mediated direct amination of benzoxazoles: tuning the amino group source from formamides to parent amines. *Angew Chem Int Ed Engl* **2009,** *48* (48), 9127-30.

80. Wang, G.-N.; Zhu, T.-H.; Wang, S.-Y.; Wei, T.-Q.; Ji, S.-J., $NiCl_2$-catalyzed cascade reaction of isocyanides with functionalized anilines. *Tetrahedron* **2014,** *70* (43), 8079-8083.
81. Yella, R.; Patel, B. K, One-Pot Synthesis of Five and Six Membered N, O, S-Heterocycles Using a Ditribromide Reagent. *J. Comb. Chem.* **2010,** *12*, 754-763.
82. Yadav, V. K.; Srivastava, V. P.; Yadav, L. D. S., Iodide catalyzed synthesis of 2-aminobenzoxazoles via oxidative cyclodesulfurization of phenolic thioureas with hydrogen peroxide. *Tetrahedron Letters* **2018,** *59* (3), 252-255.
83. Murata, Y.; Matsumoto, N.; Miyata, M.; Kitamura, Y.; Kakusawa, N.; Matsumura, M.; Yasuike, S., One-pot reaction for the synthesis of *N*-substituted 2-aminobenzoxazoles using triphenylbismuth dichloride as cyclodesulfurization reagent. *Journal of Organometallic Chemistry* **2018,** *859*, 18-23.
84. Khatik, G. L.; Dube, N.; Pal, A.; Nair, V. A., Highly Efficient One-Pot Synthesis of 2-Aminobenzoxazoles Using Triflic Acid as a Cyclodesulfurizing Reagent. *Synthetic Communications* **2011,** *41* (17), 2631-2639.
85. Bitzer, J.; Grosse, T.; Wang, L.; Lang, S.; Beil, W.; Zeeck, A., New aminophenoxazinones from a marine Halomonas sp.: fermentation, structure elucidation, and biological activity. *J Antibiot (Tokyo)* **2006,** *59* (2), 86-92.
86. Beaulieu, C.; Wang, Z.; Denis, D.; Greig, G.; Lamontagne, S.; O'Neill, G.; Slipetz, D.; Wang, J., Benzimidazoles as new potent and selective DP antagonists for the treatment of allergic rhinitis. *Bioorg Med Chem Lett* **2004,** *14* (12), 3195-9.
87. Madsen, P.; Knudsen, L. B.; Wiberg, F. C.; Carr, R. D. Discovery and Structure-Activity Relationship of the First Non-Peptide Competitive Human Glucagon Receptor Antagonists. *J. Med. Chem.* **1998,** *41*, 5150-5157.
88. Palmer, B. D.; Kraker, A. J., Hartl, B. G.; Panopoulos, A. D.; Panek, R. L.; Batley, B. L.; Lu, G. H.; Trumpp-Kallmeyer, S.; Hollis Showalter, H. D. and Denny, W. A., Structure-Activity Relationships for 5-Substituted 1-Phenylbenzimidazoles as Selective Inhibitors of the Platelet-Derived Growth Factor Receptor. **1999,** (42), 2373-2382.
89. Sørensen, U. S.; Strøbæk, D.; Christophersen, P.; Hougaard, C.; Jensen, M. L.; Nielsen, E. Ø. Synthesis and Structure-Activity Relationship Studies of 2-(*N*-Substituted)-aminobenzimidazoles as Potent Negative Gating Modulators of Small Conductance Ca^{2+}-Activated K^+ Channels. *J. Med. Chem.* **2008,** *51*, 7625–7634.
90. Morningstar, M. L.; Roth, T.; Farnsworth, D. W.; Smith, M. K.; Watson, K.; Buckheit, R. W.; Jr., K. D.; Zhang, W.; Arnold, E.; Julias, J. G.; Hughes, S. H.; Michejda, C. J. Synthesis, Biological Activity, and Crystal Structure of Potent Nonnucleoside Inhibitors of HIV-1 Reverse Transcriptase That Retain Activity against Mutant Forms of the Enzyme. *J. Med. Chem.* **2007,** *50*, 4003-4015.
91. Janssens, F.; Torremans, J.; Janssen, M.; Stokbroekx, R. A.; Luyckx, M.; Janssen, P. A. J. New Antihistaminic N-Heterocyclic 4-Piperidinamines. 1. Synthesis and Antihistaminic Activity of JV-(4-Piperidinyl)-lfT-benzimidazol-2-amines. *J. Med. Chem.* **1985,** *28*, 1925-1933.
92. Valdez, J.; Cedillo, R.; Hernández-Campos, A.; Yépez, L.; Hernández-Luis, F.; Navarrete-Vázquez, G.; Tapia, A.; Cortés, R. Hernándezc M.; and Castillo, R. Synthesis and Antiparasitic Activity of 1*H*-Benzimidazole Derivatives. *Bioorganic & Medicinal Chemistry Letters* **2002,** *12*, 2221–2224.
93. Snow, R. J.; Cardozo, M. G.; Morwick, T. M.; Busacca, C. A.; Dong, Y.; Eckner, R. J.; Jacober, S.; Jakes, S.; Kapadia, S.; Lukas, S.; Panzenbeck, M.; Peet, G. W.; Peterson, J. D.; Prokopowicz. A. S., Sellati, R.; Tolbert, R. M.; Tschantz, M. A. and Moss, N. Discovery of 2-

Phenylamino-imidazo[4,5-h]isoquinolin-9-ones: A New Class of Inhibitors of Lck Kinase. *J. Med. Chem.* **2002,** *45*, 3394-3405.
94. Zhong, M.; Bui, M.; Shen, W.; Baskaran, S.; Allen, D. A.; Elling, R. A.; Flanagan, W. M.; Fung, A. D.; Hanan, E. J.; Harris, S. O.; Heumann, S. A.; Hoch, U.; Ivy, S. N.; Jacobs, J. W.; Lam, S.; Lee, H.; McDowell, R. S.; Oslob, J. D.; Purkey, H. E.; Romanowski, M. J.; Silverman, J. A.; Tangonan, B. T.; Taverna, P.; Yang, W.; Yoburn, J. C.; Yu, C. H.; Zimmerman, K. M.; O'Brien, T.; Lew, W., 2-Aminobenzimidazoles as potent Aurora kinase inhibitors. *Bioorg Med Chem Lett* **2009,** *19* (17), 5158-61.
95. Kling, A.; Backfisch, G.; Delzer, J.; Geneste, H.; Graef, C.; Hornberger, W.; Lange, U. E. W.; Lauterbach, A.; Seitz, W.; Subkowski, T., Design and synthesis of 1,5- and 2,5-substituted tetrahydrobenzazepinones as novel potent and selective integrin α V β 3 antagonists. *Bioorganic & Medicinal Chemistry* **2003,** *11* (7), 1319-1341.
96. Mukhopadhyay, T.; Sasaki, J.-i.; Ramesh, R.; Roth, J. A. Mebendazole Elicits a Potent Antitumor Effect on Human Cancer Cell Lines Both in Vitro and in Vivo. *Clin Cancer. Res.* **2002,** *8*, 2963–2969.

97. Chong, C. R.; Chen, X.; Shi, L.; Liu, J. O.; Sullivan, D. J., Jr. A clinical drug library screen identifies astemizole as an antimalarial agent. *Nat Chem Biol* **2006,** *2* (8), 415-6.
98. Bonfanti, J.-F.; Doublet, F.; Fortin, J.; Lacrampe, J.; Guillemont, J.; Muller, P.; Queguiner, L.; Arnoult. E., Gevers, T.; Janssens, P.; Szel, H.; Willebrords, R.; Timmerman, P.; Wuyts, K.; Janssens, F.; Sommen, C.; Wigerinck, P.; and Andries, K. Selection of a Respiratory Syncytial Virus Fusion Inhibitor Clinical Candidate, Part 1: Improving the Pharmacokinetic Profile Using the Structure-Property Relationship. *J. Med. Chem.* **2007,** *50*, 4572-4584.
99. Hasegawa, M.; Nishigaki, N.; Washio, Y.; Kano, K.; Harris, P. A.; Sato, H.; Mori, I.; West, R. I.; Shibahara, M.; Toyoda, H.; Wang, L.; Nolte, R. T.; Veal, J. M.; Cheung, M. Discovery of Novel Benzimidazoles as Potent Inhibitors of TIE-2 and VEGFR-2 Tyrosine Kinase Receptors. *J. Med. Chem.* **2007,** *50*, 4453-4470.
100. Charton, J.; Girault-Mizzi, S.; Debreu-Fontaine, M. A.; Foufelle, F.; Hainault, I.; Bizot-Espiard, J. G.; Caignard, D. H.; Sergheraert, C., Synthesis and biological evaluation of benzimidazole derivatives as potent AMP-activated protein kinase activators. *Bioorg Med Chem* **2006,** *14* (13), 4490-518.
101. Danneberg, F.; Ghidini, A.; Dogandzhiyski, P.; Kalden, E.; Stromberg, R.; Gobel, M. W., Sequence-specific RNA cleavage by PNA conjugates of the metal-free artificial ribonuclease tris(2-aminobenzimidazole). *Beilstein J Org Chem* **2015,** *11*, 493-8.
102. Carpenter, R. D.; DeBerdt, P. B.; Lam, K. S.; Kurth, M. J. Carbodiimide-Based Benzimidazole Library Method. *J. Comb. Chem.* **2006,** *8*, 907-914.
103. Walchshofer, N.; Delabre-Defayolle, I.; Paris, J.; Petavy, A. F. In Vitro Morphological Damage Induced by a New Benzimidazole Prodrug in Echinococcus multiocularis Metacestodes. *J. Pharm. Sci.* **1990,** *79*, 606-608.
104. Scheffer, U.; Strick, A.; Ludwig, V.; Peter, S.; Kalden, E.; Göbel, M. W. Metal-Free Catalysts for the Hydrolysis of RNA Derived from Guanidines, 2-Aminopyridines, and 2-Aminobenzimidazoles. *J Am Chem Soc* **2005,** *127*, 2211-2217.
105. J Perkins, J. J.; Zartman, A. E.; Meissner, R. S. Synthesis of 2-(Alkylamino)benzimidazoles. *Tetrahedron Letters* **1999,** *40*, 1103-1106.
106. Hamley, P.; Tinker, A. C. 1,2-Diaminobenzimidazoles: Selective Inhibitors of Nitric Oxide Synthase Derived From Aminoguanidine. *Bioorganic & Medicinal Chemistry Letters* **1995,** *5*, 1573-1576.

107. Gudmundsson, K. S.; Tidwell, J.; Lippa, N.; Koszalka, G. W.; Draanen, N. v.; Ptak, R. G.; Drach, J. C.; Townsend, L. B. Synthesis and Antiviral Evaluation of Halogenated â-D- and -L-Erythrofuranosylbenzimidazoles. *J. Med. Chem.* **2000,** *43*, 2464-2472.
108. Murphy, D. B., Carbonimidoyl Dihalides as Organic Intermediates. I. The Preparation of 2-Aryl Aminobenzimidazoles. *J. Org. Chem.* **1964,** *29*, 1613-1615.
109. Carpenter, R. D.; Kurth, M. J., A rapid and efficient route to benzazole heterocycles. *Nat Protoc* **2010,** *5* (11), 1731-6.
110. Phakhodee, W.; Duangkamol, C.; Wiriya, N.; Pattarawarapan, M., Ultrasound-assisted synthesis of substituted 2-aminobenzimidazoles, 2-aminobenzoxazoles, and related heterocycles. *Tetrahedron Letters* **2016,** *57* (47), 5290-5293.
111. Wang, Z.; Zhao, Q.; Hou, J.; Yu, W.; Chang, J., Iodine-mediated direct synthesis of multifunctional 2-aminobenzimidazoles from *N*-substituted *o*-diaminoarenes and isothiocyanates. *Tetrahedron* **2018,** *74* (19), 2324-2329.
112. Chanda, K.; Maiti, B.; Chung, W.-S.; Sun, C.-M., Novel approach towards 2-substituted aminobenzimidazoles on imidazolium ion tag under focused microwave irradiation. *Tetrahedron* **2011,** *67* (34), 6214-6220.
113. Heinelt, U.; Schultheis, D.; Jäger, S.; Lindenmaier, M.; Pollex, A.; Beckmann, H. S. g., A convenient method for the synthesis of 2-amino substituted aza-heterocycles from N,N′-disubstituted thioureas using TsCl/NaOH. *Tetrahedron* **2004,** *60* (44), 9883-9888.
114. Cee, V. J.; Downing, N. S., A one-pot method for the synthesis of 2-aminobenzimidazoles and related heterocycles. *Tetrahedron Letters* **2006,** *47* (22), 3747-3750.
115. Clark, P. R.; Williams, G. D.; Tomkinson, N. C. O., Copper-catalysed C-H functionalisation gives access to 2-aminobenzimidazoles. *Org Biomol Chem* **2019,** *17* (34), 7943-7955.
116. Wang, X.-j.; Zhang, L.; Xu, Y.; Krishnamurthy, D.; Senanayake, C. H., A practical synthesis of 2-(N-substituted)-aminobenzimidazoles utilizing CuCl-promoted intramolecular cyclization of N-(2-aminoaryl)thioureas. *Tetrahedron Letters* **2004,** *45* (38), 7167-7170.
117. Wang, F.; Cai, S.; Liao, Q.; Xi, C., A protocol to 2-aminobenzimidazoles via copper-catalyzed cascade addition and cyclization of o-haloanilines and carbodiimides. *J Org Chem* **2011,** *76* (9), 3174-80.
118. Yin, J.; Zhao, M. M.; Huffman, M. A.; McNamara, J. M. Pd-Catalyzed N-Arylation of Heteroarylamines. *Org Lett* **2002,** *4*, 3481-3484.
119. Devine, W. G.; Diaz-Gonzalez, R.; Ceballos-Perez, G.; Rojas, D.; Satoh, T.; Tear, W.; Ranade, R. M.; Barros-Alvarez, X.; Hol, W. G.; Buckner, F. S.; Navarro, M.; Pollastri, M. P., From Cells to Mice to Target: Characterization of NEU-1053 (SB-443342) and Its Analogues for Treatment of Human African Trypanosomiasis. *ACS Infect Dis* **2017,** *3* (3), 225-236.
120. Martin, M. W.; Newcomb, J.; Nunes, J. J.; Boucher, C.; Chai, L.; Epstein, L. F.; Faust, T.; Flores, S.; Gallant, P.; Gore, A.; Gu, Y.; Hsieh, F.; Huang, X.; Kim, J. L.; Middleton, S.; Morgenstern, K.; Oliveira-dos-Santos, A.; Patel, V. F.; Powers, D.; Rose, P.; Tudor, Y.; Turci, S. M.; Welcher, A. A.; Zack, D.; Zhao, H.; Zhu, L.; Zhu, X.; Ghiron, C.; Ermann, M.; Johnston, D.; Saluste, C. G., Structure-based design of novel 2-amino-6-phenyl-pyrimido[5',4':5,6]pyrimido[1,2-a]benzimidazol-5(6H)-ones as potent and orally active inhibitors of lymphocyte specific kinase (Lck): synthesis, SAR, and in vivo anti-inflammatory activity. *J Med Chem* **2008,** *51* (6), 1637-48.

121. Barrett, l. C.; Kerr, M. A. The High-Pressure SNAr Reaction of N-p-Fluorobenzyl-2-chlorobenzimidazole With Amines; An Approach to Norastemizole and Analogues. *Tetrahedron Letters* **1999,** *40*, 2439-2442.
122. Saha, P.; Ramana, T.; Purkait, N.; Ali, M. A.; Paul, R.; Punniyamurthy, T., Ligand-free copper-catalyzed synthesis of substituted benzimidazoles, 2-aminobenzimidazoles, 2-aminobenzothiazoles, and benzoxazoles. *J Org Chem* **2009,** *74* (22), 8719-25.
123. Deng, X.; McAllister, H.; Mani, N. S., CuI-catalyzed amination of arylhalides with guanidines or amidines: a facile synthesis of 1-H-2-substituted benzimidazoles. *J Org Chem* **2009,** *74* (15), 5742-5.
124. Chi, Y.; Zhang, W. X.; Xi, Z., Oxidant-switchable selective synthesis of 2-aminobenzimidazoles via C-H amination/acetoxylation of guanidines. *Org Lett* **2014,** *16* (24), 6274-7.
125. Zhu, T. S.; Chen, J. P.; Xu, M. H., Rhodium-catalyzed enantioselective addition to unsymmetrical alpha-diketones: tandem one-pot synthesis of optically active 3-tetrasubstituted isochroman derivatives. *Chemistry* **2013,** *19* (3), 865-9.
126. Liu, J.; Hoover, J. M., Cobalt-Catalyzed Aerobic Oxidative Cyclization of 2-Aminophenols with Isonitriles: 2-Aminophenol Enabled O_2 Activation by Cobalt(II). *Org Lett* **2019,** *21* (12), 4510-4514.
127. Pitzer, L.; Schafers, F.; Glorius, F., Rapid Assessment of the Reaction-Condition-Based Sensitivity of Chemical Transformations. *Angew Chem Int Ed Engl* **2019,** *58* (25), 8572-8576.
128. Ravindranathan, T.; Wakharkar, R. D.; Landge, A. B., Synthesis of Mebendazole and Enviroxime. Acylation of 2-Amino-5-Benzoylbenzimidazole. *Organic Preparations and Procedures International* **1987,** *19* (1), 9-16.
129. Ravindranathan, T.; Wakharkar, R. D.; Landge, A. B., Preparation of 2-Chloro- and 2-Amino-5-Benzoylbenzimidazoles. *Organic Preparations and Procedures International* **1986,** *18* (2), 95-98.
130. Pal, S., Chapter 4 : Synthesis of other Isocoumarin derivatives. In *Isocoumarin, Thiaisocoumarin and Phosphaisocoumarin : natural occurrences, synthetic approaches and pharmaceutical applications*, Elsevier Science: 2019; pp 109-151.
131. Marco-Contelles, J.; Pérez-Mayoral, E.; Ballesteros, P., 11.05 - Bicyclic 5-5 Systems with One Bridgehead (Ring Junction) Nitrogen Atom: Three Extra Heteroatoms 2:1. In *Comprehensive Heterocyclic Chemistry III*, ScienceDirect: 2008; pp 199-305.
132. Wamhoff, H.; Richardt, G.; Stölben, S., Iminophosphoranes: Versatile Tools in Heterocyclic Synthesis. In *Advances in Heterocyclic Chemistry*, 1995; Vol. 64, pp 159-249.
133. Ke, F.; Zhang, P.; Lin, C.; Lin, X.; Xu, J.; Zhou, X., Synthesis of benzimidazoles by CuI-catalyzed three-component reaction of 2-haloaniline, ammonia and aldehyde in water. *Org Biomol Chem* **2018,** *16* (43), 8090-8094.
134. Kalas, S.; Patil, S.; Jadhav, V., Synthesis and Characterization of Impurities of an Broad-Spectrum Anthelmintic Drug, Albendazole. *Chemical Science Transactions* **2016,** *5* (1), 79-86.
135. Fulmer, G. R.; Miller, A. J. M.; Sherden, N. H.; Gottlieb, H. E.; Nudelman, A.; Stoltz, B. M.; Bercaw, J. E.; Goldberg, K. I., NMR Chemical Shifts of Trace Impurities: Common Laboratory Solvents, Organics, and Gases in Deuterated Solvents Relevant to the Organometallic Chemist. *Organometallics* **2010,** *29* (9), 2176-2179.
136. Zhu, J.; Wu, C. F.; Li, X.; Wu, G. S.; Xie, S.; Hu, Q. N.; Deng, Z.; Zhu, M. X.; Luo, H. R.; Hong, X., Synthesis, biological evaluation and molecular modeling of substituted 2-

aminobenzimidazoles as novel inhibitors of acetylcholinesterase and butyrylcholinesterase. *Bioorg Med Chem* **2013,** *21* (14), 4218-24.
137. Xie, Y.; Zhang, F.; Li, J.; Shi, X., Novel Synthesis of 2-Aminobenzimidazoles from Isoselenocyanates. *Synlett* **2010,** *2010* (06), 901-904.
138. Quast, H.; Ross, K.-H.; Philipp, G.; Hagedorn, M.; Hahn, H.; Banert, K., Syntheses and ^{15}N NMR Spectra of Iminodiaziridines - Ring-Expansions of 1-Aryl-3-iminodiaziridines to 1H- and 3aH-Benzimidazoles, 2H-Indazoles, and 5H-Dibenzo[d,f][1,3]diazepines. *European Journal of Organic Chemistry* **2009,** *2009* (23), 3940-3952.
139. Lyaskovskyy, V.; de Bruin, B., Redox Non-Innocent Ligands: Versatile New Tools to Control Catalytic Reactions. *ACS Catalysis* **2012,** *2* (2), 270-279.
140. Butschke, B.; Fillman, K. L.; Bendikov, T.; Shimon, L. J.; Diskin-Posner, Y.; Leitus, G.; Gorelsky, S. I.; Neidig, M. L.; Milstein, D., How Innocent are Potentially Redox Non-Innocent Ligands? Electronic Structure and Metal Oxidation States in Iron-PNN Complexes as a Representative Case Study. *Inorg Chem* **2015,** *54* (10), 4909-26.
141. Broere, D. L.; Plessius, R.; van der Vlugt, J. I., New avenues for ligand-mediated processes--expanding metal reactivity by the use of redox-active catechol, *o*-aminophenol and *o*-phenylenediamine ligands. *Chem Soc Rev* **2015,** *44* (19), 6886-915.
142. Alaji, Z.; Safaei, E.; Chiang, L.; Clarke, R. M.; Mu, C.; Storr, T., A Copper Complex of a Noninnocent Iminophenol-Amidopyridine Hybrid Ligand: Synthesis, Characterization, and Aerobic Alcohol Oxidation. *European Journal of Inorganic Chemistry* **2014,** *2014* (35), 6066-6074.
143. Safaei, E.; Balaghi, S. E.; Chiang, L.; Clarke, R. M.; Martelino, D.; Webb, M. I.; Wong, E. W. Y.; Savard, D.; Walsby, C. J.; Storr, T., Stabilization of different redox levels of a tridentate benzoxazole amidophenoxide ligand when bound to Co(III) or V(V). *Dalton Trans* **2019,** *48* (35), 13326-13336.
144. Alaji, Z.; Safaei, E.; Yi, H.; Cong, H.; Wojtczak, A.; Lei, A., Redox active ligand and metal cooperation for C(sp^2)-H oxidation: extension of the galactose oxidase mechanism in water-mediated amide formation. *Dalton Trans* **2018,** *47* (43), 15293-15297.
145. Chaudhuri, P.; Verani, C. N.; Bill, E.; Bothe, E.; Weyhermuller, T.; Wieghardt, K., Electronic structure of bis(o-iminobenzosemiquinonato)metal complexes (Cu, Ni, Pd). The art of establishing physical oxidation states in transition-metal complexes containing radical ligands. *J Am Chem Soc* **2001,** *123* (10), 2213-23.
146. Leconte, N.; Moutet, J.; Constantin, T.; Molton, F.; Philouze, C.; Thomas, F., Coordination Chemistry of the Redox Non-Innocent Ligand Bis(2-amino-3,5-di-*tert*-butylphenyl)amine with Group 10 Metal Ions (Ni, Pd, Pt). *European Journal of Inorganic Chemistry* **2018,** *2018* (16), 1752-1761.
147. Nasibipour, M.; Safaei, E.; Masoumpour, M. S.; Wojtczak, A., Ancillary ligand electro-activity effects towards phenyl acetylene homocoupling reaction by a nickel(ii) complex of a non-innocent O-amino phenol ligand: a mechanistic insight. *RSC Advances* **2020,** *10* (41), 24176-24189.
148. Metzinger, R.; Demeshko, S.; Limberg, C., A Novel Pentadentate Redox-Active Ligand and Its Iron(III) Complexes: Electronic Structures and O2Reactivity. *Chemistry - A European Journal* **2014,** *20* (16), 4721-4735.
149. Matson, E. M.; Franke, S. M.; Anderson, N. H.; Cook, T. D.; Fanwick, P. E.; Bart, S. C., Radical Reductive Elimination from Tetrabenzyluranium Mediated by an Iminoquinone Ligand. *Organometallics* **2014,** *33* (8), 1964-1971.

150. Boyer, J. L.; Cundari, T. R.; DeYonker, N. J.; Rauchfuss, T. B.; Wilson, S. R., Redox activation of alkene ligands in platinum complexes with non-innocent ligands. *Inorg Chem* **2009,** *48* (2), 638-45.
151. Blackmore, K. J.; Ziller, J. W.; Heyduk, A. F., "Oxidative addition" to a Zirconium(IV) redox-active ligand complex. *Inorg Chem* **2005,** *44* (16), 5559-61.
152. Herebian, D.; Bothe, E.; Bill, E.; Weyhermuller, T.; Wieghardt, K., Experimental evidence for the noninnocence of o-aminothiophenolates: coordination chemistry of o-iminothionebenzosemiquinonate(1-) pi-radicals with Ni(II), Pd(II), Pt(II). *J Am Chem Soc* **2001,** *123* (41), 10012-23.
153. Chun, H.; Bill, E.; Bothe, E.; Weyhermuller, T.; Wieghardt, K., Octahedral (cis-cyclam)iron(III) complexes with O,N-coordinated o-iminosemiquinonate(1-) pi radicals and o-imidophenolate(2-) anions. *Inorg Chem* **2002,** *41* (20), 5091-9.
154. Sun, X.; Chun, H.; Hildenbrand, K.; Bothe, E.; Weyhermuller, T.; Neese, F.; Wieghardt, K., o-Iminobenzosemiquinonato(1-) and o-amidophenolato(2-) complexes of palladium(II) and platinum(II): a combined experimental and density functional theoretical study. *Inorg Chem* **2002,** *41* (16), 4295-303.
155. Chun, H.; Bill, E.; Weyhermuller, T.; Wieghardt, K., S = (3)/(2) <==> S = (1)/(2) spin crossover behavior in five-coordinate halido- and pseudohalido-bis(o-iminobenzosemiquinonato)iron(III) complexes. *Inorg Chem* **2003,** *42* (18), 5612-20.
156. Min, K. S.; Weyhermuller, T.; Bothe, E.; Wieghardt, K., Tetradentate bis(o-iminobenzosemiquinonate(1-)) π radical ligands and their o-aminophenolate(1-) derivatives in complexes of nickel(II), palladium(II), and copper(II). *Inorg Chem* **2004,** *43* (9), 2922-31.
157. Gray, H. B.; Williams, R.; Bernal, I.; Billig, E. A Spin-Free Square Planar Cobaltous Complex. *J. Am. Chem. Soc.* **1962,** *84* (18), 3596–3597.
158. Billig, E.; Williams, R.; Bernal, I.; Waters, J. H.; Gray, H. B. The Electronic Structures of Square-Planar Metal Complexes. II. The Complexes of Maleonitriledithiolate with Copper(II), Nickel(II), Palladium(II), and Platinum(II). *Inorg. Chem.* **1963,** *3* (5), 663-666.
159. Chirik, P. J.; Wieghardt, K., Chemistry. Radical ligands confer nobility on base-metal catalysts. *Science* **2010,** *327* (5967), 794-5.
160. Bachler, V.; Olbrich, G.; Neese, F.; Wieghardt, K., Theoretical evidence for the singlet diradical character of square planar nickel complexes containing two o-semiquinonato type ligands. *Inorg Chem* **2002,** *41* (16), 4179-93.
161. Chaudhuri, P.; Hess, M.; Muller, J.; Hildenbrand, K.; Bill, E.; Weyhermuller, T.; Wieghardt, K., Aerobic oxidation of primary alcohols (including methanol) by copper(II)- and zinc(II)-phenoxyl radical catalysts. *Journal of the American Chemical Society* **1999,** *121* (41), 9599-9610.
162. Boyer, J. L.; Rochford, J.; Tsai, M.-K.; Muckerman, J. T.; Fujita, E., Ruthenium complexes with non-innocent ligands: Electron distribution and implications for catalysis. *Coordination Chemistry Reviews* **2010,** *254* (3-4), 309-330.
163. Balaghi, S. E.; Safaei, E.; Chiang, L.; Wong, E. W.; Savard, D.; Clarke, R. M.; Storr, T., Synthesis, characterization and catalytic activity of copper(II) complexes containing a redox-active benzoxazole iminosemiquinone ligand. *Dalton Trans* **2013,** *42* (19), 6829-39.
164. Chakraborty, B.; Paine, T. K., Aromatic ring cleavage of 2-amino-4-tert-butylphenol by a nonheme iron(II) complex: functional model of 2-aminophenol dioxygenases. *Angew Chem Int Ed Engl* **2013,** *52* (3), 920-4.

165. Costas, M.; Mehn, M. P.; Jensen, M. P.; Que, L., Jr., Dioxygen activation at mononuclear nonheme iron active sites: enzymes, models, and intermediates. *Chem Rev* **2004,** *104* (2), 939-86.
166. Baltrun, M.; Watt, F. A.; Schoch, R.; Wolper, C.; Neuba, A. G.; Hohloch, S., A new bis-phenolate mesoionic carbene ligand for early transition metal chemistry. *Dalton Trans* **2019,** *48* (39), 14611-14625.

Appendix

NMR Characterization of Aminobenzoxazoles and Aminobenzimidazoles

^{1}H and ^{13}C NMR Spectra of 2-Aminobenzoxazoles

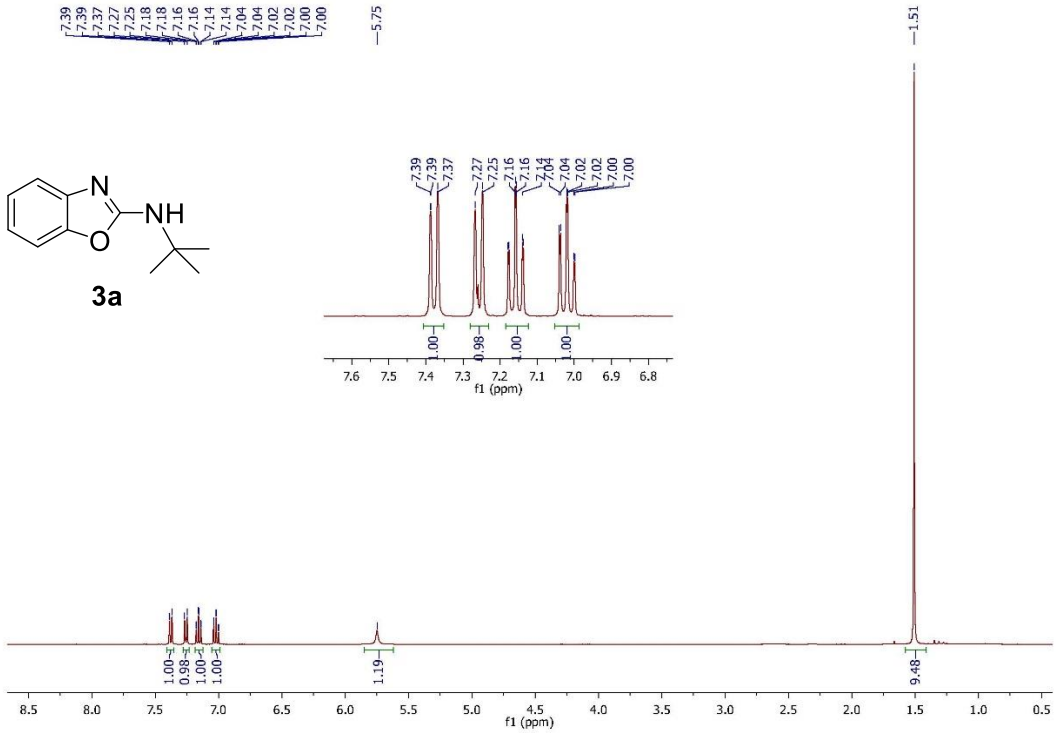

Figure A1. ^{1}H NMR spectrum of 2-(*tert*-butylamino)benzoxazole (3a) in $CDCl_3$ at 400 MHz.

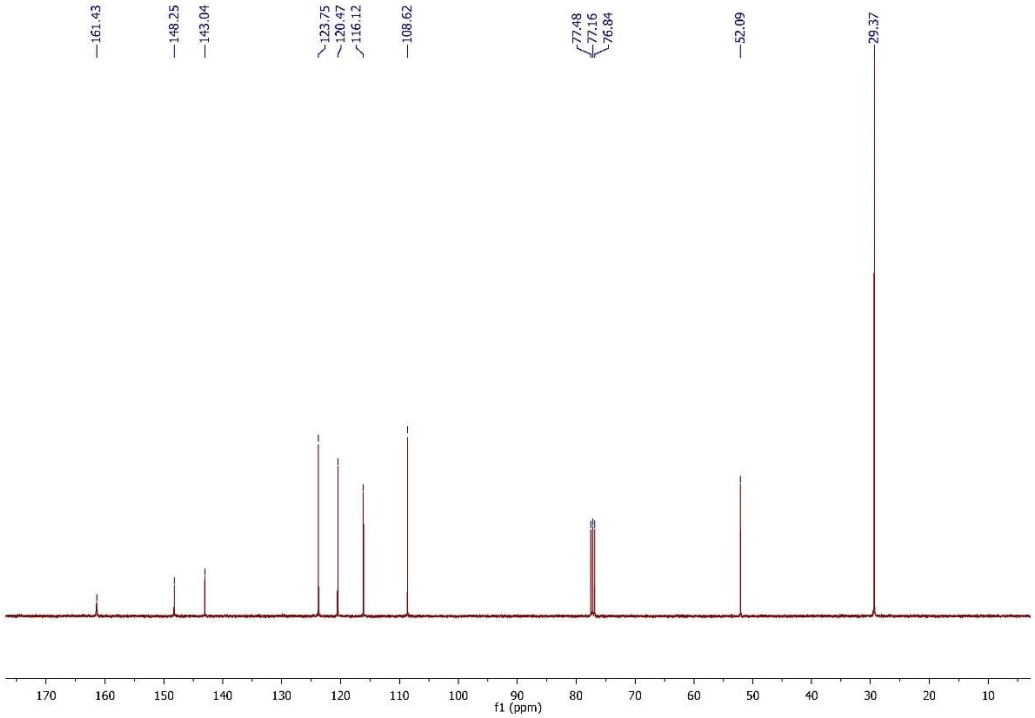

Figure A2. ^{13}C NMR spectrum of 2-(*tert*-butylamino)benzoxazole (3a) in $CDCl_3$ at 100 MHz.

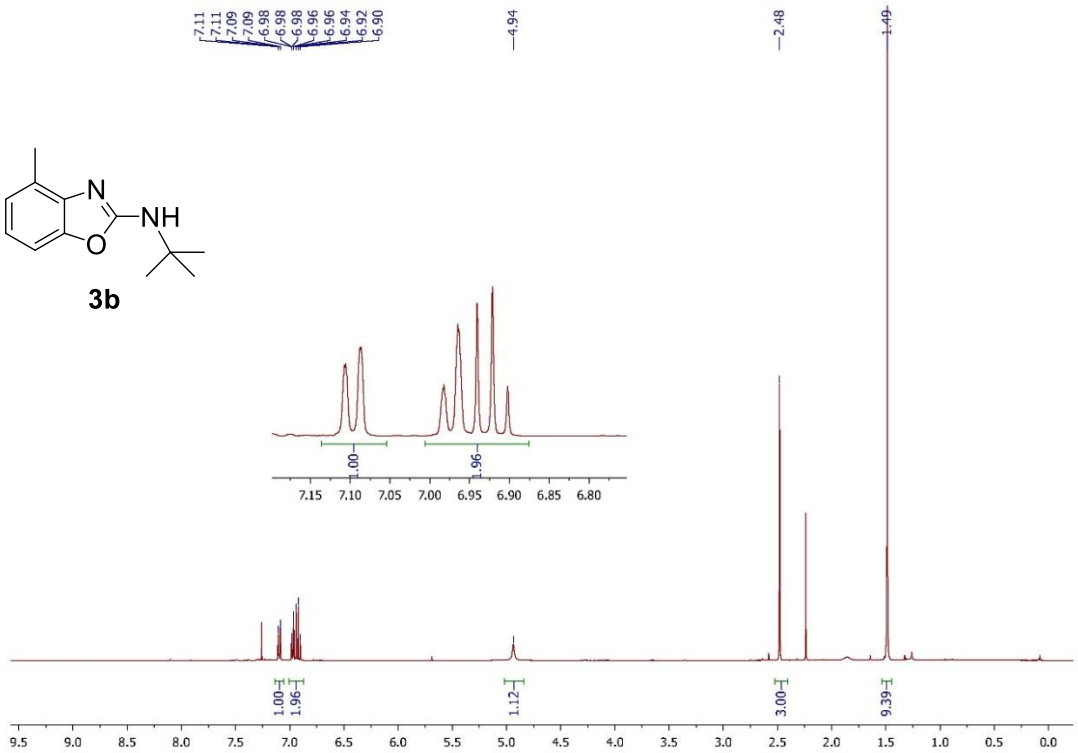

Figure A3. ^{1}H NMR spectrum of 4-methyl-2-(*tert*-butylamino)benzoxazole (3b) in $CDCl_3$ at 400 MHz.

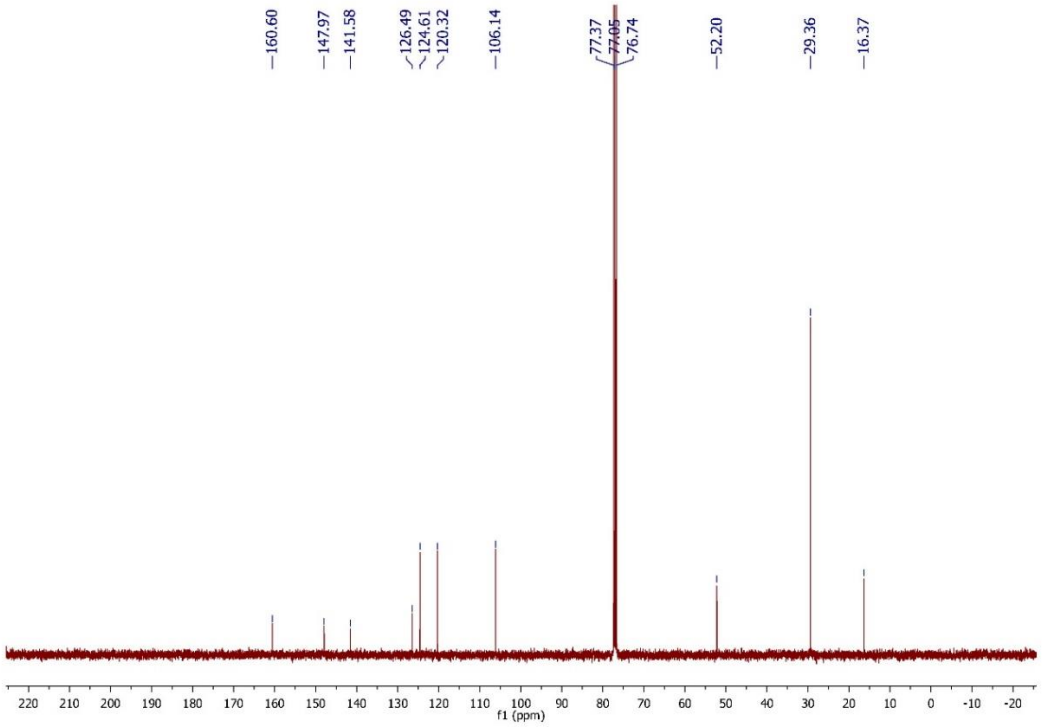

Figure A4. ^{13}C NMR spectrum of 4-methyl-2-(*tert*-butylamino)benzoxazole (3b) in $CDCl_3$ at 100 MHz.

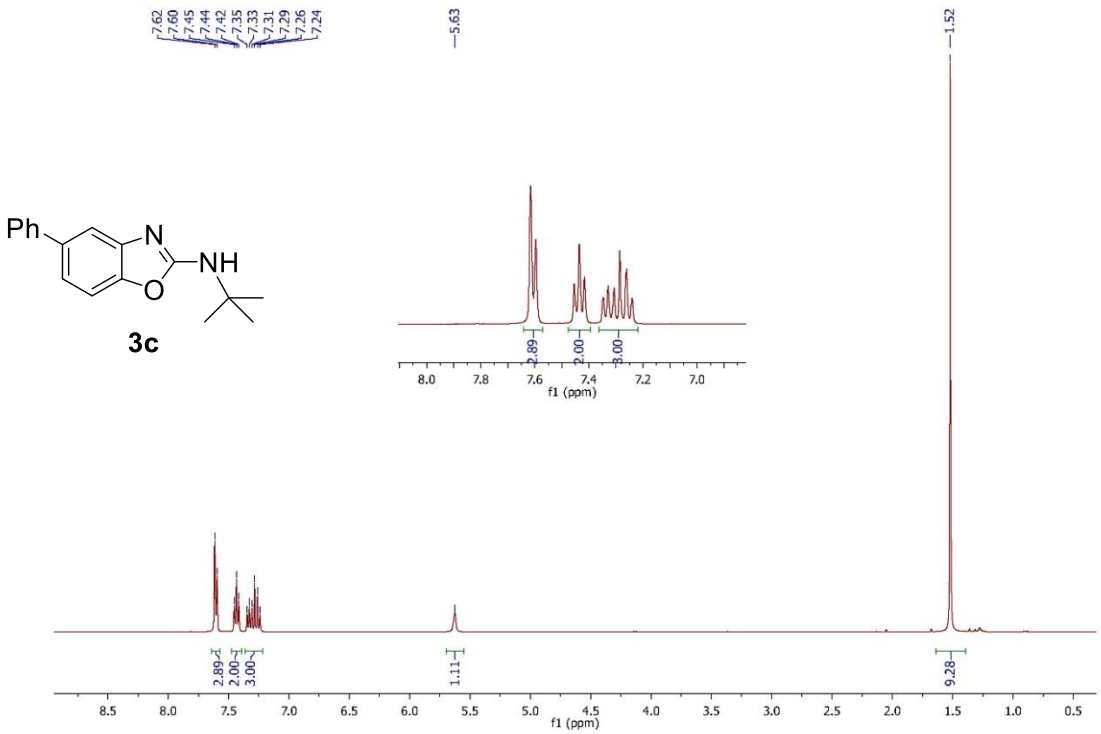

Figure A5. ^{1}H-NMR spectrum of 5-phenyl-2-(*tert*-butylamino) benzoxazole (3c) in $CDCl_3$ at 400 MHz.

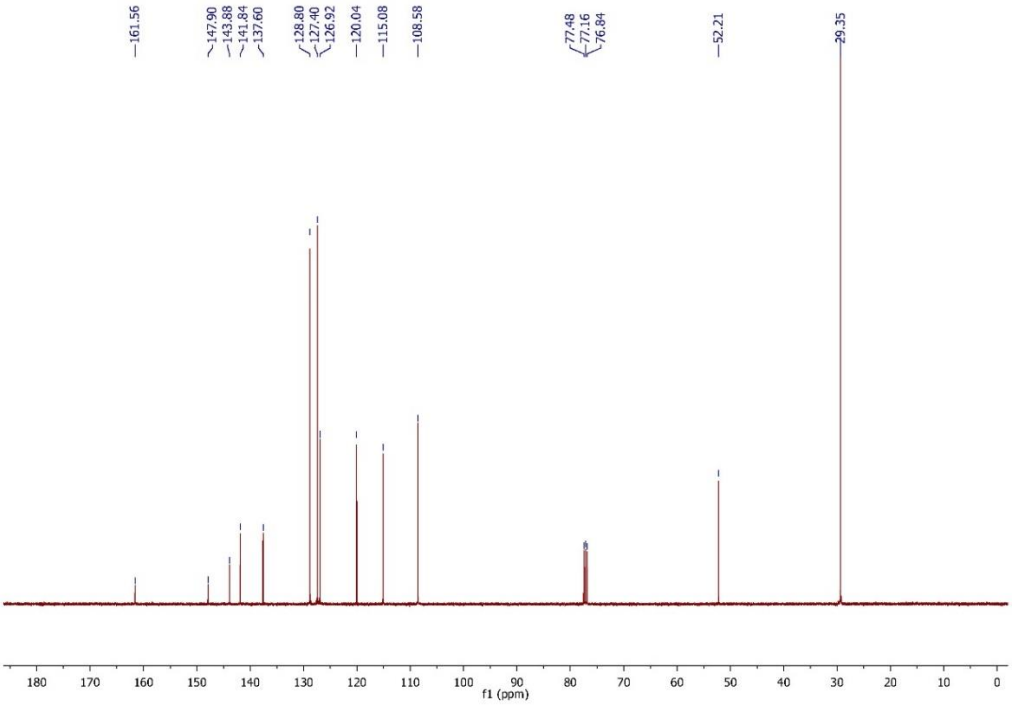

Figure A6. ^{13}C NMR spectrum of 5-phenyl-2-(*tert*-butylamino)benzoxazole (3c) in $CDCl_3$ at 100 MHz.

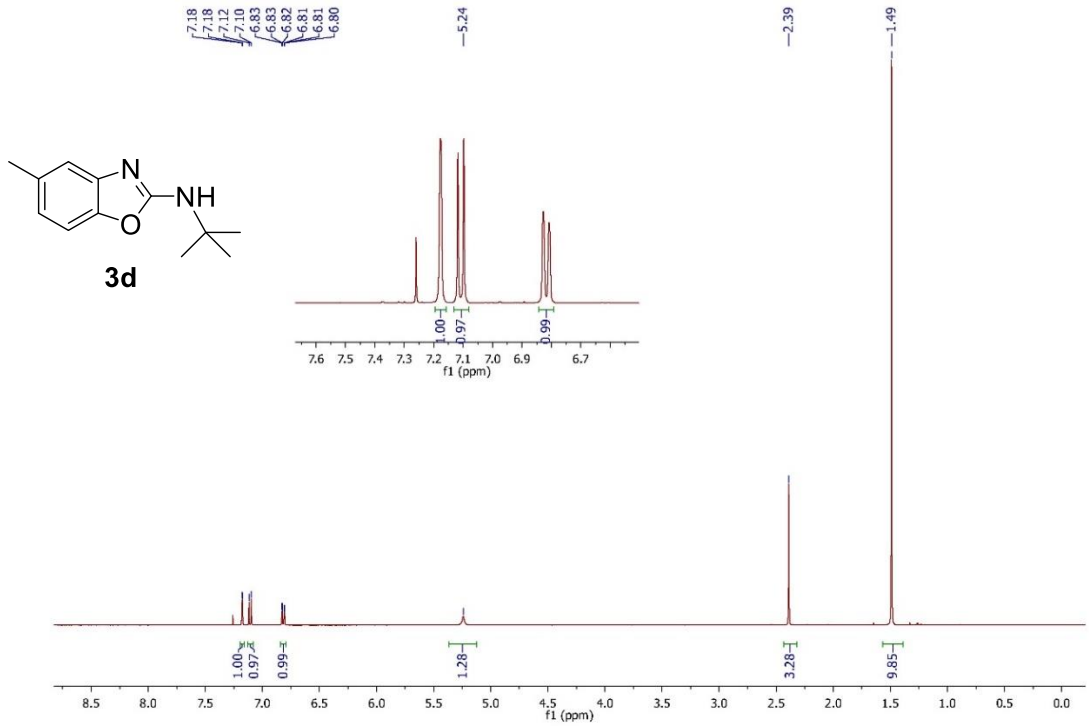

Figure A7. ^{1}H NMR spectrum of 5-methyl-2-(*tert*-butylamino)benzoxazole (3d) in $CDCl_3$ at 400 MHz.

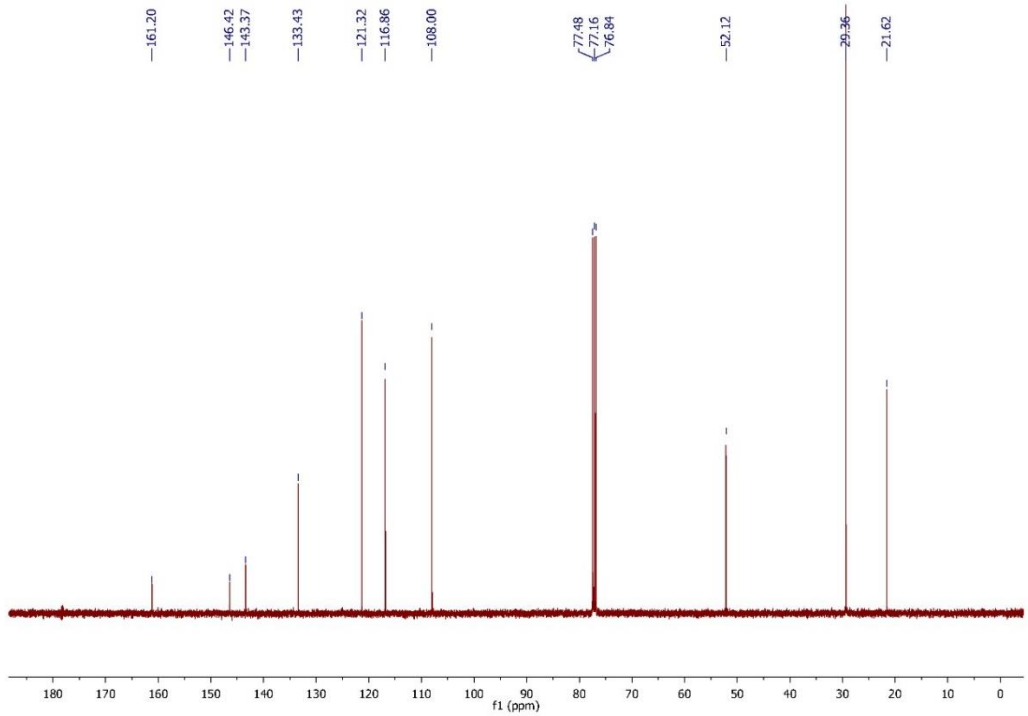

Figure A8. ^{13}C NMR spectrum of 5-methyl-2-(*tert*-butylamino) benzoxazole (3d) in $CDCl_3$ at 100 MHz.

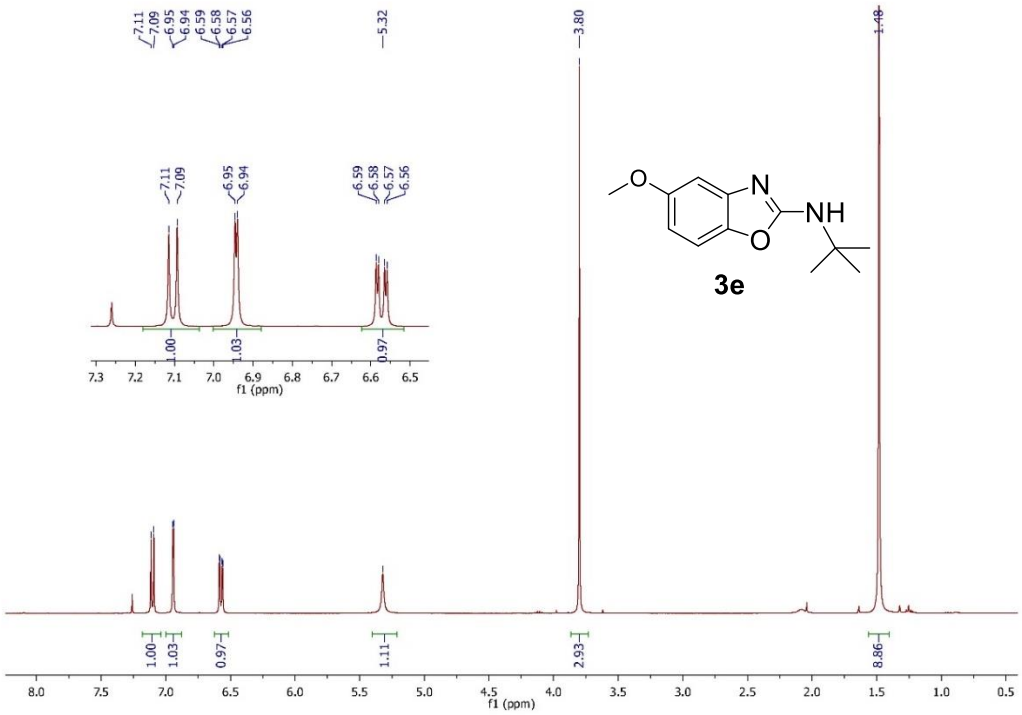

Figure A9. ^{1}H NMR spectrum of 5-methoxy-2-(*tert*-butylamino)benzoxazole (3e) in $CDCl_3$ at 400 MHz.

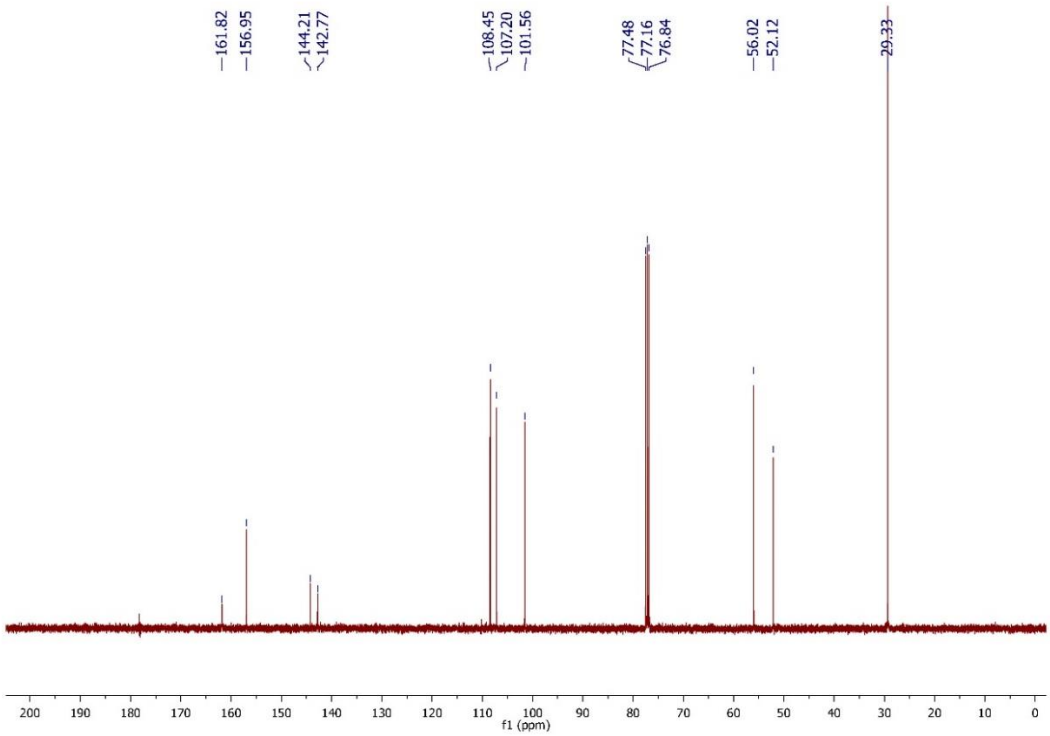

Figure A10. ^{13}C NMR spectrum of 5-methoxy-2-(*tert*-butylamino)benzoxazole (3e) in $CDCl_3$ at 100 MHz.

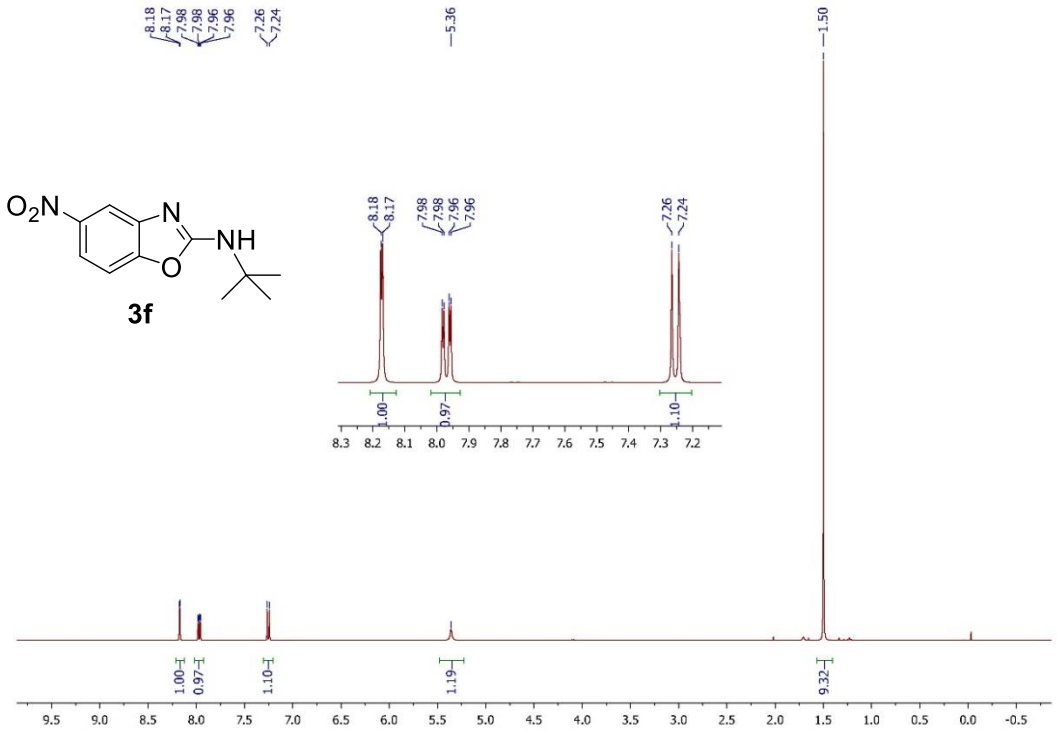

Figure A11. ^{1}H NMR spectrum of 5-nitro-2-(*tert*-butylamino)benzoxazole (3f) in $CDCl_3$ at 400 MHz.

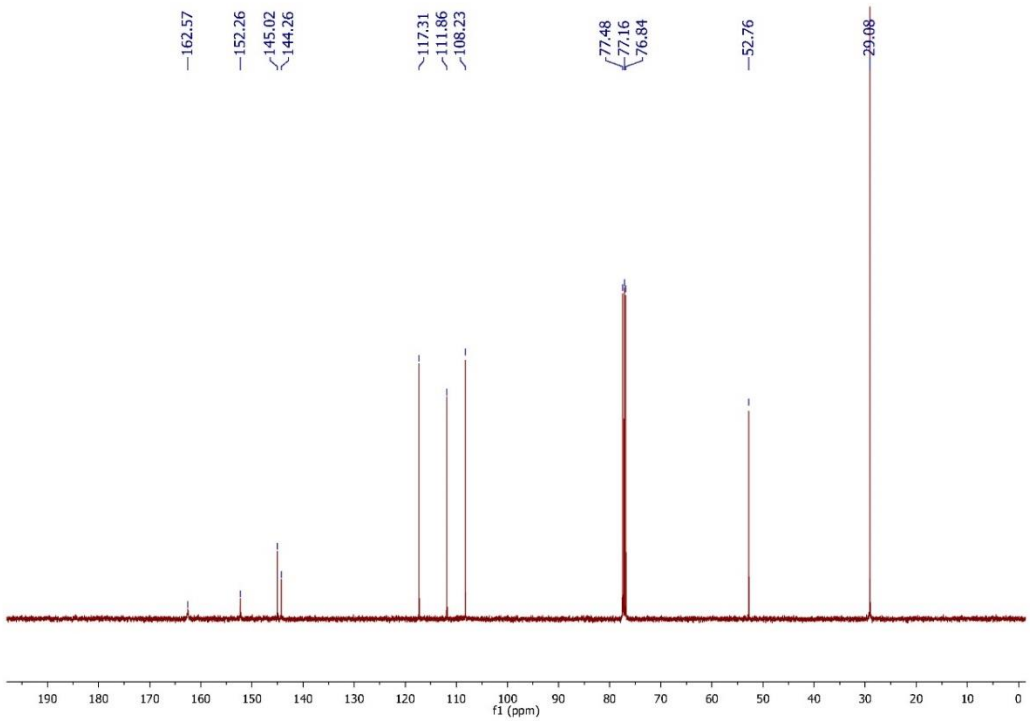

Figure A12. ^{13}C NMR spectrum of 5-nitro-2-(*tert*-butylamino)benzoxazole (3f) in $CDCl_3$ at 100 MHz.

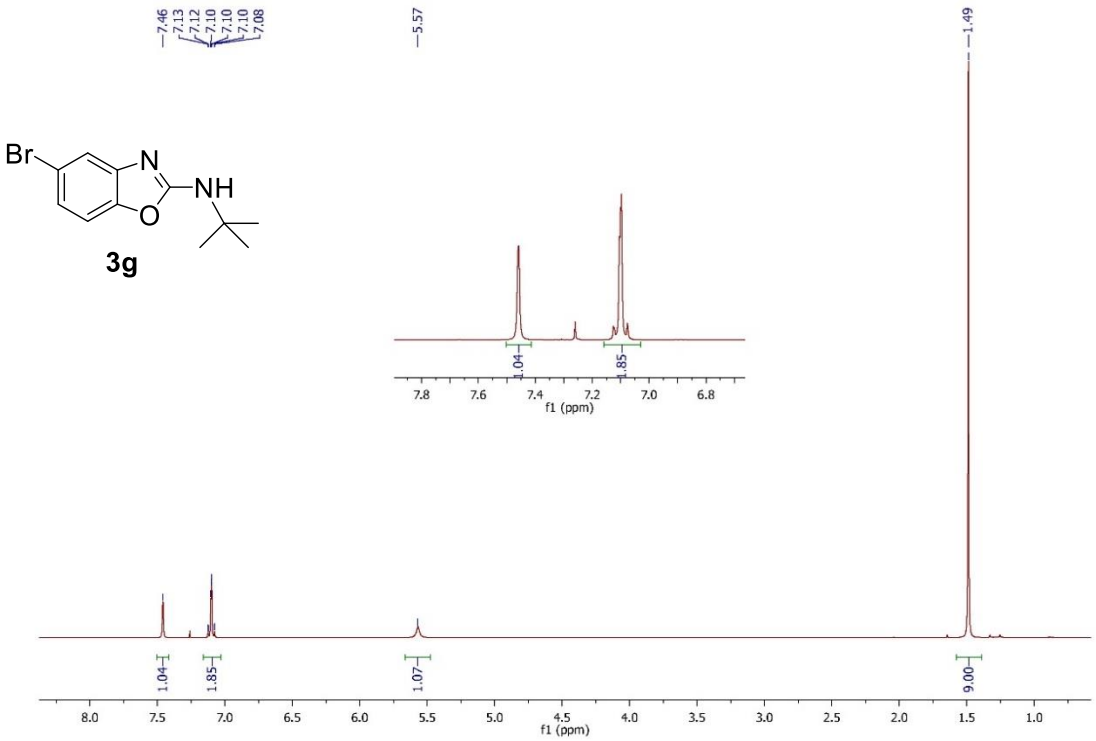

Figure A13. ^{1}H NMR spectrum of 5-bromo-2-(*tert*-butylamino)benzoxazole (3g) in $CDCl_3$ at 400 MHz.

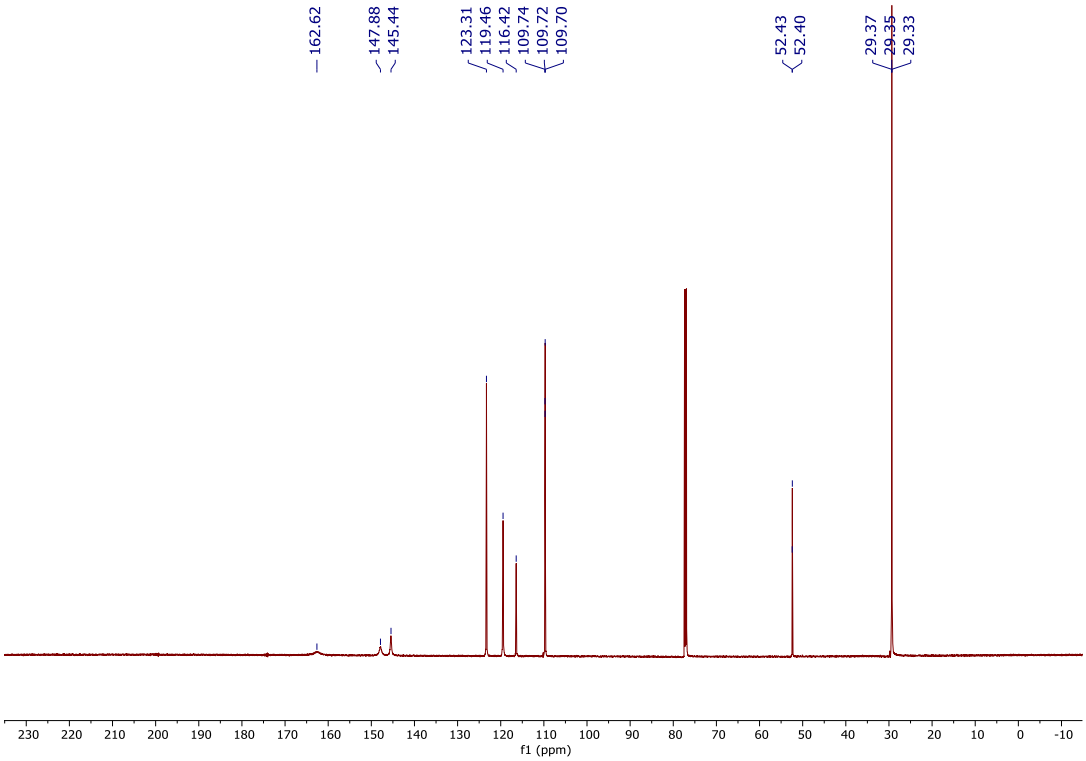

Figure A14. ^{13}C NMR spectrum of 5-bromo-2-(*tert*-butylamino)benzoxazole (3g) in $CDCl_3$ at 100 MHz.

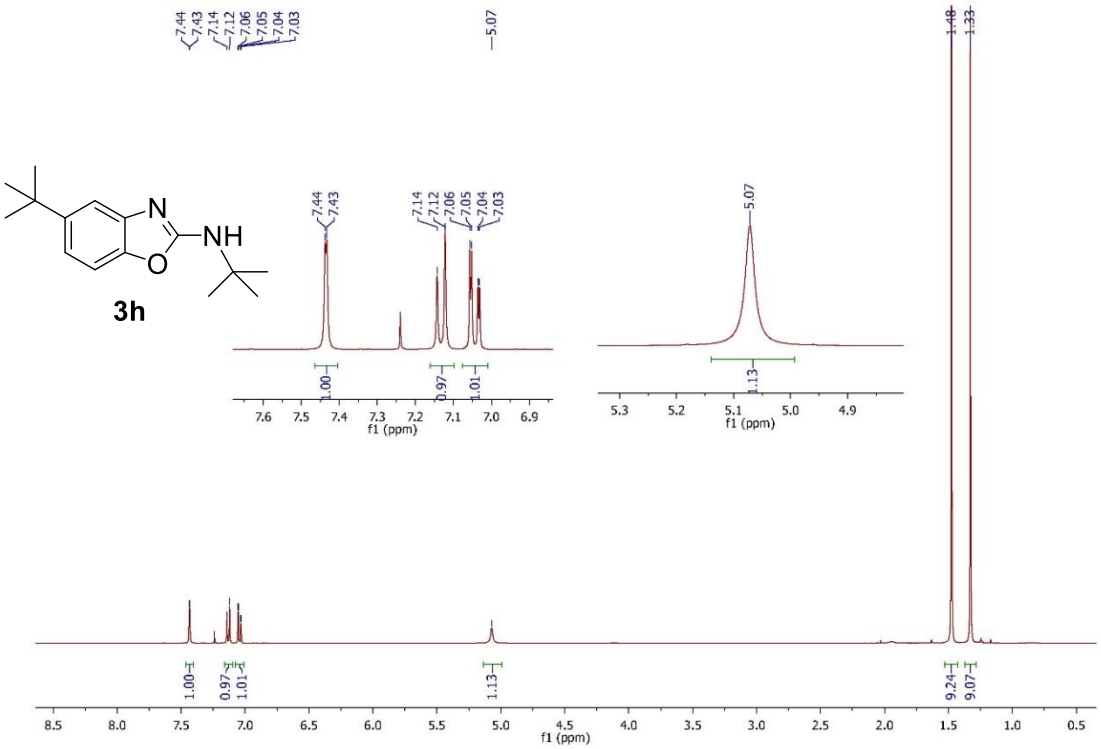

Figure A15. ^{1}H NMR spectrum of 5-tert-butyl-2-(tert-butylamino)benzoxazole (3h) in $CDCl_3$ at 400 MHz.

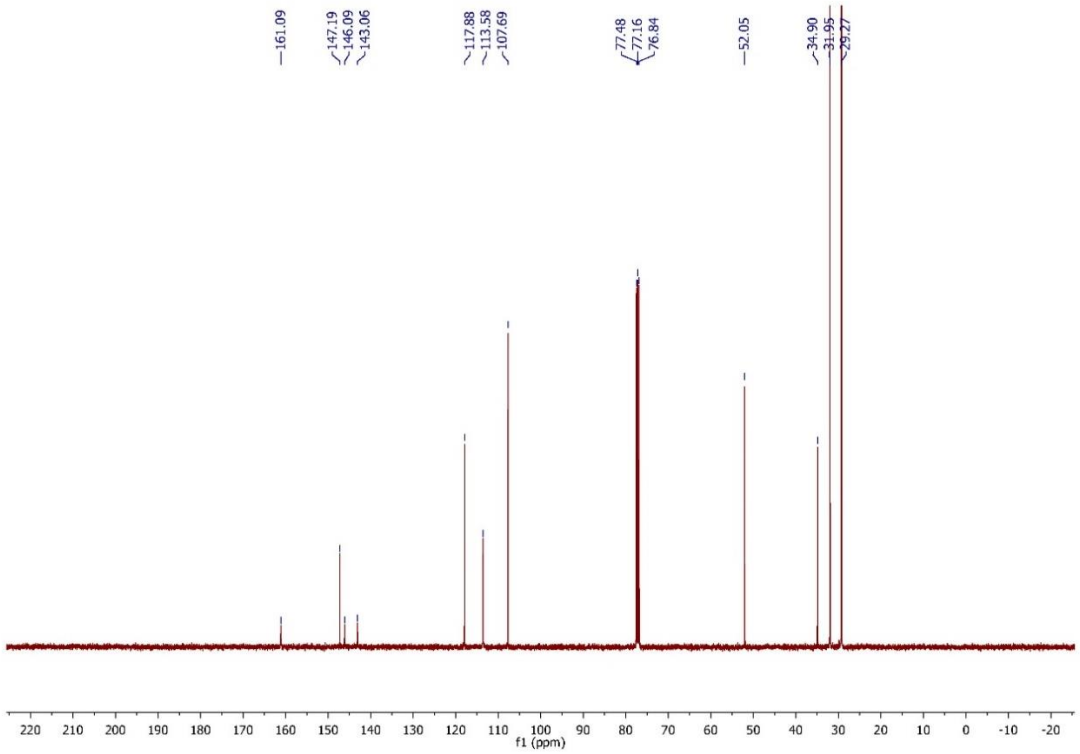

Figure A16. ^{13}C NMR spectrum of 5-tert-butyl-2-(tert-butylamino)benzoxazole (3h) in $CDCl_3$ at 100 MHz.

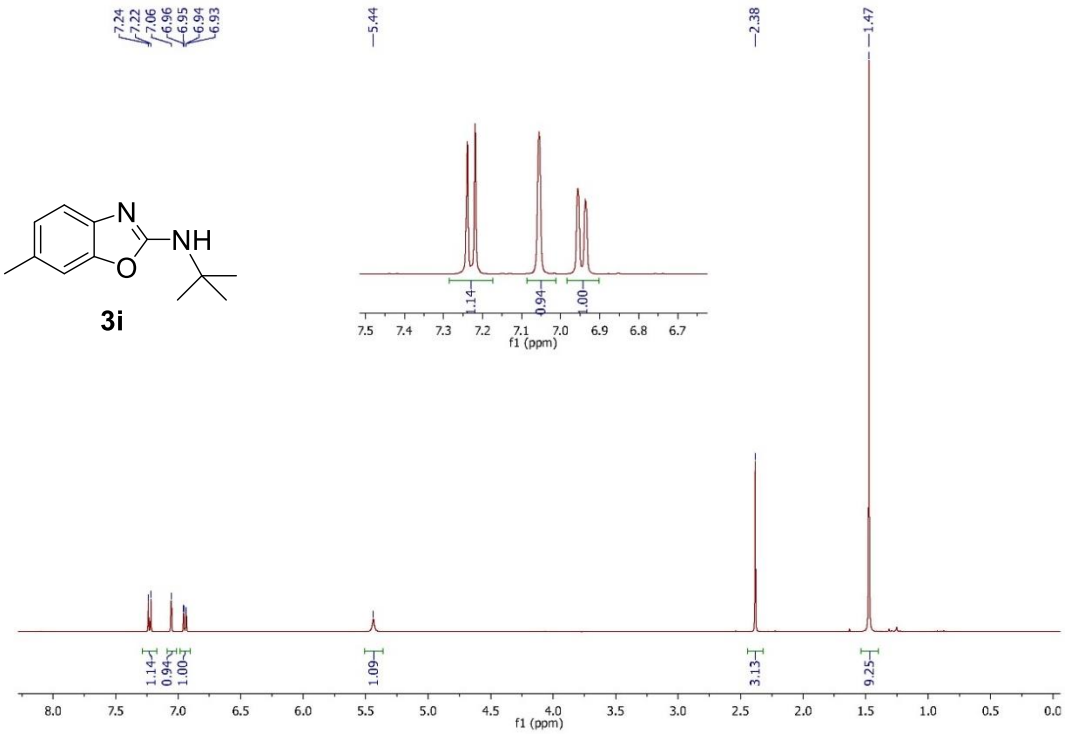

Figure A17. ^{1}H NMR spectrum of 6-methyl-2-(*tert*-butylamino)benzoxazole (3i) in $CDCl_3$ at 400 MHz.

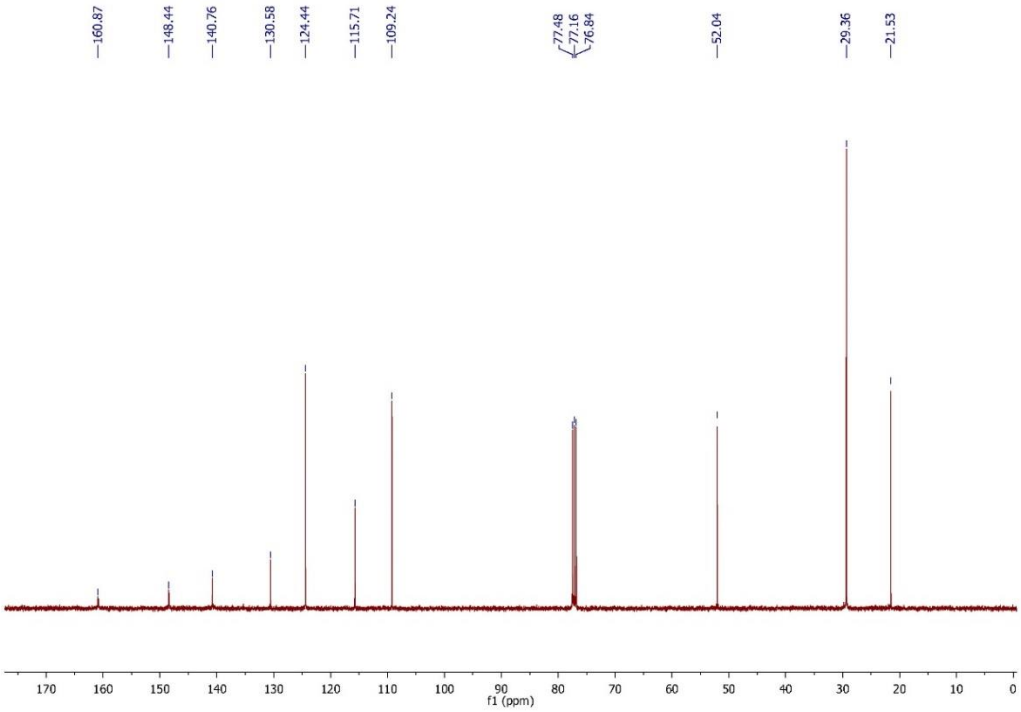

Figure A18. ^{13}C NMR spectrum of 6-methyl-2-(*tert*-butylamino) benzoxazole(3i) in $CDCl_3$ at 100 MHz.

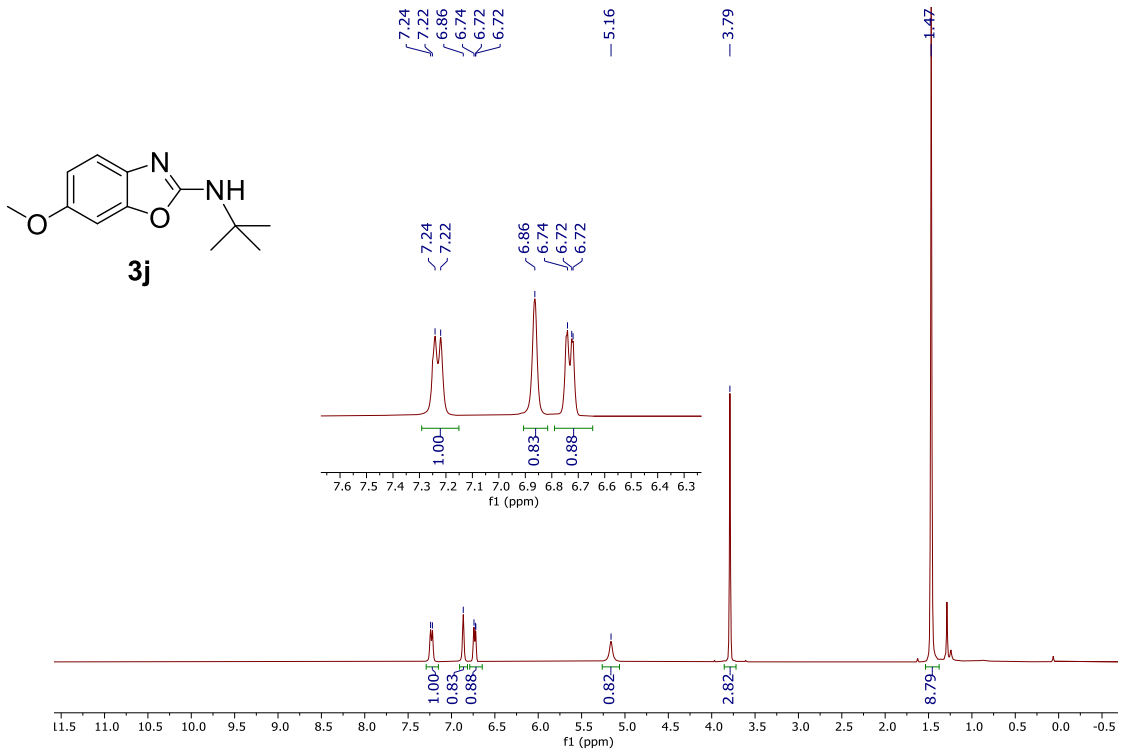

Figure A19. ^{1}H NMR spectrum of 6-methoxy-2-(*tert*-butylamino)benzoxazole (3j) in $CDCl_3$ at 400 MHz.

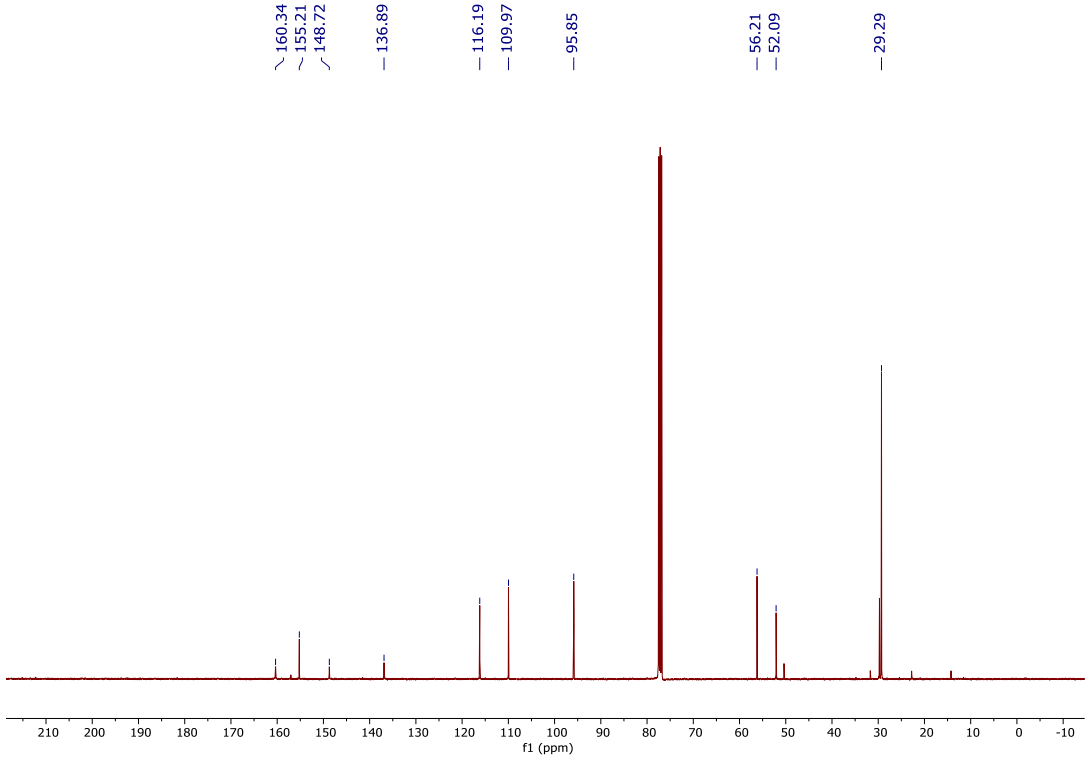

Figure A20. ^{13}C NMR spectrum of 6-methoxy-2-(*tert*-butylamino)benzoxazole (3j) in $CDCl_3$ at 100 MHz.

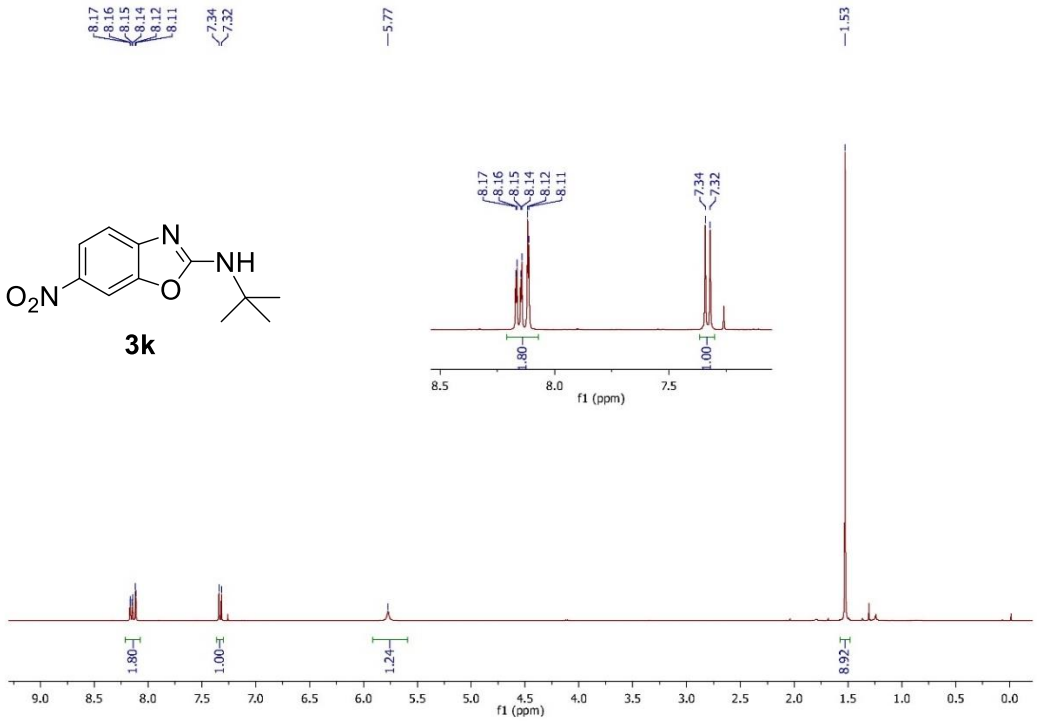

Figure A21. ^{1}H NMR spectrum of 6-nitro-2-(*tert*-butylamino)benzoxazole (3k) in $CDCl_3$ at 400 MHz.

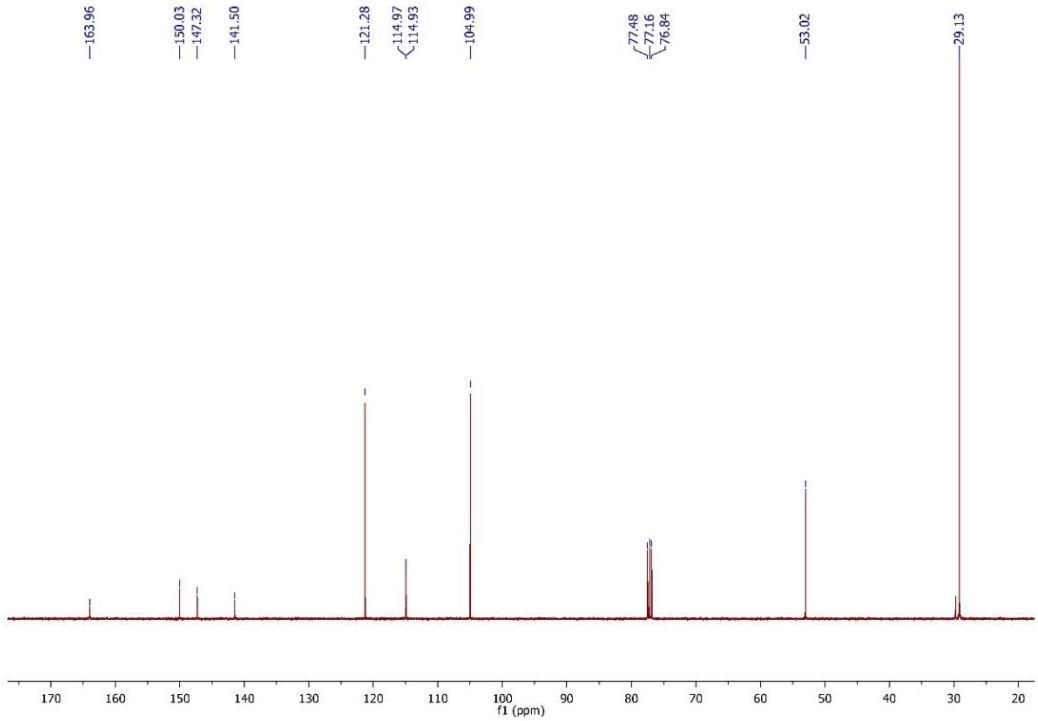

Figure A22. ^{13}C NMR spectrum of 6-nitro-2-(*tert*-butylamino)benzoxazole (3k) in $CDCl_3$ at 100 MHz.

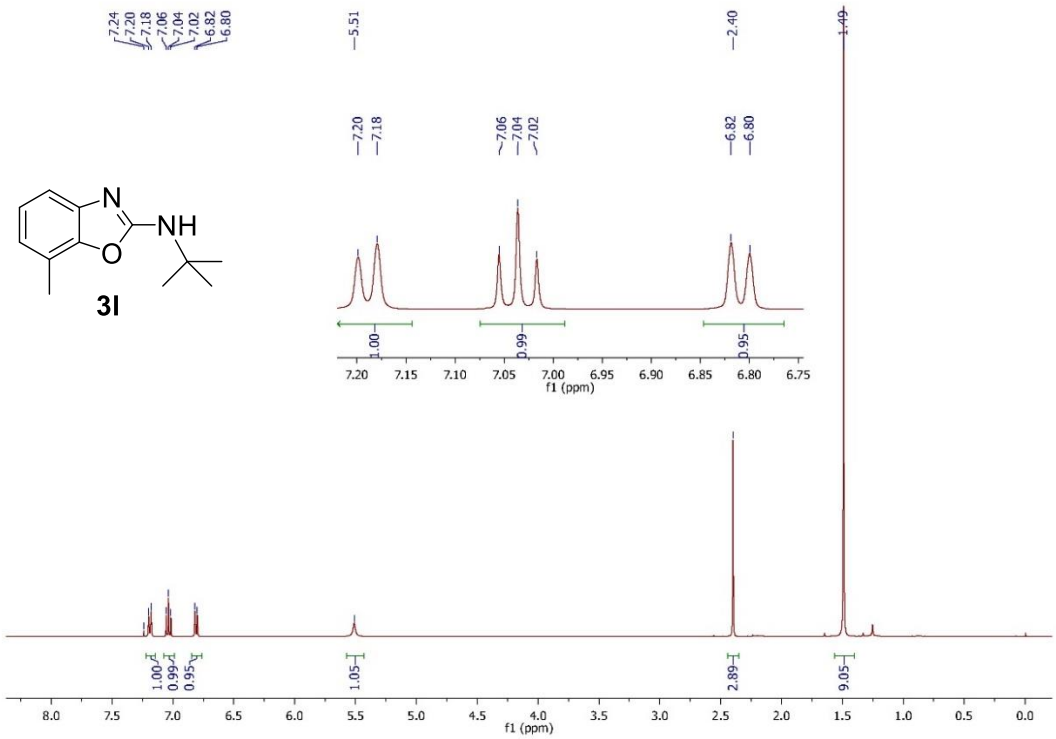

Figure A23. ^{1}H NMR spectrum of 7-methyl-2-(*tert*-butylamino)benzoxazole (3l) in $CDCl_3$ at 400 MHz.

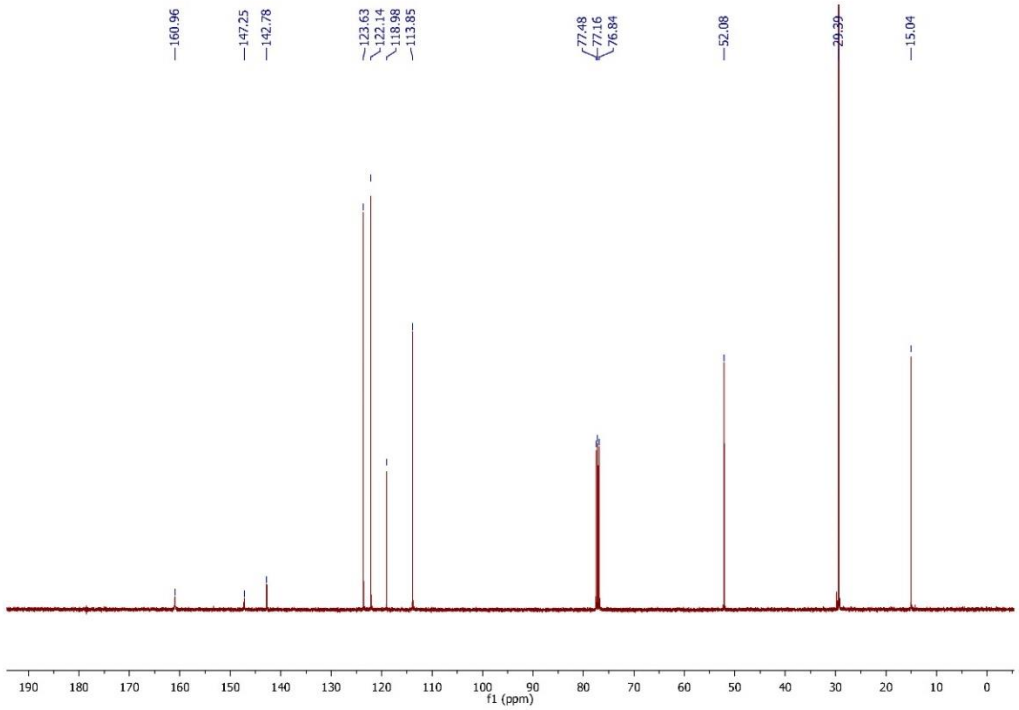

Figure A24. ^{13}C NMR spectrum of 7-methyl-2-(*tert*-butylamino)benzoxazole (3l) in $CDCl_3$ at 100 MHz.

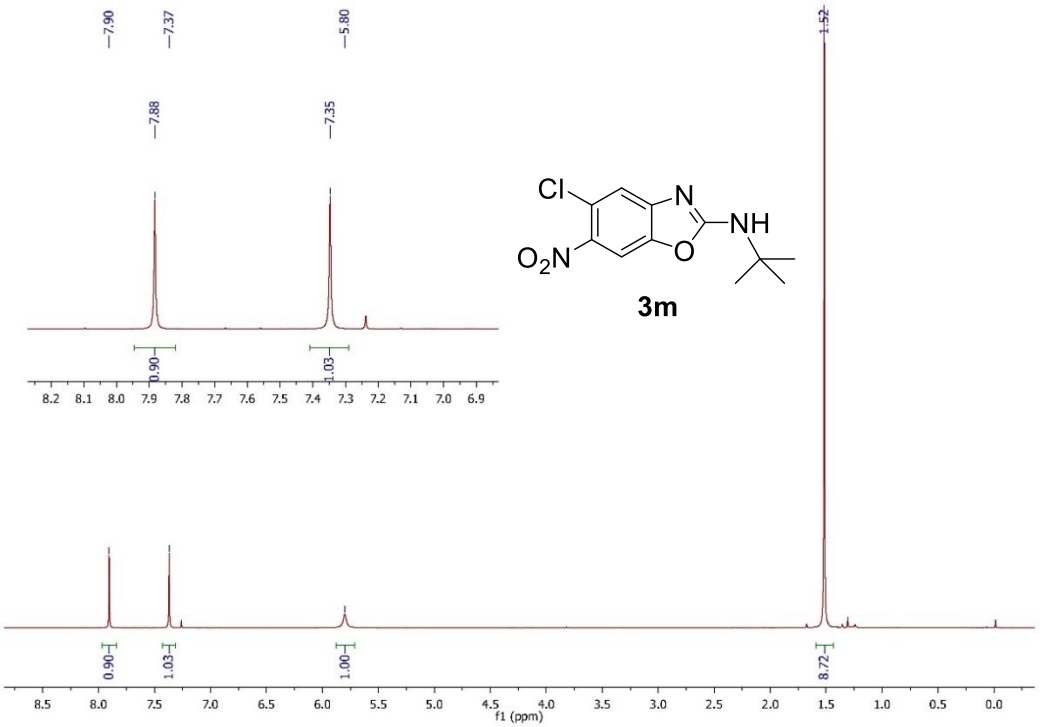

Figure A25. ^{1}H NMR spectrum of 6-nitro-5-chloro-2-(*tert*-butylamino)benzoxazole (3m) in $CDCl_3$ at 400 MHz.

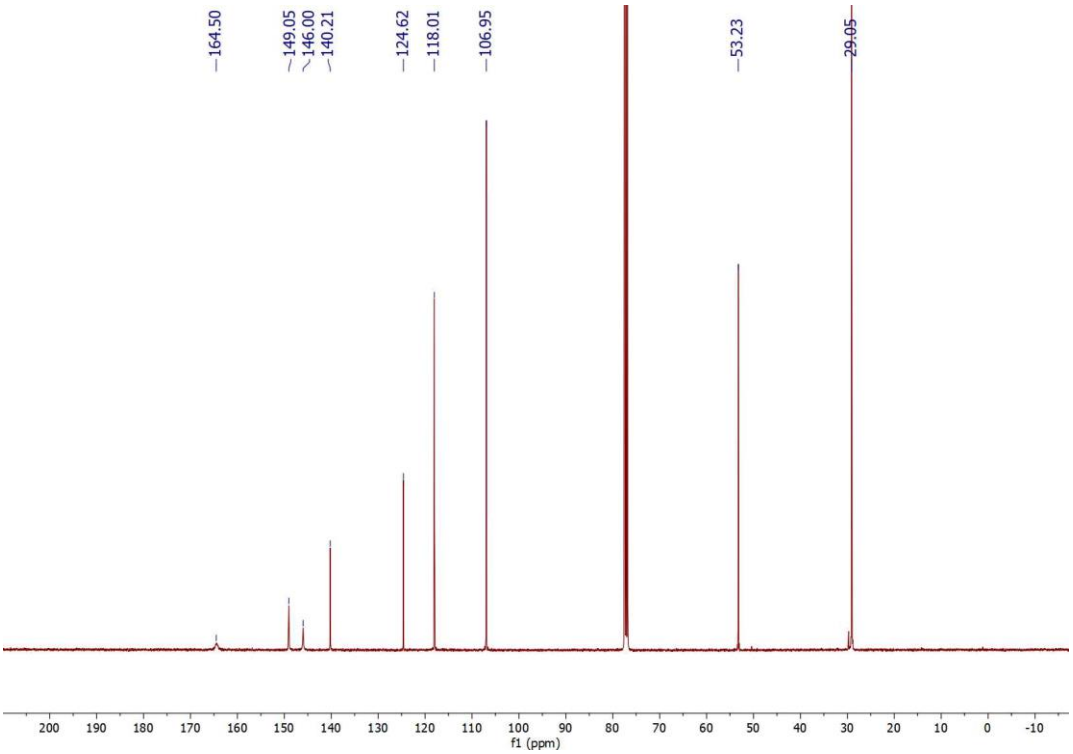

Figure A26. ^{13}C NMR spectrum of 6-nitro-5-chloro-2-(*tert*-butylamino)benzoxazole (3m) in $CDCl_3$ at 100 MHz.

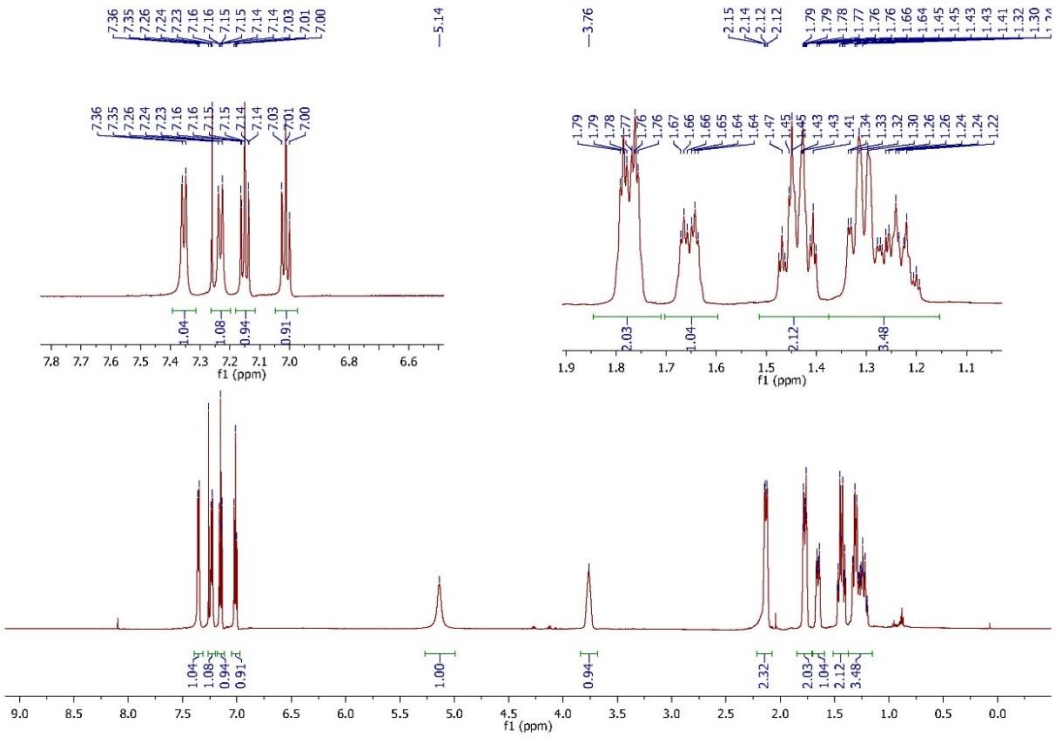

Figure A27. ^{1}H NMR spectrum of 2-(cyclohexylamino)benzoxazole (3n) in $CDCl_3$ at 400 MHz.

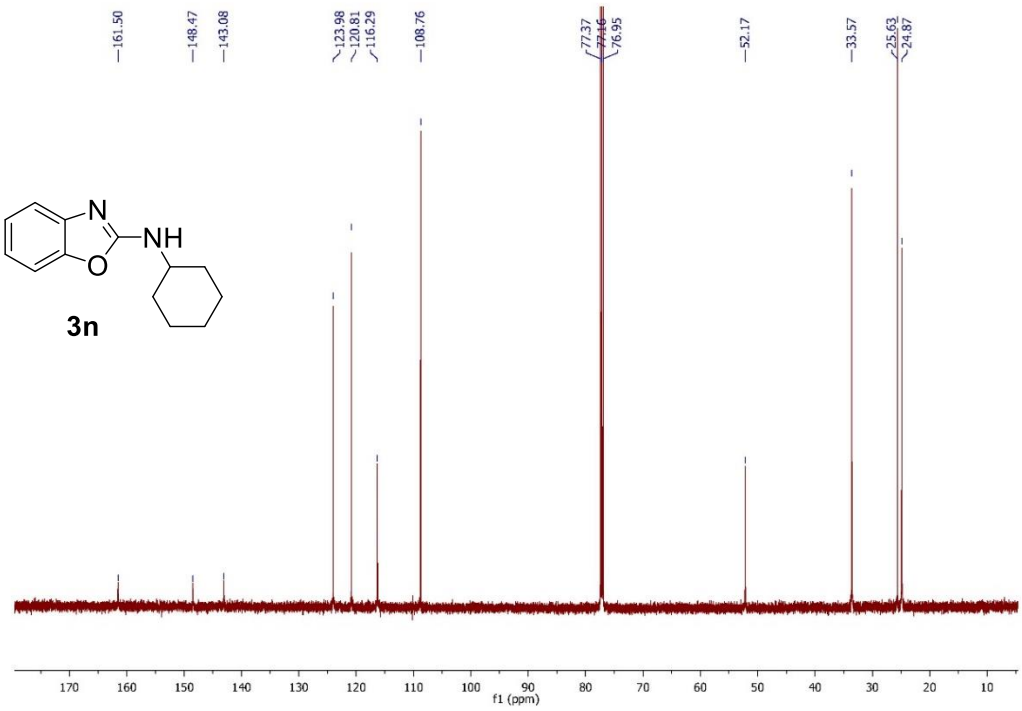

Figure A28. ^{13}C NMR spectrum of 2-(cyclohexylamino)benzoxazole (3n) in $CDCl_3$ at 100 MHz.

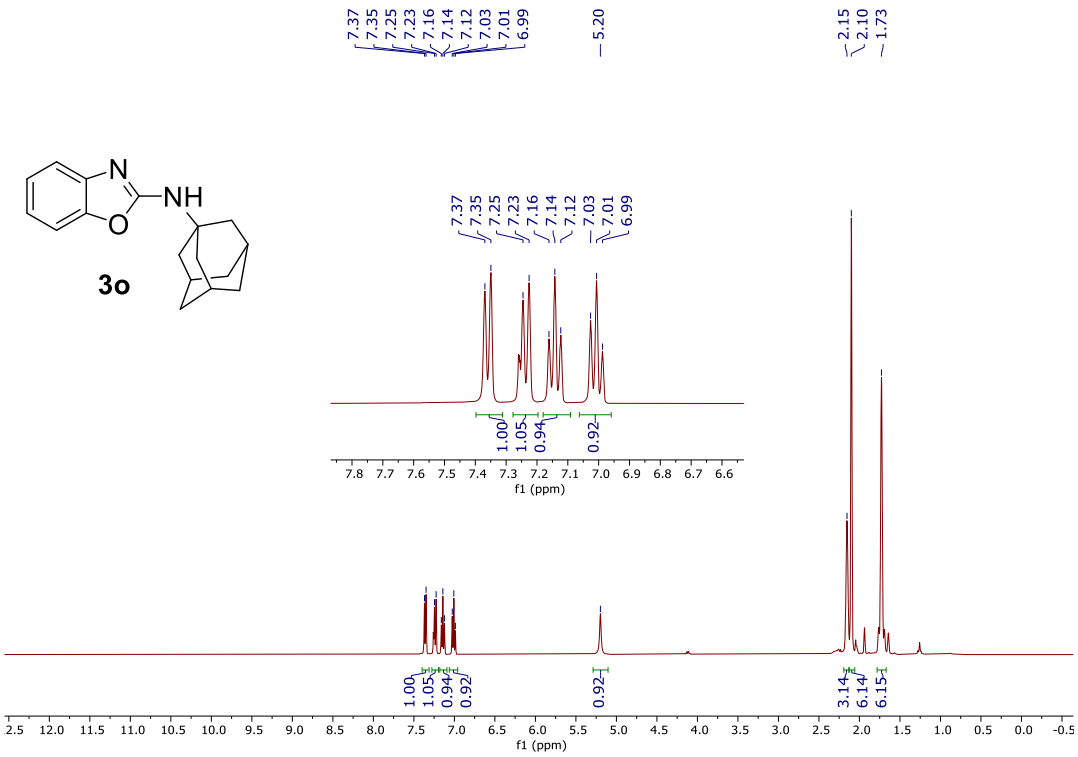

Figure A29. ^{1}H NMR spectrum of 2-(1-admantylamino)benzoxazole (3o) in $CDCl_3$ at 400 MHz.

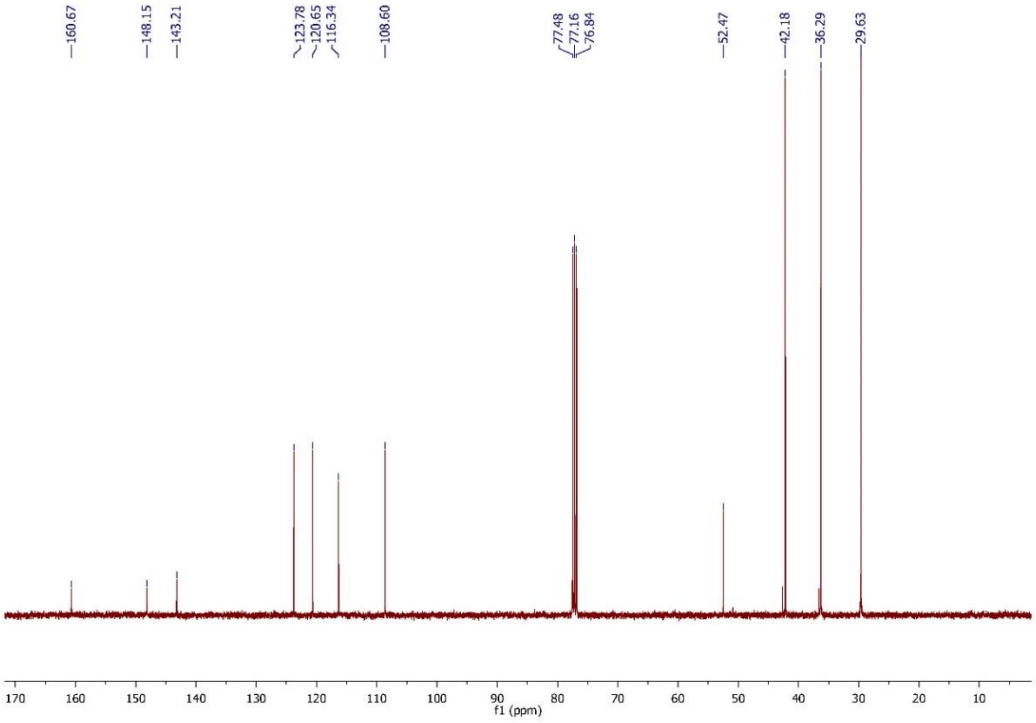

Figure A30. ^{13}C-NMR spectrum of 2-(1-admantylamino)benzoxazole (3o) in $CDCl_3$ at 100 MHz.

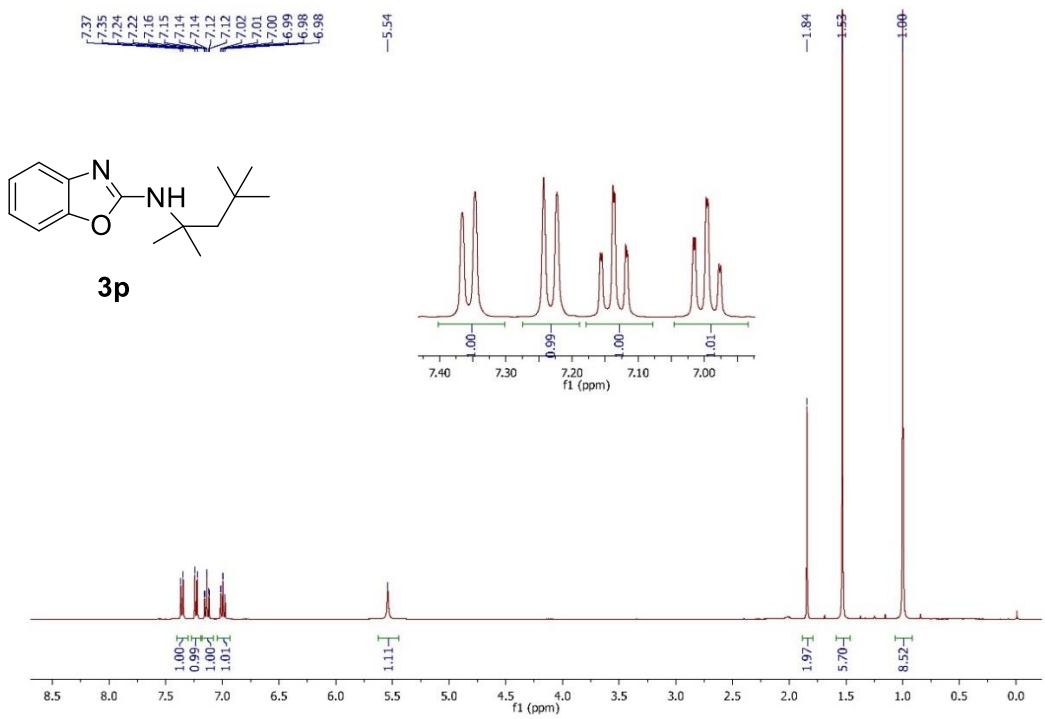

Figure A31. ^{1}H NMR spectrum of 2-(1,1,3,3-tetramethylbutylamino)benzoxazole (3p) in $CDCl_3$ at 400 MHz.

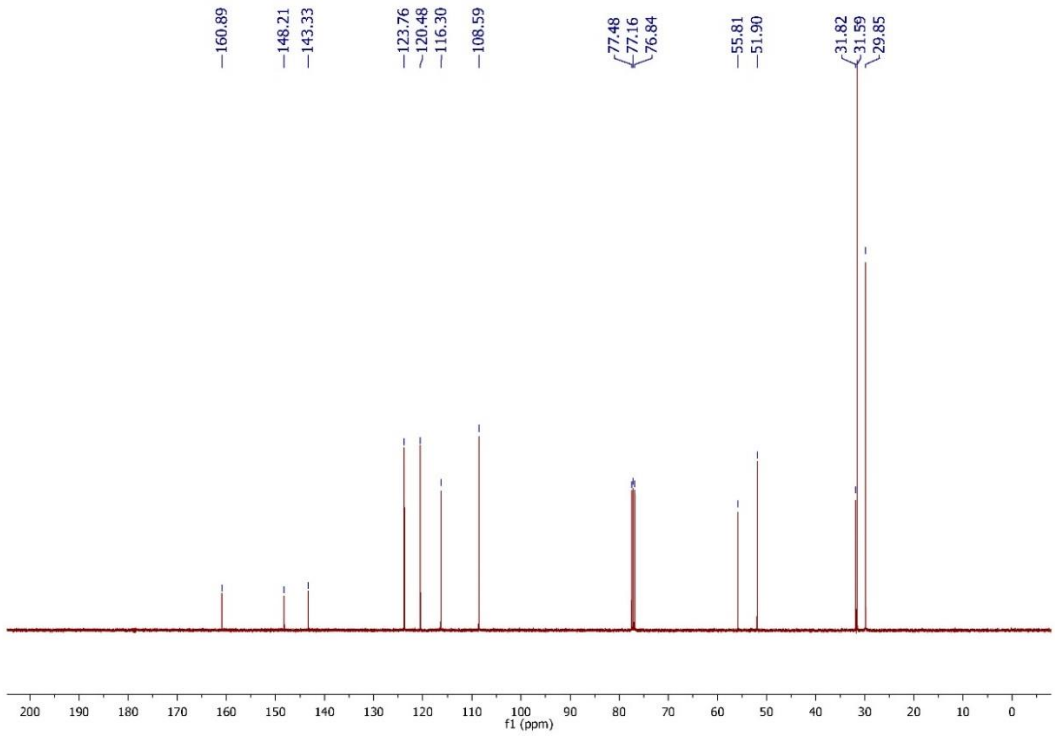

Figure A32. ^{13}C NMR spectrum of 2-(1,1,3,3-tetramethylbutylamino)benzoxazole (3p) in $CDCl_3$ at 100 MHz.

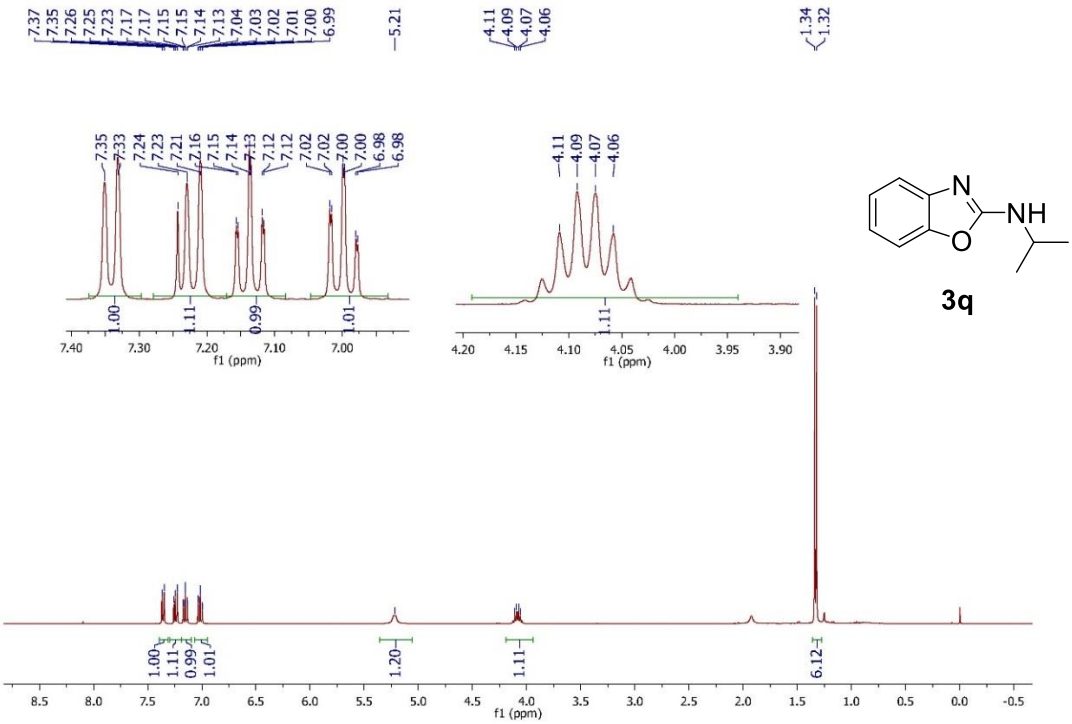

Figure A33. ^{1}H NMR spectrum of 2-(isopropylamino)benzoxazole (3q) in $CDCl_3$ at 400 MHz.

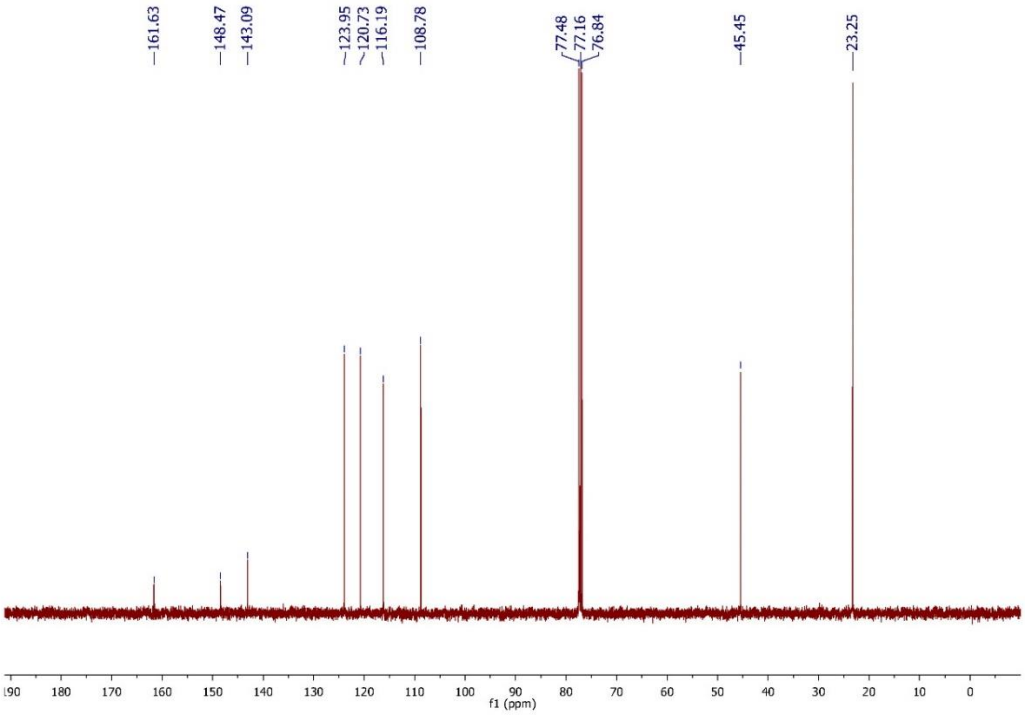

Figure A34. ^{13}C NMR spectrum of 2-(isopropylamino)benzoxazole (3q) in $CDCl_3$ at 100 MHz.

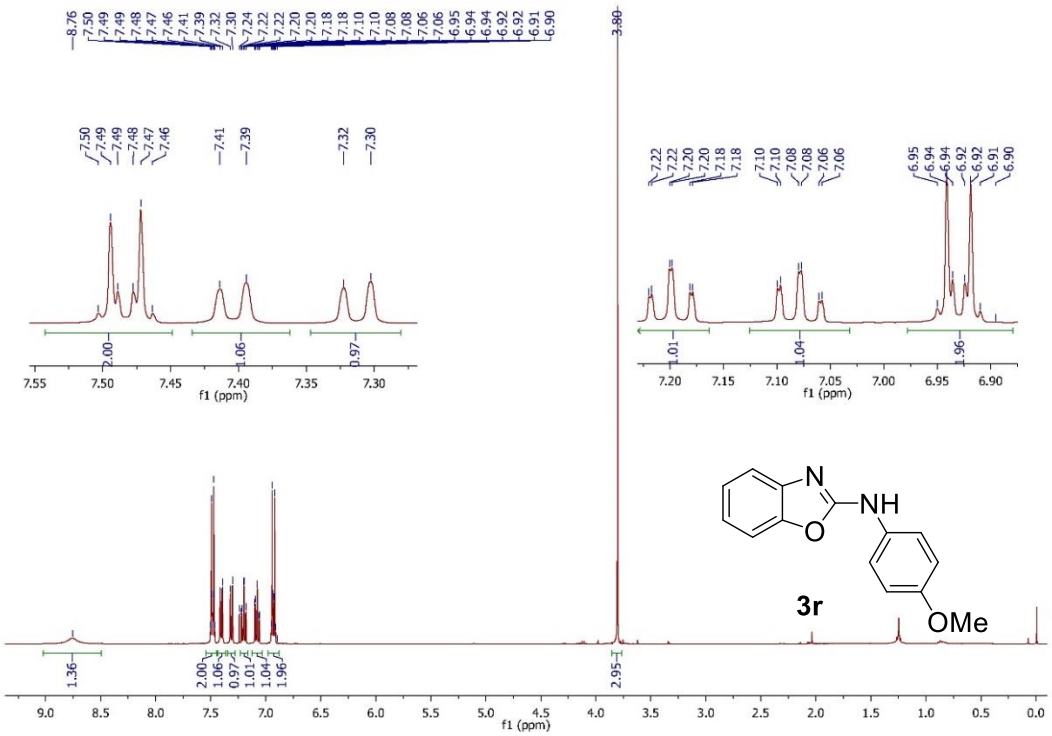

Figure A35. ^{1}H NMR spectrum of 2-(4-methoxyphenylamino)benzoxazole (3r) in $CDCl_3$ at 400 MHz.

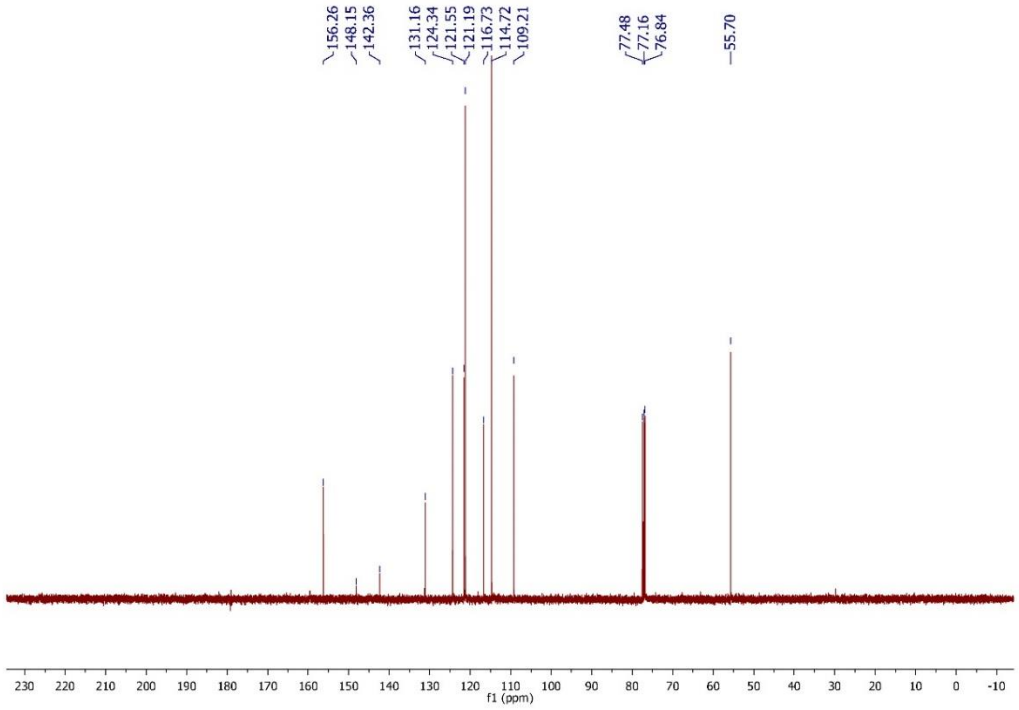

Figure A36. ^{13}C NMR spectrum of 2-(4-methoxyphenylamino)benzoxazole (3r) in $CDCl_3$ at 100 MHz.

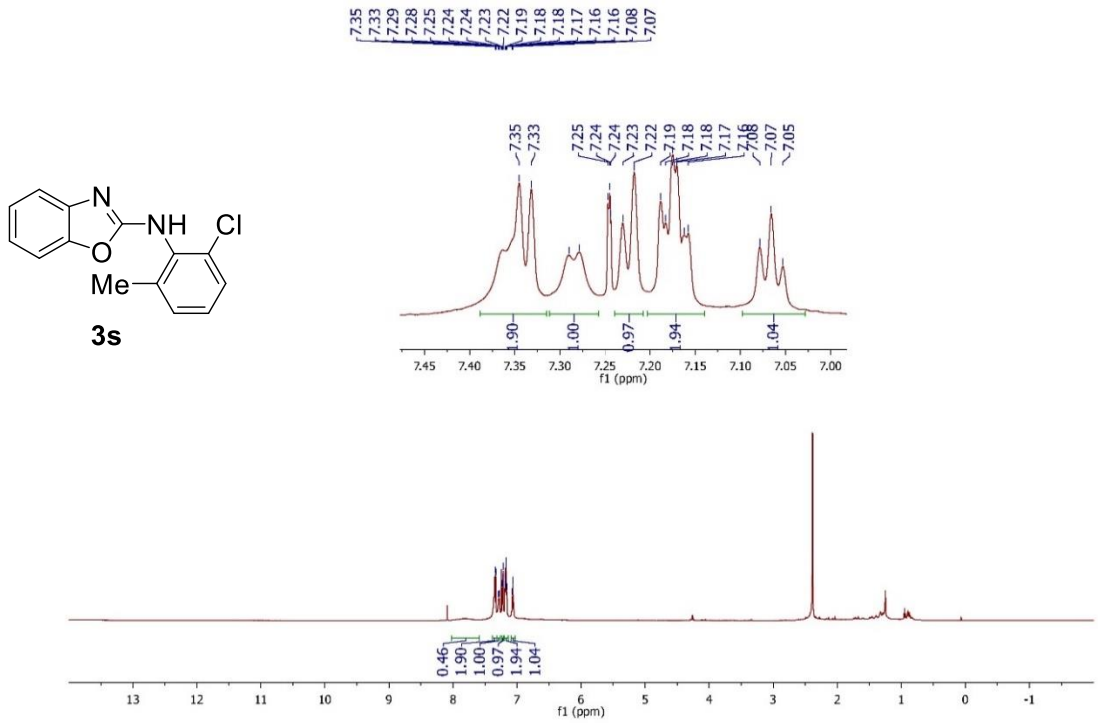

Figure A37. ^{1}H NMR spectrum of 2-(6-chloro-2-methylphenylamino)benzoxazole (3s) in $CDCl_3$ at 400 MHz.

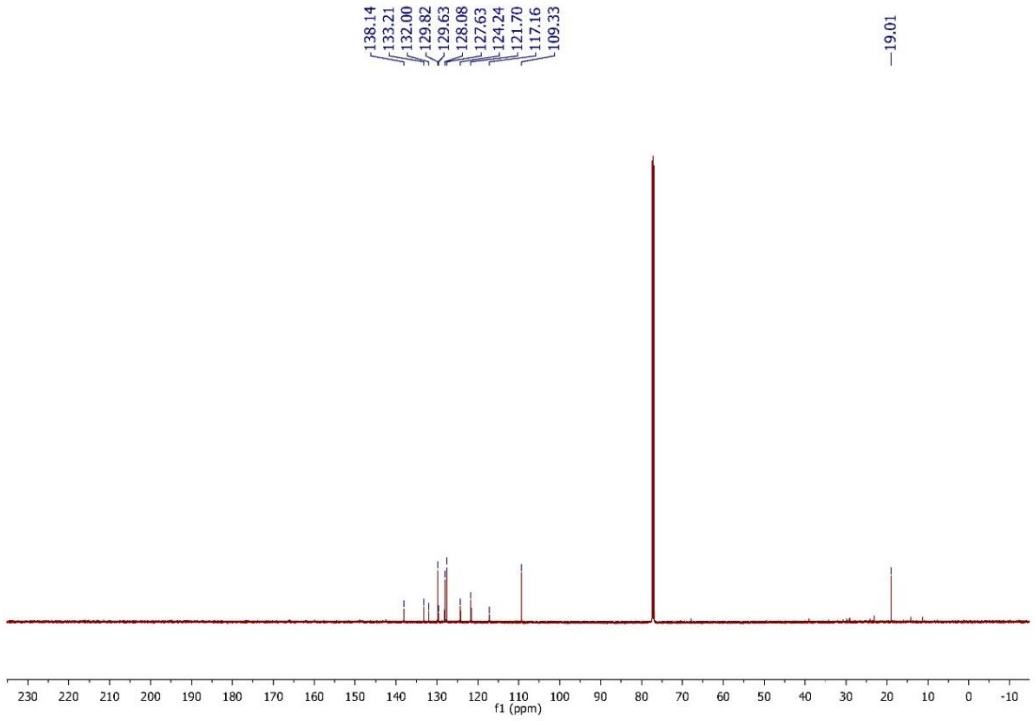

Figure A38. ^{13}C NMR spectrum of 2-(6-chloro-2-methylphenylamino)benzoxazole (3s) in $CDCl_3$ at 100 MHz.

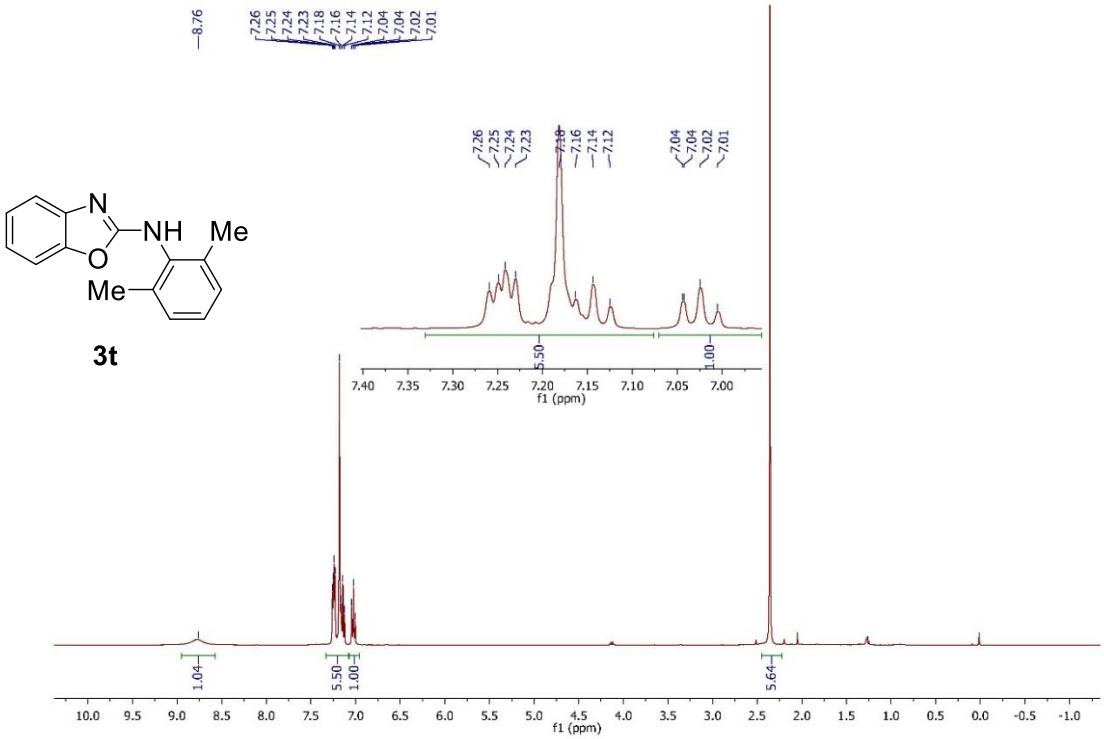

Figure A39. ^{1}H NMR spectrum of 2-(2,6-dimethylphenylamino)benzoxazole (3t) in $CDCl_3$ at 400 MHz.

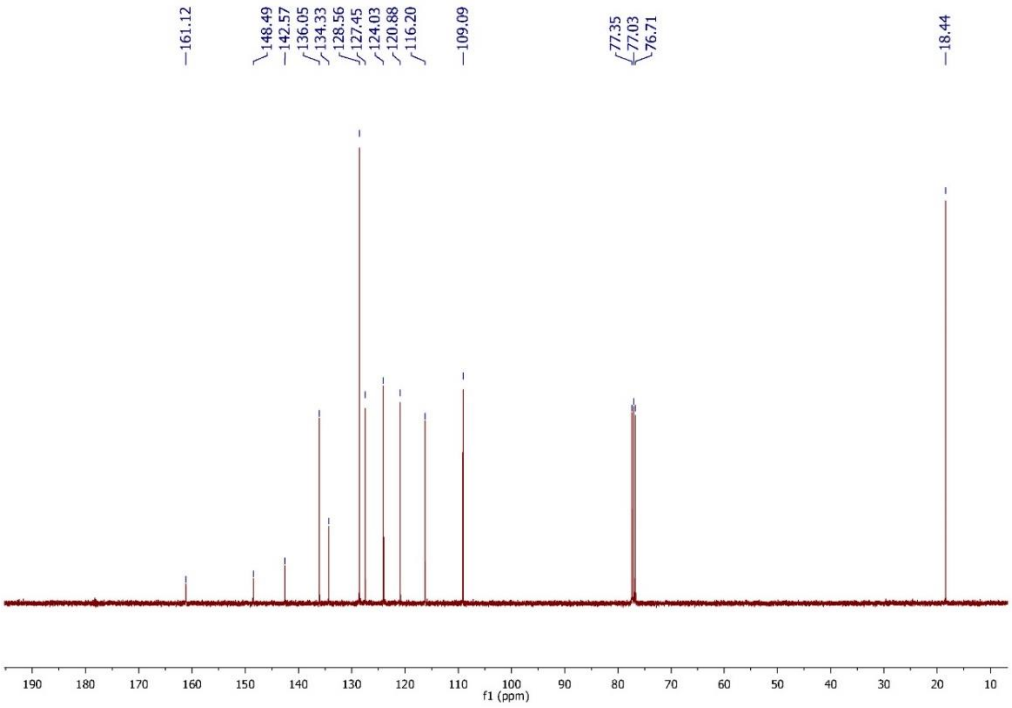

Figure A40. ^{13}C NMR spectrum of 2-(2,6-dimethylphenylamino)benzoxazole (3t) in $CDCl_3$ at 100 MHz.

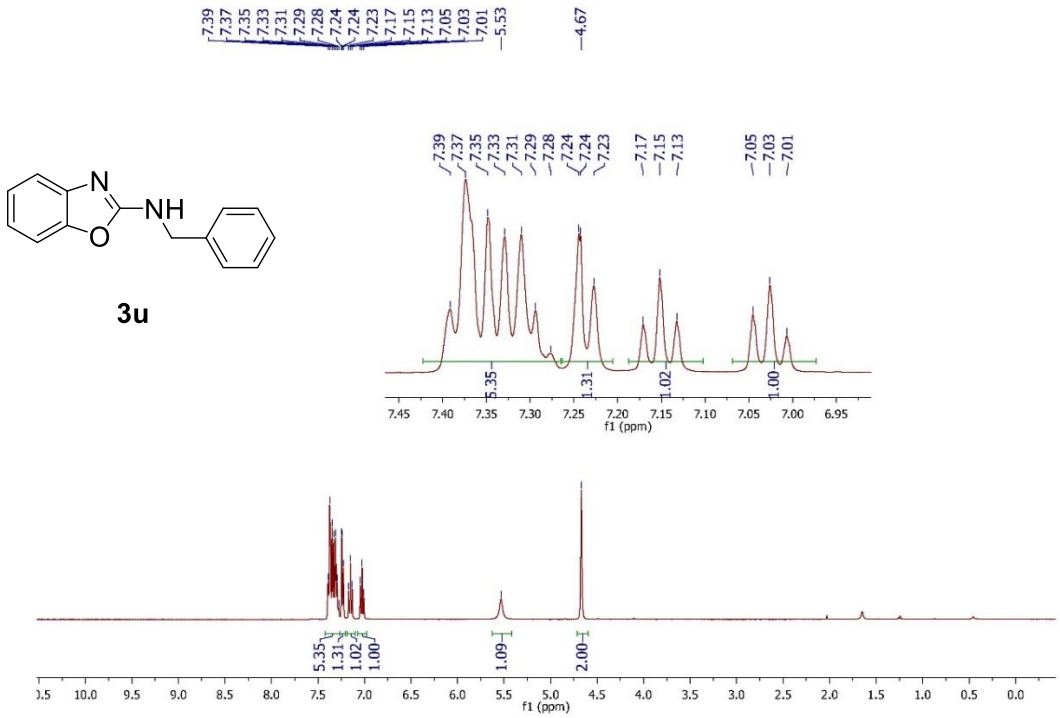

Figure A41. ^{1}H NMR spectrum of *N*-(phenylmethyl)-2-benzoxazolamine (3u) in $CDCl_3$ at 400 MHz.

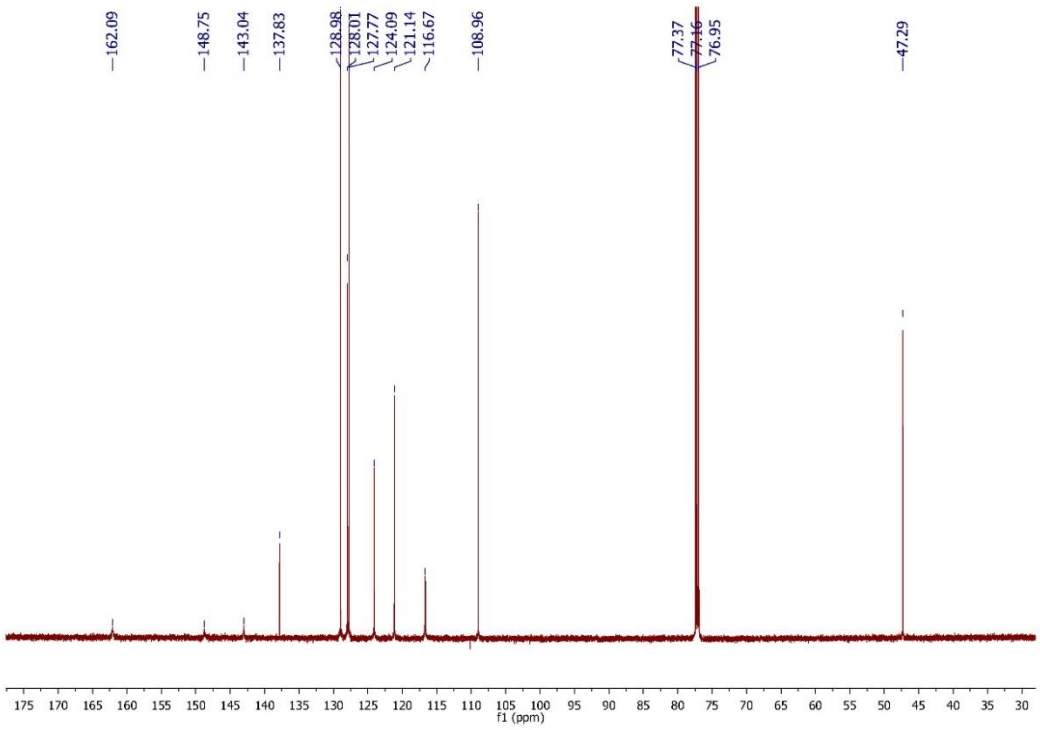

Figure A42. ^{13}C NMR spectrum of *N*-(phenylmethyl)-2-benzoxazolamine (3u) in $CDCl_3$ at 100 MHz.

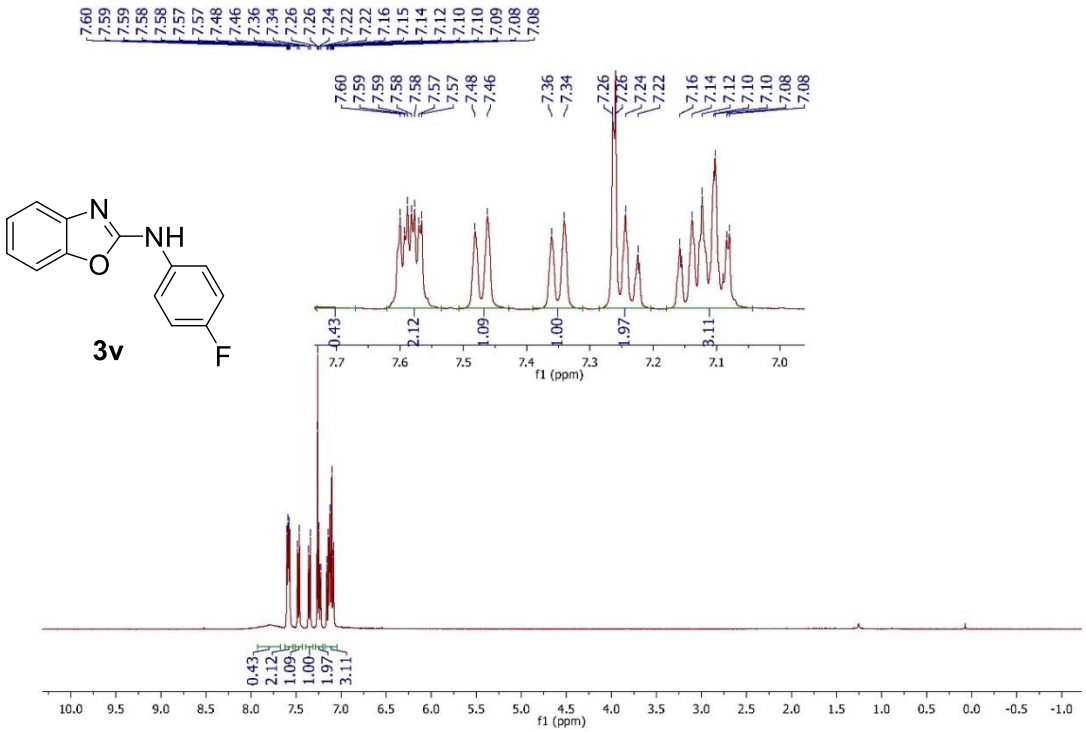

Figure A43. ^{1}H NMR spectrum of 2-(4-fluorophenylamino)benzoxazole (3v) in $CDCl_3$ at 400 MHz.

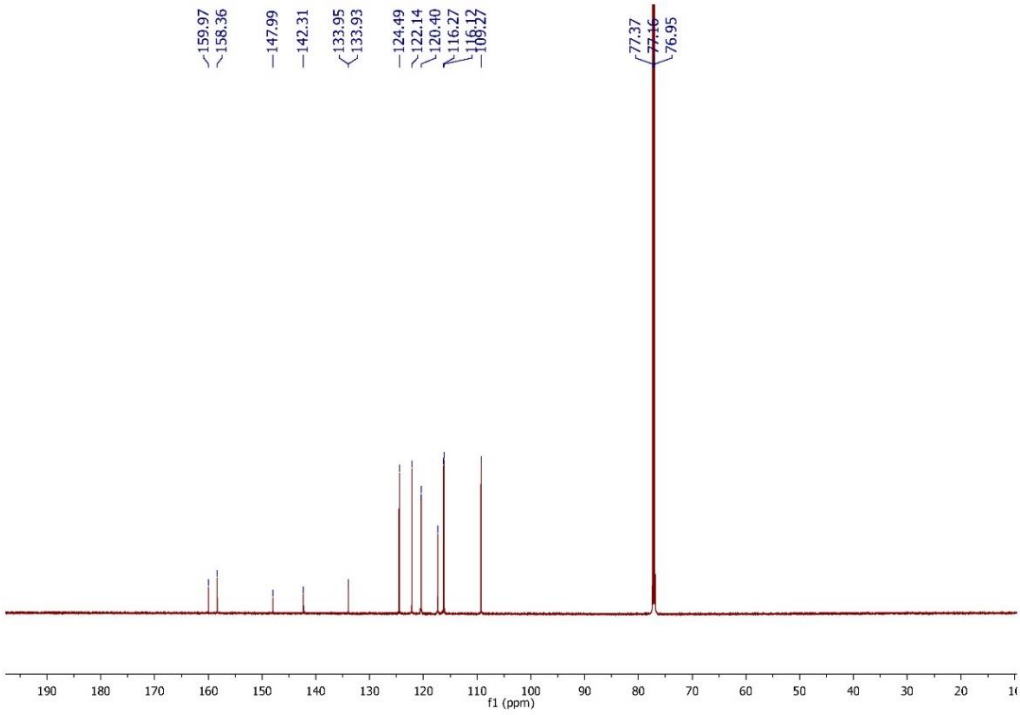

Figure A44. ^{13}C NMR spectrum of 2-(4-fluorophenylamino)benzoxazole (3v) in $CDCl_3$ at 100 MHz.

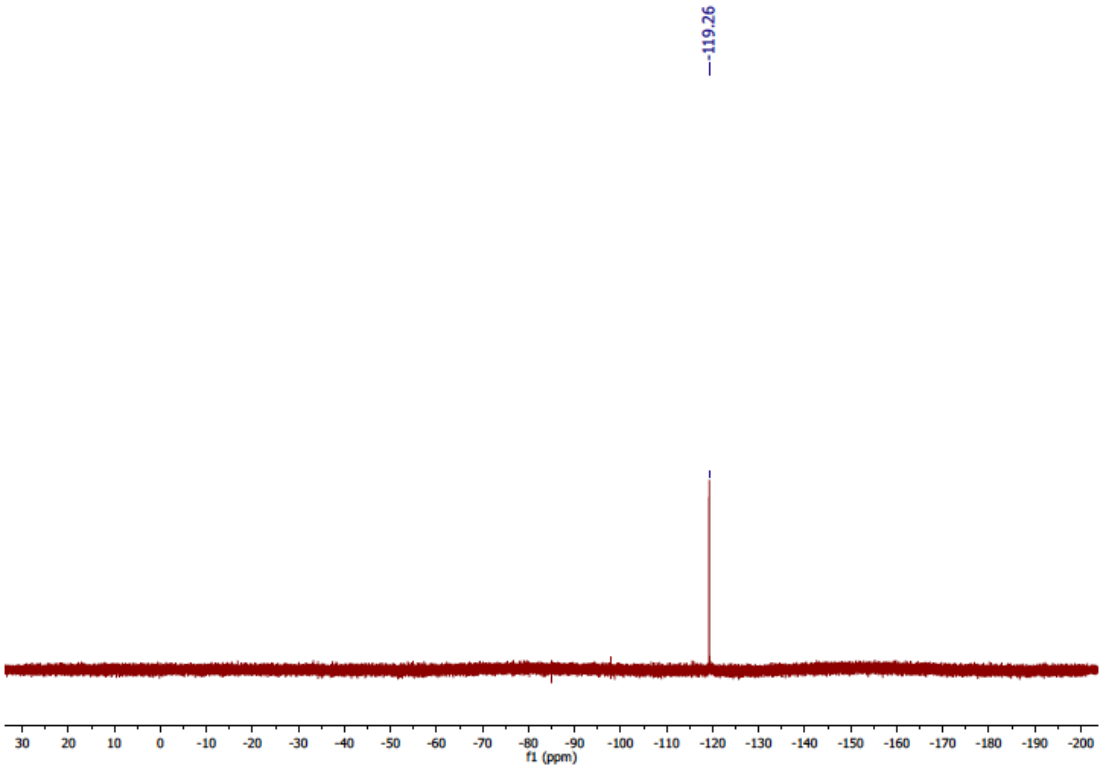

Figure A45. ^{19}F NMR spectrum of 2-(4-fluorophenylamino)benzoxazole (3v) in $CDCl_3$ at 376 MHz.

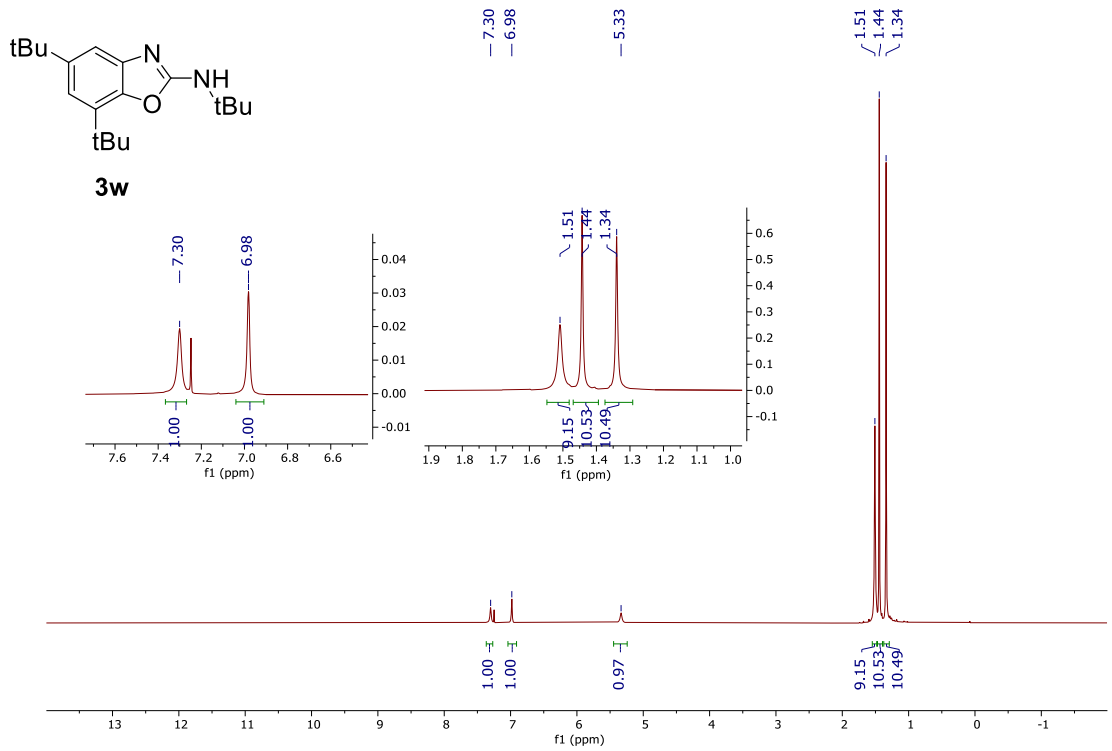

Figure A46. ^{1}H NMR spectrum of 5,7-di-tertbutyl -2-(tert-butylamino)benzoxazole (3w) in $CDCl_3$ at 400 MHz.

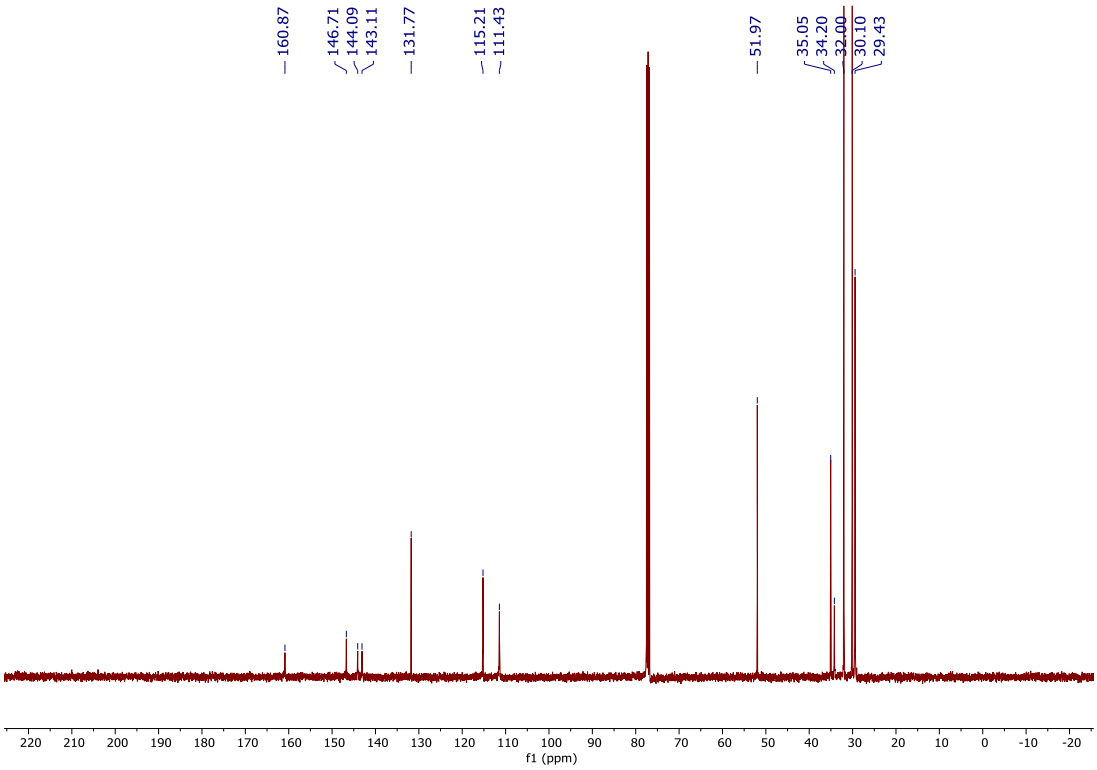

Figure A47. ^{13}C NMR spectrum of 5,7-di-tertbutyl -2-(tert-butylamino)benzoxazole (3w) in $CDCl_3$ at 400 MHz.

^{1}H and ^{13}C NMR Spectra of 2-Aminobenzimidazoles

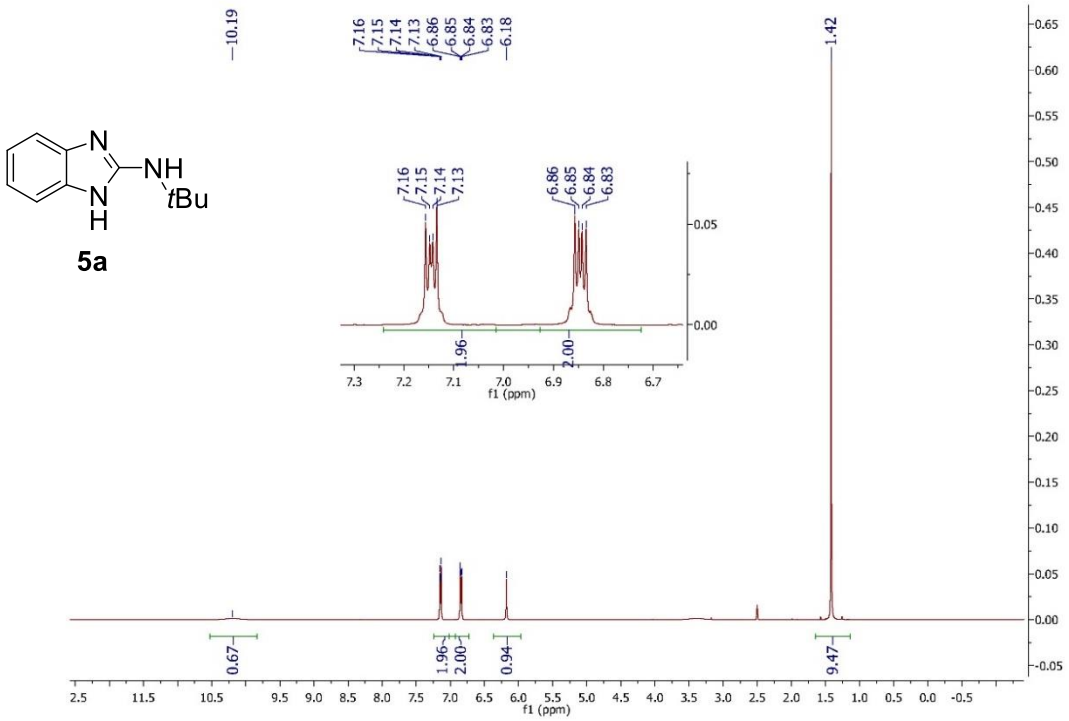

Figure A48. ^{1}H NMR spectrum of 2-(*tert*-butylamino)benzimidazole (5a) in DMSO-*d*6 at 400 MHz.

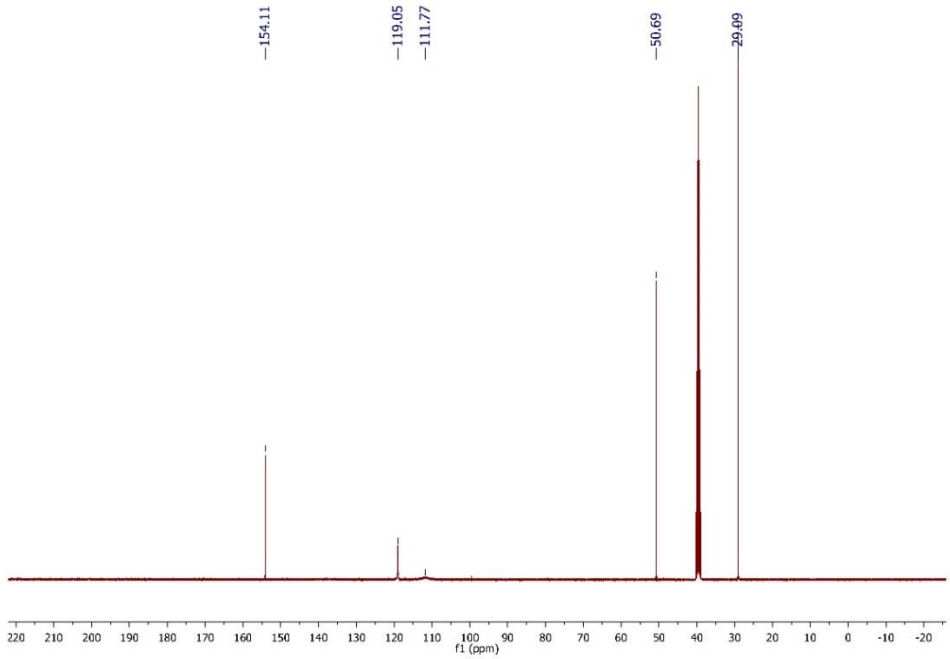

Figure A49. ^{13}C NMR spectrum of 2-(*tert*-butylamino)benzimidazole (5a) in DMSO-*d*6 at 100 MHz.

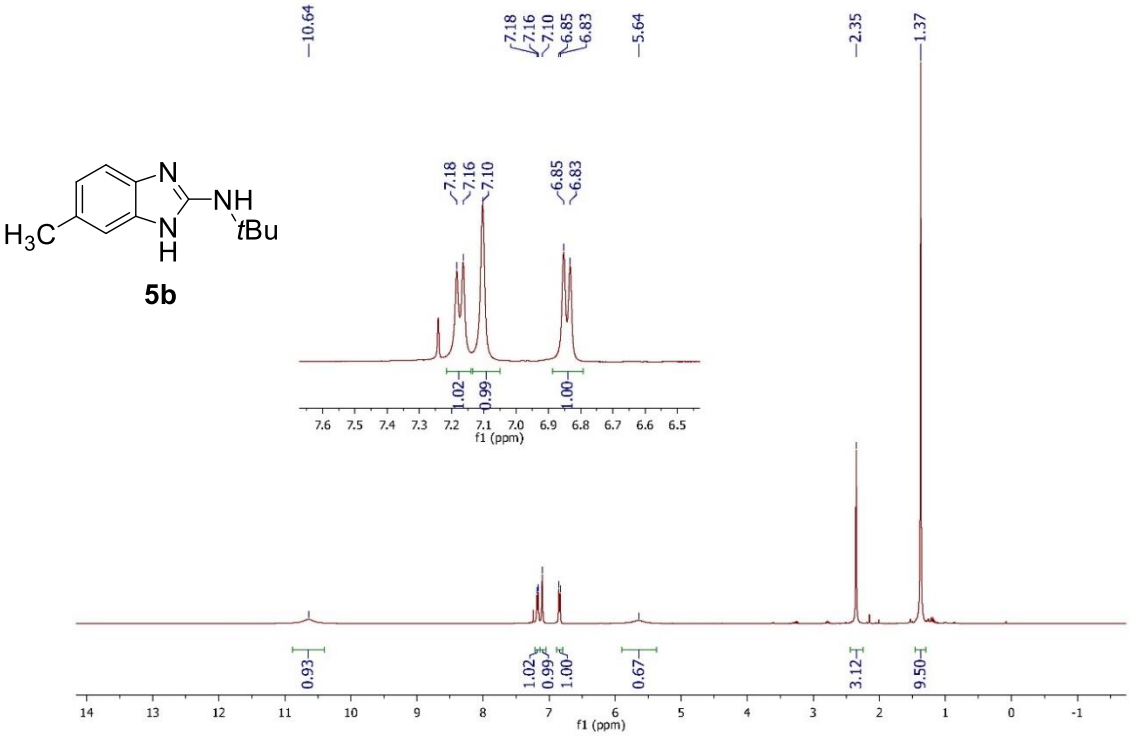

Figure A50. ^{1}H NMR spectrum of 2-(*tert*-butylamino)-5-methylbenzimidazole (5b) in $CDCl_3$ at 400 MHz.

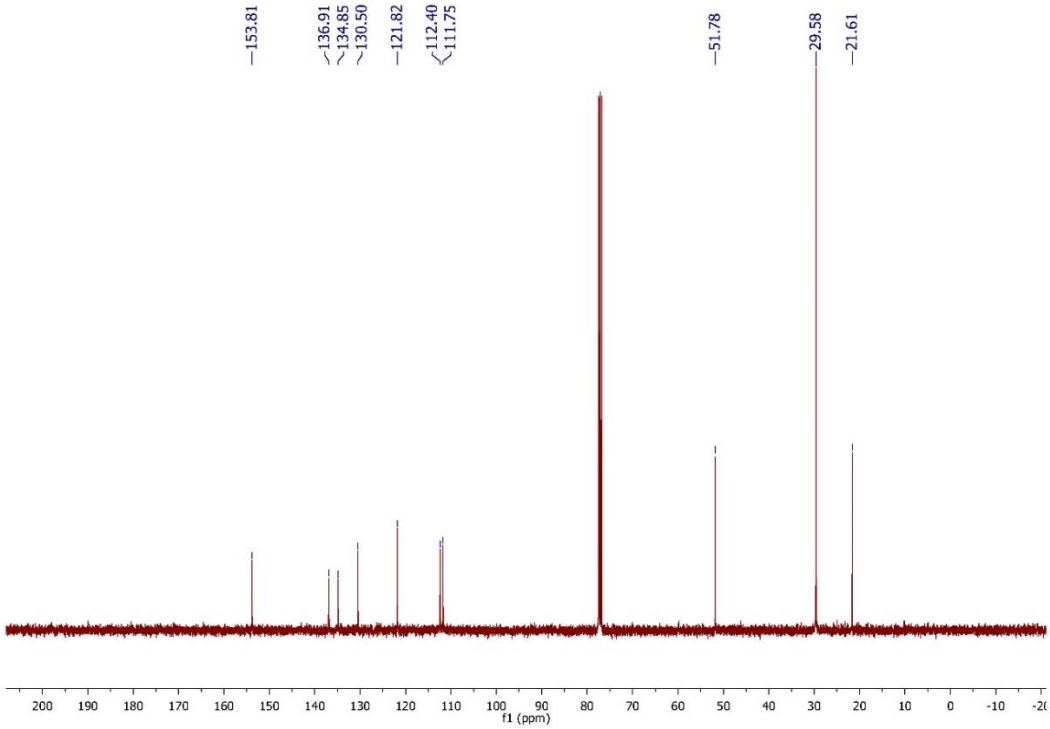

Figure A51. ^{13}C NMR spectrum of 2-(*tert*-butylamino) benzimidazole (5b) in $CDCl_3$ at 100 MHz.

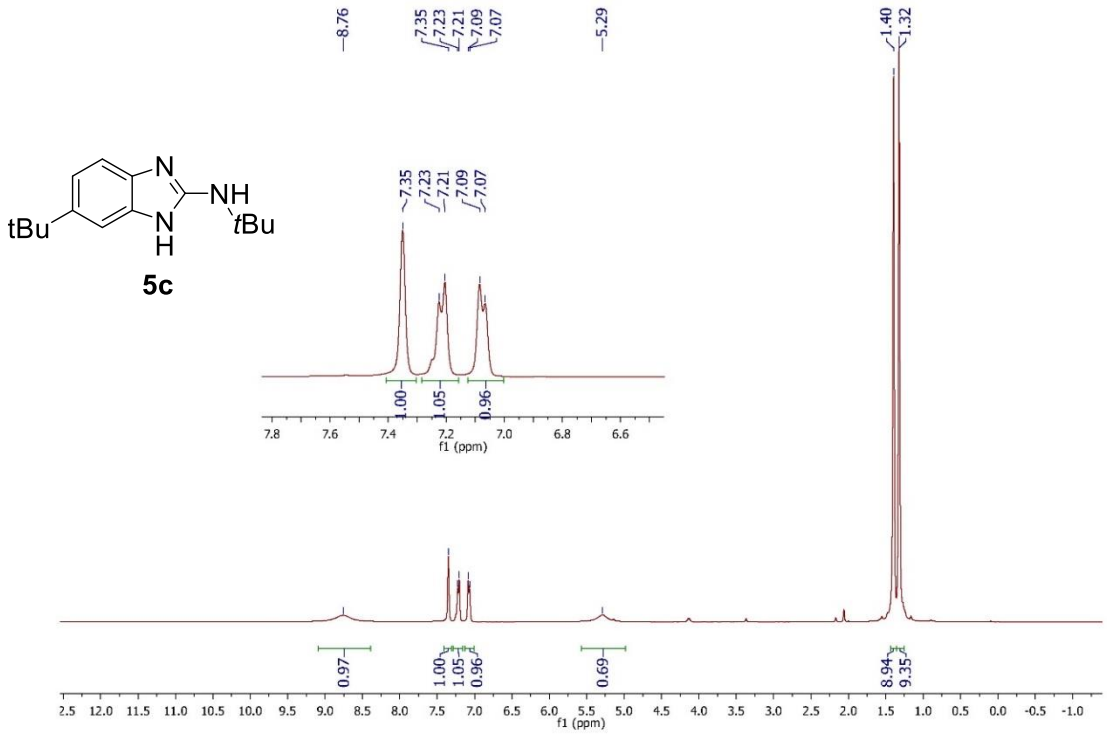

Figure A52. ^{1}H NMR spectrum of 2-(*tert*-butylamino)-5-*tert*-butylbenzimidazole (5c) in $CDCl_3$ at 400 MHz.

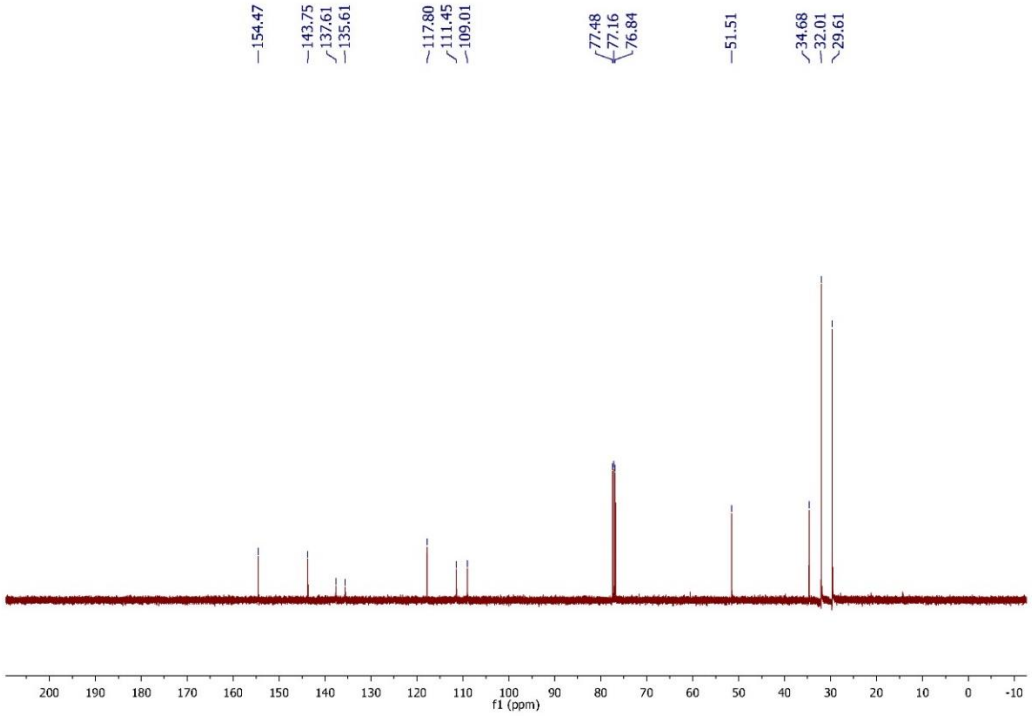

Figure A53. ^{13}C NMR spectrum of 2-(*tert*-butylamino)-5-*tert*-butylbenzimidazole (5c) in $CDCl_3$ at 100 MHz.

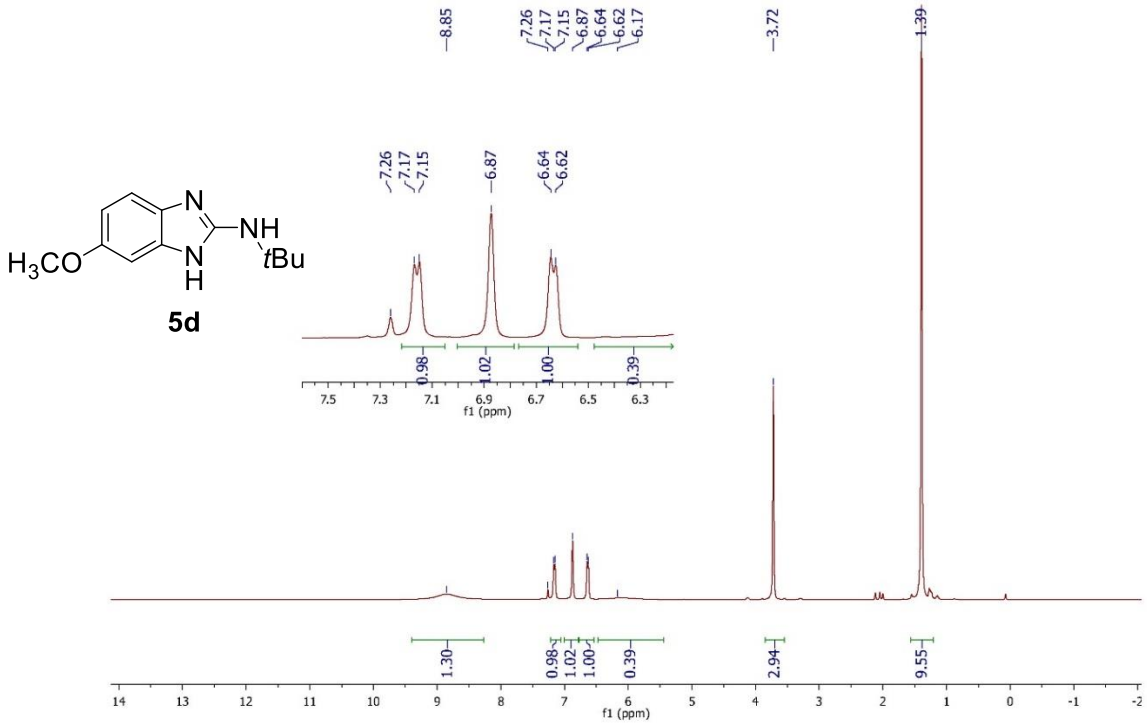

Figure A54. ^{1}H NMR spectrum of 2-(*tert*-butylamino)-5-methoxybutylbenzimidazole (5d) in CDCl3 at 400 MHz.

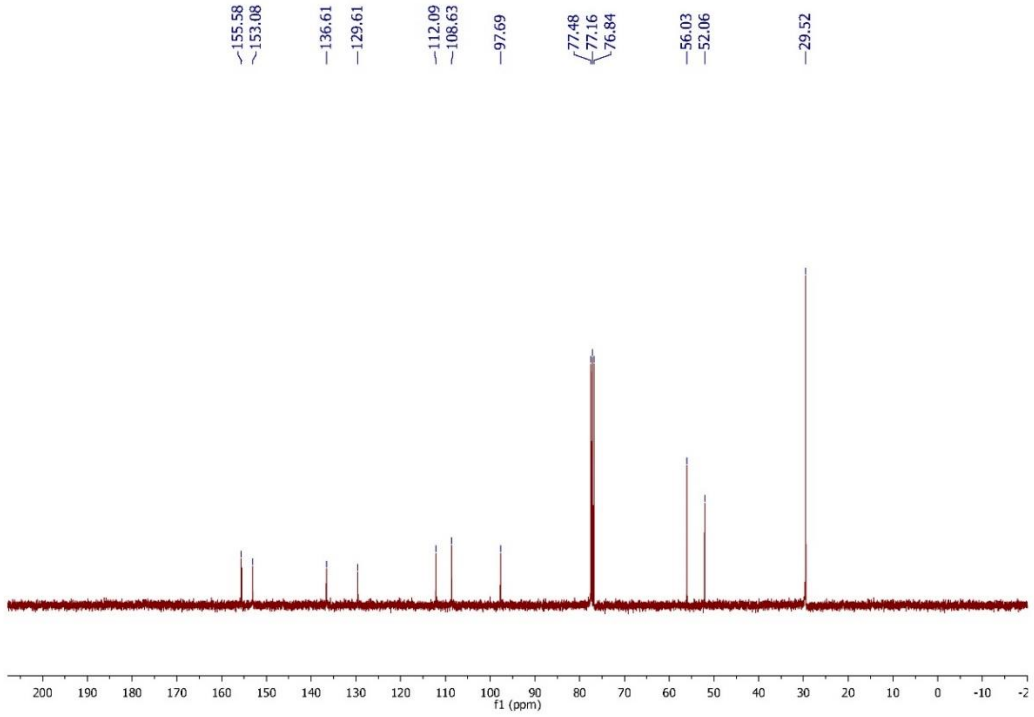

Figure A55. ^{13}C NMR spectrum of 2-(*tert*-butylamino)-5-methoxybenzimidazole (5d) in CDCl3 at 100 MHz.

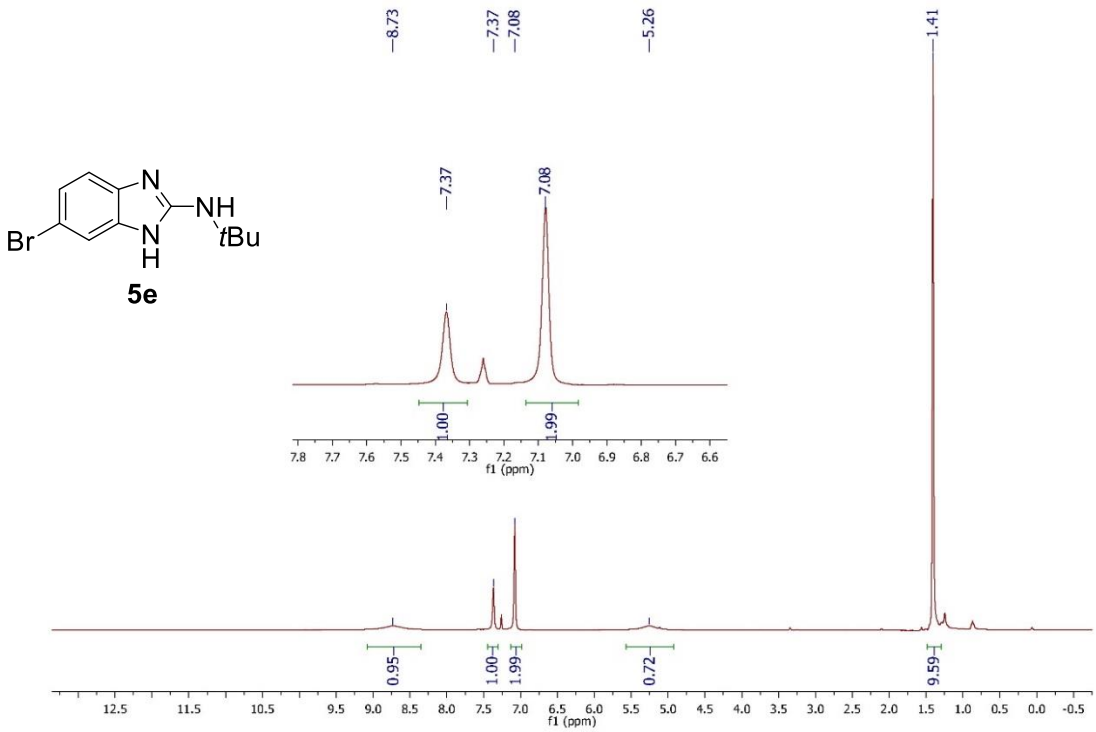

Figure A56. ^{1}H NMR spectrum of 2-(*tert*-butylamino)-5-bromobenzimidazole (5e) in CDCl3 at 400 MHz.

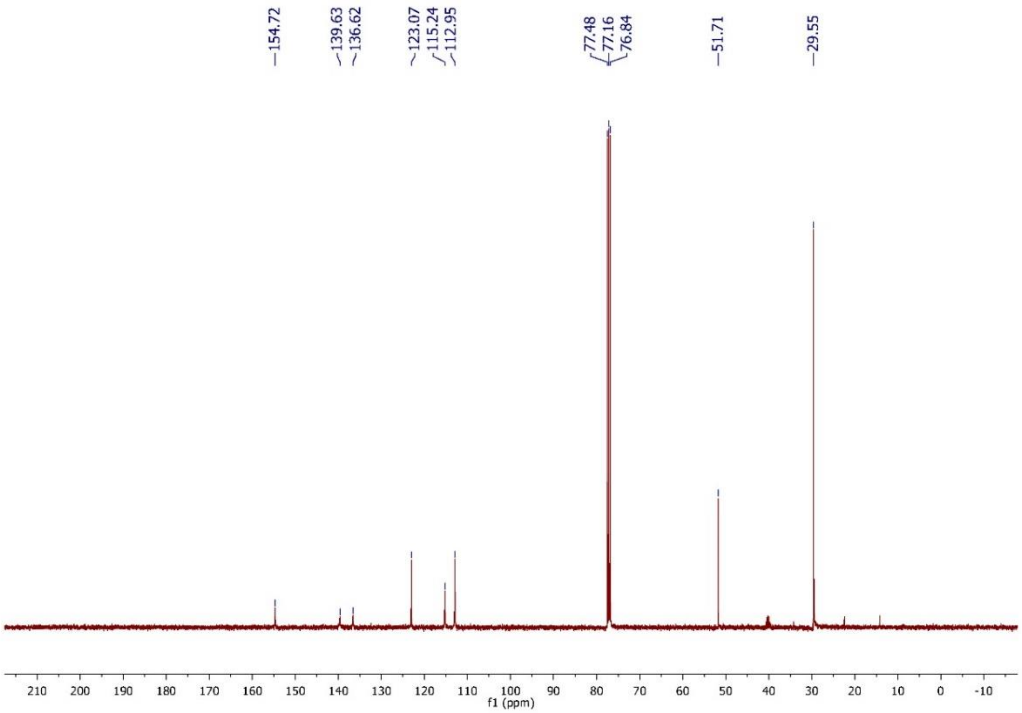

Figure A57. ^{13}C NMR spectrum of 2-(*tert*-butylamino)-5-bromobenzimidazole (5e) in CDCl3 at 100 MHz.

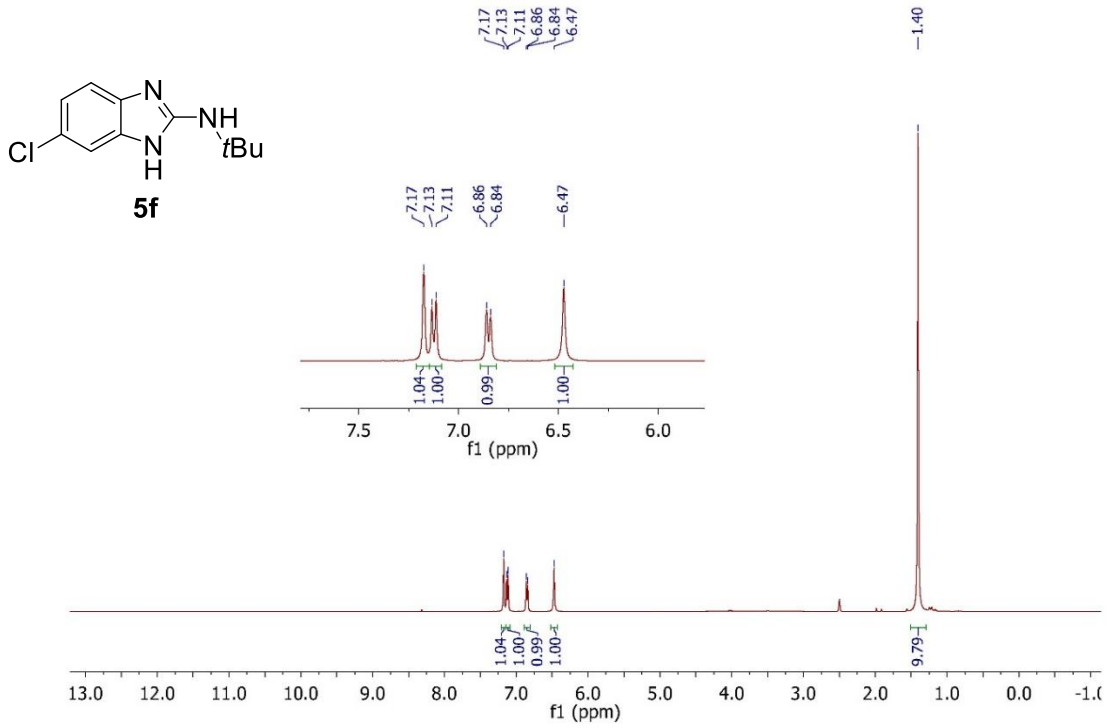

Figure A58. ^{1}H NMR spectrum of 2-(*tert*-butylamino)-5-chlorobenzimidazole (5f) in DMSO-d_6 at 400 MHz.

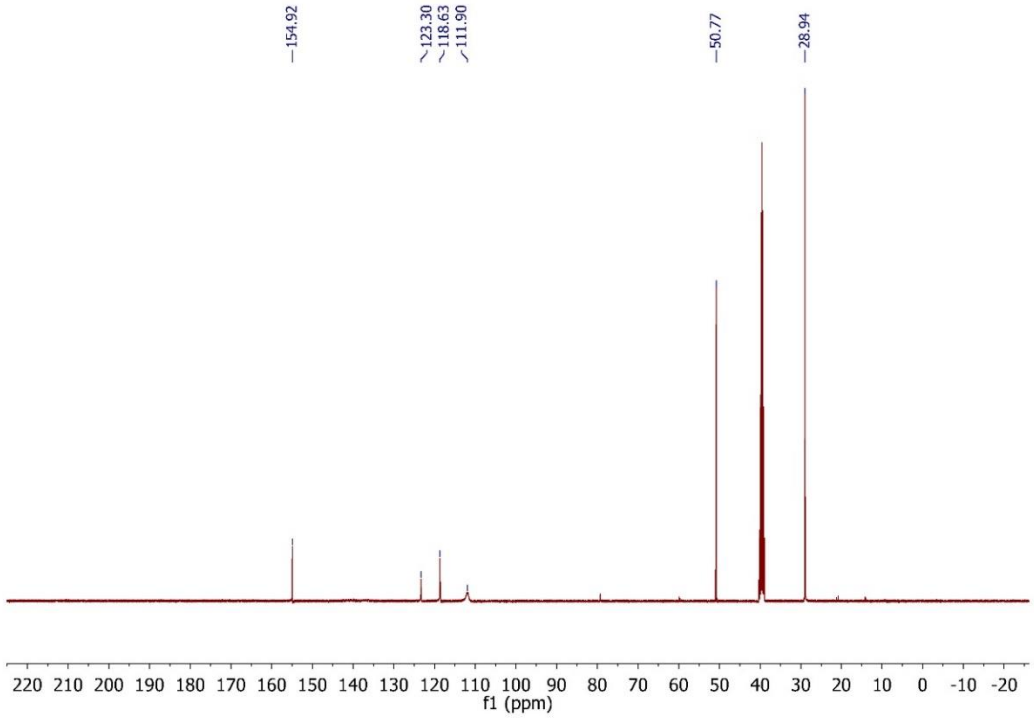

Figure A59. ^{13}C NMR spectrum of 2-(*tert*-butylamino)-5-chlorobenzimidazole (5f) in DMSO-d_6 at 100 MHz.

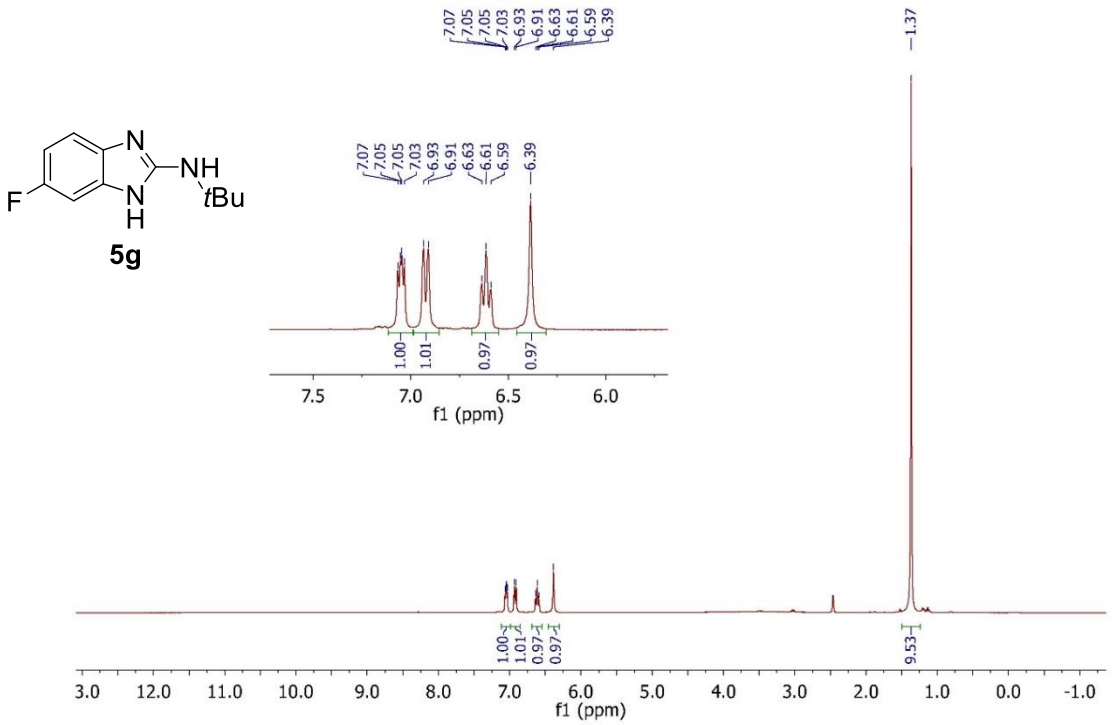

Figure A60. ^{1}H NMR spectrum of 2-(*tert*-butylamino)-5-fluorobenzimidazole (5g) in DMSO-d_6 at 400 MHz.

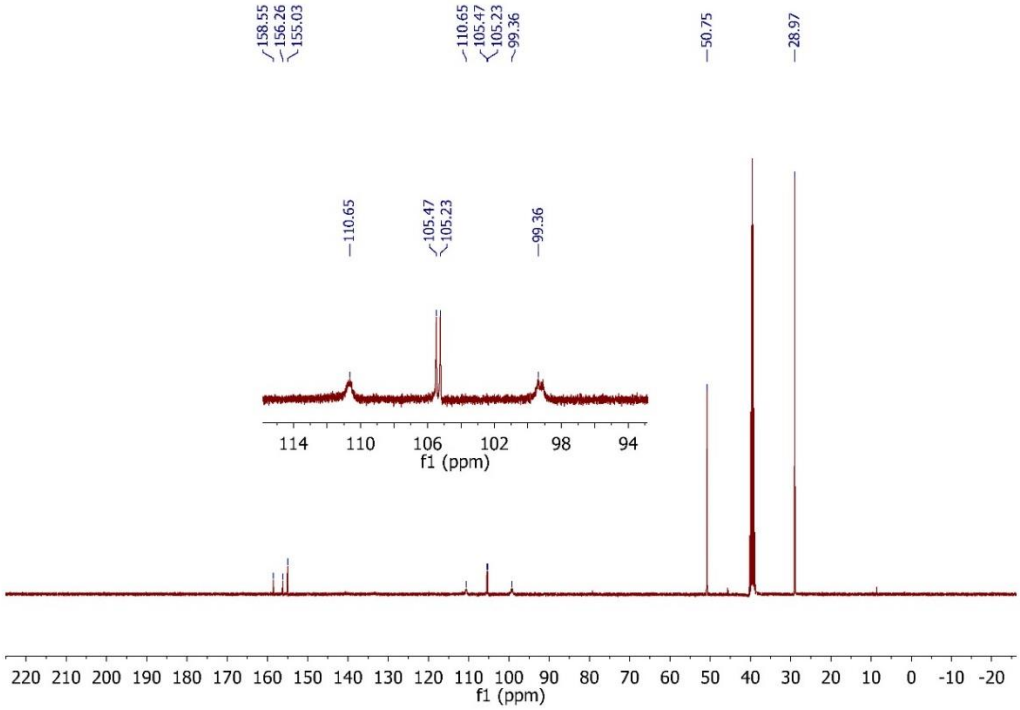

Figure A61. ^{13}C NMR spectrum of 2-(*tert*-butylamino)-5-fluorobenzimidazole (5g) in DMSO-d_6 at 100 MHz.

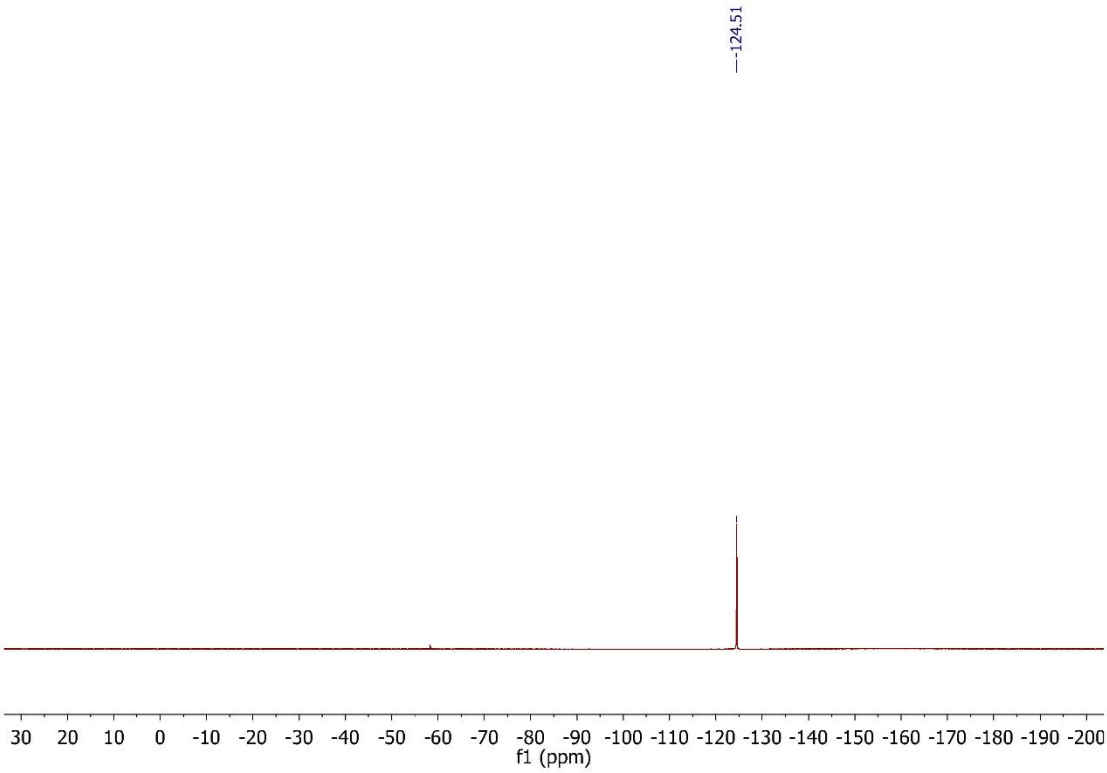

Figure A62. ^{19}F NMR spectrum of 2-(*tert*-butylamino)-5-fluorobenzimidazole (5g) in DMSO-d_6 at 376 MHz.

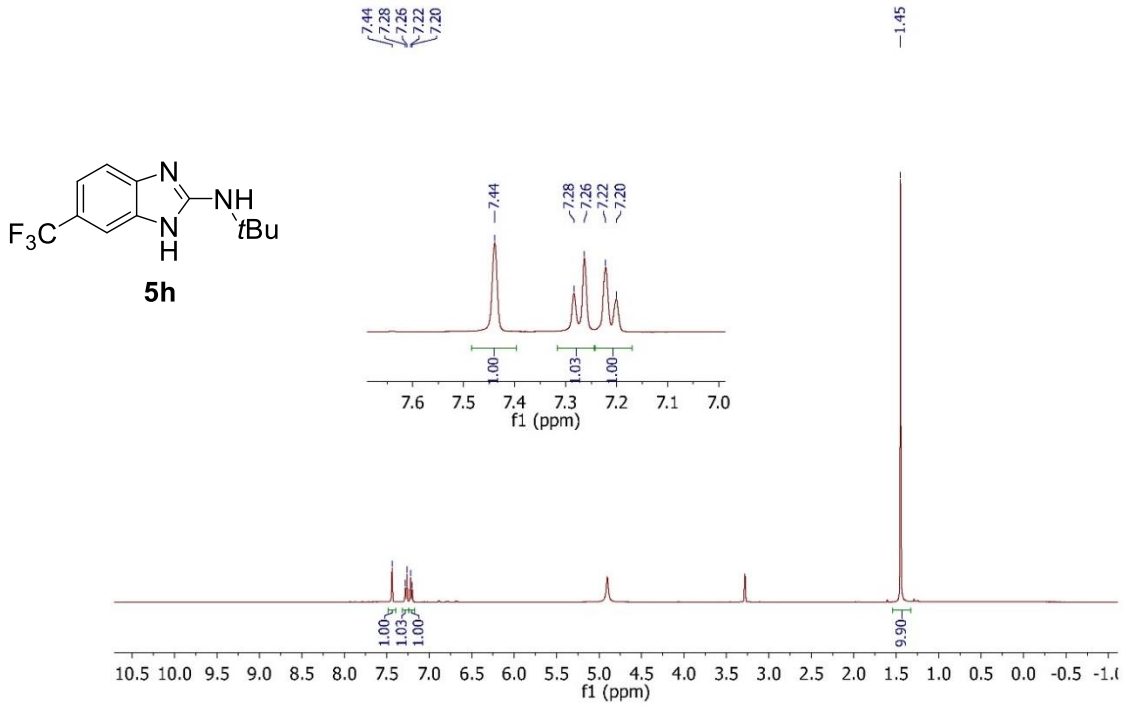

Figure A63. ^{1}H NMR spectrum of 2-(*tert*-butylamino)-5-trifluoromethylbenzimidazole (5h) in CD_3OD at 400 MHz.

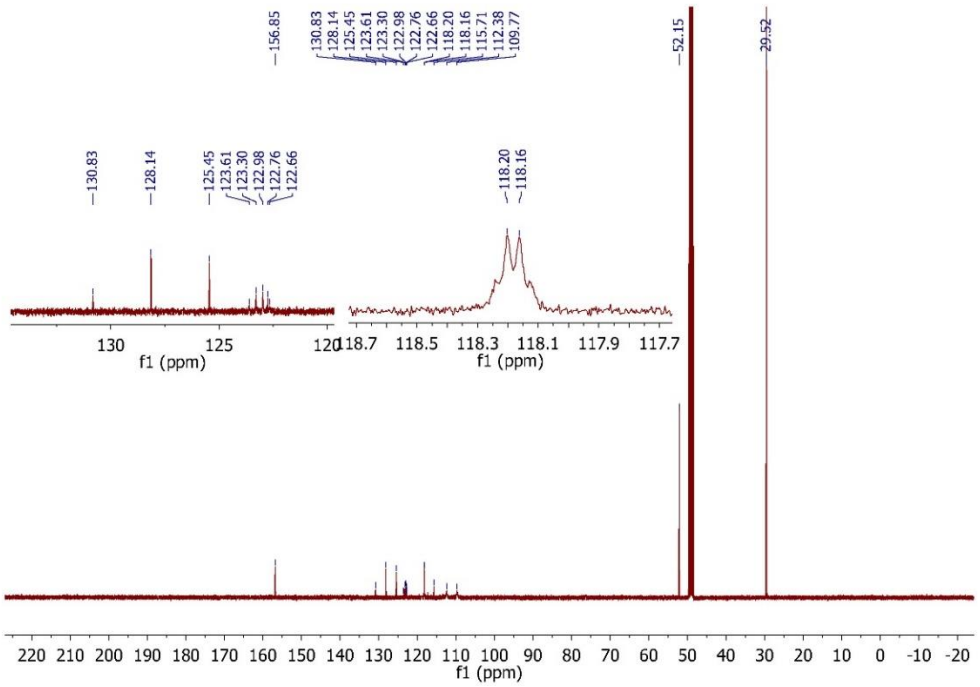

Figure A64. ^{13}H NMR spectrum of 2-(*tert*-butylamino)-5-trifluoromethylbenzimidazole (5h) in CD_3OD at 100 MHz.

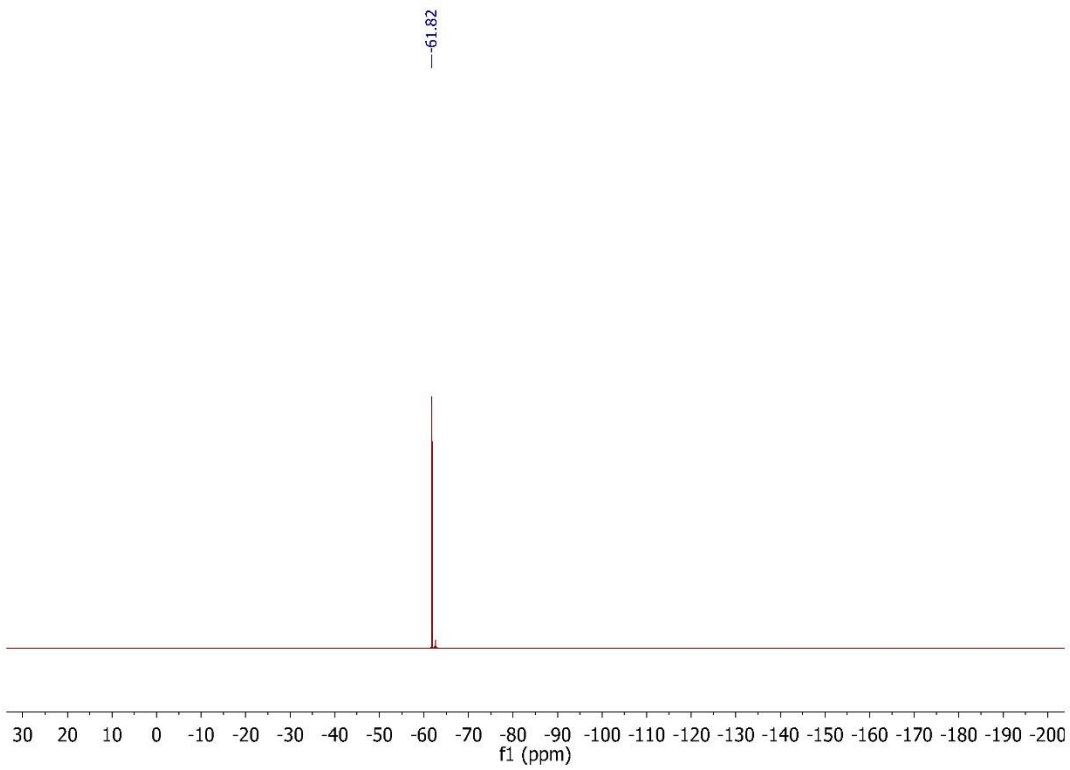

Figure A65. ^{19}F NMR spectrum of 2-(*tert*-butylamino)-5-trifluoromethylbenzimidazole (5h) in CD_3OD at 376 MHz.

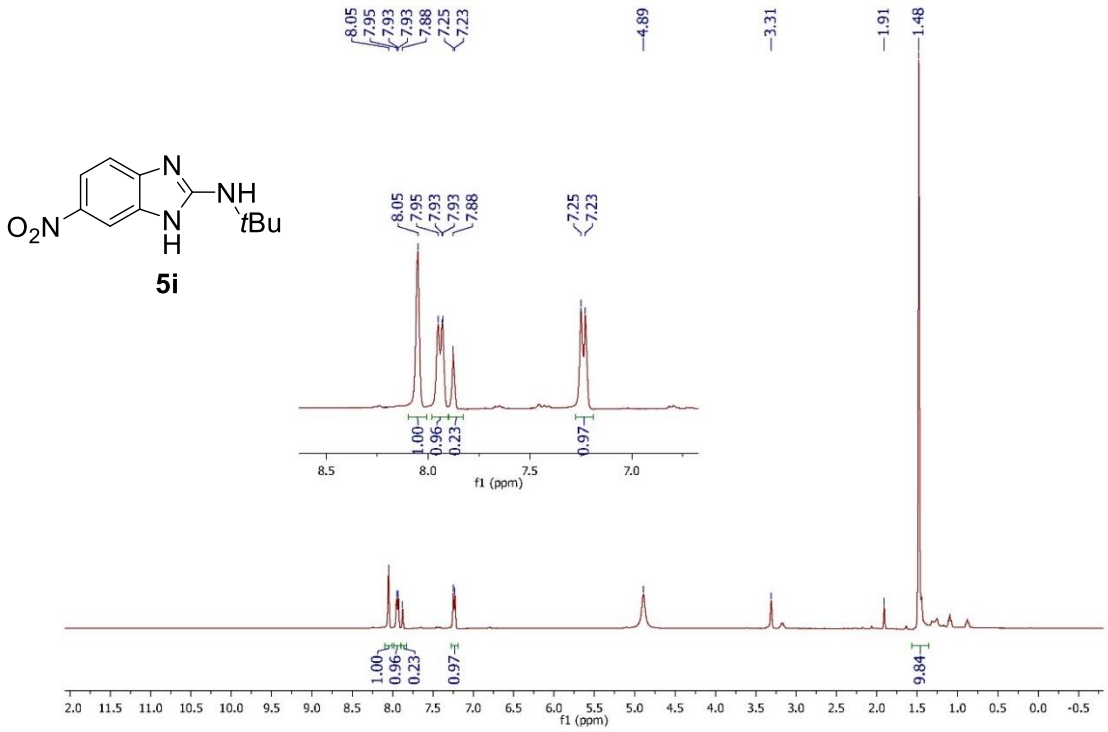

Figure A66. ^{1}H NMR spectrum of 2-(*tert*-butylamino)-5-nitrobenzimidazole (5i) in CD_3OD at 400 MHz.

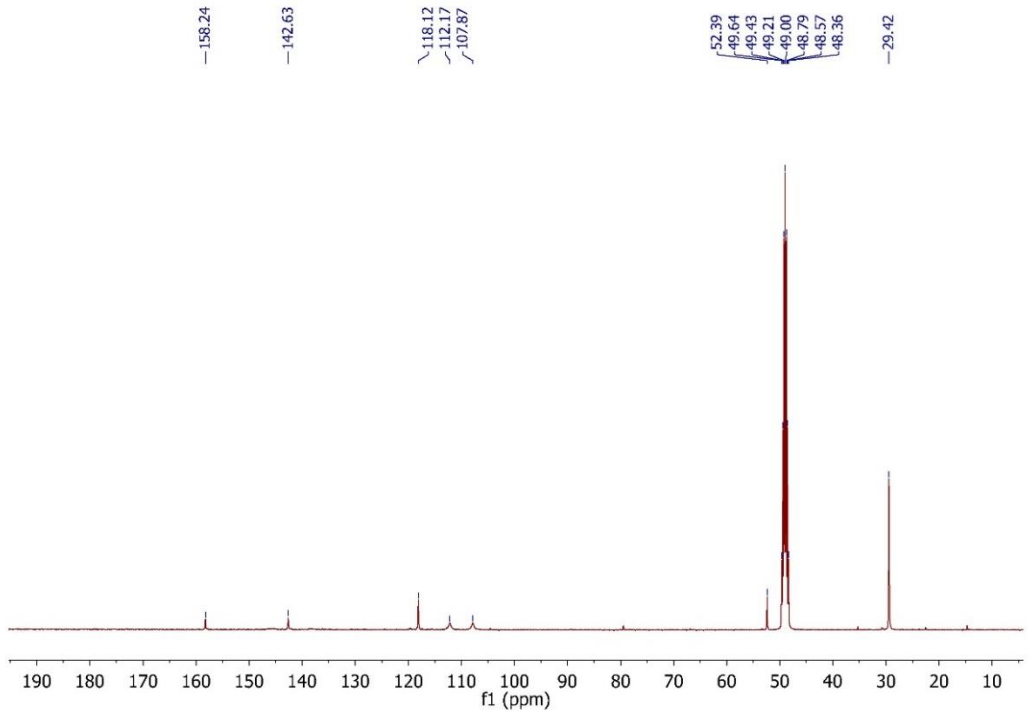

Figure A67. ^{13}C NMR spectrum of 2-(*tert*-butylamino)-5-nitrobenzimidazole (5i) in CD_3OD at 100 MHz.

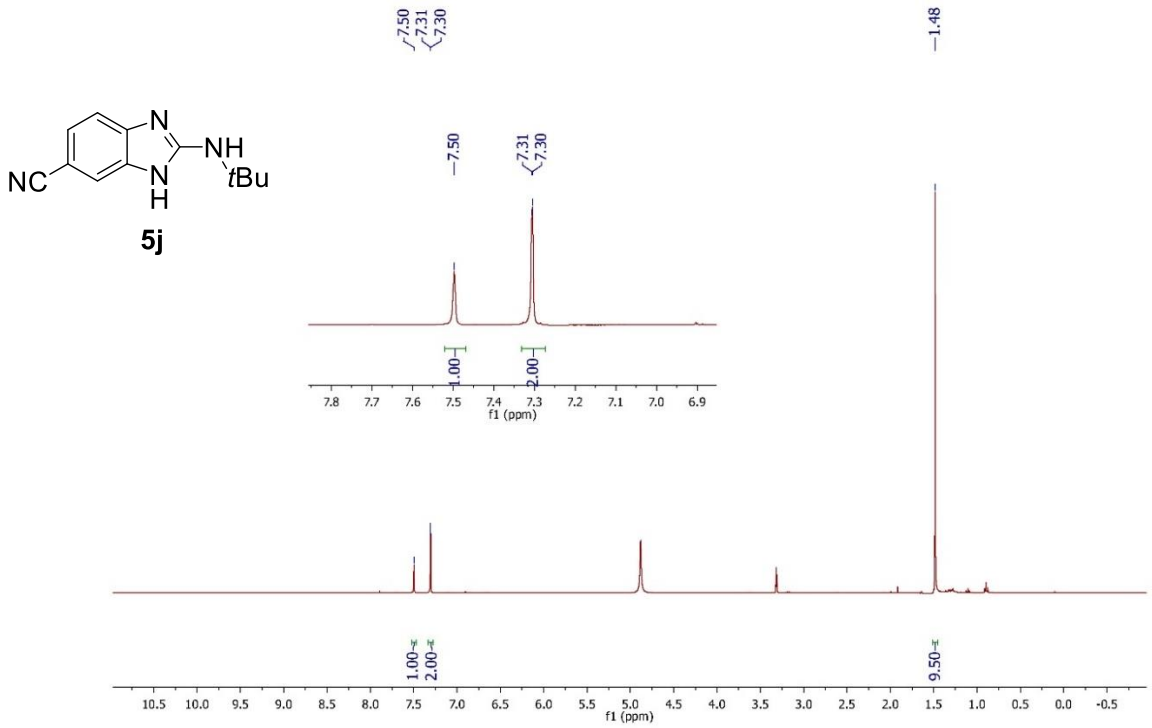

Figure A68. ^{1}H NMR spectrum of 2-(*tert*-butylamino)-5-cyanobenzimidazole (5j) in CD3OD at 400 MHz.

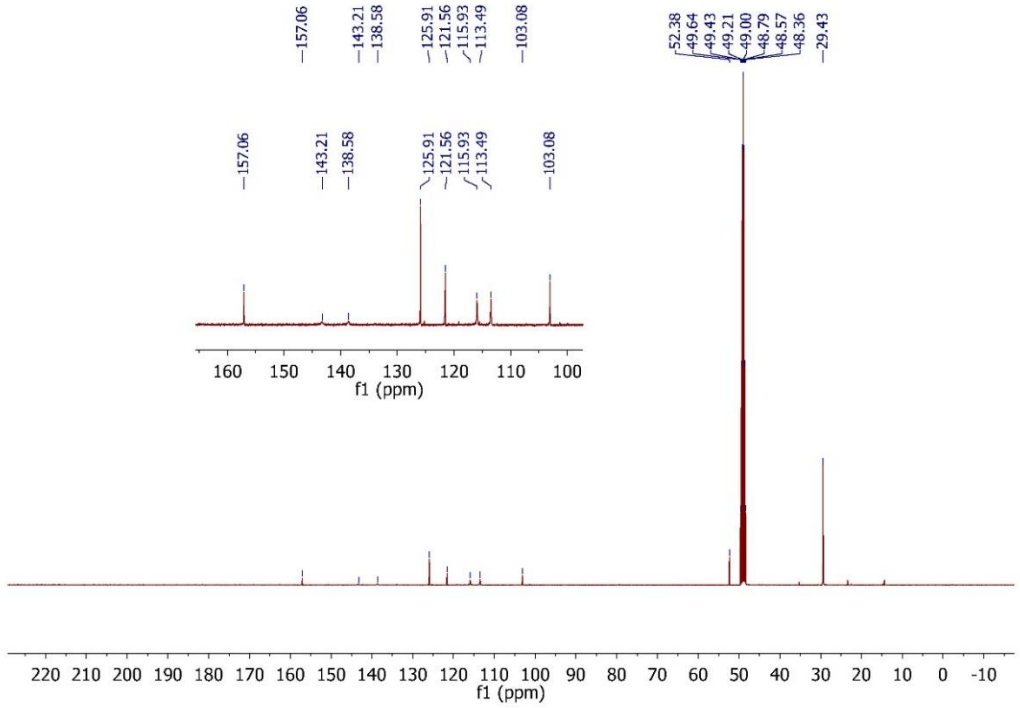

Figure A69. ^{13}C NMR spectrum of 2-(*tert*-butylamino)-5-cyanobenzimidazole (5j) in CD3OD at 100 MHz.

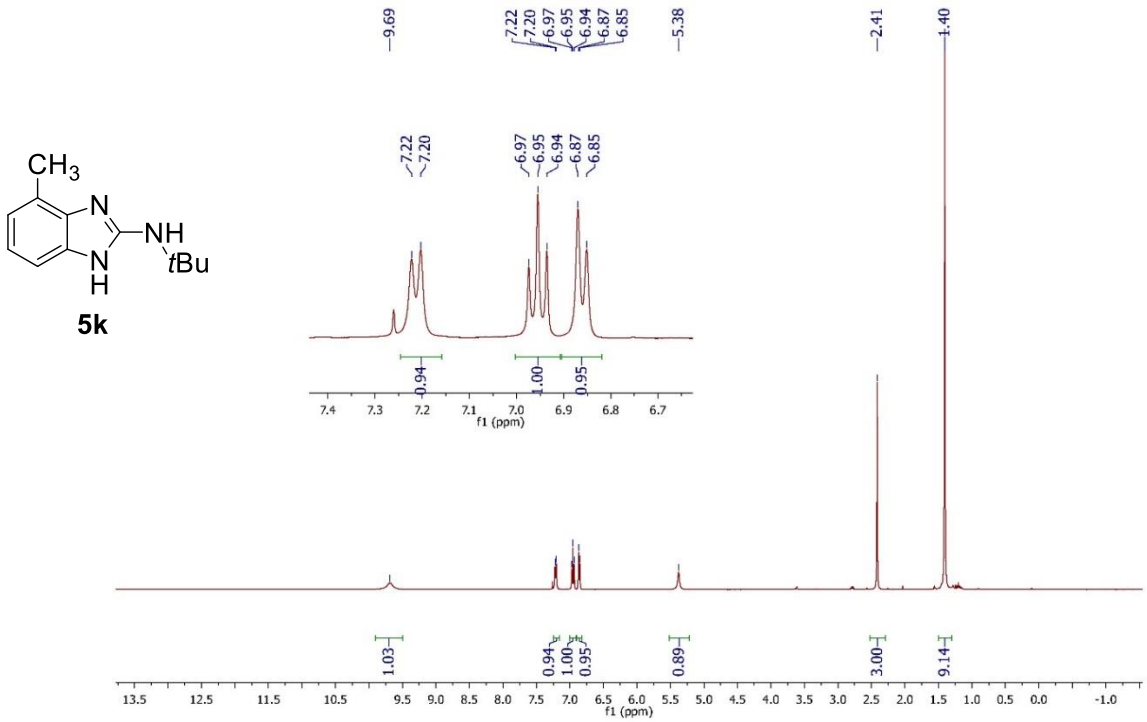

Figure A70. ^{1}H NMR spectrum of 2-(*tert*-butylamino)-7-methylbenzimidazole (5k) in $CDCl_3$ at 400 MHz.

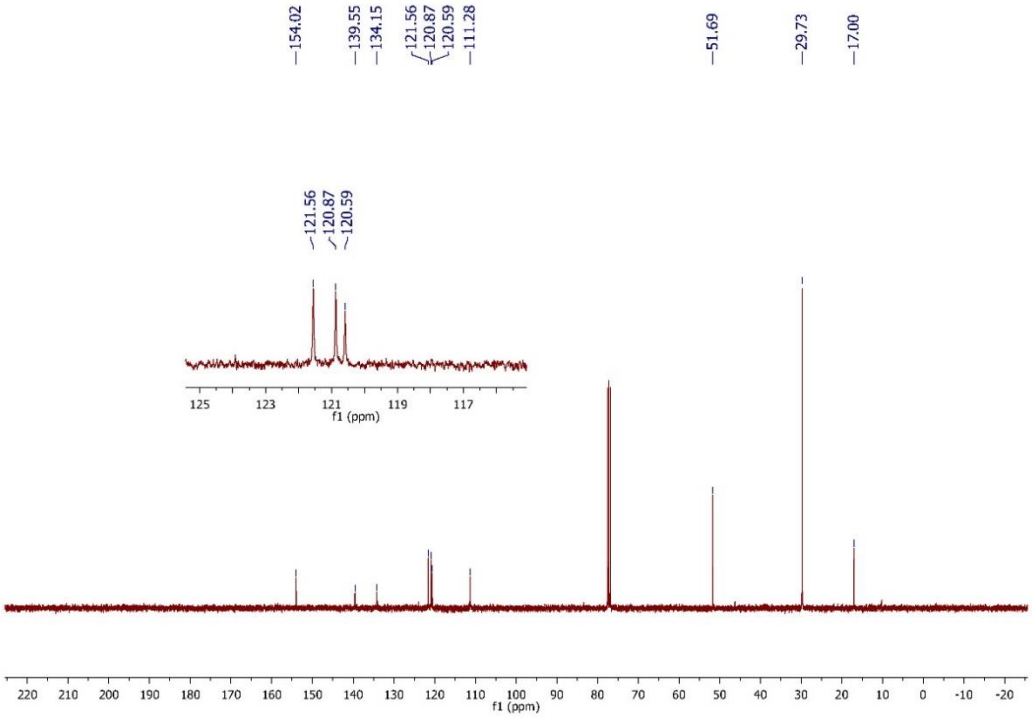

Figure A71. ^{13}C NMR spectrum of 2-(*tert*-butylamino)-7-methylbenzimidazole (5k) in $CDCl_3$ at 100 MHz.

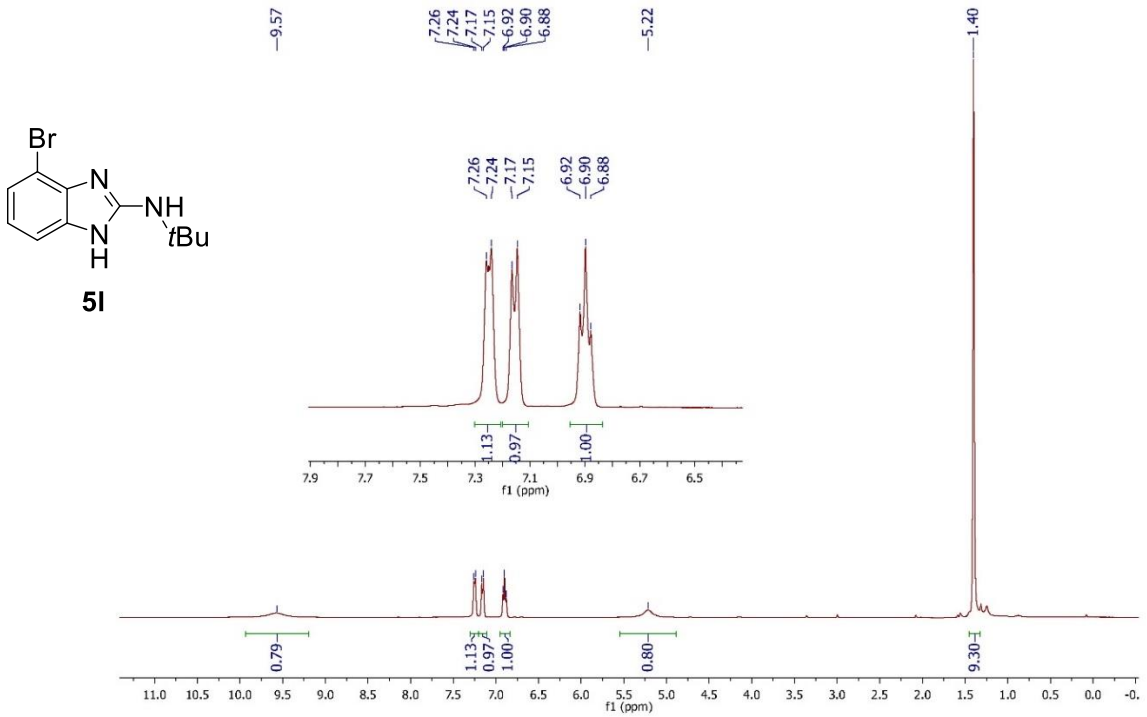

Figure A72. ^{1}H NMR spectrum of 2-(*tert*-butylamino)-7-bromobenzimidazole (5l) in $CDCl_3$ at 400 MHz.

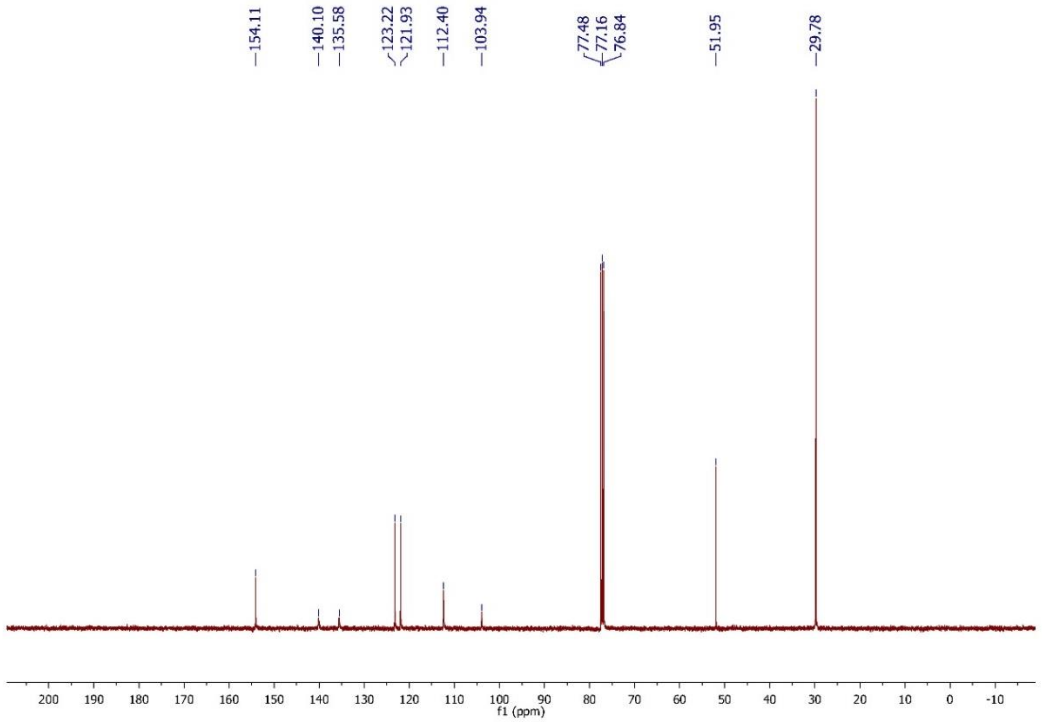

Figure A73. ^{13}C NMR spectrum of 2-(*tert*-butylamino)-7-bromobenzimidazole (5l) in $CDCl_3$ at 100 MHz.

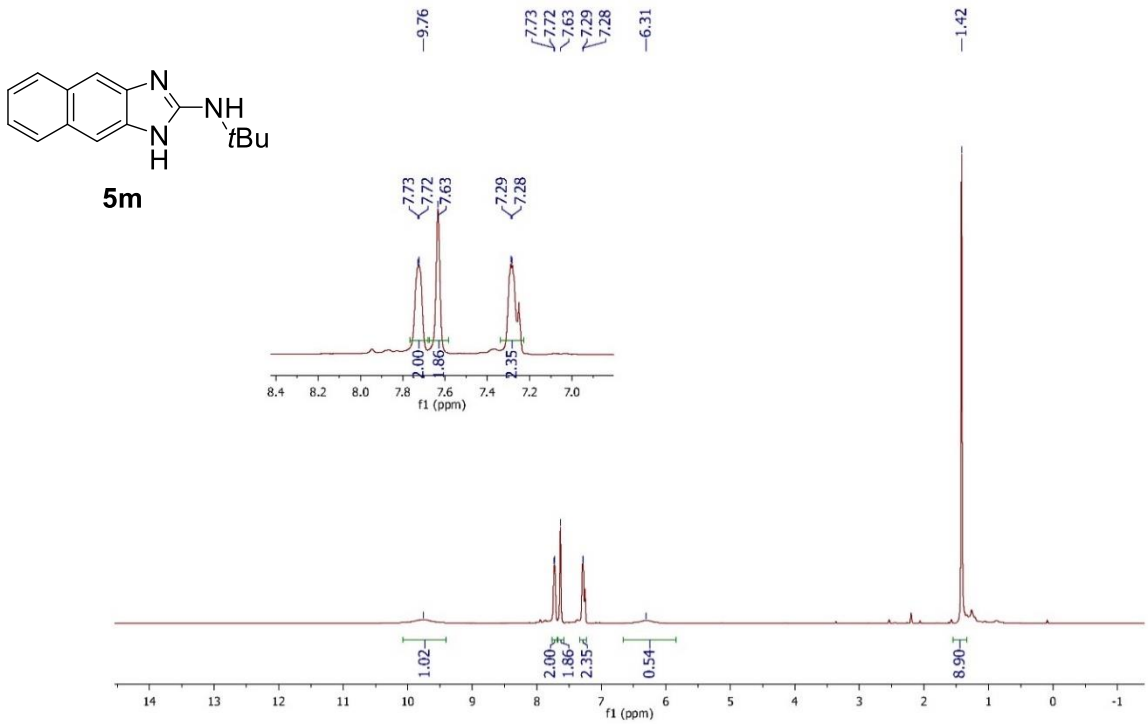

Figure A74. ^{1}H NMR spectrum of 2-(*tert*-butylamino)naphtho[2,3-d]imidazole (5m) in $CDCl_3$ at 400 MHz.

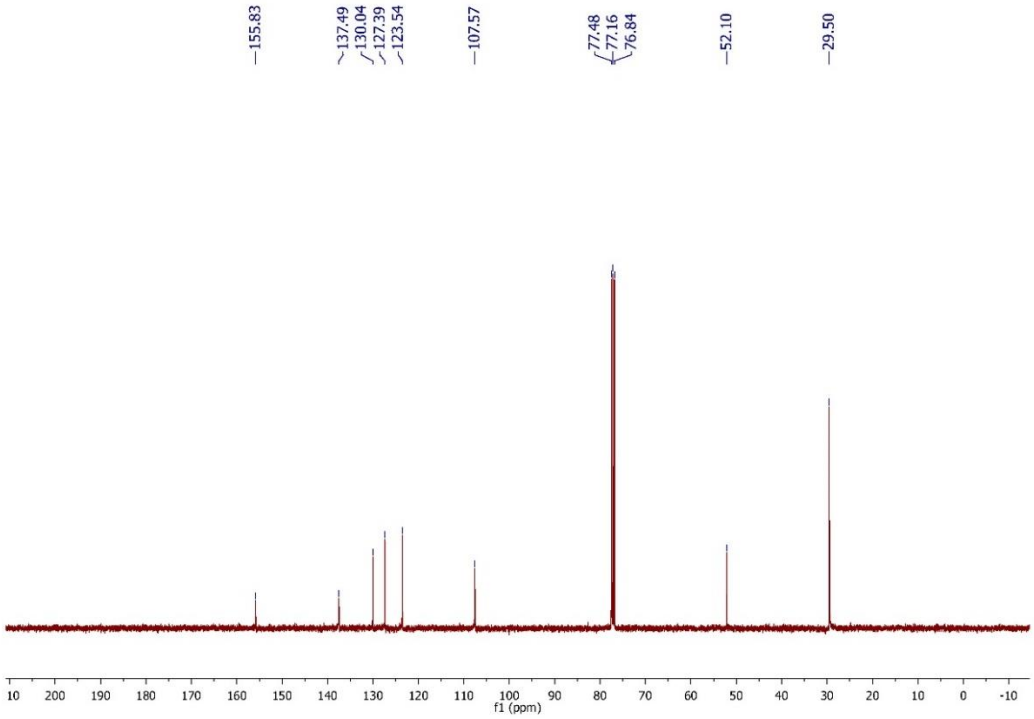

Figure A75. ^{13}C NMR spectrum of 2-(*tert*-butylamino)naphtho[2,3-d]imidazole (5m) in $CDCl_3$ at 100 MHz.

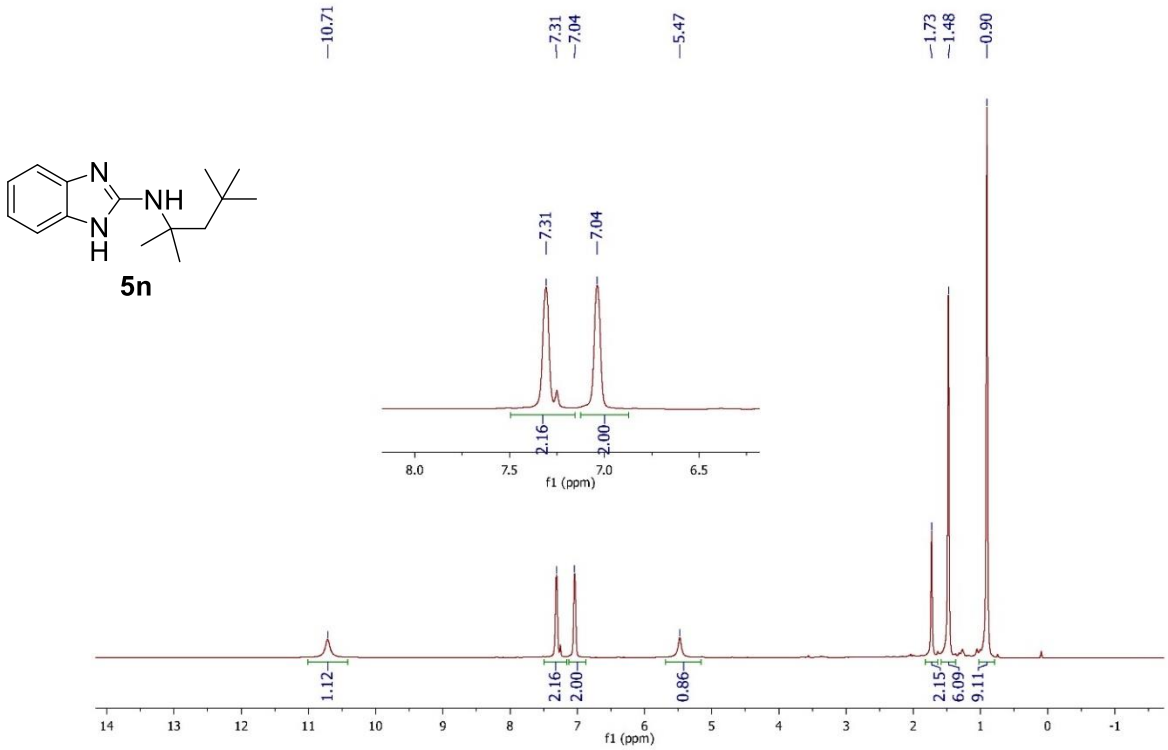

Figure A76. ^{1}H NMR spectrum of 2-(1,1,3,3-tetramethylbutylamino)benzimidazole (5n) in $CDCl_3$ at 400 MHz.

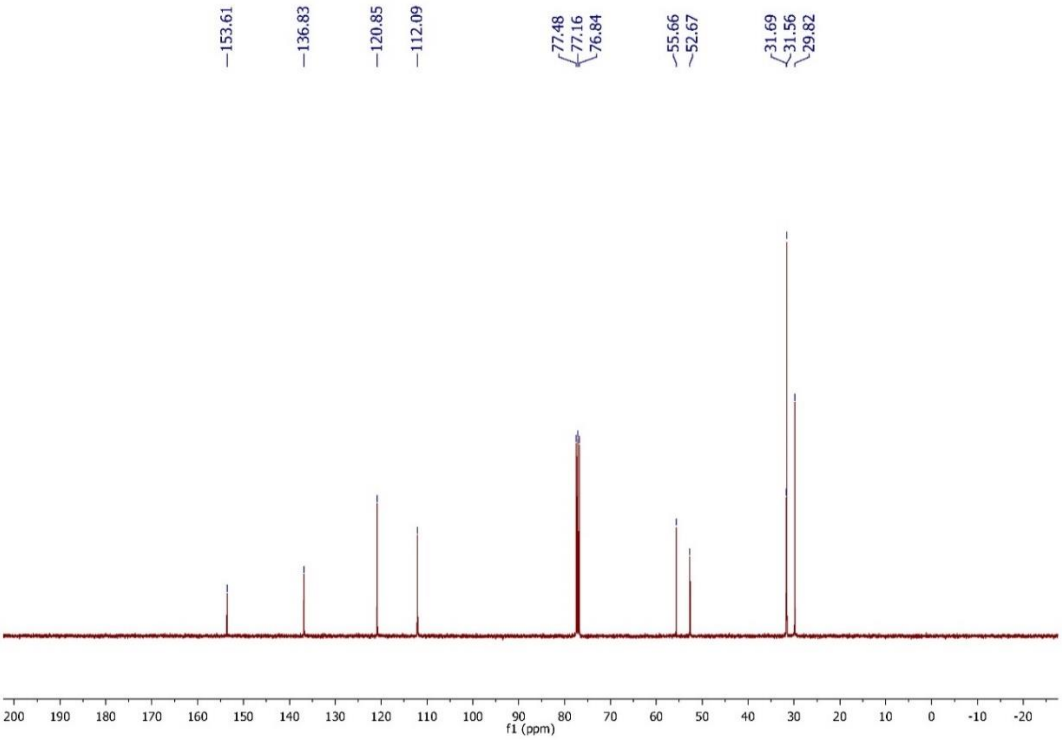

Figure A77. ^{13}C NMR spectrum of 2-(1,1,3,3-tetramethylbutylamino)benzimidazole (5n) in $CDCl_3$ at 100 MHz.

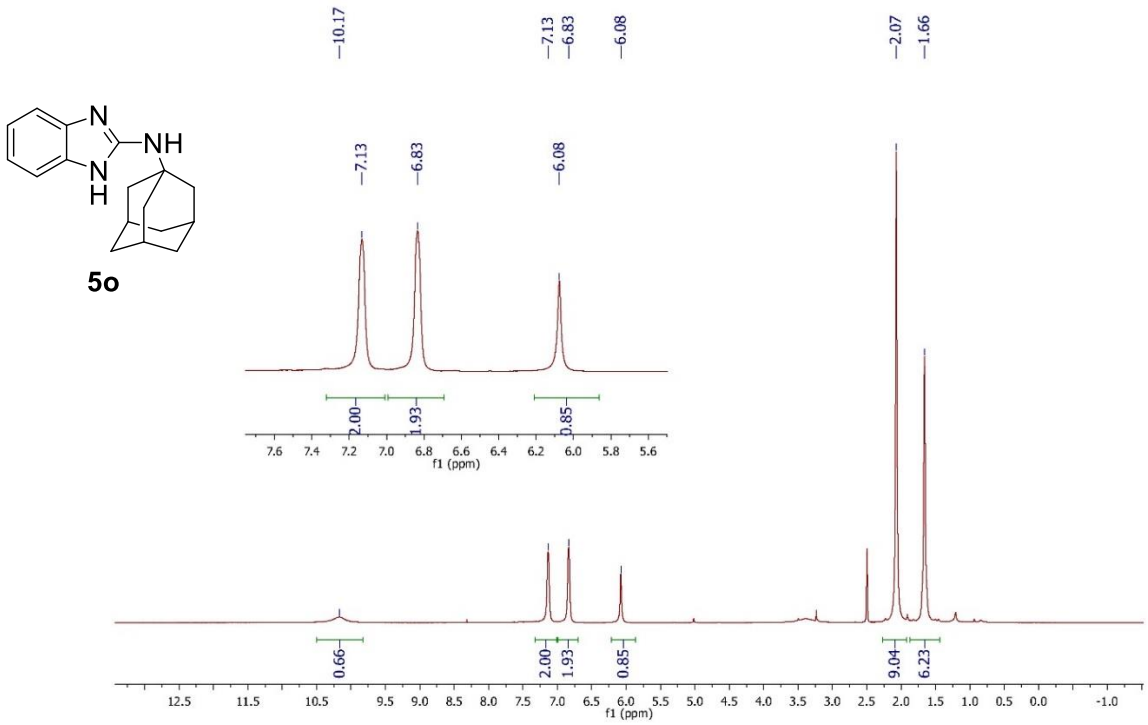

Figure A78. ^{1}H NMR spectrum of 2-(1-adamantylamino)benzimidazole (5o) in DMSO-*d*$_6$ at 400 MHz.

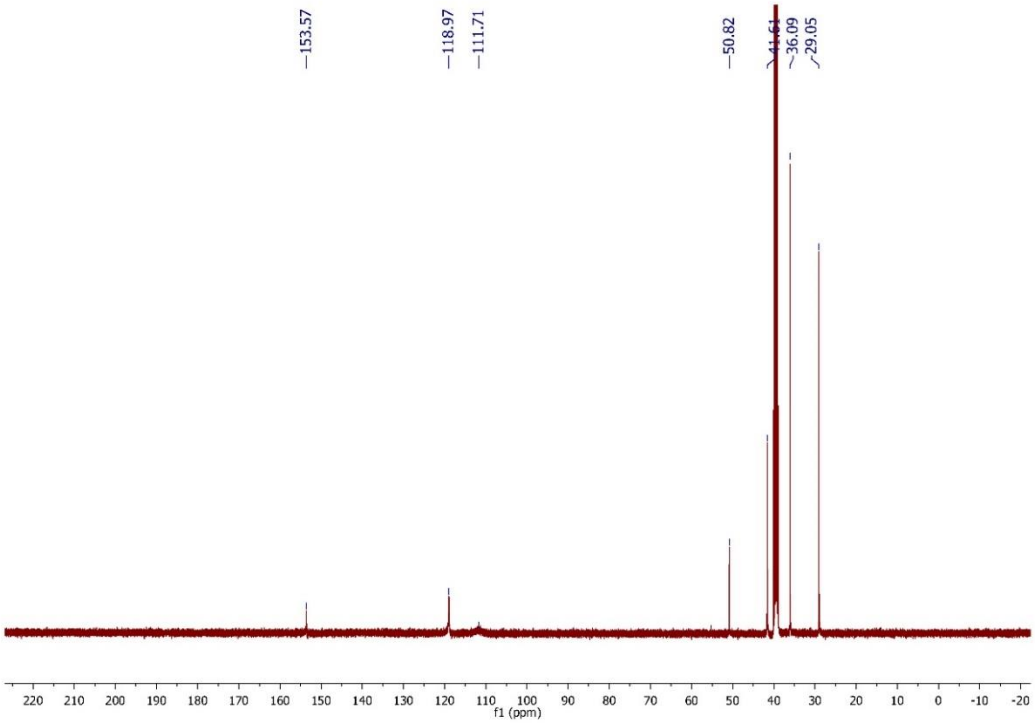

Figure A79. ^{13}C NMR spectrum of 2-(1-adamantylamino)benzimidazole (5o) in DMSO-*d*$_6$ at 100 MHz.

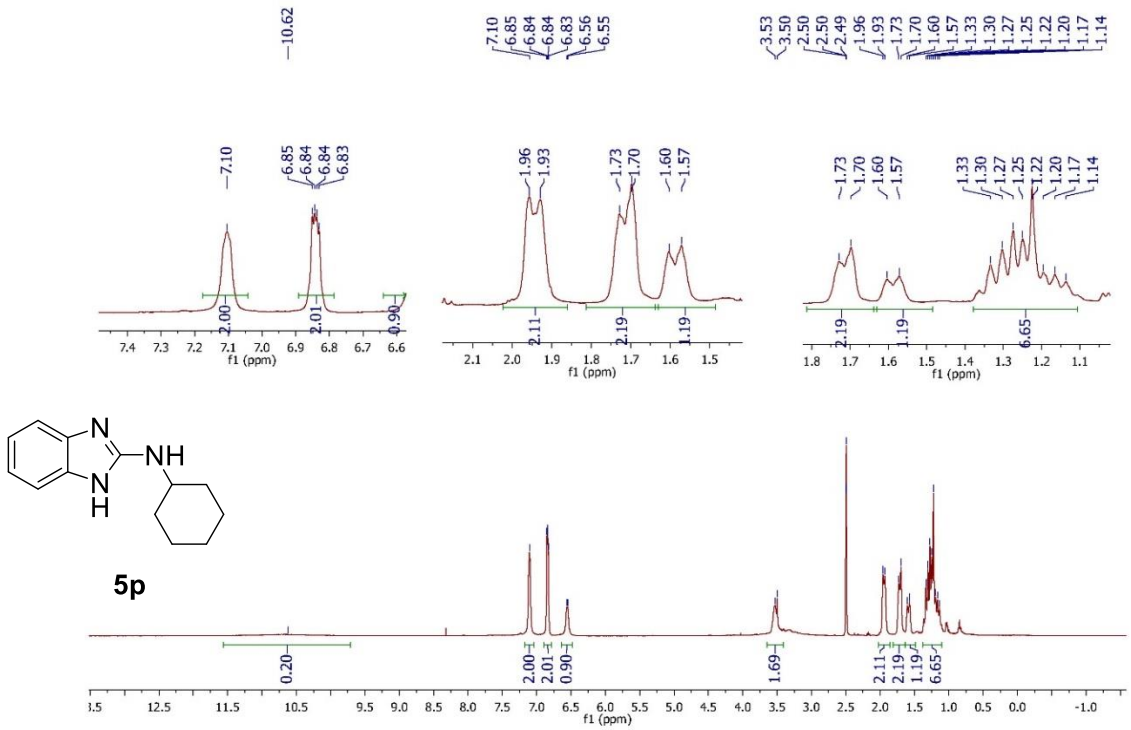

Figure A80. ^{1}H NMR spectrum of 2-(cyclohexylamino)benzimidazole (5p) in DMSO-*d*$_6$ at 400 MHz.

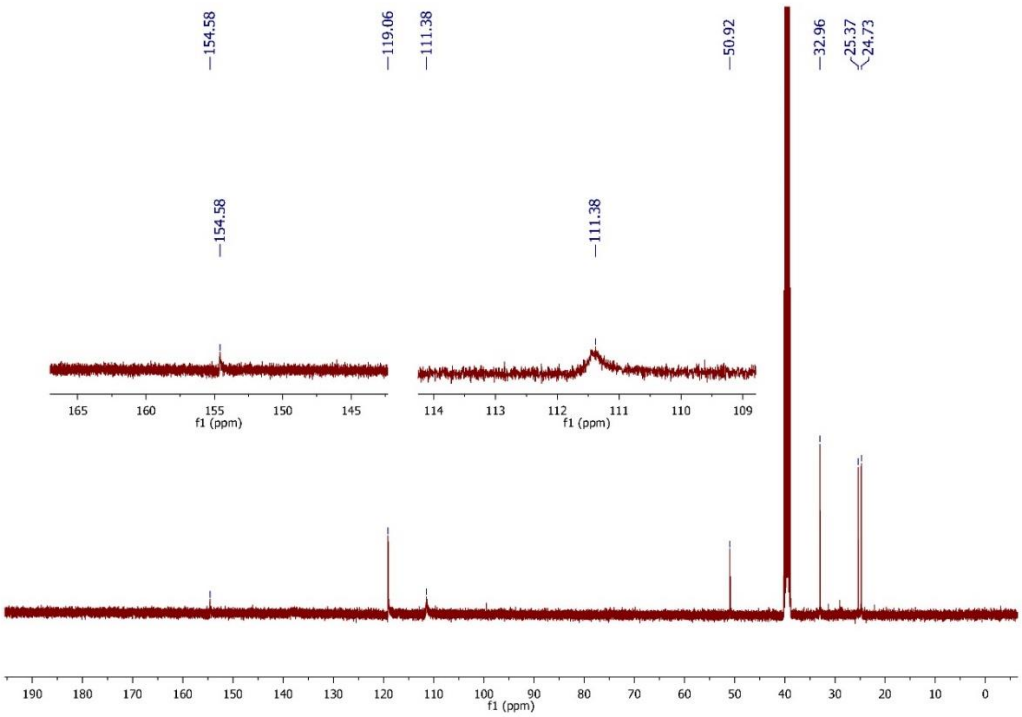

Figure A81. ^{13}C NMR spectrum of 2-(cyclohexylamino)benzimidazole (5p) in DMSO-*d*$_6$ at 100 MHz.

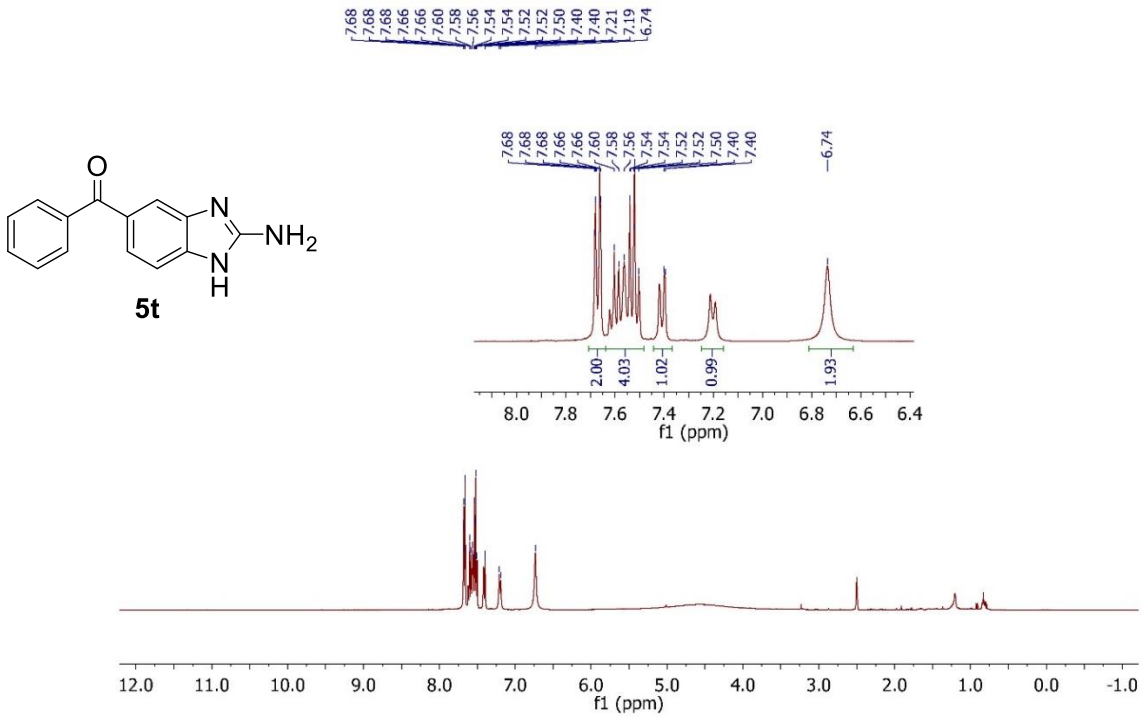

Figure A82. ^{1}H NMR spectrum of 2-amino-5-benzoyl-*1H*-benzimidazole (5t) in DMSO-*d*$_6$ at 400 MHz.

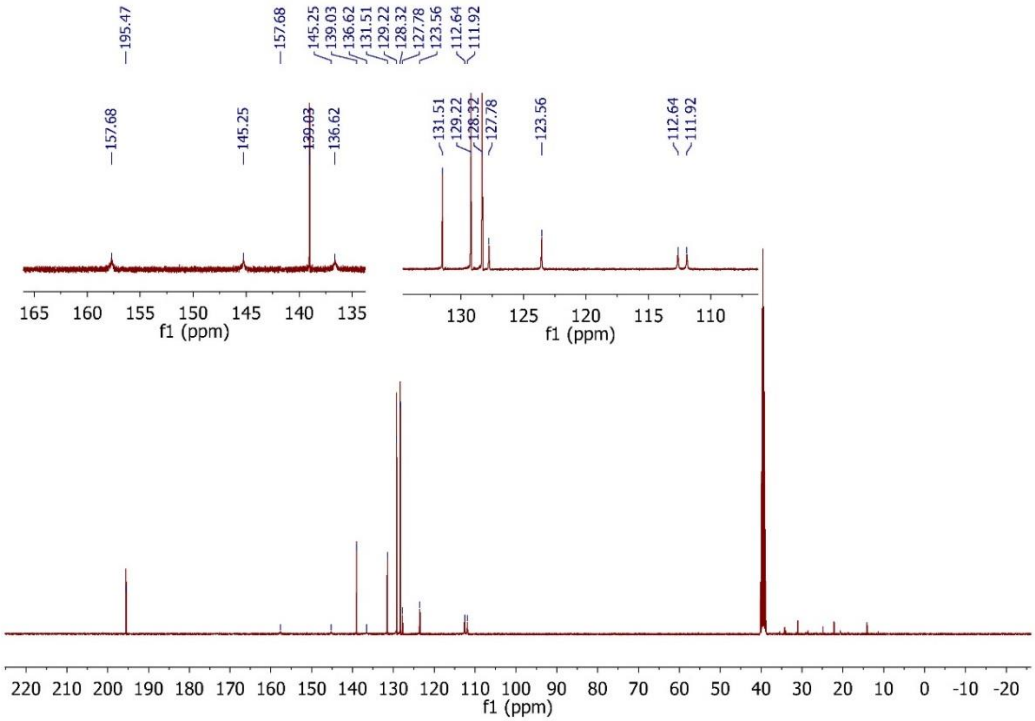

Figure A83. ^{13}C NMR spectrum of 2-amino-5-benzoyl-*1H*-benzimidazole (5t) in DMSO-*d*$_6$ at 100 MHz.

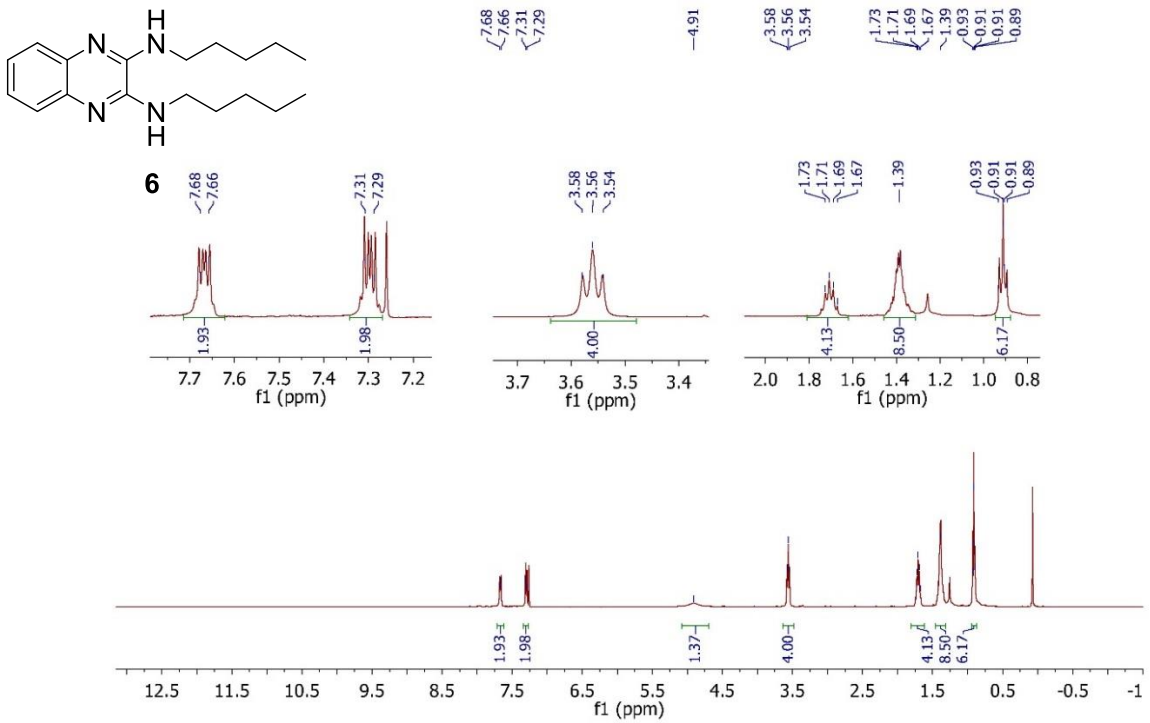

Figure A84. ^{1}H NMR spectrum of *N*2,*N*3-dipentylquinoxaline-2,3-diamine (6) in CDCl3 at 400 MHz.

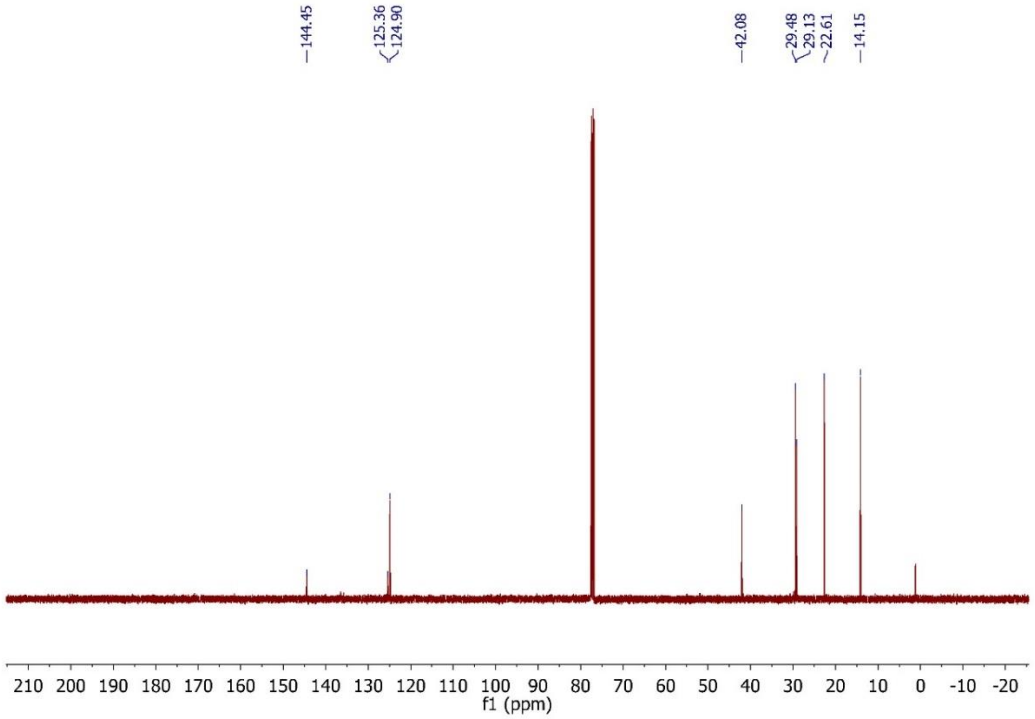

Figure A85. ^{13}C NMR spectrum of *N*2,*N*3-dipentylquinoxaline-2,3-diamine (6) in CDCl3 at 100 MHz.